

Study of Electromagnetic Field Induced Transparency in Y, Gate systems and their variants.

A thesis submitted for the degree of
Doctor of Philosophy

by
V.S.Ashoka



School of Physics
University of Hyderabad
Hyderabad - 500 046
October 1998

CERTIFICATE

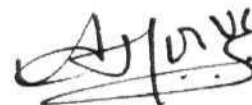
School of Physics

University of Hyderabad

HYDERABAD 500 046

This is to certify that the work presented in this thesis has been carried out by me, V. S. Ashoka for the full period prescribed under Ph.D. ordinances of the university.

I declare to the best of my knowledge that no part of this thesis was earlier submitted for the award of research degree of any University.



Name: V. S. Ashoka

Enrollment No: PP 5980



Supervisor: Prof. S. P. Tewari



Dean

School of Physics

DEAN,
SCHOOL OF PHYSICS,
UNIVERSITY OF HYDERABAD

I owe my gratitude to my thesis supervisor Prof. S. P. Tewari. Due to his constant encouragement and patient tutoring, I relished every moment of my learning.

I thank the Dean, School of Physics for extending all the facilities and support during my stay here.

I thank each one of the faculty members of the School for all their support and help. I specially thank Dr. D. Naryana Rao, Dr. Dutta Gupta and Dr. Ranjit Singh. I also remember with gratitude my constant wellwishers, Profs. V. Srinivasan, S. Chaturvedi and Dr. Prashant Panigrahi. I also thank all the supporting staff at School of Physics.

And then there is an endless list of people who otherwise made every moment of my stay at University a cherished memory. My close friends Chandan, Goutam, Nirmal and Kavita, Harsha and Jolly, other colleagues at the department Siva, Sree Ramana, Venu, Satheesh, Sreenath and Anitha and many many more, who by their affection and friendship have made my University years full of pleasant memories.

I finally thank University Grants Commission, India for the financial support extended for my work.

Abstract

The thesis presents results of theoretical studies on Electromagnetic Field Induced Transparency (EIT) of two multilevel configurations **Y** and **Gate**, so called according to their appearance. The probe absorption behaviour for Y and Gate are examined using four methods viz, (i) numerical solutions of density matrix equations, (ii) analytical solutions to first order in probe absorption and to all orders in pump, (iii) analytical solutions in wavefunction approach and (iv) Semiclassical dressed state picture. These solutions are used to develop an understanding of the underlying mechanism.

The Y configuration shows complete transparency while **Gate** has a residual absorption under certain conditions. It is demonstrated that an externally injected coherence in ground state of Gate system affects its EIT behaviour. Thus, depending on the value of the coherence the **EIT** can be enhanced or destroyed. Using the dressed state picture it is demonstrated that these results are a consequence of the quantum mechanical interference from the superposition states in the excited and the ground states which are connected by the probe transition.

Examples of Y and Gate systems that can exist in real atomic systems are examined. Also studied briefly are subconfigurations which show **Y**-like and Gate-like behaviour.

A case of Gate-like system - comprising of $F=1 \rightarrow F'=1 \rightarrow F''=1$ levels is shown to demonstrate complete transparency. This is because of the resonant action of the pump beam on the excited levels $F' \rightarrow F''$ as well as the non-resonant action on $F \rightarrow F'$, while the probe field is resonantly interacting on $F \rightarrow F'$ transitions. The solution of this bichromatic problem is presented in matrix continued fraction, and has been analysed in terms of the dressed states.

Possibility of obtaining gain without population inversion is studied in both **Y** and **Gate** using (i) incoherent population pumping and (ii) injected atomic coherence. The gain mechanism in $F=1 \leftrightarrow F'=1 \leftrightarrow F''=1$ transition is studied where required coherence already exists and incoherent population pumping is incorporated.

Finally, spatial variation of the induced transparency as a result of spatial variation of pump beam intensity is considered in the limit when, the pump beam is assumed a focussed Gaussian beam and the probe beam a plane wave. In a simple example of a three level ladder scheme, the induced transparency shows a threshold character as a function of pump intensity. This threshold phenomena is described as a puncture of the length L of the sample by a dumbbell shaped absorption profile within which the medium is transparent. The factors affecting the length of this dumbbell are discussed.

| | | |
|------------|--|-----------|
| I | Introduction | 1 |
| 1.1 | Mechanism of EIT | 3 |
| 1.1.1 | Coherence induced Transparency | 8 |
| 1.2 | Plan of this thesis | 11 |
| | References | 15 |
| II | Y and Gate schemes: Semiclassical study | 18 |
| 2.1 | The Y Configuration | 18 |
| 2.1.1 | Analytical Solution for Y system | 29 |
| 2.1.2 | Determination of f - values | 30 |
| 2.2 | Gate configuration | 31 |
| 2.2.1 | Analytical Solution for the Gate system | 40 |
| 2.2.2 | Anomalous absorption | 42 |
| 2.2.3 | Determination of f - values | 43 |
| 2.3 | Conclusion | 43 |
| | References | 44 |
| III | Dressed state analysis | 45 |
| 3.1 | Semiclassical Dressed States | 45 |
| 3.2 | Y configuration | 46 |
| 3.2.1 | Bare state analysis | 46 |
| 3.2.2 | Dressed State picture | 49 |
| 3.2.3 | Interference between spontaneous emission pathways | 54 |
| 3.3 | The Gate System | 59 |
| 3.3.1 | The Bare state picture | 59 |

| | | |
|--|--|------------|
| 3.3.2 | Dressed State picture. | 63 |
| 3.3.3 | Interference between Spontaneous emission pathways. | 67 |
| 3.4 | Conclusion | 71 |
| References | | 73 |
| IV Groundstate Coherences | | 74 |
| 4.1 | Coupling of Non-Coupling States. | 79 |
| 4.2 | Density matrix solutions. | 82 |
| 4.3 | Stability of ground state coherence. | 86 |
| 4.4 | Conclusion. | 88 |
| References | | 89 |
| V Configurations in Real atomic systems | | 91 |
| 5.1 | Case I: $F=1 \rightarrow F'=1 \rightarrow F''=1$ | 92 |
| 5.2 | Case II: $F=2 \rightarrow F'=1 \rightarrow F''=1$ | 94 |
| 5.3 | Case III : $F=1$ and $F=2 \leftrightarrow F'=2 \leftrightarrow F''=1$ | 95 |
| References | | 123 |
| VI Gain without population inversion | | 125 |
| 6.1 | Y configuration: incoherent pumping. | 127 |
| 6.2 | Gate configuration: injected atomic coherence. | 130 |
| 6.3 | Bichromatic approach. | 131 |
| References | | 135 |

| | |
|--------------------------------------|------------|
| VII Threshold of Transparency | 136 |
| References | 144 |
| A Equation 2.3 | i |
| B Equation 2.13 | III |
| C Clebsch-Gordon Coefficients | v |
| D Dipole matrix elements | vii |

Note: Figures corresponding to each chapter are at the end of the chapter

Chapter I

Introduction

A strong electromagnetic field can considerably alter atomic response functions. Such alterations can effectively be exploited for practical purposes. For instance, a simple Stark effect on atomic energy levels by a d.c. electric field has led to an enhanced second harmonic generation in atomic Hydrogen [1]. Similar useful modifications are induced by an oscillating electric field as a consequence of dynamic Stark effect [2, 3]. Oscillating electric fields at optical frequencies can be obtained by use of lasers, which are sources of intense radiation at optical frequencies. This has led to considerable interest in studies of a variety of electromagnetic field induced phenomena. Diverse applications of such phenomena like Electromagnetic Field Induced Transparency (EIT) [4], Lasing Without Inversion (LWI) [5], efficient VUV generation by third harmonic generation [6, 7], efficient second harmonic generation [8], ultrahigh refractive index [9], elimination of self focusing [10] or lens like behaviour [11], enhanced nonlinear sum frequency generation [12], giant kerr nonlinearities [13], efficient optical phase conjugation [14], enhanced isotope separation [15] and Velocity Selective Coherent Population Trapping (VSCPT) [16, 17], etc. have been studied recently.

An intense laser radiation, often referred to as pump beam has been shown to alter and control atomic properties of a simple two-level model (Figure 1.1) [18]. Another weak tunable beam, interacting with the same two levels can be used to probe the alterations induced by the strong beam [19]. The absorption of the probe beam is seen

to be significantly altered leading to new effects like multiple absorption bands [20] and gain in presence of the strong pump [19].

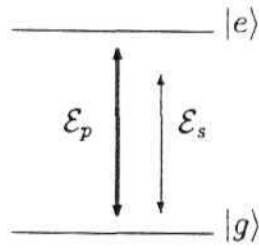


Figure 1.1: Two level atom. \mathcal{E}_p is the pump beam and \mathcal{E}_s is the probe beam.

Instead of interacting with the same strong transition, the probe beam can interact on a transition connecting one of the two levels with a third level (Figure 1.2). The pump and probe beams now interact with two different transitions sharing a common level. In this case, coherences developed between the atomic states can lead to Coherent Population Trapping (CPT) condition and as a consequence such configurations show a probe absorption behaviour different from the earlier setup (Figure 1.1). Such configurations involving three levels through their coherences offer further new control over the electromagnetic field induced phenomena. Recently a large number of studies of electromagnetic field induced phenomena involving three-level system of all possible configurations like V, A and ladder (E) have appeared in literature. As examples of different configurations see references :[13, 21, 22, 23, 24, 25, 26]. These and several

others have been covered in review articles collected in [5] and references therein.

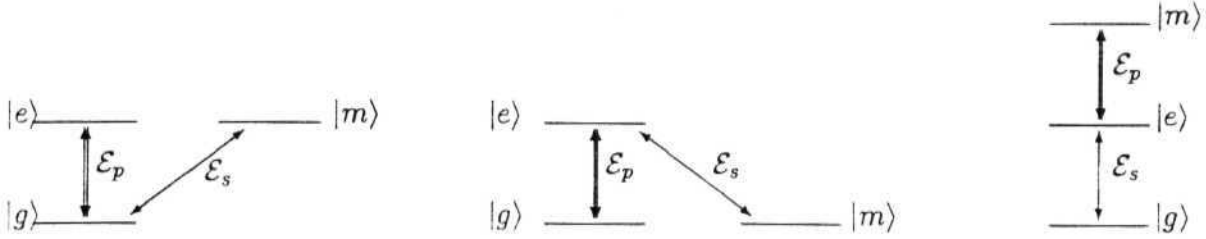


Figure 1.2: Three level configuration of V, A, and ladder. \mathcal{E}_p is the pump beam and \mathcal{E}_s is the probe beam.

In order to develop further the study of such electromagnetic field induced phenomena in more complex systems, an insight into the mechanisms of Electromagnetic Field Induced Transparency is presented below in some detail.

1.1 Mechanism of EIT

Classical absorption of probe beam by an atomic vapour follows Beer-Lambert Law. Accordingly, intensity of light after passing through a length L of the absorbing medium, is given by $I(L) = I_0 \exp(-\alpha L)$. I_0 is the incident intensity and α is the absorption

coefficient of the medium, constant throughout the length L . A high value of α implies a large absorption and a smaller value of α denotes transmission. A completely transparent medium has $\alpha = 0$. Electromagnetic Field Induced Transparency (EIT) involves reduction of value of α by a control laser beam.

Three mechanisms leading to EIT which have been studied in past are (i)AC Stark shift, (ii)Fano interferences and (iii)Coherent Population Trapping. In the first case, strong, resonant laser causes a dynamic Stark splitting of the related energy levels [2]. The resultant shift in the energy level is proportional to the Rabi frequency of the transition involving the strong laser. Stronger the pump laser, larger is the Rabi frequency and larger is the shift. The probe laser is thus detuned from the shifted levels leading to a reduced absorption. The absorption is not a complete zero, but minimized [3, 27, 28].

The other two cases are results of 'Quantum interferences' (QI). Effect of destructive interference between quantum mechanical pathways was first pointed out by Ugo Fano who attributed the dark lines in photoionization spectra of Helium to destructive interference between two ionization pathways [29]. A similar mechanism was adopted by Harris and coworkers to obtain EIT, in which two spontaneous emission pathways destructively interfere to give rise to a non-absorption condition [30]. For this interference to take place, these two spontaneous emission pathways should couple to the same mode of radiation field. Such condition is readily fulfilled when the spontaneous emission takes place from two atomic states having the same J and m_J quantum numbers [30]. But such states do not frequently occur in nature. A method of obtaining such condition is to prepare a 'Dressed' superposition by a strong laser. These two 'Dressed States' will then have same effective J , m_J values [27, 31], leading to a Harris-Imamoğlu

type of interference. QI induced transparency is complete and the absorption is a total zero unlike AC Stark effect case [27].

The third case referred as Coherent Population Trapping (CPT) is also a result of Quantum Interference, but between absorption pathways. It was first observed by Alzetta, Gozzini, Moi and Orriols in their experiments in Sodium vapour[32]. In this case, a coherence between hyperfine sublevels caused a destructive interference of absorption pathways [33]. In a typical CPT setup, two ground states $|a\rangle$ and $|b\rangle$ couple simultaneously to a third state $|c\rangle$ via the laser beam. There develops in the system a superposition state $|Q_-\rangle = (|a-b\rangle)/\sqrt{2}$. The total transition probability for absorption of radiation field is proportional to

$$\begin{aligned} |\langle c|\vec{d} \cdot \vec{E}|Q_-\rangle|^2 &= 1/2|\langle c|\vec{d} \cdot \vec{E}|a-b\rangle|^2 \\ &= 1/2\{|\langle a|\vec{d} \cdot \vec{E}|c\rangle|^2 + |\langle b|\vec{d} \cdot \vec{E}|c\rangle|^2 - 2\langle a|\vec{d} \cdot \vec{E}|c\rangle\langle b|\vec{d} \cdot \vec{E}|c\rangle\} \quad (1.1) \end{aligned}$$

When $\langle a|\vec{d} \cdot \vec{E}|c\rangle = \langle b|\vec{d} \cdot \vec{E}|c\rangle \neq 0$, the total transition probability (1.1) is zero and therefore the population is trapped in level $|Q_-\rangle$. The state $|Q_-\rangle$ is termed a CPT state [34, 35]. Superposition states are obtained even in the previous case, where 'dressed states' are superpositions of 'bare states'. But the population stays in bare states which do not form part of superposition state. In CPT condition on the other hand, population is trapped in the superposition states. Unlike AC Stark effect, creation of coherences does not call for strong lasers. Nominal intensity lasers will be sufficient to induce transparency by the above two methods. But coherences between atomic levels, especially between degenerate atomic levels are destroyed by collision mechanisms. The laser light in such cases has to be strong enough to overcome such coherence destroying collisions [36].

The **Y** and the **Gate** systems to be introduced below and discussed in detail in the thesis are more complicated compared to the two and three level models discussed so far. However before we motivate for their studies we consider briefly the phenomenon of **LWI** which has benefitted considerably by the **EIT** phenomenon, and has been reported later in the thesis for the **Y** and the **Gate** systems.

The lasing without inversion is a phenomenon related to EIT. Two processes are required to achieve Lasing without **Inversion**. (i) Increased emission and (ii) cancellation of absorption. There are two methods of achieving these processes. (a) Fano interferences and (b) preparation of CPT states. Fano interference processes **affect** emission and absorption processes differently. Absorption is cancelled due to destructive interference while the emission probability is **unaffected**[37]. This concept was used to achieve **sufficient** gain without the need for population inversion [30]. In this case, energy of pump beam is fed into the probe beam. The second method is to first create a CPT state and thus cancel the absorption. Then, some population is pumped to the upper level by an incoherent process which **will** not destroy the coherences that lead to CPT state. Lasing occurs in this case even when the population pumped to the upper state is less than the population in the lower state [5, 38]. An added effect that was observed in this case was the reduction of spontaneous emission which would otherwise add to the noise in lasing [21, 39, 40, 41, 42, 43]

Practical advantage of EIT and LWI effects may be summarised as follows. EIT effect is useful when resonant absorption of generated light is to be avoided. Such cases occur in higher order harmonic generations in atomic vapours and is especially troublesome while dealing with **VUV** light. Added effect of the refractive index being modified

in presence of strong laser is also applicable in these cases [6, 12]. Usually, In experiments involving atom -light interaction, higher refractive index is always accompanied by high absorption. Using the **EIT** effect to achieve low absorption even at substantial refractive index values was proposed for experiments where ultra high refractive index could be achieved [9]. Both these features will be beneficial for experiments using nonlinear optics and magnetometry [44].

Lasing without inversion eliminates the need for long lived states. Conventional lasing is possible only among those levels where the population inversion holds till the stimulated emission takes place. This condition is relaxed for LWI process which extends the range of atomic levels that can be used for lasing. Frequency ranges and materials hitherto forbidden for lasing action can now be made use of by these methods. Atomic medium where the transition from ground state to first excited state is in UV range while the higher transitions are in visible light energies can be used to obtain gain in UV. Using a weak probe beam in UV and a high powered pump beam in visible range, a lasing action can be achieved wherein the probe beam experiences a gain at the cost of pump beam energy. Thus a practical source of high energy UV and VUV can be obtained.

In order to motivate the study of EIT and LWI phenomena in more complex atomic models like the Y and the Gate studied in this thesis we introduce now briefly a treatment of EIT as a coherence induced effect using the density matrix formalism.

1.1.1 Coherence induced Transparency

The absorption coefficient α is related to imaginary part of atomic susceptibility by

$$\alpha(\omega) = \frac{2\pi\omega}{c} \chi''.$$

ω is the frequency of light and c is the velocity of light in vacuum. χ'' is the imaginary part of atomic susceptibility $\chi = \chi' + i \chi''$.

From a two-level model atom, the susceptibility can be obtained in density matrix formalism as

$$\chi(\omega) = \frac{\mathcal{N} d_{eg}}{\mathcal{E}} \rho_{eg} \quad (1.2)$$

where \mathcal{N} is the number of atoms in unit volume and \mathcal{E} is the amplitude of the incident light. $d_{eg} = \langle e | q \cdot \hat{\mathbf{r}} | g \rangle$ is the dipole moment between the ground state $|g\rangle$ and the excited state $|e\rangle$. q is the charge on the electron and $\hat{\mathbf{r}}$ is its displacement from mean position. ρ_{eg} is the off-diagonal element of the density matrix denoting the coherence between states $|g\rangle$ and $|e\rangle$. For a two-level atom, the value ρ_{eg} is governed by the equation

$$\partial_t \rho_{eg} = [i(\omega - \omega_{eg}) - \gamma_{eg}] \rho_{eg} - i \frac{d_{eg} \cdot \mathcal{E}_1}{\hbar} (\rho_{ee} - \rho_{gg}) \quad (1.3)$$

ρ_{ee} and ρ_{gg} are populations of level $|e\rangle$ and $|g\rangle$ respectively. $\omega_{eg} = (E_e - E_g)/\hbar$ is the energy difference in radian frequency between the two levels. γ_{eg} is the decay rate of coherence ρ_{eg} . When the field amplitude \mathcal{E}_1 is small, the variations in populations ρ_{ee} and ρ_{gg} vary very slowly, and thus the populations can be assumed to be constant. Then, a steady state value of ρ_{eg} is obtained by setting the time derivative to zero, which gives,

$$\rho_{eg} = \frac{d_{eg} \cdot \mathcal{E}_1 (\rho_{ee} - \rho_{gg})}{\hbar(\omega - \omega_{eg} + i\gamma_{eg})}$$

A weak field amplitude \mathcal{E}_1 does not alter the thermal statistical distribution which has $\rho_{ee} < \rho_{gg}$. This condition, used in above equation leads to the probe absorption, i.e., $\text{Im}(\rho_{eg}) > 0$. Therefore, $\alpha > 0$ which represents here an absorption.

If there exists a third level $|m\rangle$ in the atom such that a pump laser beam connects transition between $|e\rangle$ and $|m\rangle$, then the equation (1.3) becomes

$$\partial_t \rho_{eg} = [i(\omega - \omega_{eg}) - \gamma_{eg}] \rho_{eg} - i \frac{u_{eg} \cdot \mathcal{E}_1}{\hbar} (\rho_{ee} - \rho_{gg}) + i \frac{u_{em} \cdot \mathcal{E}_2}{\hbar} \rho_{mg} \quad (1.4)$$

where ρ_{mg} is the coherence between $|g\rangle$ and $|m\rangle$. \mathcal{E}_1 is the amplitude of probe beam and \mathcal{E}_2 is that of the pump beam. It is seen that ρ_{mg} modifies the value of ρ_{eg} and its coupling is controlled by value of $d \cdot \mathcal{E}_2$.

Under suitable conditions, ρ_{mg} can completely cancel the effect of $(\rho_{ee} - \rho_{gg})$, and make the coherence $\rho_{eg} = 0$. The medium is then transparent. It is also possible for ρ_{mg} to exceed the contribution of $(\rho_{ee} - \rho_{gg})$ and make ρ_{eg} negative, which implies gain in the medium. For such a 'coherence induced gain' situation, the population inversion $\rho_{ee} > \rho_{gg}$ is not required, and a Lasing Without Population Inversion is hence possible [45]. Thus, EIT and LWI are results of coherence between atomic levels. This makes it necessary that in multilevel schemes, all possible coherences should be considered.

For further development of the EIT like phenomena one might consider modifications of atomic response due to a strong pump forming a three-level-configuration by itself. This is different from the two-level-strong-field-configuration discussed so far in the literature. The weak probe beam probing it may act on another connected transition e.g. by dipole transition to a fourth level. Behaviour of such a model will be dramatically different from the three level systems already studied in literature.

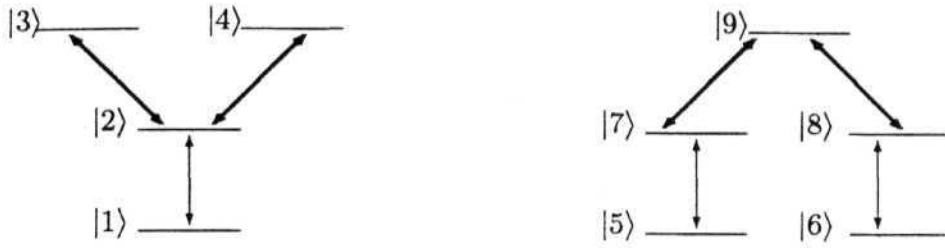


Figure 1.3: **Y** and **Gate** configurations. Thicker lines represent pump beams and the thinner lines are probe beams.

Analysis of two such models are presented in this thesis. In these models, the conventional three level systems are formed in the excited state, and the probe beam interacts with the ground state. For the sake of simplicity, only a A and a V system in the excited states are considered since they involve a strong beam of a single frequency. The first model is a four level system, called Y configuration. It involves a V system in the excited state and the probe beam interacting with the common level of the three states and the ground state (Figure 1.3). The second model is a five level system, called the **Gate** configuration. It has a A in the excited states while the probe beam connects transitions between the two lower levels to two degenerate ground states (Figure 1.3). They are thus named due to their appearances.

An analysis is presented in this thesis for Electromagnetic Field Induced Transparency in these two configurations. It reveals the distinct behaviour of these two systems. For instance Y configuration shows a complete induced transparency, while the Gate configuration does not. An understanding of such behaviour is important when, as shown in the later part of the thesis, complex systems are analysed as combinations of Y and **Gate** systems.

1.2 Plan of this thesis

At first, behaviour of isolated Y and Gate configurations are analysed in the density matrix formalism in Chapter II. Numerical calculations are used to show the effect of atomic coherences which cancel the absorption process in the Y configuration and reduce the absorption in the Gate configuration. Analytical solutions are then obtained in first order of probe amplitude, for both the configurations. These analytical solutions agree well with the numerical solutions at a weak probe beam limit. An application of these analytical solutions is suggested using which Rabi frequencies of excited state transitions can be experimentally determined.

The dressed state picture shows the mechanism of transparency in a straightforward way. In order to discuss the dressed state picture we consider next the wave function approach for the analysis of the Y and Gate configurations in Chapter III. Solutions in the long-time limit are presented in both bare state and dressed state picture. These two solutions confirm the earlier results of the density matrix method. These solutions are used to develop an understanding of the mechanism of EIT in **Y** and **Gate** systems.

The Fourth chapter deals with a situation when the atom is initially prepared in a superposition state of the two ground states of **Gate** system. The behaviour of the configuration is affected by such a preparation. The injected coherences either enhance or reduce the transparency of the **Gate** configuration depending upon their sign. Such externally injected coherences offer a control over the transparency of the **Gate** system. Analysis of this behaviour leads to a new insight on interaction between superposition states. Behaviour of Coherent Population Trapping is reexamined in this light and the knowledge of such behaviour is extended.

In the fifth chapter, energy level schemes of certain real atomic systems are analysed where **Gate** and **Y** systems can be realized. Configurations formed with magnetic hyperfine sublevels of Sodium atom are considered as an example. Three configurations are studied, the first one is an isolated **Gate** system, a second one is when a **Y** and a **Gate** configuration exist together. Third one is a more complex configuration involving many levels, all of them interacting with the same pump and probe beams. This configuration is shown to reduce into uncoupled groups which individually show either **Gate** -like and **Y** -like behaviour. This means that **Gate** and **Y** can be considered as generic systems and can be added to the class of other generic systems such as **A**, Ξ and **V**.

In previous chapters II to IV, the pump and probe beams have been assumed to interact only with their respective transitions. Due to differences in their frequencies, the pump beam is assumed far detuned from the probe transition frequency and vice versa. Note however that even far detuned beams can generate coherences between atomic levels. For example in the **Gate** configuration, the pump beam can create extra coherences while interacting with the probe transition. Considering such coherences

can lead to further modification of the **EIT** phenomena. Such a case is presented in the real atomic system. In this case since both pump and probe beams, which are of two different frequencies, are interacting with both the transitions, a **bichromatic approach** is used to solve this problem in Chapter V. Solutions are obtained in continued fraction method. The coherences created by the pump beam is seen to render the **Gate configuration** completely transparent. An examination into the dressed state picture reveals that the pump beam creates coherences which lead to the same effects as studied in Chapter IV by the injected coherence method.

Lasing without inversion in **Y** and **Gate** systems is examined in Chapter VI. Three cases of achieving Gain without population inversion are presented. (A) Incoherent pumping method : By transferring some population incoherently to the first excited states, but not creating a population inversion. Since absorption and spontaneous emission is inhibited due to coherence induced effects, population decay to lower levels is via stimulated emission. A gain is observed even in absence of population inversion. The **Y** configuration, which shows a complete induced transparency is suitable for this method.

(B) **Injected coherence method**: The role of coherences between ground states, which in an earlier chapter was shown to effect the absorption properties significantly, is exploited here. A coherence between the two ground levels of **Gate** can be created externally. This coherence is in general a complex number and its magnitude and phase can be controlled separately. For particular values of such magnitude and phase, gain is observed and the frequency region of this gain can be controlled by controlling the phase and magnitude.

(C) A combination of the above methods is used to achieve gain in the realistic configuration. The **bichromatic** problem reveals that the pump beam acting off-resonant on the probe transition creates a coherence between the ground states which will render the **Gate** system completely transparent. Thus, the necessary coherence is created by the pump beam itself. Once this coherence is created, an incoherent pumping can be used to obtain a gain in the medium. Continuing from the bichromatic problem of previous chapter, **the real** configuration with an isolated **Gate** system is used to achieve such a gain.

In Chapter VII, we consider an effect of the pump beam being a focussed Gaussian beam. This results in a spatial variation of the strength of the pump laser, along the length of the sample. A relation between the strength of the pump laser and the EIT signal observed is explored. This gives a condition for the threshold intensity of the pump laser for which **EIT** is achieved [46].

References

- [1] K. Hakuta, L. Marmet and B. P. Stoicheff, *prl*, 66, 596 (1991)
- [2] S. H. Autler and C. H. Townes, *Phys. Rev.* **100**, 707 (1955)
- [3] T. Hänsch, R. Keil, A. Schabert, Ch. Schmelzer and P. Toschek, *Z. Phys.* **226**, 293 (1969)
- [4] K.-J. Boiler, A. Imamoglu and S. E. Harris, *Phys. Rev. Lett.*, 66, 2593 (1990); A. Kasapi, M. Jain, G. Y. Yin and S. E. Harris, *Phys. Rev. Lett.* 74 2447 (1995)
- [5] O. Kocharovskaya *Phys. Rep.* **219**, 175 (1992); M. O. Scully, *ibid*, 191 and references therein, E. Arimondo, *Progress in Optics*, Vol.XXXV, Ed: E. Wolf. Elsivier, 1996, pp 259; S. E. Harris, *Phys. Today*, July 1997, pp36; M. O. Scully and M. S. Zubairy *Quantum Optics*, Cambridge Univeristy Press (1997)
- [6] Surya P. Tewari and G. S. Agarwal, *Phys. Rev. Lett.* 56, 1811 (1986); Surya P. Tewari and G. S. Agarwal, *Phys. Rev. Lett.* 66, 1797 1991; G. S. Agarwal and Surya P. Tewari, *Phys. Rev. Lett.* 70, 1417 (1993)
- [7] G. Z. Zhang, D. W. Tokaryk, B. P. Stoicheff and K. Hakuta, *Phys. Rev. A* 56, 813 (1997)
- [8] S. E. Harris, J. E. Field and A. Imamoglu, *Phys. Rev.* 1, 64, 1107 (1990)
- [9] M. Fleischhauer, C. H. Keitel, M. O. Scully, C. Su, B. T. Ulrich, and S-Y. Zhu, *Phys. Rev. A***46**, 1468 (1992)
- [10] M. Jain, A. J. Merrin, A. Kasapi, G. V. Yin and S. E. Harris, *Phys. Rev. Lett.* 75, 4385 (1995)
- [11] Richard R. Mosley, Sara Shepherd, David J. Fulton, Bruce D. Sinclair and Malcom S. Dunn, *Phys. Rev. Lett.* 74, 670 (1995)
- [12] G. Z. Zhang, K. Hakuta and B. P. Stoicheff, *Phys. Rev. Lett.* 71 3099 (1993)
- [13] H. Schmidt and A. Imamoglu. *Opt. Lett.* 21, 1936 (1996)

- [14] P. R. Hemmer, D. P. Katz, J. Donghue, M. Cronin - Golomb, M. S. Shahriar and P. Kumar, Opt. Lett., 20, 982 (1995)
- [15] A. Kasapi, Phys. Rev. Lett. **77**, 1035 (1996)
- [16] E. Arimondo, "*Laser Manipulation of Atoms and Ions*", *Proceedings of School of Physics - Enrico Fermi*, ed:- E. Arimondo, W. D. Phillips and F. Strumia, North Holland (Pisa) 1992, pp 191 and references therein
- [17] A. Hemmerich, M. Weidemüller, T. Esslinger, C. Zimmermann and T. Hänsch, Phys. Rev. Lett. 75, 37 (1995)
- [18] B. R. Mollow, Phys. Rev. **188** 1969)
- [19] B. R. Mollow, Phys. Rev. bf A 5, 2217 (1972)
- [20] For recent work and other references see Z. Ficek and H. S. Freedhoff, Phys. Rev. A 53, 4275 (1996)
- [21] P. Zhou and S. Swain, Phys. Rev. Lett. **78**, 832, (1997)
- [22] J. Gao, C. Guo, X. Guo, G. Jin, P. Wang, J. Zho, H. Zhang, Y. Jiang, D. Waig, D. Jiang, Opt. Comm. **93**, 323 (1992)
- [23] M. O. Scully and M. S. Zubairy, Phys. Rev. A 35, 752 (1987)
- [24] B. Lü, W. H. Burkett and M. Xiao, Phys. Rev. a 56, 976 (1997)
- [25] J. A. Bergou, P. Bogár, Phys. Rev. A **43**, 4889 (1991)
- [26] D. J. Fulton, S. Shepherd, R. R. Moseley, B. D. Sinclair and M. H. Dunn, Phys. Rev., A 52, 2302 (1995)
- [27] Y-q Li and M. Xiao, Phys. Rev. A 51, 4959 (1995) and references therein.
- [28] P. T. H. Fisk, H. -A. Bachor and R. J. Sandeman Phys. Rev A **33** 2418 (1986); *ibid* 2424; *ibid* A **34** 4762 (1986)
- [29] U. Fano, Phys. Rev. **124**, 1866 (1961)
- [30] S. E. Harris, Phys. Rev. Lett. **62**, 1033(1989); A. Imamoğlu Phys. Rev. A 40, 2835 (1989); A. Imamoğlu, S. E. Harris, Opt. Lett **14**, 134, (1989); J. E. Field, K. H. Hahn & S. E. Harris, Phys. Rev. Lett. **67**, 3062 (1992)
- [31] C. Cohen-Tannoudji and S. Reynaud, J. Phys. B 10 345, (1976)
- [32] G. Alzetta, A. Gozzini, L. Moi and G. Orriols Nu.Cm **36B**, 5 (1976)

- [33] G. Orriols, Lett. Nu. Cm, **53B**, 1 (1978)
- [34] H. R. Gray, R. M. Whitely and C. R. Stroud Jr., Opt. Lett. 3, 218 (1978); R. M. Whitely and C. R. Stroud Jr., Phys. Rev. A 14, 1498 (1976)
- [35] S. Swain, J. Phys. B 10, 3405 (1982)
- [36] E. Arimondo, *Fundamentals of Quantum Optics III*, Lecture Notes in Physics, **Vol. 420**, Ed:- F. Ehlotzky, Springer Verlag, Heidelberg, 1993. pp 170;
- [37] Y. G. Arkhipin, Yu. I. Heller, Phys. Lett. A 98, 12 (1983)
- [38] E.Fry, X.Li, D.Nikonov, G.G.Padmabandu, M.O.Scully, A.V. Smith, F.K.Tittel, C.Wong, S.R.Wilkinson and S.Y.Zhu, Phys.Rev. Lett. 70, 3235 (1993)
- [39] S-Y. Zhu & M. O. Scully, Phys. Lett. A **201**, 85 (1995)
- [40] S. -Y. Zhu, M. O. Scully, Phys. Rev. Lett. 76, 385 (1996); H. Lee, P. Polykin, M. O. Scully and S. -Y. Zhu, Phys. Rev. A **55**, 4454 (1997)
- [41] G. S. Agarwal, Phys. Rev. A **54**, 3734 (1996)
- [42] H. -R. Xia, C. -Y. Ye, S. -Y. Zhu, Phys. Rev. Lett. 77, 1032 (1996)
- [43] L. M. Narducci, M. O. Scully, G. -L. Oppo, P. Ru and J. R. Tredicce, Phys. Rev. A **42**, 1630 (1990)
- [44] M. O. Scully and M. Fleischhauer, Phys. Rev. Lett. , 69, 1360 (1992)
- [45] T. Hänsch and P. Toscheck, Z. Physik, **236**, 213 (1970)
- [46] S.P.Tewari & V.S.Ashoka, Proceedings of Workshop on Advanced Laser Spectroscopy, Indian Instt. of Technology, Kanpur, ed. H.D.Bist et. al., Allied Publishers, New Delhi, pp 213, (1996)

Chapter II

Y and Gate schemes: Semiclassical study

*Detailed study of two model configurations, viz., **Y** and **Gate** are presented in this chapter. These two configurations are individually analysed in semiclassical picture using density matrix formalism. Numerical solutions are studied and analytical solutions are obtained to first order in probe amplitude and to all orders in the pump using linear response theory. Analytical solutions are shown to agree with the numerical solutions obtained to all orders of probe amplitude. It is seen that the **Y** system can be made completely transparent while there is only a reduction to a final residual absorption in the **Gate** system. Use of these effects to measure the dipole matrix elements of excited states is suggested.*

2.1 The Y Configuration

The **Y** configuration is shown in the fig. 2.1. A weak probe beam, of small amplitude, denoted by $E_s = \mathcal{E}_s^0 \exp(i \omega_s t) + c.c.$, connects transition between levels $|1\rangle$ and $|2\rangle$. The strong pump beam (E_p) is polarized perpendicular to the polarization of E_s beam. The subscript s in E_s refers to the smallness of the amplitude and the subscript p in E_p refers to the pump. The E_p may be considered as a **sum** of two circularly polarized lights denoted by $E_p^\pm = \mathcal{E}_p^\pm \exp(i \omega_p t) + c.c.$, which connects $|2\rangle \leftrightarrow |3\rangle$ and $|2\rangle \leftrightarrow |4\rangle$ transitions respectively. \mathcal{E}_p^+ and \mathcal{E}_p^- denote the slowly varying amplitudes of the beams of two different circular polarizations needed to connect the two different transitions

characterized for example by angular momentum selection rule $\Delta m_F = \pm 1$. It is assumed that the field E_p is too far detuned to interact with $|1\rangle \leftrightarrow |2\rangle$ and the field E_s is far detuned from $|4\rangle \leftrightarrow |2\rangle \leftrightarrow |3\rangle$ transitions.

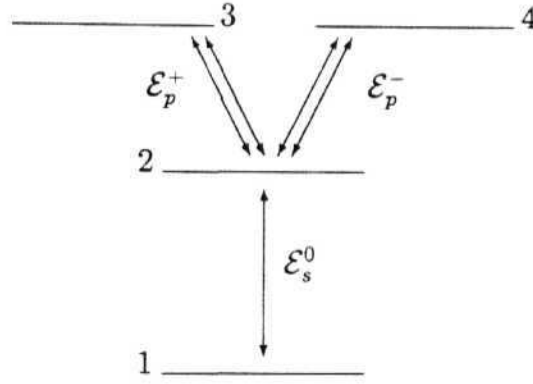


Fig. 2.1

Although levels $|3\rangle$, $|2\rangle$ and $|4\rangle$ form a V configuration which has been extensively studied in past [1, 2, 3], study of Y is more than just an extension of earlier studies as shall become clear shortly. Note that earlier studies of V configuration involved a pump and a probe beam together forming a V configuration. In the present configuration, the probe beam lies outside the V system, which is formed by two pump beams of different polarizations. The V shaped configuration is formed only among excited states, whereas all the population is assumed to be settled in the ground state $|1\rangle$ to begin with. Therefore, the probe absorption behaviour of Y system will be different from that of the V system. We will show that it is more like that of Ξ system.

Let the Hamiltonian of the system be written as

$$\mathcal{H} = \begin{pmatrix} \omega_1 & -d_{21} \cdot E_s & 0 & 0 \\ -d_{21} \cdot E_s & \omega_2 & -d_{32} \cdot E_p & -d_{42} \cdot E_p \\ 0 & -d_{32} \cdot E_p & \omega_3 & 0 \\ 0 & -d_{42} \cdot E_p & 0 & \omega_4 \end{pmatrix} \quad (2.1)$$

Where, d_{ij} is the the dipole moment of the transition between i and j and ω_i is the energy eigenvalue of the i th level in radian frequency. \hbar is taken to be 1.

The density matrix ρ is formed by

$$\rho = \begin{pmatrix} \rho_{11} & \rho_{12} & \rho_{13} & \rho_{14} \\ \rho_{21} & \rho_{22} & \rho_{23} & \rho_{24} \\ \rho_{31} & \rho_{32} & \rho_{33} & \rho_{34} \\ \rho_{41} & \rho_{42} & \rho_{43} & \rho_{44} \end{pmatrix}$$

The Liouville equation which governs the dynamics of this system is obtained in the Born Markov approximation to be [4]

$$\partial_t \rho = -i [\mathcal{H}, \rho] - \mathcal{L} \rho. \quad (2.2a)$$

The Liouville operator $\mathcal{L} \rho$ denotes the matrix containing the decay terms, which is given by

$$[\mathcal{L} \rho]_{lm} = -\delta_{lm} \sum_{k \neq l} 2\gamma_{lk} \rho_{kk} + \left(\sum_{k \neq l} \gamma_{kl} + \sum_{k \neq m} \gamma_{km} \right) \rho_{lm}. \quad (2.2b)$$

Here, γ_{ij} is the decay rate of coherence ρ_{ij} and $2\gamma_{ii} = \Gamma_{ii}$ is the decay of the population from level $|i\rangle$.

On using (i) the transformations

$$\begin{aligned}
\rho_{12} &= \bar{\rho}_{12} \exp(i\omega_s t), \\
\rho_{23} &= \bar{\rho}_{23} \exp(i\omega_p t), \quad \rho_{24} = \bar{\rho}_{24} \exp(i\omega_p t), \\
\rho_{13} &= \bar{\rho}_{13} \exp(i(\omega_s + \omega_p)t), \quad \rho_{14} = \bar{\rho}_{14} \exp(i(\omega_s + \omega_p)t) \\
\rho_{ii} &= \bar{\rho}_{ii}, \text{ for } i = 1, 2, 3, 4 \\
\rho_{nm} &= \rho_{mn}^*, (m \neq n); (m, n = 1, 2, 3, 4)
\end{aligned}$$

in the Liouville equation (2.2) and (ii) the rotating wave approximation which implies neglecting the fast oscillating terms, one gets

$$\begin{aligned}
\partial_t \bar{\rho}_{11} &= \Gamma_{22} \bar{\rho}_{22} - i d_{21} \mathcal{E}_s^- \bar{\rho}_{12} + i d_{21}^* \mathcal{E}_s^{+*} \bar{\rho}_{21} \\
\partial_t \bar{\rho}_{12} &= (i \Delta_s - \gamma_{12}) \bar{\rho}_{12} - i d_{21}^* \mathcal{E}_s^{+*} (\bar{\rho}_{11} - \bar{\rho}_{22}) - i d_{32} \mathcal{E}_p^+ \bar{\rho}_{13} - i d_{42} \mathcal{E}_p^- \bar{\rho}_{14} \\
\partial_t \bar{\rho}_{13} &= [i (\Delta_s + \Delta_p) - (\gamma_{23} + \gamma_{43})] \bar{\rho}_{13} + i d_{21}^* \mathcal{E}_s^{+*} \bar{\rho}_{23} - i d_{32}^* \mathcal{E}_p^{+*} \bar{\rho}_{12} \\
\partial_t \bar{\rho}_{14} &= [i (\Delta_s + \Delta_p) - (\gamma_{24} + \gamma_{34})] \bar{\rho}_{14} + i d_{21}^* \mathcal{E}_s^{+*} \bar{\rho}_{24} - i d_{42}^* \mathcal{E}_p^{+*} \bar{\rho}_{12} \\
\partial_t \bar{\rho}_{22} &= -\Gamma_{22} \bar{\rho}_{22} + 2\gamma_{23} \bar{\rho}_{33} + 2\gamma_{24} \bar{\rho}_{44} + i d_{21} \mathcal{E}_s^- \bar{\rho}_{12} - i d_{21}^* \mathcal{E}_s^{+*} \bar{\rho}_{21} - i d_{32} \mathcal{E}_p^+ \bar{\rho}_{23} \\
&\quad + i d_{32}^* \mathcal{E}_p^{+*} \bar{\rho}_{32} - i d_{42} \mathcal{E}_p^- \bar{\rho}_{24} + i d_{42}^* \mathcal{E}_p^{+*} \bar{\rho}_{42} \\
\partial_t \bar{\rho}_{23} &= [i \Delta_p - (\gamma_{12} + \gamma_{23} + \gamma_{43})] \bar{\rho}_{23} + i d_{21} \mathcal{E}_s^- \bar{\rho}_{13} - i d_{32}^* \mathcal{E}_p^{+*} (\bar{\rho}_{22} - \bar{\rho}_{33}) + i d_{42}^* \mathcal{E}_p^{+*} \bar{\rho}_{43} \\
\partial_t \bar{\rho}_{24} &= [i \Delta_p - (\gamma_{12} + \gamma_{24} + \gamma_{34})] \bar{\rho}_{24} + i d_{21} \mathcal{E}_s^- \bar{\rho}_{14} - i d_{42}^* \mathcal{E}_p^{+*} (\bar{\rho}_{22} - \bar{\rho}_{44}) + i d_{32}^* \mathcal{E}_p^{+*} \bar{\rho}_{34} \\
\partial_t \bar{\rho}_{33} &= -(\Gamma_{33} + \Gamma_{34}) \bar{\rho}_{33} + \Gamma_{43} \bar{\rho}_{44} + i d_{32} \mathcal{E}_p^+ \bar{\rho}_{23} - i d_{32}^* \mathcal{E}_p^{+*} \bar{\rho}_{32} \\
\partial_t \bar{\rho}_{34} &= [i \Delta_{34} - (\gamma_{23} + \gamma_{24} + \gamma_{34} + \gamma_{43})] \bar{\rho}_{34} + i d_{32} \mathcal{E}_p^+ \bar{\rho}_{24} - i d_{42}^* \mathcal{E}_p^{+*} \bar{\rho}_{32} \\
\partial_t \bar{\rho}_{44} &= -(\Gamma_{44} + \Gamma_{34}) \bar{\rho}_{44} + \Gamma_{43} \bar{\rho}_{33} + i d_{42} \mathcal{E}_p^- \bar{\rho}_{24} - i d_{42}^* \mathcal{E}_p^{+*} \bar{\rho}_{42}
\end{aligned} \tag{2.3}$$

and

$$\bar{\rho}_{ji} = \bar{\rho}_{ij}^*,$$

Where

$$\Delta_s = \omega_{21} - \omega_s,$$

$$\begin{aligned}
\Delta_p &= \omega_{32} - \omega_p = \omega_{42} - \omega_p, \\
\Delta_{34} &= \omega_3 - \omega_4, \\
\omega_{mn} &= \omega_m - \omega_n.
\end{aligned}$$

Absorption of the probe laser is related to imaginary part of $\bar{\rho}_{21}$ (1.2). Equation for ρ_{12} in (2.3) and $\rho_{21} = \rho_{12}^*$ show that the evolution of $\bar{\rho}_{21}$ is governed by three factors, viz., the population difference $\bar{\rho}_{11} - \bar{\rho}_{22}$ and the two coherences $\bar{\rho}_{31}$ **and** $\bar{\rho}_{41}$. The two coherence terms are, in turn, coupled to the coherence terms $\bar{\rho}_{32}$ **and** $\bar{\rho}_{42}$ respectively, by the pump field. Therefore, a strong pump beam will obviously create a strong $\bar{\rho}_{32}$ ($\bar{\rho}_{42}$) and hence a $\bar{\rho}_{31}$ ($\bar{\rho}_{41}$) with a value high enough to overcome the effect of $\bar{\rho}_{22} - \bar{\rho}_{11}$. At steady state, when the time derivatives on LHS are zero, the probe absorption is governed by the steady state values of these factors as

$$\bar{\rho}_{21}^{ss} = \frac{id_s \mathcal{E}_s^0 (\bar{\rho}_{11}^{ss} - \bar{\rho}_{22}^{ss})}{i\Delta_s + \gamma_{21}} + \frac{id_{32}^* \mathcal{E}_p^- \bar{\rho}_{31}^{ss}}{i\Delta_s + \gamma_{21}} + \frac{id_{42}^* \mathcal{E}_p^+ \bar{\rho}_{41}^{ss}}{i\Delta_s + \gamma_{21}}. \quad (2.4)$$

Different terms of (2.4) shall be analyzed extensively in steady state below. The steady state solution for $\bar{\rho}$ is obtained in the following manner. Assuming that the **Y** is a closed configuration, closure condition $\sum_i \bar{\rho}_{ii} = 1$ is used to substitute $\bar{\rho}_{11} = 1 - (\bar{\rho}_{22} + \bar{\rho}_{33} + \bar{\rho}_{44})$ in equation (2.3). Then the set of equations can be rewritten in matrix form,

$$\partial_t \psi = M \cdot \psi + \phi \quad (2.5a)$$

where, ψ is the column matrix

$$(\bar{\rho}_{12} \ \bar{\rho}_{13} \ \bar{\rho}_{14} \ \bar{\rho}_{21} \ \bar{\rho}_{22} \ \bar{\rho}_{23} \ \bar{\rho}_{24} \ \bar{\rho}_{31} \ \bar{\rho}_{32} \ \bar{\rho}_{33} \ \bar{\rho}_{34} \ \bar{\rho}_{41} \ \bar{\rho}_{42} \ \bar{\rho}_{43} \ \bar{\rho}_{44}).$$

ϕ is another column vector containing terms independent of $\bar{\rho}$. Explicit form of M and ϕ are given in Appendix A.

The steady state solution of equation (2.5 a), and hence of (2.3) is

$$\psi = -M^{-1} \cdot \phi \quad (2.5b)$$

where M^{-1} denotes the inverse of matrix M . A spectrum of probe absorption is obtained numerically from $\text{Im}\rho_{21}$ by scanning the detuning Δ_s , which is equivalent to scanning the probe frequency. For such a computation, all frequency parameters are scaled to the coherence decay rate γ_{12} of $\bar{\rho}_{21}$. For the decay rates of upper transition, a typical ratio of $\gamma_{23} = \gamma_{24} = 0.25$ is assumed. For a ‘Strong’ beam, $\Omega_{s,p} = 6.0$ is used and for a ‘Weak’ beam, a value of $\Omega_{s,p} = 0.2$ and $\gamma_{34} = 0$ is used. Here, $\Omega_{s,p}$ are the Rabi frequencies such that $\Omega_s = d_{21}\mathcal{E}_s^0$ and $\Omega_p = |d_{32}\mathcal{E}_p^{-*}| = |d_{42}\mathcal{E}_p^{+*}|$. Imaginary part of $\bar{\rho}_{21}$ gives the absorption of the weak field E_s and the absorption of the pump field Ω_p is given by $\text{Im}(\bar{\rho}_{32} + \bar{\rho}_{42})$.

At first, both pump and probe beam are taken to be weak, with the Rabi frequencies $\Omega_p = \Omega_s = 0.2$. The pump is resonant and the probe frequency is scanned. We first describe all the figures and then summarize the observations on their basis. Figure 2.2a shows the result of probe absorption for such a condition. A dip at zero detuning is evident in Figure 2.2a. With reference to (2.4) note that since the pump beam is weak, the coherences $\bar{\rho}_{31}$ and $\bar{\rho}_{41}$ are not large enough to compete with the contribution of the term $\bar{\rho}_{11} - \bar{\rho}_{22}$ (see 2.4). But there is a contribution from the $\bar{\rho}_{31}$ and $\bar{\rho}_{41}$ terms for small detuning region, which results in the dip at the center of the absorption profile. The corresponding behaviour of populations are shown in Figures 2.2 (b),(c). Figure 2.2 (b) shows population of ground level $|1\rangle$ and Figure 2.2 (c) shows the population of

excited states: that of $|2\rangle$ is represented by the solid line and those of $|3\rangle$ and $|4\rangle$ are represented by the dashed line. Figure 2.2 (d) shows the contribution from two factors which make up $\bar{\rho}_{21}$. The solid line shows the factor $A = \text{Im}[(\bar{\rho}_{11}^- - \bar{\rho}_{22})/(\Delta_s - i\gamma_{21})]$, and the dashed line shows factor $B = \text{Im}[(\bar{\rho}_{31}^- + \bar{\rho}_{41})/(\Delta_s - i\gamma_{21})]$. From equation (2.4), these two add up to give $\text{Im}(\bar{\rho}_{21})$. These two are of opposite signs in $\Delta_s \approx 0$ range. This shows the origin of the small dip of probe absorption at zero detuning at Figure 2.2 (a). The population values from Figure 2.2 (b) and (c) show that during the dip in probe absorption, the population is depleted in level $|1\rangle$ while the populations of level $|3\rangle$ and $|4\rangle$ increase, showing that there is a direct population transfer from ground state to these two upper levels.

Figure 2.2 d which presents an explanation of the dip in Figure 2.2 a is further elaborated in Figures 2.2 e and 2.2 f. In Figure 2.2 e are plotted separately the functions BR and BL where

$$\begin{aligned} B &= BR + BL \\ BR &= \frac{\Delta_s}{\Delta_s^2 + \gamma_{21}^2} \text{Im} [d_{32}\mathcal{E}_p^- \rho_{31} + d_{42}\mathcal{E}_p^+ \rho_{41}] \\ BL &= \frac{\gamma_{21}}{\Delta_s^2 + \gamma_{21}^2} \text{Re} [d_{32}\mathcal{E}_p^- \rho_{31} + d_{42}\mathcal{E}_p^+ \rho_{41}] \end{aligned}$$

The insets in the Figure 2.2 e show the skew symmetric behaviour of $\text{Im}[d_{32}\mathcal{E}_p^- \rho_{31} + d_{42}\mathcal{E}_p^+ \rho_{41}]$ and the symmetric behaviour of $\text{Re}[d_{32}\mathcal{E}_p^- \rho_{31} + d_{42}\mathcal{E}_p^+ \rho_{41}]$. Multiplication of these respectively with the skew symmetric dispersion curve $\Delta_s/(\gamma_s^2 + \Delta_s^2)$ and the Lorentzian $\gamma_s/(\gamma_s^2 + \Delta_s^2)$ produces the curves BR and BL shown in Figure 2.2 e. Since the major part of cancellation is brought out by A+BL which contain the Lorentzian $\gamma_{21}/(\Delta^2 + \gamma_{21}^2)$ as common factor, we take the coefficient in A+BL merely

$$d.\mathcal{E}_s^0(\rho_{11} - \rho_{22}) + \text{Re}(d_{32}\mathcal{E}_p^- \rho_{31} + d_{42}\mathcal{E}_p^+ \rho_{41})$$

as characterizing the magnitude of residual absorption at $\Delta_s = 0$. Figure 2.2 f shows its behaviour in the domain of the dip $\Delta_s = 0$.

We may summarize the characteristics of the system for weak probe and weak pump beams, shown in Figure 2.2 as follows.

- (α) Probe absorption shows Lorentzian peak with peculiar dip in absorption at line center.
- (β) Population of level |1) is depleted along with the probe absorption but does not show any reduction in its depletion at the line center.
- (7) Population of level |2) on the other hand follows the probe absorption along the broad Lorentzian peak as well as the peculiar dip at the line center.
- (8) Population in level |3) and |4) do not follow the probe absorption along its broad Lorentzian but show a narrow Lorentzian peak in concurrence with the dip in probe absorption, and with the dip in the population of level |2) at the center.
- (η) The minimum of the dip in probe absorption occurs at $\Delta_s = 0$. It is controlled by the value of condition $d_{21} \cdot \mathcal{E}_s^0 (\rho_{11} - \rho_{22}) + d_{32} \cdot \mathcal{E}_{32} \text{Re} [\rho_{31}] + d_{42} \cdot \mathcal{E}_{42} \text{Re} [\rho_{41}]$ at $\Delta_s = 0$ as shown in Figure 2.2 f.

We consider next a case when the pump beam is strong and resonant. The probe absorption then shows a different behaviour. Figure 2.3 (a) shows the probe absorption, for a pump value of $\Omega_p = 6.0$ and a probe beam value of $\Omega_s = 0.2$. There is a marked transparency window between the two absorption side bands. These side bands

correspond to the Rabi frequency of the pump beam transitions and are placed at $\Delta_s = \pm\sqrt{|\Omega_{32}|^2 + \Omega_{42}|^2}$. Figure 2.3 (b) shows the population of level $|1\rangle$ for these conditions and the corresponding populations of levels $|2\rangle$ and levels $|3\rangle$ and $|4\rangle$ are shown in Figure 2.3 (c) by a solid line and a dashed line respectively. It can be seen that with the exception of side bands, the population is settled in level $|1\rangle$ for all other detunings. The coherence terms corresponding to this case are plotted in Figure 2.3 (d), where the solid line represents the factor $A = \text{Im} [(d_{21} \cdot \mathcal{E}_s^0 (\bar{\rho}_{11} - \bar{\rho}_{22}) / (-i\Delta_s - \gamma_{21}))]$ and the dashed line represents $B = \text{Im} [(d_{32} \cdot \mathcal{E}_p^* \bar{\rho}_{31} + d_{42} \cdot \mathcal{E}_p^* \bar{\rho}_{41}) / (-i\Delta_s - \gamma_{21})]$. The complete cancellation of normal absorption by the coherent terms $\bar{\rho}_{31}$ and $\bar{\rho}_{41}$ is evident at $\Delta_s = 0$ neighbourhood.

It is very interesting to discuss the Figure 2.3 (d) further. The plot of term A reflects only a single Lorentzian at the line center. This is surprising because we know from Figure 2.3 b and Figure 2.3 c that $\rho_{11} - \rho_{22}$ does show Rabi side bands. The features of the sidebands due to $\rho_{11} - \rho_{22}$ in A is however suppressed because of multiplication by the tail of the Lorentzian function $\gamma_{21} / (\Delta_s^2 + \gamma_{21}^2)$, which is involved in A. It is further surprising to note that the Lorentzian implied by A is ultimately missing from Figure 2.3 a. This implies that the term B must behave in such a way that the Lorentzian of A is totally annulled and Rabi side bands show up. Both these features are there, then, due to the build up of coherences $\bar{\rho}_{31}$ and $\bar{\rho}_{41}$. The two features required, are indeed seen in B, by isolating them as the terms BR and BL. BR contains the part which develops the two Rabi side bands and BL contains that part which cancels the Lorentzian from A in the neighbourhood of the line center $\Delta_s \approx 0$. The two insets in Figures 2.3 e show $\text{Im} [d_{32}^* \mathcal{E}_p^- \bar{\rho}_{31} + d_{42}^* \mathcal{E}_p^+ \bar{\rho}_{41}]$ and $\text{Re} [d_{32}^* \mathcal{E}_p^- \bar{\rho}_{31} + d_{42}^* \mathcal{E}_p^+ \bar{\rho}_{41}]$ separately. The $\text{Im} [d_{32}^* \mathcal{E}_p^- \bar{\rho}_{31} + d_{42}^* \mathcal{E}_p^+ \bar{\rho}_{41}]$ shows flipped Lorentzian which on multiplication with skew symmetric dispersion function $\Delta_s / (\gamma_{21}^2 + \Delta_s^2)$ shows in BR the symmetric Rabi side

bands for resonant pump case. It also shows a broad inverted Lorentzian centered at $\Delta_s = 0$. $\text{Re}[d_{32}^* \mathcal{E}_p^- \bar{\rho}_{31} + d_{42}^* \mathcal{E}_p^+ \bar{\rho}_{41}]$ when multiplied by the symmetric function shows in BL the negative Lorentzian dominant when $\Delta_s \approx 0$. From this discussion the behaviour at $\Delta_s \approx 0$ can be characterized by

$$d\mathcal{E}_s^0(\rho_{11} - \rho_{22}) + \text{Re}[d_{32}^* \mathcal{E}_p^- \bar{\rho}_{31}^{(ss)} + d_{42}^* \mathcal{E}_p^+ \rho_{41}] \approx 0;$$

and in the neighbourhood of Rabi side bands one notes the domination of BR term. Particularly interesting in this regard is the observation that the final Lorentzian looking shape of the Rabi side bands are not truly Lorentzian about their own center. The inner portion, towards the transparency window, is made up of the difference between a Lorentzian and dispersion curves, while the outer sides of the Rabi side bands are composed of a sum of a Lorentzian and a dispersion (local) curve. (BR + BL behaviour)

To summarize the differences in the characteristics of the system created by going to strong pump case we note:

(SP α) The probe absorption develops three distinct regions

(a) two Lorentzian peaks separated by the Rabi frequency of the three level-V- system as shall be shown in Chapter III.

(b) the line center continues to show little absorption, though some changes occur as required by the modification of the dip by the development of large Rabi frequency sidebands. Thus the small dip in weak pump case has now fully developed into a broad transmission window.

(SP β) Population of level |1) continues to show depletion whenever probe absorption is large as for example at the two Rabi side bands. The broad transparency window

now is accompanied by very little depletion in ρ_{11} . This is very much in contrast to what was happening in weak pump case. There was little indication through the behaviour of $\bar{\rho}_{11}$ of the reduction in absorption at the line center.

- (SP7) Population of level $|2\rangle$ continues to reflect probe absorption feature in that it is large at Rabi side bands and nearly zero at line center inside the transparency window.
- (SP δ) Population of level $|3\rangle$ and $|4\rangle$ now do follow the probe absorption peak at the Rabi side bands as well as reduced values through transparency window. However the values are finite through transparency window and as well as at line center—that is they are not zero.

(SP η) The minimum of the dip in probe absorption at $\Delta_s = 0$ is characterized by

$$d_{21} \cdot \mathcal{E}_s^0 (\bar{\rho}_{11} - P_{22}) + (d_{23} \mathcal{E}_p^{-*} \bar{\rho}_{31} + d_{24} \mathcal{E}_p^{+*} \bar{\rho}_{41}) \approx 0$$

Let us recall that these peculiar behaviour are similar to a simple ladder like configuration which may be obtained from the Y system by simply putting say $d_{42} = 0$. Analysis of a ladder in terms of A, BR and BL has however not appeared in print before. The Y system has distinctly different behaviour because of possible coherence among $|3\rangle$ and $|4\rangle$ levels which can be fairly high for $\gamma_{34} \neq 0$ situation considered so far. We now consider a case where $\gamma_{34} = 1.0$ implying a large collision relaxation between levels $|3\rangle$ and $|4\rangle$. In the weak field case shown in Figure 2.2g and 2.2 h we see that the dip phenomenon vanishes, although some change does occur. For the case of strong pump, there are two effects (a) the peak heights of Rabi side bands is reduced (b) the absorption at $\Delta_s = 0$ is increased, i.e., the transparency is reduced. The analytical results obtained in next section are valid for $\gamma_{34} \neq 0$ as well as for $\Delta_p \neq 0$.

2.1.1 Analytical Solution for Y system

For the case of strong Ω_p (pump) and weak Ω_s (probe), an approximate analytical solution is obtained in the first order of probe intensity, using linear response theory and all orders of the pump field. Then, the coherences ρ_{23} and ρ_{24} and population ρ_{22} get significant values only in the second order in probe amplitude. Thus, for a weak probe, the zeroth order terms in probe can be assumed to be zero. i.e.,

$$\bar{\rho}_{23}^{(0)} = 0 = \bar{\rho}_{24}^{(0)} = \bar{\rho}_{34}^{(0)}$$

$$\bar{\rho}_{22}^{(0)} = 0 = \bar{\rho}_{33}^{(0)} = \bar{\rho}_{44}^{(0)}$$

Such an assumption is valid because a weak probe will not generate a significant ρ_{22} and hence ρ_{23} and ρ_{24} will be negligible. For other cases, such assumptions are invalid.

From equation (2.3), the relevant equations, upto the first order in probe amplitude are

$$i \partial_t \bar{\rho}_{21}^{(1)} = (-\Delta_s + i \gamma_{12}) \bar{\rho}_{21}^{(1)} + d_{21} \mathcal{E}_s^0 \bar{\rho}_{11}^{(0)} + d_{32}^* \mathcal{E}_p^+ \bar{\rho}_{31}^{(1)} + d_{42}^* \mathcal{E}_p^- \bar{\rho}_{41}^{(1)} \quad (2.6)$$

$$i \partial_t \bar{\rho}_{31}^{(1)} = [-(\Delta_s + \Delta_p) + i (\gamma_{23} + \gamma_{43})] \bar{\rho}_{31}^{(1)} + d_{32} \mathcal{E}_p^+ \bar{\rho}_{21}^{(1)} \quad (2.7)$$

$$i \partial_t \bar{\rho}_{41}^{(1)} = [-(\Delta_s + \Delta_p) + i (\gamma_{24} + \gamma_{34})] \bar{\rho}_{41}^{(1)} + d_{42} \mathcal{E}_p^- \bar{\rho}_{21}^{(1)} \quad (2.8)$$

Steady state solutions for (2.7) and (2.8) are

$$\bar{\rho}_{31}^{(1)} = \frac{d_{32} \mathcal{E}_p^+ \bar{\rho}_{21}^{(1)}}{(\Delta_s + \Delta_p) - i(\gamma_{23} + \gamma_{43})}$$

$$\bar{\rho}_{41}^{(1)} = \frac{d_{42} \mathcal{E}_p^- \bar{\rho}_{21}^{(1)}}{(\Delta_s + \Delta_p) - i(\gamma_{24} + \gamma_{34})}$$

By substituting in equation (2.6), the steady state solution for $\bar{\rho}_{21}^{(1)}$ is obtained as

$$\bar{\rho}_{21}^{(1)} = \frac{-d_{21}\mathcal{E}_s^0\bar{\rho}_{11}^{(0)}}{[-\Delta_s + i\gamma_{12} + F_{32} + F_{42}]} \quad (2.9)$$

where,

$$F_{32} = \frac{|d_{32}\mathcal{E}_p^+|^2}{(\Delta_s + \Delta_p) - i(\gamma_{23} + \gamma_{43})}$$

and

$$F_{42} = \frac{|d_{42}\mathcal{E}_p^-|^2}{(\Delta_s + \Delta_p) - i(\gamma_{24} + \gamma_{43})}$$

For small values of probe field (\mathcal{E}_s), this solution shows an excellent agreement with the numerical solution obtained to all orders using equation (2.5 b), validating the approximation. Figure 2.4 shows a comparison of the analytical solution (symbols) to the numerical result (solid line) showing that they agree well with each other. We may employ the condition of these analytical solutions to determine the oscillator strengths of levels lying in the excited states of atoms. This is described below.

2.1.2 Determination of f - values

In the classical picture of an atom as a dipole oscillator, the strength of emission or absorption of light from a single such oscillator is quantified by 'Oscillator strength' or the 'f-value'. The total light emitted or absorbed by a system of \mathcal{N} oscillators is then given by $\mathcal{N}f$. Comparing with the quantum picture of atom, f-value is found to be proportional to the Einstein A coefficient, which in turn is related to the dipole matrix element of the transition between two atomic levels [7] as

$$f_{ji} = \frac{2m\omega_{ji}}{3g_j} |\langle i|\mathbf{r}|j\rangle|^2 \quad (2.10)$$

The accurate measurement of f-value is important in the field of astrophysics and spectroscopy. **The** existing methods of measurements are based on **plasma** excitation

and require an accurate measurement of population in the excited states involved. Accurate knowledge of population in excited states is difficult to obtain. The analytical solutions of EIT helps to devise a method to experimentally determine the dipole matrix elements of excited states without pumping any population to the excited states.

Using AC Stark splitting for measurement of dipole matrix elements has been suggested earlier [8]. Accordingly, in an absorption profile obtained as a function of probe detuning, the distance between two absorption peaks is directly proportional to the Stark splitting of the energy levels, which is equal to 2Ω , where $\Omega = d \cdot E$. By using the analytical expression (2.9) to fit the set of experimental data over the entire detuning range, value of $|\Omega_{32}|^2 + |\Omega_{42}|^2$ can be determined to a better accuracy. Using these values in (2.10), the oscillator strengths for excited state transitions $\langle 2 | \vec{r} | 3 \rangle$ and $\langle 2 | \vec{r} | 4 \rangle$ can be determined.

Having discussed the numerical and analytical results for Y configuration we next consider the **Gate** configuration.

2.2 Gate configuration

This configuration is as shown in fig. 2.6. A single probe beam denoted by $E_s \propto \mathcal{E}_s^0 \exp(i \omega_s t) + c.c$ connects both $|5\rangle \leftrightarrow |7\rangle$ and $|6\rangle \leftrightarrow |8\rangle$ transitions. The strong beam $E_p \propto \mathcal{E}_p^0 \exp(i \omega_p t) + c.c$ connects the transition $|8\rangle \leftrightarrow |9\rangle$ and $|7\rangle \leftrightarrow |9\rangle$. Levels $|5\rangle$, $|6\rangle$ and $|7\rangle$, $|8\rangle$ are assumed degenerate for the sake of simplicity. The results are valid even otherwise, as long as the single probe laser and a single pump laser connects the transitions as described.

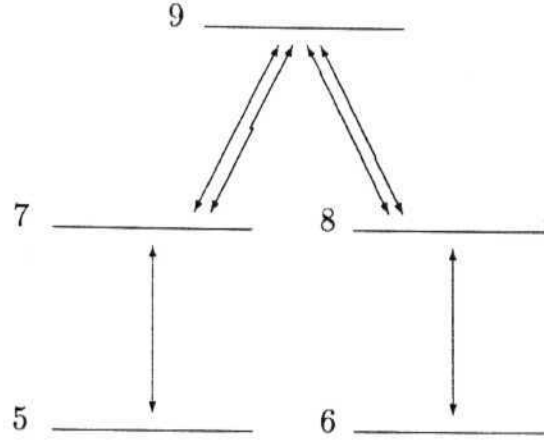


Fig. 2.6

In this case, levels $|7\rangle$, $|9\rangle$ and $|8\rangle$ form a Λ configuration involving the excited states. The probe beam connects levels of this Λ to two levels $|5\rangle$ and $|6\rangle$ outside the Λ . The population is assumed to be confined to levels $|5\rangle$ and $|6\rangle$ to begin with and not in $|7\rangle$ and $|8\rangle$. The pump and probe beam are of different polarizations. The pump is polarized in x-y plane, and probe is polarized along z- axis. So the angular momentum selection rule allows Λ configuration, and coupling of probe beam to transitions $|5\rangle \leftrightarrow |7\rangle$ and $|6\rangle \leftrightarrow |8\rangle$ which are of same azimuthal quantum number m . Note that the configuration is simultaneously probed by the two ground states $|5\rangle$ and $|6\rangle$. Therefore, the probe absorption behaviour is expected to be different from that of the Λ configuration which has been studied earlier [5, 9]. The Λ configurations are usually made of one weak and one strong transition. The Gate configuration can not be interpreted as two ladder (Ξ) configurations. Because the pump beam creates a coherence between the states $|7\rangle$ and $|8\rangle$ and such coherences for two connected ladders have not yet been studied. Therefore, this configuration requires further analysis.

Let the Hamiltonian for this configuration be

$$\mathcal{H} = \begin{pmatrix} \omega_5 & 0 & -d_{75}^* \cdot E_s^* & 0 & 0 \\ 0 & \omega_6 & 0 & -d_{86}^* \cdot E_s^* & 0 \\ -d_{75} \cdot E_s & 0 & \omega_7 & 0 & -d_{97}^* \cdot E_p^{*-} \\ 0 & -d_{86} \cdot E_s & 0 & \omega_8 & -d_{98}^* \cdot E_p^{*+} \\ 0 & 0 & -d_{97} \cdot E_p^- & -d_{98} \cdot E_p^+ & \omega_9 \end{pmatrix} \quad (2.11)$$

which acts on the density matrix

$$\rho = \begin{pmatrix} \rho_{55} & \rho_{56} & \rho_{57} & \rho_{58} & \rho_{59} \\ \rho_{65} & \rho_{66} & \rho_{67} & \rho_{68} & \rho_{69} \\ \rho_{75} & \rho_{76} & \rho_{77} & \rho_{78} & \rho_{79} \\ \rho_{85} & \rho_{86} & \rho_{87} & \rho_{88} & \rho_{89} \\ \rho_{95} & \rho_{96} & \rho_{97} & \rho_{98} & \rho_{99} \end{pmatrix}$$

ω_i denotes the energy eigenvalue in radian frequency, of level $|i\rangle$ and $d_{ij} = \langle i|d|j\rangle$ is the dipole matrix element of transition between levels $|i\rangle$ and $|j\rangle$, for $i, j = 5, 6, 7, 8, 9$. \hbar is taken to be 1.

The dynamics of the system is determined by the Liouville equation, which in Born Markov approximation is

$$\partial_t \rho = -i [H, \rho] - C\rho$$

The Liouville operator $C\rho$ denote the matrix containing damping mechanisms, which follow the master equation [4]

$$[\mathcal{L}\rho]_{lm} = -\delta_{lm} \sum_{k \neq l} 2\gamma_{lk} \rho_{kk} + \left(\sum_{k \neq l} \gamma_{kl} + \sum_{k \neq m} \gamma_{km} \right) \rho_{lm}; \quad l, m = 5, 6, 7, 8$$

γ_{ij} is the decay rate of coherence $\bar{\rho}_{ij}$.

On using (i) the transformations

$$\begin{aligned}\rho_{ij} &= \bar{\rho}_{ij} \exp(i\omega_s t) \quad \text{for } i = 5, 6 \text{ and } j = 7, 8 \\ \rho_{ij} &= \bar{\rho}_{ij} \exp(i\omega_p t) \quad \text{for } i = 7, 8 \text{ and } j = 9 \\ \rho_{ij} &= \bar{\rho}_{ij} \exp(i(\omega_s + \omega_p)t) \quad \text{for } i = 5, 6 \text{ and } j = 9\end{aligned}$$

and (ii) the rotating wave approximation as before, one gets,

$$\begin{aligned}\partial_t \bar{\rho}_{55} &= -2\gamma_{65}\bar{\rho}_{55} + 2\gamma_{57}\bar{\rho}_{77} + 2\gamma_{56}\bar{\rho}_{66} + i d_{75}^* \mathcal{E}_s^{0*} \bar{\rho}_{75} - i d_{75} \mathcal{E}_s^0 \bar{\rho}_{57} \\ \partial_t \bar{\rho}_{57} &= [i \Delta_{75} - (\gamma_{57} + \gamma_{65} + \gamma_{87})] \bar{\rho}_{57} + i d_{75}^* \mathcal{E}_s^{0*} (\bar{\rho}_{77} - \bar{\rho}_{55}) - i d_{97} \mathcal{E}_p^+ \bar{\rho}_{59} \\ \partial_t \bar{\rho}_{58} &= [i \Delta_{85} - (\gamma_{68} + \gamma_{65} + \gamma_{78})] \bar{\rho}_{58} + i d_{75}^* \mathcal{E}_s^{0*} \bar{\rho}_{78} - i d_{86}^* \mathcal{E}_s^{0*} \bar{\rho}_{56} \\ &\quad - i d_{98} \mathcal{E}_p^- \bar{\rho}_{59} \\ \partial_t \bar{\rho}_{59} &= [i (\Delta_{97} + (\Delta_{75}) - (\gamma_{79} + \gamma_{89} + \gamma_{65}))] \bar{\rho}_{59} + i d_{75}^* \mathcal{E}_s^{0*} \bar{\rho}_{79} \\ &\quad - i d_{97} \mathcal{E}_p^+ \bar{\rho}_{57} - i d_{98} \mathcal{E}_p^- \bar{\rho}_{58} \\ \partial_t \bar{\rho}_{65} &= (-i \Delta_{65} - (\gamma_{65} + \gamma_{65})) \bar{\rho}_{65} + i d_{86}^* \mathcal{E}_s^{0*} \bar{\rho}_{85} - i d_{75} \mathcal{E}_s^0 \bar{\rho}_{67} \\ \partial_t \bar{\rho}_{66} &= -2\gamma_{56}\bar{\rho}_{66} + 2\gamma_{68}\bar{\rho}_{88} + 2\gamma_{65}\bar{\rho}_{55} + i d_{86}^* \mathcal{E}_s^{0*} \bar{\rho}_{86} - i d_{86} \mathcal{E}_s^0 \bar{\rho}_{68} \\ \partial_t \bar{\rho}_{67} &= [i \Delta_{76} - (\gamma_{57} + \gamma_{56} + \gamma_{87})] \bar{\rho}_{67} + i d_{86}^* \mathcal{E}_s^{0*} \bar{\rho}_{87} - i d_{75} \mathcal{E}_s^0 \bar{\rho}_{65} \\ &\quad - i d_{97} \mathcal{E}_p^+ \bar{\rho}_{69} \\ \partial_t \bar{\rho}_{68} &= [i \Delta_{86} - (\gamma_{68} + \gamma_{56} + \gamma_{78})] \bar{\rho}_{68} + i d_{86}^* \mathcal{E}_s^{0*} (\bar{\rho}_{88} - \bar{\rho}_{66}) - i d_{98} \mathcal{E}_p^- \bar{\rho}_{69} \\ \partial_t \bar{\rho}_{69} &= [i (\Delta_{86} + \Delta_{98}) - (\gamma_{79} + \gamma_{89} + \gamma_{56})] \bar{\rho}_{69} + i d_{86}^* \mathcal{E}_s^{0*} \bar{\rho}_{89} \\ &\quad - i d_{97} \mathcal{E}_p^+ \bar{\rho}_{67} - i d_{98} \mathcal{E}_p^- \bar{\rho}_{68} \\ \partial_t \bar{\rho}_{77} &= 2\gamma_{79}\bar{\rho}_{99} + 2\gamma_{78}\bar{\rho}_{88} - (2\gamma_{57} + 2\gamma_{87})\bar{\rho}_{77} + i d_{75} \mathcal{E}_s^0 \bar{\rho}_{57} + i d_{97} \mathcal{E}_p^+ \bar{\rho}_{97} \\ &\quad - i d_{75}^* \mathcal{E}_s^{0*} \bar{\rho}_{75} - i d_{97} \mathcal{E}_p^- \bar{\rho}_{79} \\ \partial_t \bar{\rho}_{78} &= [i \Delta_{87} - (\gamma_{57} + \gamma_{68} + \gamma_{87} + \gamma_{78})] \bar{\rho}_{78} + i d_{75} \mathcal{E}_s^0 \bar{\rho}_{58} \\ &\quad + i d_{97} \mathcal{E}_p^+ \bar{\rho}_{98} - i d_{86}^* \mathcal{E}_s^{0*} \bar{\rho}_{76} - i d_{98} \mathcal{E}_p^- \bar{\rho}_{79} \\ \partial_t \bar{\rho}_{79} &= [i \Delta_{97} - (\gamma_{57} + \gamma_{79} + \gamma_{89} + \gamma_{87})] \bar{\rho}_{79} + i d_{75} \mathcal{E}_s^0 \bar{\rho}_{59}\end{aligned}$$

$$\begin{aligned}
& + i d_{97}^* \mathcal{E}_p^{-*} (\bar{\rho}_{99} - \bar{\rho}_{77}) - i d_{98}^* \mathcal{E}_p^{-*} \bar{\rho}_{78} \\
\partial_t \bar{\rho}_{88} & = 2\gamma_{89} \bar{\rho}_{99} + 2\gamma_{87} \bar{\rho}_{77} - 2(\gamma_{68} + \gamma_{78}) \bar{\rho}_{88} + i d_{86} \mathcal{E}_s^0 \bar{\rho}_{68} + i d_{98}^* \mathcal{E}_p^{-*} \bar{\rho}_{98} \\
& - i d_{86}^* \mathcal{E}_s^{0*} \bar{\rho}_{86} - i d_{98} \mathcal{E}_p^- \bar{\rho}_{89} \\
\partial_t \bar{\rho}_{89} & = [i \Delta_{98} - (\gamma_{58} + \gamma_{68} + \gamma_{79} + \gamma_{89} + \gamma_{78})] \bar{\rho}_{89} + i d_{86} \mathcal{E}_s^0 \bar{\rho}_{69} \\
& + i d_{98}^* \mathcal{E}_p^{-*} (\bar{\rho}_{99} - \bar{\rho}_{88}) - i d_{97}^* \mathcal{E}_p^{+*} \bar{\rho}_{87} \\
\partial_t \bar{\rho}_{99} & = -2(\gamma_{79} + \gamma_{89}) \bar{\rho}_{99} + i d_{97} \mathcal{E}_p^+ \bar{\rho}_{79} + i d_{98} \mathcal{E}_p^- \bar{\rho}_{89} + i d_{97}^* \mathcal{E}_p^{-*} \bar{\rho}_{97} \\
& + i d_{98}^* \mathcal{E}_p^{-*} \bar{\rho}_{98}
\end{aligned} \tag{2.12}$$

and

$$\bar{\rho}_{ji} = \bar{\rho}_{ij}^*; i \neq j; i, j = 5, 6, 7, 8, 9$$

Where, the detunings are defined as

$$\Delta_{75} = \omega_{75} - \omega_s$$

$$\Delta_{86} = \omega_{86} - \omega_s$$

$$\Delta_{97} = \omega_{97} - \omega_p$$

$$\Delta_{98} = \omega_{98} - \omega_p$$

Since the probe connects both $|5\rangle \rightarrow |7\rangle$ and $|6\rangle \rightarrow |8\rangle$ transitions, total probe absorption is given by the sum of individual probe absorptions $\text{Im}(\bar{\rho}_{75} + \bar{\rho}_{86})$. Because of the symmetry that is assumed in the similarity of transitions $|5\rangle \leftrightarrow |7\rangle$ and $|6\rangle \rightarrow |8\rangle$ the two probe absorptions are identical. From the ρ_{75} equation in (2.12), evolution of $\bar{\rho}_{75}$ is seen to be governed by population difference $\bar{\rho}_{77} - \bar{\rho}_{55}$ and the coherence $\bar{\rho}_{95}$. Similarly, evolution of $\bar{\rho}_{86}$ is governed by $\bar{\rho}_{88} - \bar{\rho}_{66}$ and $\bar{\rho}_{96}$. At steady state, the probe

absorption can be written as

$$\rho_{75}^{ss} = \frac{id_{75}\mathcal{E}_s^0(\rho_{55} - \rho_{77})}{i\Delta_{75} + (\gamma_{57} + \gamma_{65} + \gamma_{87})} + \frac{id_{97}\mathcal{E}_p^+\rho_{95}}{i\Delta_{75} + (\gamma_{57} + \gamma_{65} + \gamma_{87})} \quad (2.13)$$

$$\rho_{86}^{ss} = \frac{id_{86}\mathcal{E}_s^0(\rho_{66} - \rho_{88})}{i\Delta_{86} + (\gamma_{68} + \gamma_{56} + \gamma_{78})} + \frac{id_{98}\mathcal{E}_p^+\rho_{96}}{i\Delta_{86} + (\gamma_{68} + \gamma_{56} + \gamma_{78})} \quad (2.14)$$

Note that γ_{56} (γ_{65}) is the decay rate of coherence of ρ_{56} (ρ_{65}) between the ground states |5) and |6). Similarly γ_{78} (γ_{87}) is the decay rate of coherence ρ_{78} (ρ_{87}) between levels |7) and |8). Because of the degeneracy assumed in ground and excited levels the rates γ_{78} and γ_{56} are dependent on collisions and different values of γ_{78} will be used in the following.

The steady state solution to be used in 2.14 and 2.15 is obtained by the method similar to the one used for *Y* configuration. A closure condition is imposed on the system and ρ_{55} is substituted by $\rho_{55} = 1 - (\bar{\rho}_{66} + \bar{\rho}_{77} + \bar{\rho}_{88} + \bar{\rho}_{99})$. The set of equations (2.12) are rewritten in matrix notation as

$$\partial_t \psi = M \cdot \psi + \phi \quad (2.15)$$

Here ψ is a (24 x 1) column vector consisting of elements of density matrix, M is a 24 x 24 matrix denoting the couplings and ϕ is a column vector arising due to use of closure condition. Explicit form of these matrices are given in appendix B.

The steady state solution of (2.15) is

$$\psi_{ss} = -M^{-1} \cdot \phi$$

Numerical solutions are investigated for specific parameters. As in the case of Y system, all the frequency parameters are normalized to the coherence decay rate γ_{57} .

Figure 2.7 (a) shows $\text{Im}(\rho_{75})$ and $\text{Im}(\rho_{86})$ for a case when both pump and probe beam are weak with their Rabi frequencies $\Omega_s = \Omega_p = 0.2$. Here we have $\gamma_{56} = \gamma_{75} = \gamma_{86}$ and $\gamma_{78} = 0$. It shows that the probe absorption has a Lorentzian profile, indicating a behaviour similar to that of a two-level atom in the weak fields. Figure 2.7 (b) shows behaviour of population of ground levels $|5\rangle$ and $|6\rangle$ where the decrease in population of $|5\rangle$ and $|6\rangle$ is indicated along with absorption of the probe (fig. 2.7 a). Figure 2.7 (c) shows populations of excited states $|7\rangle$, $|8\rangle$ and $|9\rangle$. Their profiles are compatible with that of probe absorption. Figure 2.7(d) shows two factors which add to make up steady state value of $\text{Im}(\rho_{75})$, according to (2.14). The factor $B = \text{Im}[d_{75}\mathcal{E}_s^0(\rho_{55} - \rho_{77})/(\Delta_{75} - i(\gamma_{57} + \gamma_{65} + \gamma_{87}))]$ is too small to make any change to the absorption factor $A = \text{Im}\left[(-d_{97}\mathcal{E}_p^+\rho_{95})/(\Delta_{75} - i(\gamma_{57} + \gamma_{65} + \gamma_{87}))\right]$ which shows the Lorentzian. Therefore, their sum is absorptive.

Summarizing the observations from Fig. 2.7 for the weak probe and weak pump case we have for the **Gate** system,

- (α_G) Individual absorption of $|7\rangle \leftrightarrow |5\rangle$ and $|6\rangle \leftrightarrow |8\rangle$ transitions show a single peak Lorentzian line shape. Unlike Y system, for similar situation in terms of field intensities, the **Gate** system shows only partial noticeable reduction in absorption.
- (β_G) There is depletion of population in levels $|5\rangle$ and $|6\rangle$ accompanied by absorption of probe. This depletion is with respect to the population (0.5) in the absence of any radiation.

- (γ_G) Levels |7) and |8) show increase in population with the absorption of probe beam;
- (δ_G) However the population transfer to level |9) is rather small. This is so even at line center where the probe absorption is maximum. Nevertheless for weak fields it follows the probe absorption pattern.
- (η_G) There is no dip in probe absorption at line center. This is also characterized by the fact that for the parameter range chosen ($d.\mathcal{E}_s^0(\bar{\rho}_{55} - P77) + d.\mathcal{E}_p^+ \bar{\rho}_{99}$) and ($d.\mathcal{E}_s^0(\bar{\rho}_{66} - \bar{\rho}_{88}) + d.\mathcal{E}_p^+ \bar{\rho}_{96}$) are far from being zero. Hence there is no cancellation effect and no transparency is produced at these range of parameters.

Next we consider the case of strong pump and weak probe. Figure 2.8 (a) shows $\text{Im}(\rho_{75})$ and $\text{Im}(\rho_{86})$ when the pump beam becomes stronger, with amplitudes $\Omega_p = 6.0$, while the probe beam is weak with $\Omega_s = 0.2$. We have a three peaked profile. This profiles shows two side bands of absorption at $\Delta \approx \sqrt{|\Omega_{97}|^2 + |\Omega_{98}|^2}$, which are at Rabi frequencies of pump beam transition. A central absorption peak at zero detuning indicates a finite, nonzero absorption at center. Therefore, there is no transparency induced for this system, though the absorption at the center is less than that for a weak pump case which is seen in Figure 2.7 (a). Figure 2.8 (b) shows populations of ground states |5) and |6) and Figure 2.8 (c) shows populations of excited states |7), |8) and |9). These two Figures show a three peaked depletion in population of level |5) and |6) coincident with probe absorption. Corresponding increase in population of |7) and |8) is also a three peaked structure- However the behaviour of the change in population of level |9) shows only a double peak structure coincident with the Rabi side bands in probe absorption. Population of level |9) is not zero at zero detuning. Figure 2.8 (d) shows the behaviour of factors **A** and **B** for the **Gate** system which add up to form the probe absorption $\text{Im}(\rho_{75})$. Clearly the cancellation is not complete at $\Delta_s = 0$. i.e.,

$$(d.\mathcal{E}_s^0(\bar{\rho}_{55} - \bar{\rho}_{77}) + \text{Re}[d.\mathcal{E}_p^+ \bar{\rho}_{95}]) \neq 0 \text{ and } (d.\mathcal{E}_s^0(\bar{\rho}_{66} - \bar{\rho}_{88}) + \text{Re}[d.\mathcal{E}_p^+ \bar{\rho}_{96}]) \neq 0 \text{ at } \Delta_s = 0$$

This result is in contrast to that for the Y configuration at high intensity which shows a marked transparency. Even though the pump beam creates a coherence between the excited states, such coherences do not cancel the probe absorption.

We may now summarize the results of Figure 2.8 for the strong pump case of Gate system.

(SP α_G) The probe absorption develops three distinct regions

(a) Two Lorentzian peaks separated by the Rabi frequency of the three level A system as shall be shown in Chapter III

(b) The line center shows strong absorption peak and thus there is no transparency or zero absorption at line center.

(SP β_G) Population of levels |5) and |6) deplete at all the three places where the probe absorption is high.

(SP γ_G) Populations of levels |7) and |8) show corresponding increase in population at the three places where probe absorption is strong,

(SP δ_G) Population of level |9) shows peculiarity in the sense that it has high population at the Rabi sidebands of probe absorption, but its population at $\Delta_s = 0$ does not show a peak in spite of the fact the probe absorption and population in levels |7) and |8) is high.

(SP η_G) As noted above the cancellation of A and B in this case is not complete, so the Lorentzian also occurs at $\Delta_s = 0$. Leading to the three peaked structure.

We note that in the **Gate** system coherence decay rates γ_{78} and γ_{56} , can have a variety of values. we have chosen above a case with $\gamma_{56} = \gamma_{57}$ and $\gamma_{78} = 0$. The **Gate** system needs analysis for other values of γ_{56} & γ_{78} also. We shall take up these cases after we have given the analytical expression for the **Gate** system obtained in a manner similar to that used for **Y** system.

2.2.1 Analytical Solution for the Gate system

Using a similar method as in case of **Y** configuration, an analytical solution is obtained for the strong pump and weak probe case to the first order in probe amplitude. The zeroth order coherences $\bar{\rho}_{97}^{(0)}$ and $\bar{\rho}_{87}^{(0)}$ are assumed to be zero because they get significant value only in second order in probe intensity. The coherence between ground states $\bar{\rho}_{56}$ is assumed to be zero for the present, due to a large γ_{56} .

The relevant equations under such assumptions are

$$-i \partial_t \bar{\rho}_{75}^{(1)} = [-\Delta_{75} + i (\gamma_{57} + \gamma_{65} + \gamma_{87})] \bar{\rho}_{75}^{(1)} + d_{75} \mathcal{E}_s^0 (\bar{\rho}_{55}^{(0)} - \bar{\rho}_{77}^{(0)}) + d_{97}^* \mathcal{E}_p^+ \bar{\rho}_{95}^{(1)} \quad (2.16)$$

$$\begin{aligned} -i \partial_t \bar{\rho}_{95}^{(1)} &= [-(\Delta_{97} + \Delta_{75}) + i (\gamma_{79} + \gamma_{89})] \bar{\rho}_{95}^{(1)} + d_{97} \mathcal{E}_p^- \bar{\rho}_{75}^{(1)} \\ &+ d_{98} \mathcal{E}_p^- \bar{\rho}_{85}^{(1)} - d_{75} \mathcal{E}_s^0 \bar{\rho}_{97}^{(0)} \end{aligned} \quad (2.17)$$

$$\begin{aligned} -i \partial_t \bar{\rho}_{85}^{(1)} &= [-\Delta_{85} + i (\gamma_{68} + \gamma_{56} + \gamma_{78})] \bar{\rho}_{85}^{(1)} + d_{86} \mathcal{E}_s^0 \bar{\rho}_{65}^{(0)} + d_{98}^* \mathcal{E}_p^- \bar{\rho}_{95}^{(1)} \\ &- d_{75} \mathcal{E}_s^0 \bar{\rho}_{87}^{(0)} \end{aligned} \quad (2.18)$$

A similar set of equations are obtained for $\bar{\rho}_{86}$ as

$$-i \partial_t \bar{\rho}_{86} = [-\Delta_{86} + i (\gamma_{68} + \gamma_{56} + \gamma_{78})] \bar{\rho}_{86}^{(1)} + d_{86} \mathcal{E}_s^0 (\bar{\rho}_{66}^{(0)} - \bar{\rho}_{88}^{(0)}) + d_{98}^* \mathcal{E}_p^- \bar{\rho}_{96}^{(1)} \quad (2.19)$$

$$\begin{aligned} -i \partial_t \bar{\rho}_{96} &= [-(\Delta_{98} + \Delta_{86}) + i (\gamma_{89} + \gamma_{79})] \bar{\rho}_{96}^{(1)} + d_{98} \mathcal{E}_p^- \bar{\rho}_{86}^{(1)} \\ &+ d_{97} \mathcal{E}_p^- \bar{\rho}_{76}^{(1)} - d_{86} \mathcal{E}_s^0 \bar{\rho}_{98}^{(0)} \end{aligned} \quad (2.20)$$

$$\begin{aligned}
-i \partial_t \bar{\rho}_{76}^{(1)} &= [-\Delta_{76} + i(\gamma_{57} + \gamma_{65} + \gamma_{87})] \bar{\rho}_{76}^{(1)} + d_{86} \mathcal{E}_s^0 \bar{\rho}_{78}^{(0)} + d_{75} \mathcal{E}_s^0 \bar{\rho}_{56}^{(0)} \\
&\quad - d_{97}^* \mathcal{E}_p^+ \bar{\rho}_{96}^{(1)}
\end{aligned} \tag{2.21}$$

It can be noted at this stage itself that the two sets are independent of each other. In other words, the two components of probe absorption do not affect each other. Plugging the steady state solutions of equations 2.17 and 2.18 in 2.16, and those of equations 2.20 and 2.21 in 2.19, we obtain steady state solutions for probe absorption,

$$\bar{\rho}_{75}^{(1)} = \frac{d \mathcal{E}_s^0 \bar{\rho}_{55}^{(0)}}{\Delta_{75} - i(\gamma_{57} + \gamma_{65} + \gamma_{87}) - \frac{|d_{97} \mathcal{E}_p^+|^2}{\Delta_{95} - i\gamma_9 - \frac{|d_{98} \mathcal{E}_p^-|^2}{\Delta_{85} - i(\gamma_{68} + \gamma_{56} + \gamma_{78})}}} \tag{2.22}$$

and

$$\bar{\rho}_{86}^{(1)} = \frac{d \mathcal{E}_s^0 \bar{\rho}_{66}^{(0)}}{\Delta_{86} - i(\gamma_{68} + \gamma_{56} + \gamma_{78}) - \frac{|d_{98} \mathcal{E}_p^-|^2}{\Delta_{96} - i\gamma_9 - \frac{|d_{97} \mathcal{E}_p^+|^2}{\Delta_{76} - i(\gamma_{57} + \gamma_{65} + \gamma_{87})}}} \tag{2.23}$$

Figure 2.9 shows the comparison between analytical (symbol) and the numerical solutions (solid) for weak probe and strong pump. It shows a good agreement for small values of probe, and same parameters as used in Figure 2.8.

The analytical results given in this section are applicable not only for different values of γ_{56} and γ_{78} but also for $\Delta_s = 0$, $\Delta_p \neq 0$.

case of $\gamma_{78} \neq 0$

Figure 2.8 g compares graphs for $\gamma_{78} = \gamma_{57}$ with $\gamma_{78} = 0$ case. The three peaked structure for the **Gate** system is shown here also. However the peak heights at Rabi side bands are reduced and broadened. The behaviour of A and B factors for these cases are displayed in Figure 2.8 h. The nonzero value of $[d_s \mathcal{E}_s^0(\rho_{55} - \rho_{77} + \text{Re}(d_p \mathcal{E}_p \rho_{95}))]$ does not allow transparency to be produced in Gate system. Similar results have been found when $\Delta_p \neq 0$.

case of $\gamma_{56} = 0$

2.2.2 Anomalous absorption

It is interesting to discuss an anomalous case obtained when $\gamma_{56} = 0$ and $\gamma_{78} = 0$. In this case the numerical results give the probe absorption behaviour very different from the analytical results in Gate case. Note that the analytical result as expected, by reducing the $\gamma_{78} = \gamma_{56} = 0$, show three peaked structure, as in Figure 2.8 g, with much narrower width and high peaks. The numerical results on the other hand show only a doublet and a transparency much more than in previous cases. Figure 2.10 is a study of the effect of choosing $\gamma_{56} = 0$ for weak field situation and Figure 2.11 is the study for strong field case where the surprise lies in the absence of the central peak which occurs in Figure 2.8. The major difference in $\gamma_{56} = 0$ and $\gamma_{56} = \gamma_{57}$ case lies in the large value of the coherence ρ_{56} for $\gamma_{56} = 0$ case and its zero value for $\gamma_{56} = 1.0$ case. Clearly the approximation used in deriving the analytical results are not valid in regions where $\rho_{56}^{(0)} \neq 0$ or is developed as a result of higher order effects in probe absorption. In order to further illuminate this anomalous situation and to gain further insight into the behaviour of Y and Gate systems we examine in next chapter wave function approach in which it is possible to examine the dressed state picture of the two systems. We need to investigate further why there is a large transparency when

$\rho_{56} = 0.5$ in **Gate** system at $\Delta_s = 0$.

2.2.3 Determination of **f** - values

The analytical solutions 2.22 and 2.23 can be employed to determine the dipole matrix elements even in this case. The dipole matrix elements $\langle 7|d.E_p|9\rangle$ and $\langle 8|d.E_p|9\rangle$ can be determined using the same technique that was used for **Y** system. The separation between the two Rabi sidebands is equal to $\sqrt{|\Omega_{97}|^2 + |\Omega_{98}|^2}$. Using the analytical expression to fit the experimental data for probe absorption, the values of Rabi frequencies can be obtained with a better accuracy. The dipole matrix elements can be calculated from the values of Rabi frequencies.

2.3 Conclusion

The numerical solutions in density matrix formalism show that the coherences formed by the pump and the probe beam affect the probe absorption. In case of the **Y** configuration, these coherences can completely cancel the absorption while for the **Gate** configuration, the coherence can only partially cancel the absorption. This results in a complete transparency for the **Y** configuration while the **Gate** configuration experiences a reduced but nonzero absorption. However the **Gate** system can show transparency if one can prepare $\rho_{56} = 0.5$. In the next chapter, a further investigation of the dressed state picture of **Y** and **Gate** is presented. In Chapter IV, a detailed discussion of why the transparency of **Gate** is high for $\rho_{56} = 0.5$ is presented.

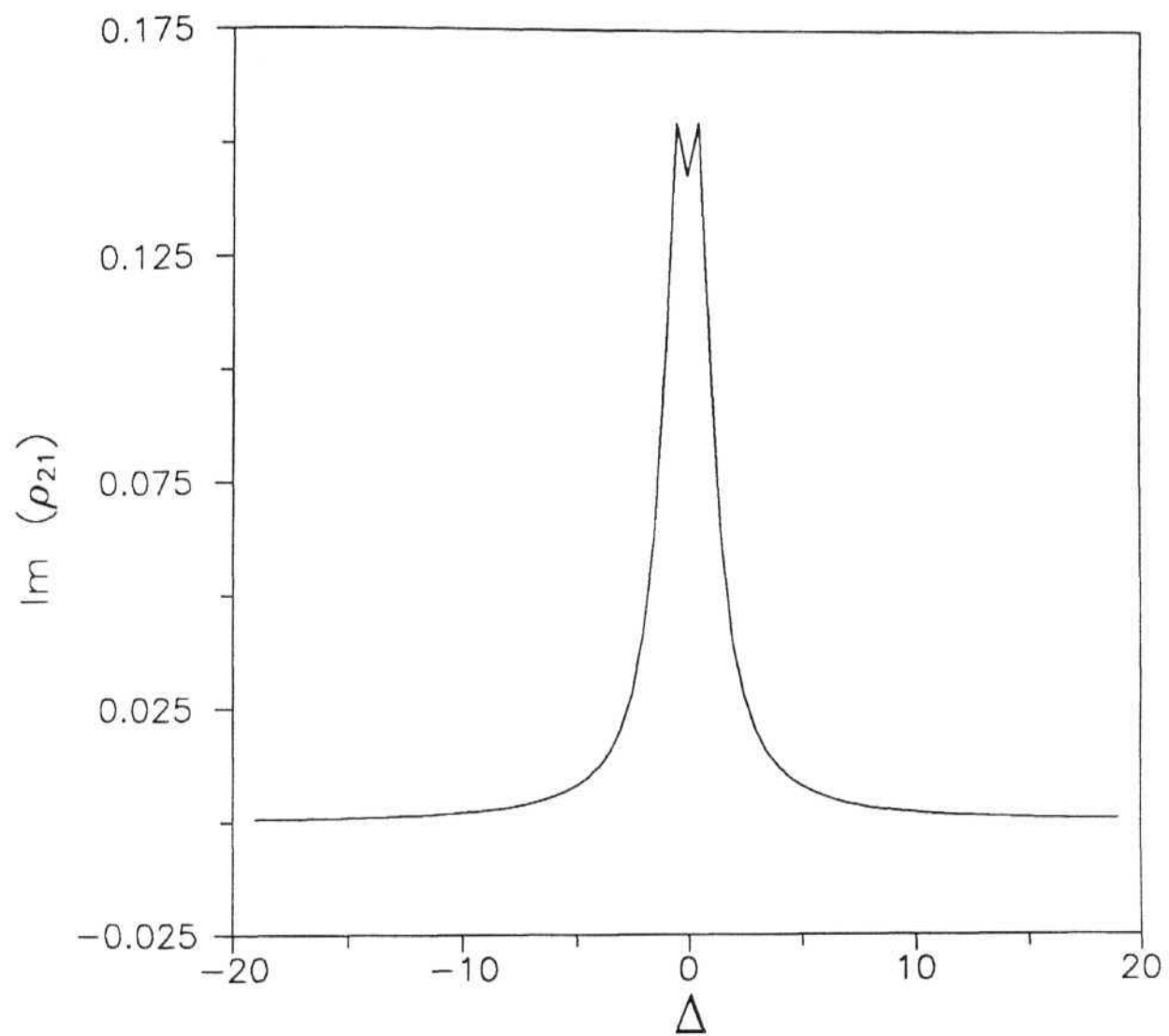


Fig. 2.2 (a): Absorption of the probe beam for for $\Omega_s = \Omega_p = 0.2$. Δ is the detuning for probe.

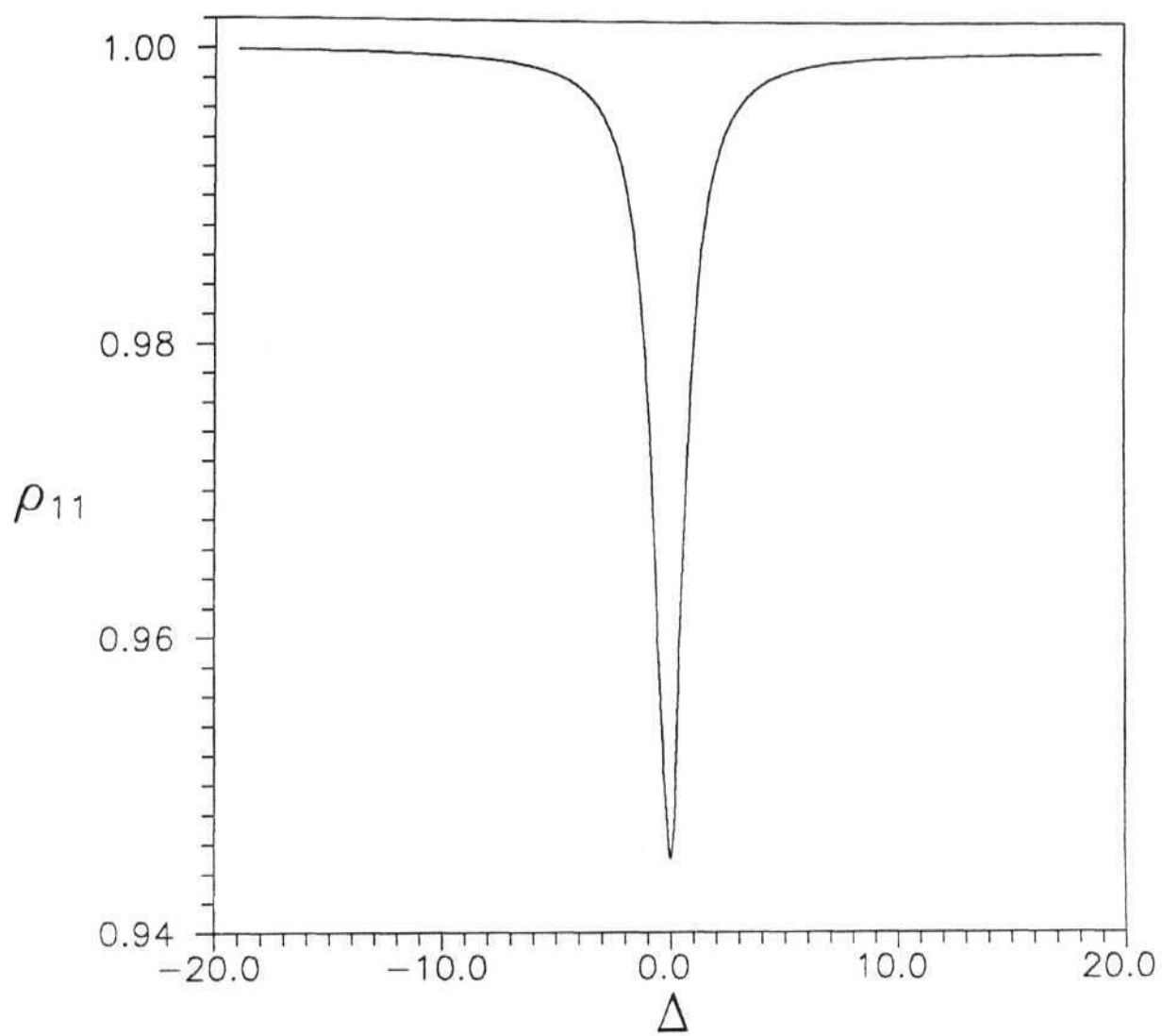


Fig. 2.2 (b): Population of level 1, for $\Omega_s = \Omega_p = 0.2$.

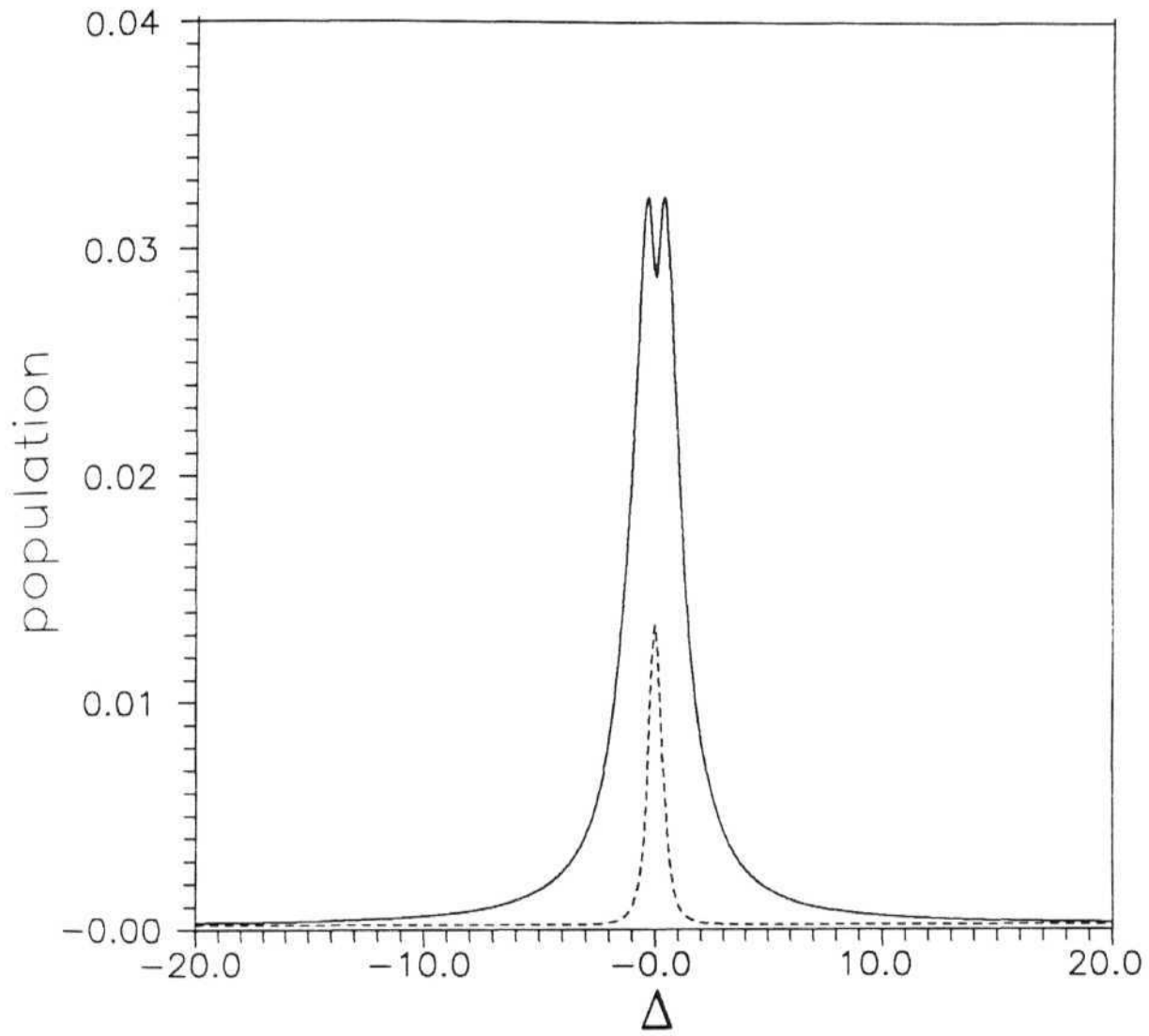


Fig. 2.2 (c): Population of level 2 (solid line) and level 3 (dotted line) for $\Omega_s = \Omega_p = 0.2$.

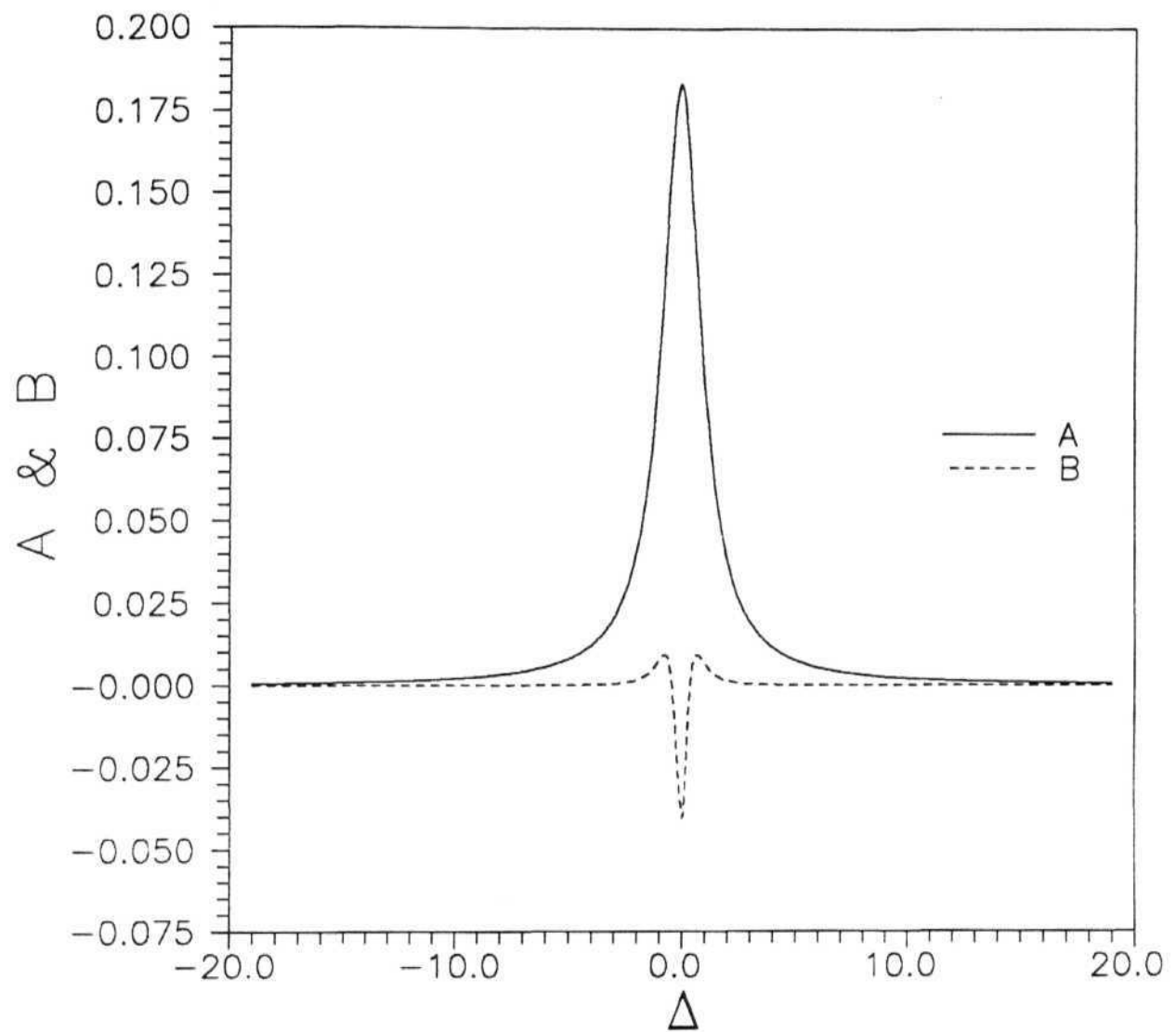


Fig. 2.2 (d): Factors A and B (See text for explanation)
for $\Omega_s = \Omega_p = 0.2$.

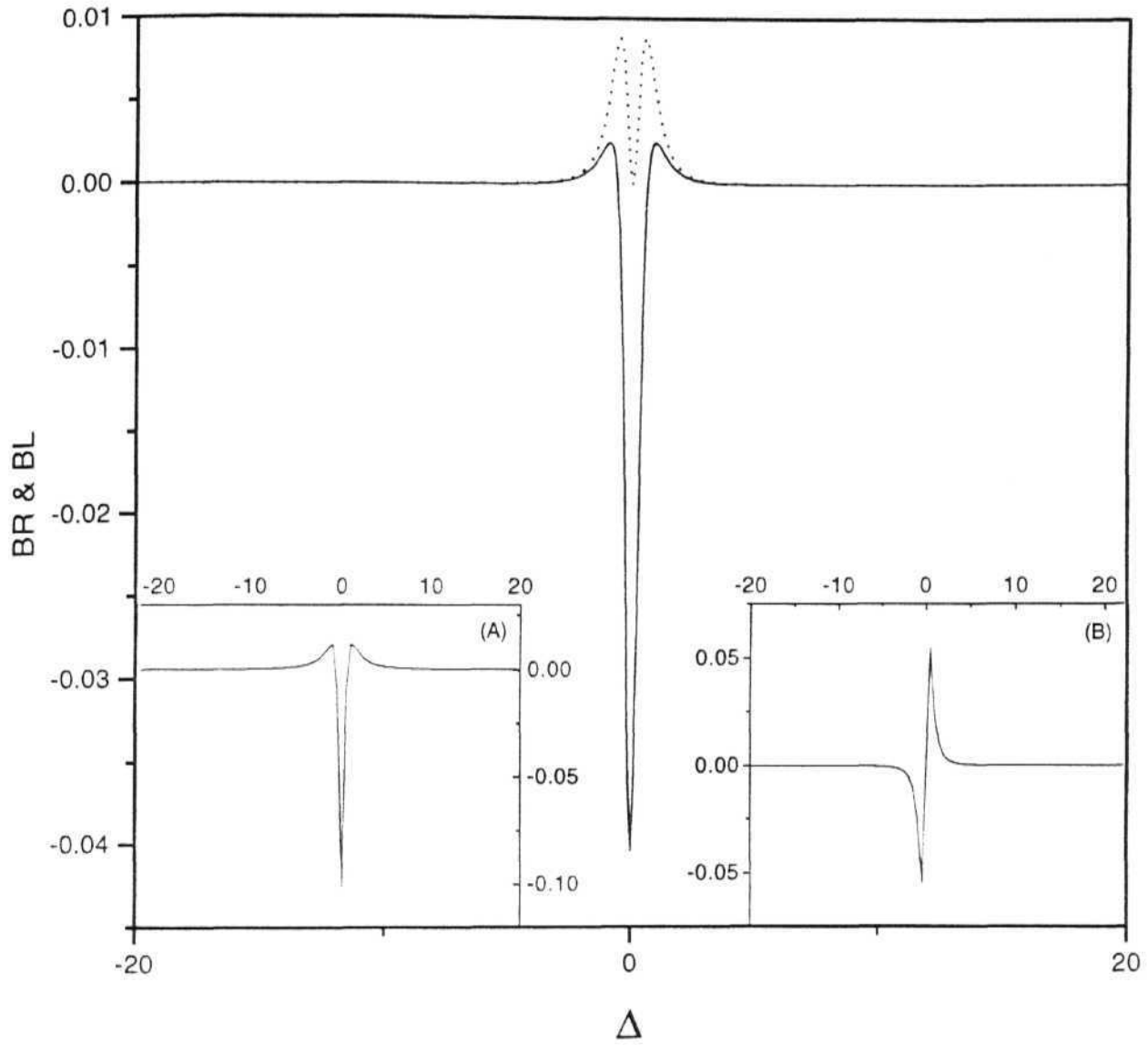


Fig. 2.2 (e): Factors BR and BL for $\Omega_s=0.2$ and $\Omega_p=0.2$. Insets (A) and (B) show $\text{Re}(\rho_{31}+\rho_{41})$ and $\text{Im}(\rho_{31}+\rho_{41})$ respectively.

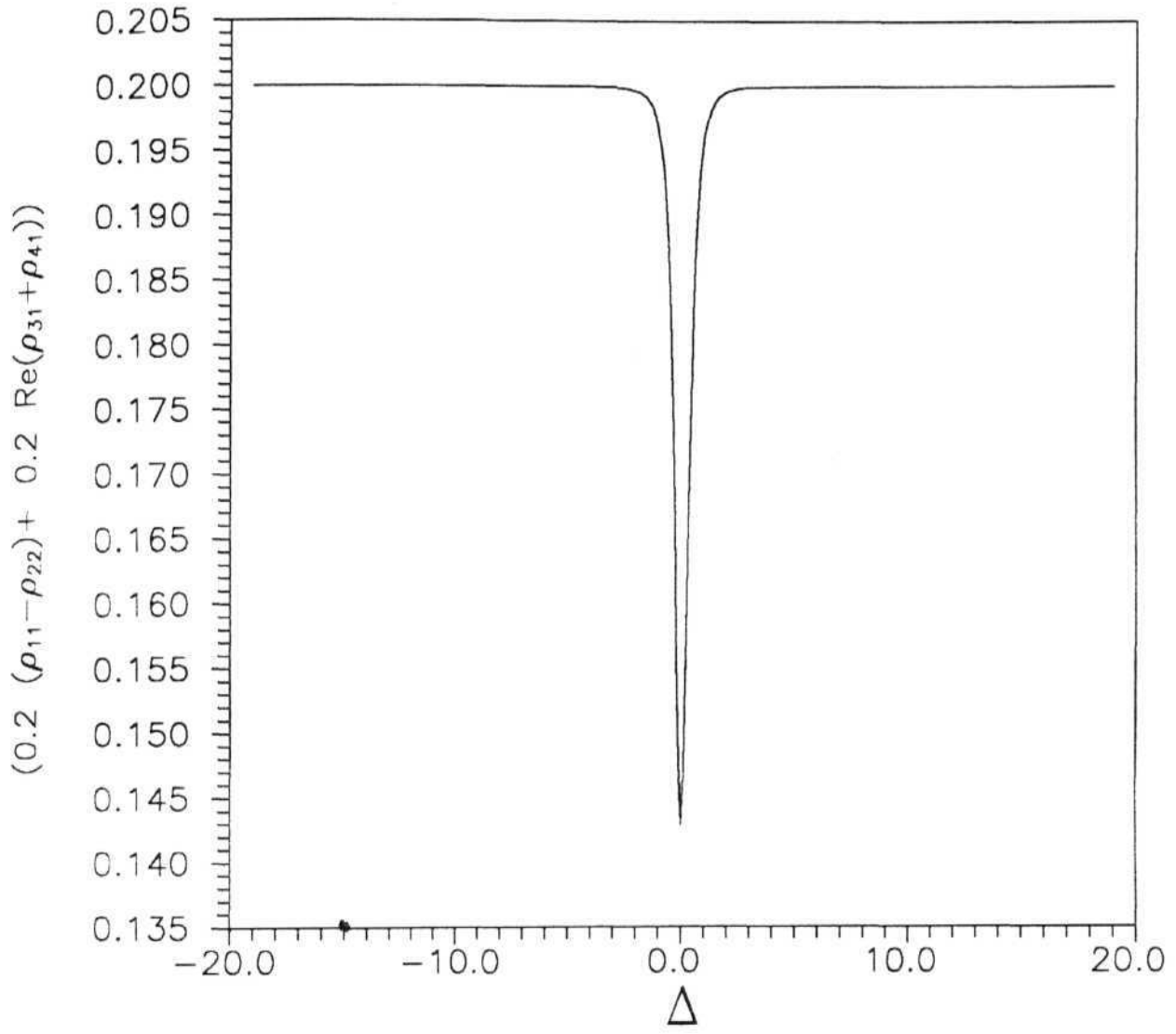


Fig. 2.2 (f): $(0.2 (\rho_{11}-\rho_{22}) + 0.2 \text{Re}(\rho_{31}+\rho_{41}))$ for $\Omega_s=\Omega_p=0.2$

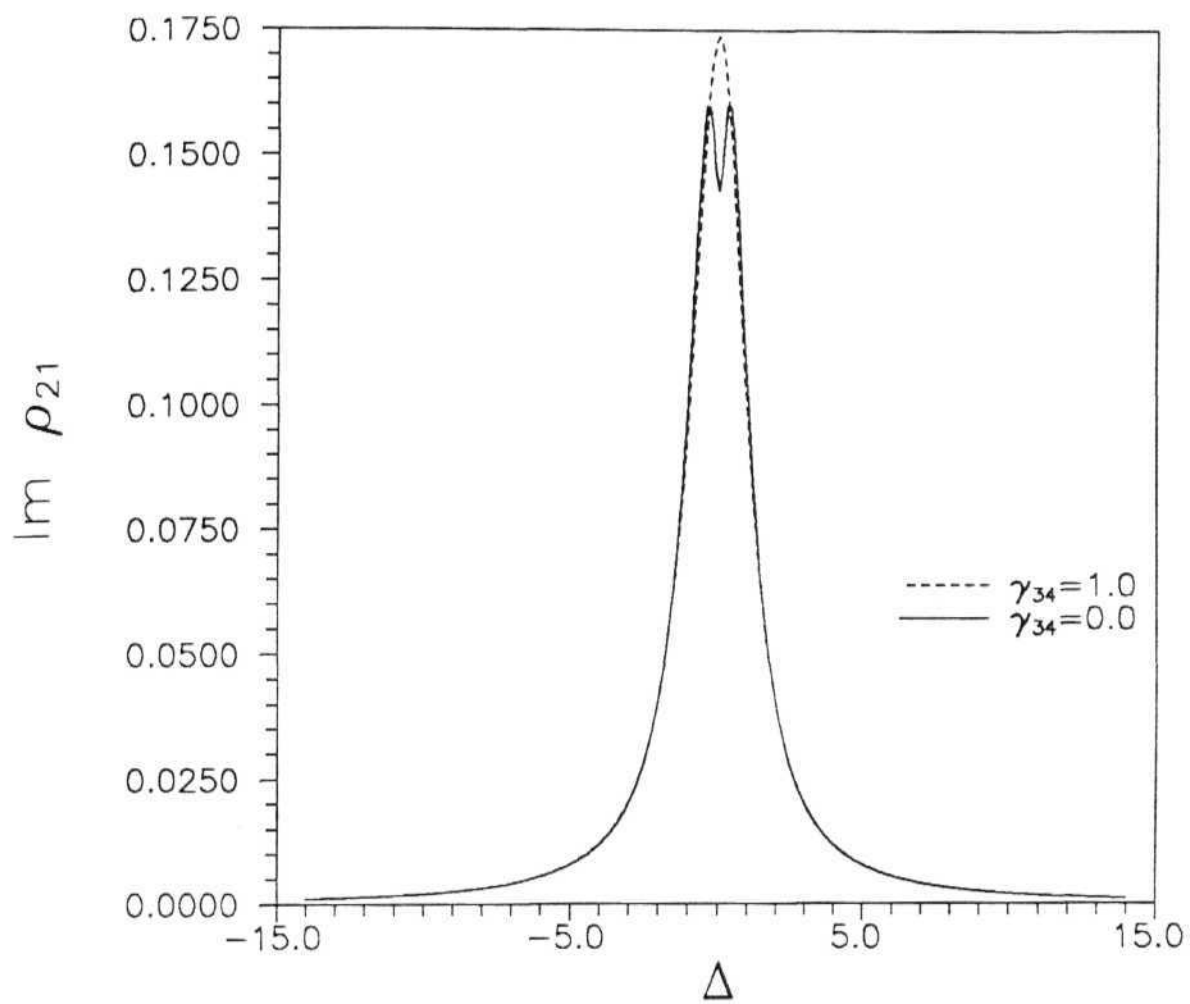


Fig. 2.2 (g): $\text{Im } \rho_{21}$ for $\gamma_{34}=0$ and $\gamma_{34}=1.0$.
for weak pump case. The dip at the line center
vanishes for a nonzero γ_{34} .

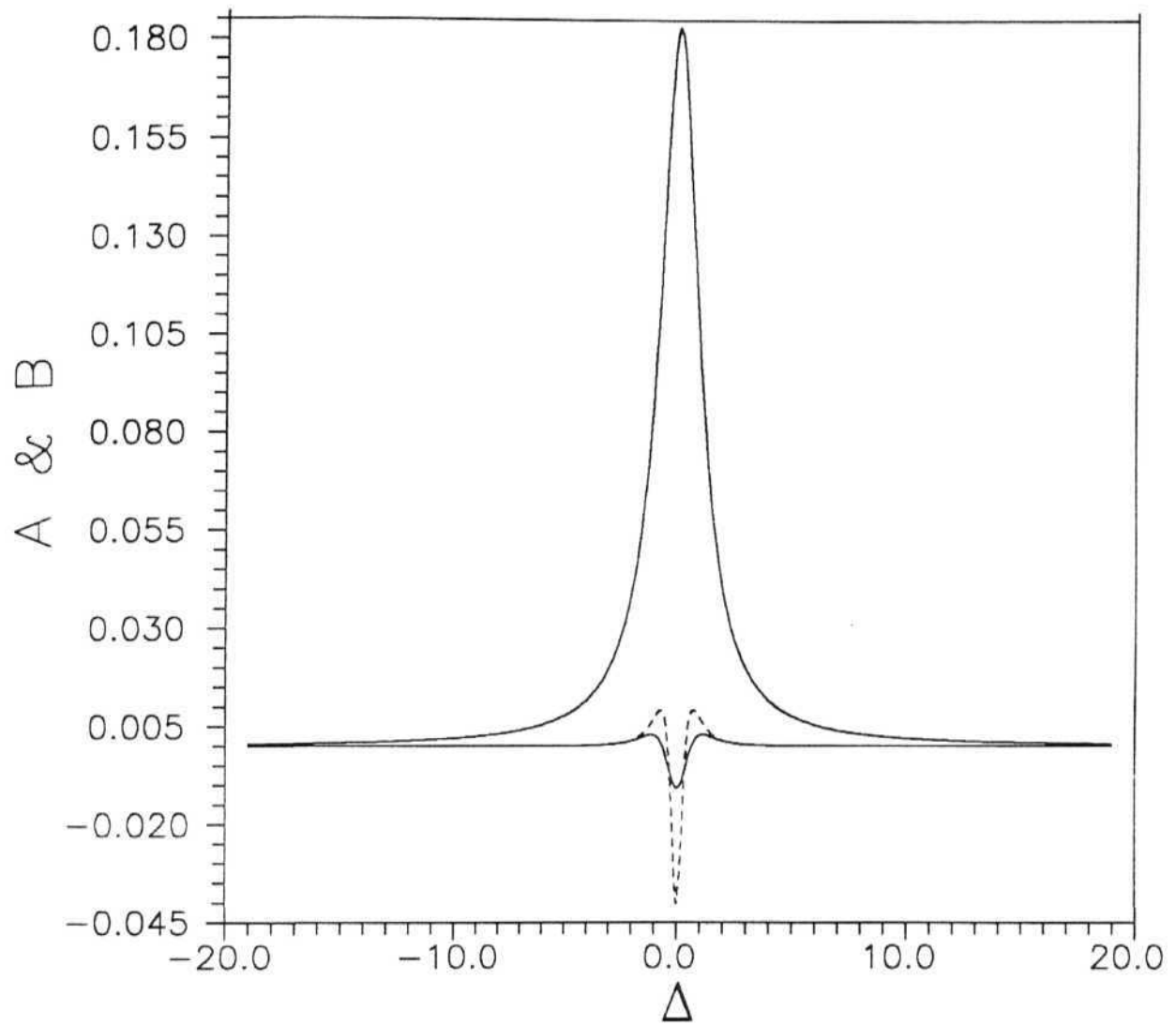


Fig.2.2 (h): Factors A and B (See text for explanation) for $\Omega_s = \Omega_p = 0.2.$, Two B lines correspond to $\gamma_{34} = 1.0$ (dashed) and $\gamma_{34} = 0.0$ (solid).

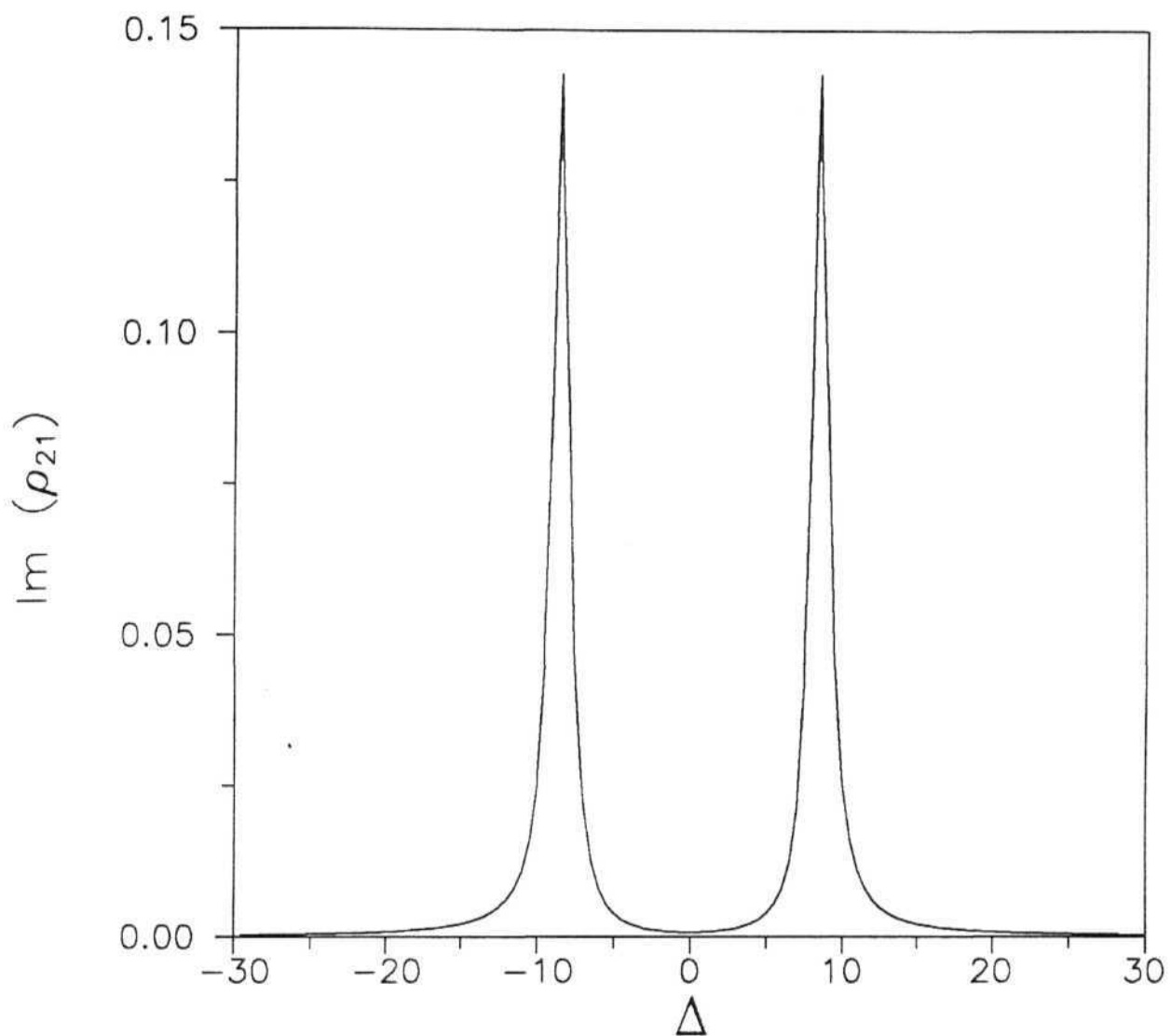


Fig. 2.3 (a): Probe absorption for weak probe ($\Omega_s=0.2$) and strong pump ($\Omega_p=6.0$) against probe detuning. Absorption is completely zero on resonance.

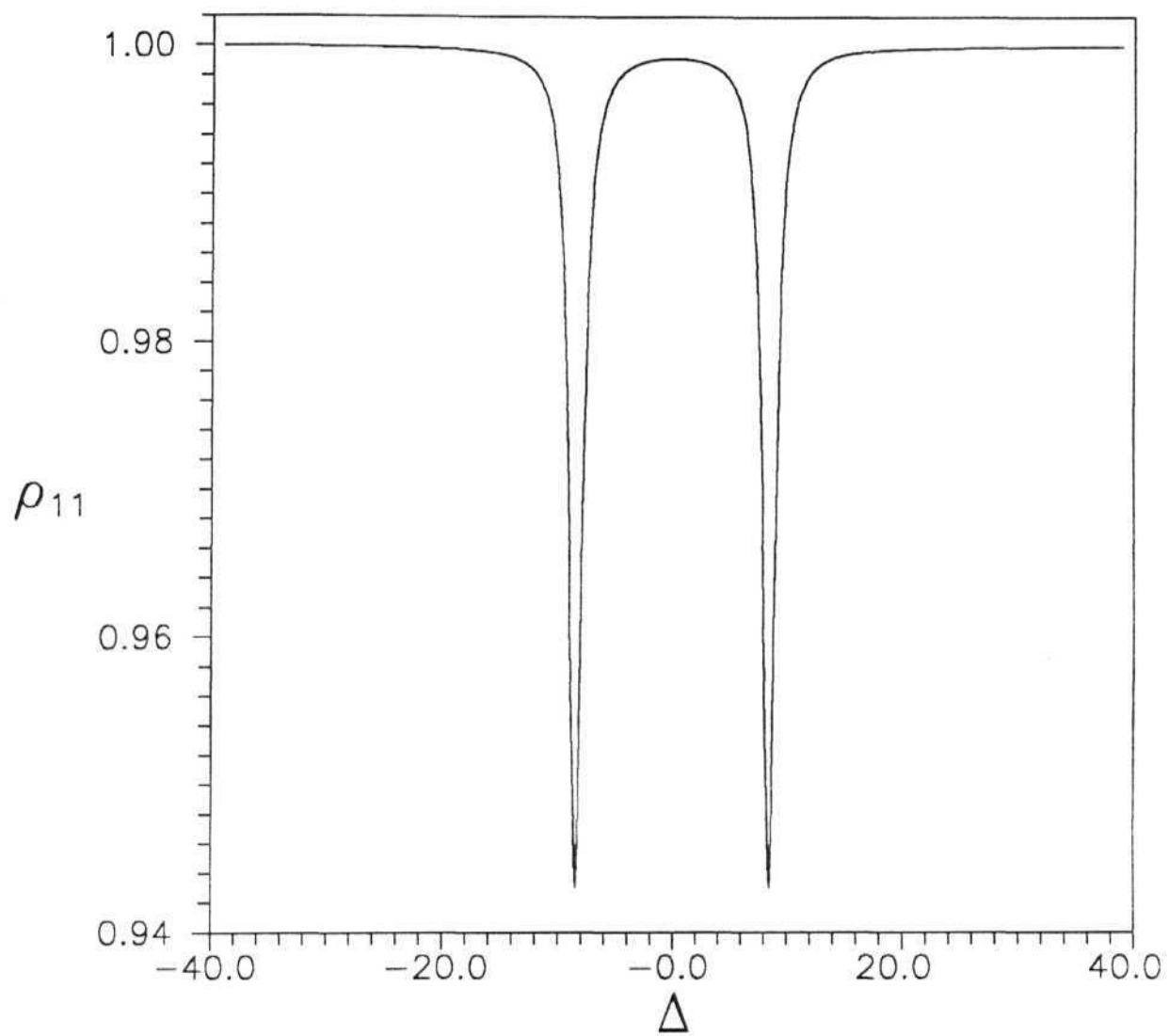


Fig. 2.3 (b): Population of level 1, for $\Omega_s=0.2$ and $\Omega_p=6.0$

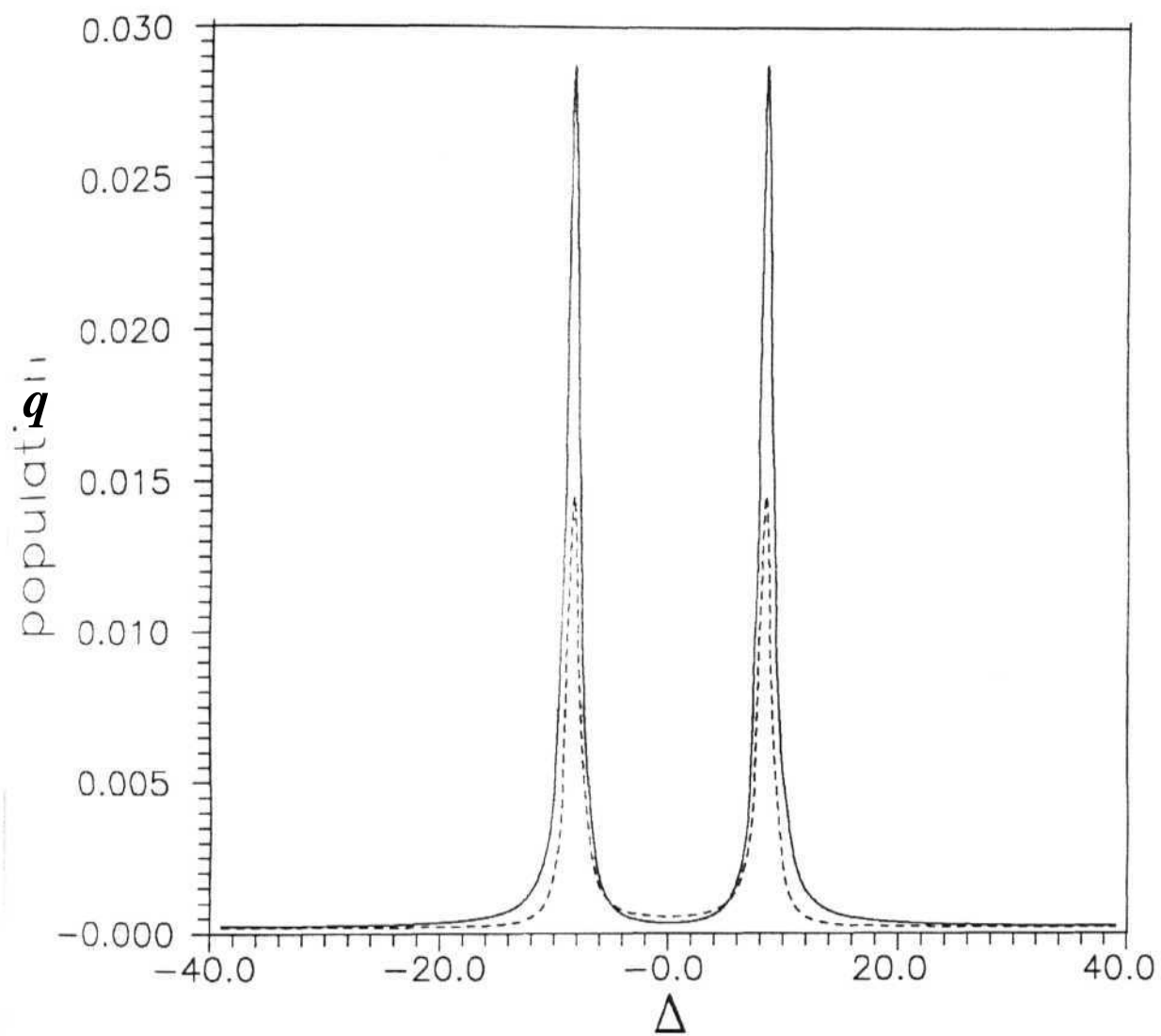


Fig. 2.3 (c): Population of level 2 (solid line) and level 3 (dotted line) for $\Omega_s=0.2$ and $\Omega_p=6.0$.

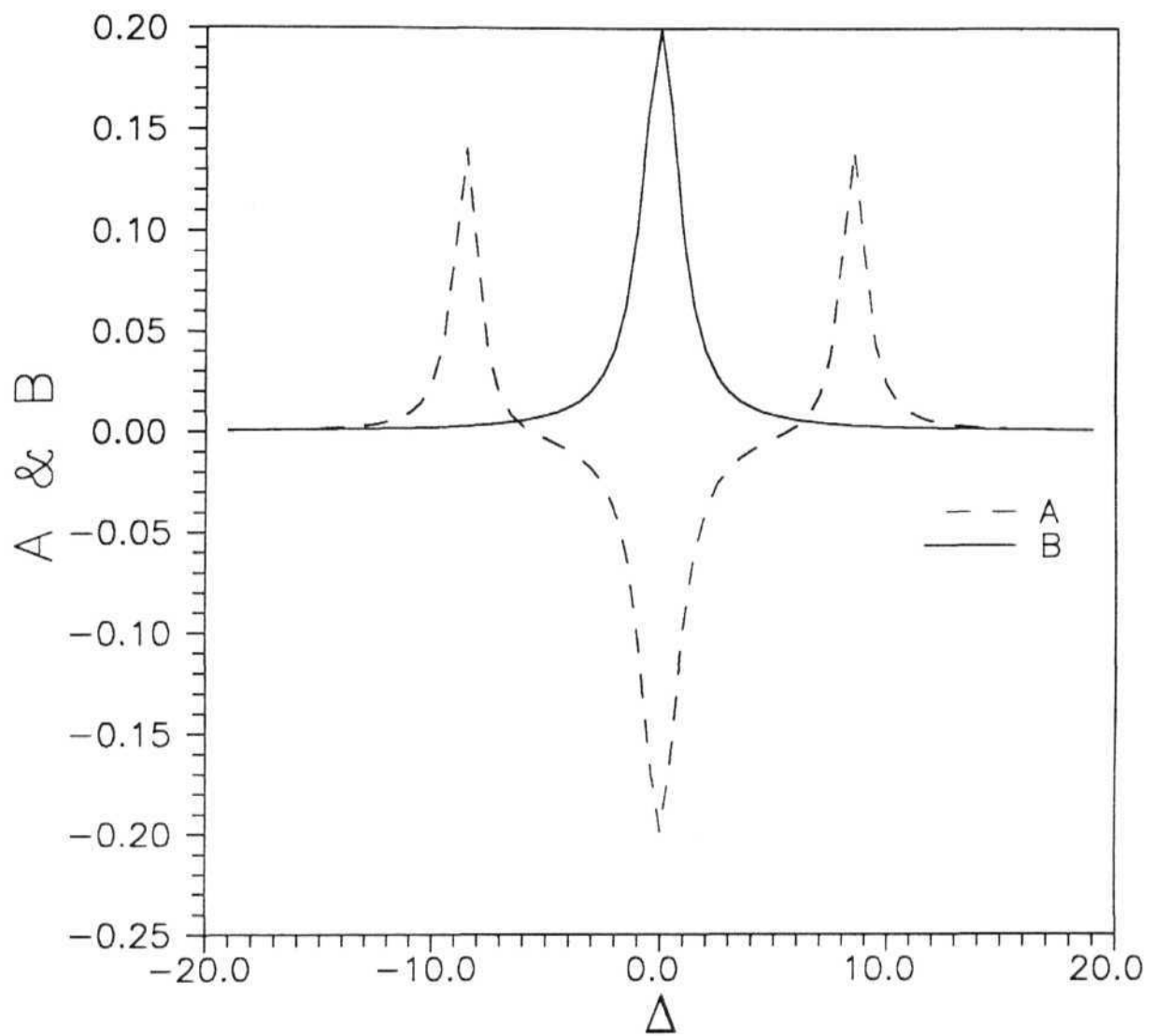


Fig. 2.3 (d): Factors A and B (See text for explanation) for $\Omega_s=0.2$ and $\Omega_p=6.0$.

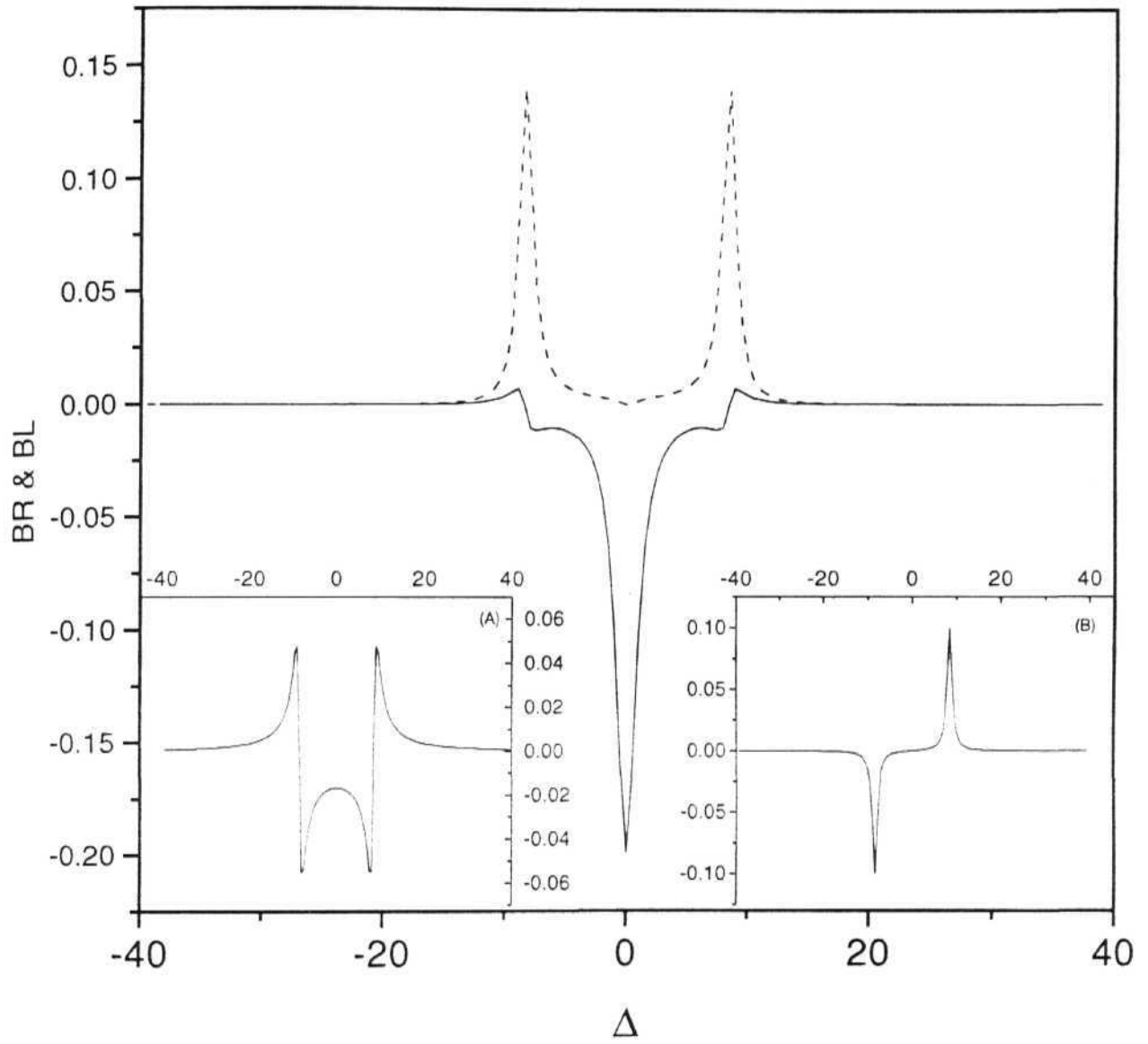


Fig. 2.3 (e): Factors BR and BL for $\Omega_s=0.2$ and $\Omega_p=6.0$. Insets (A) and (B) show $\text{Re}(\rho_{31} + \rho_{41})$ and $\text{Im}(\rho_{31} + \rho_{41})$ respectively.

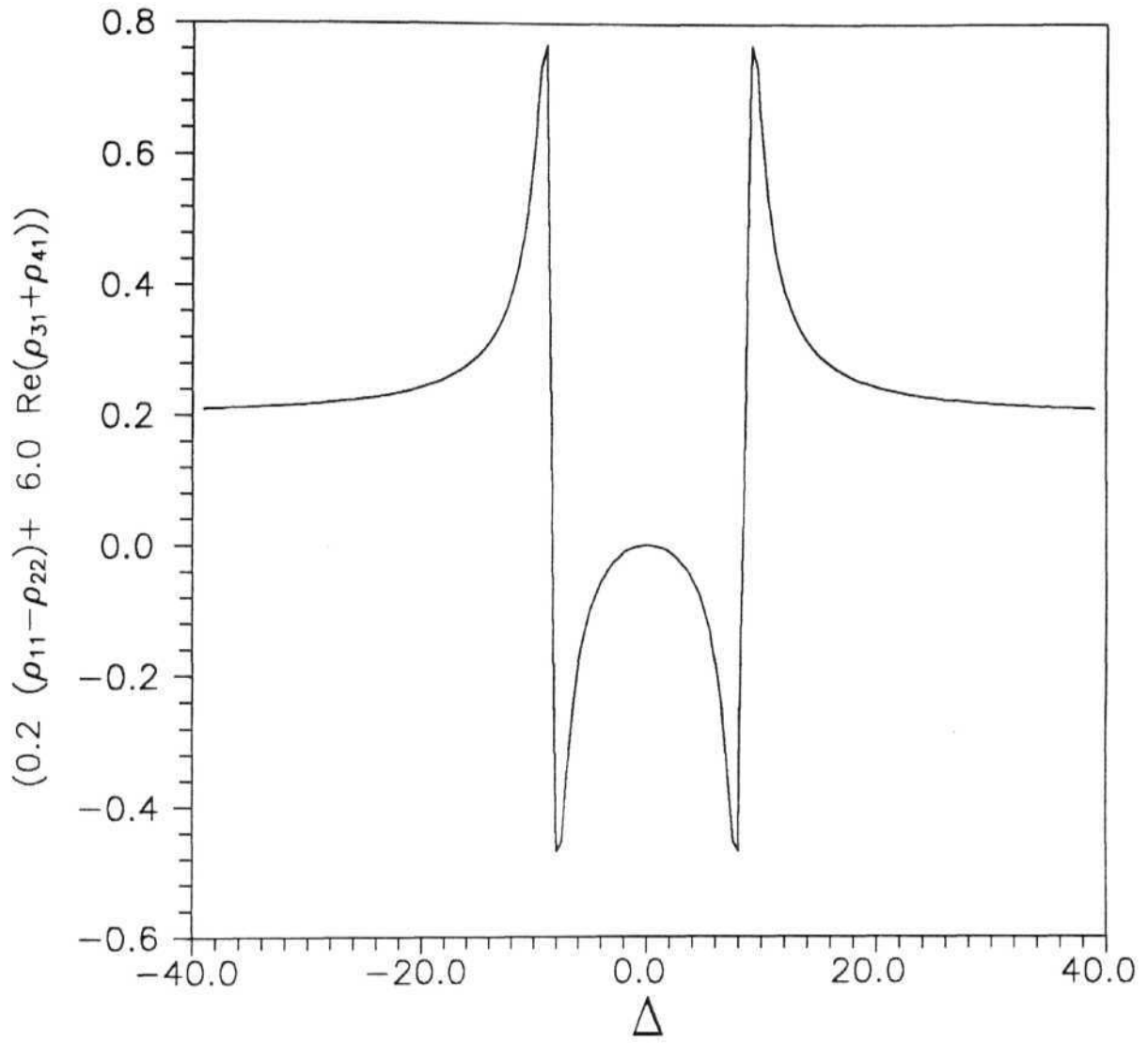


Fig. 2.3 (f): $(0.2 (\rho_{11} - \rho_{22}) + 6.0 \operatorname{Re}(\rho_{31} + \rho_{41}))$ for $\Omega_s = 0.2$ and $\Omega_p = 6.0$

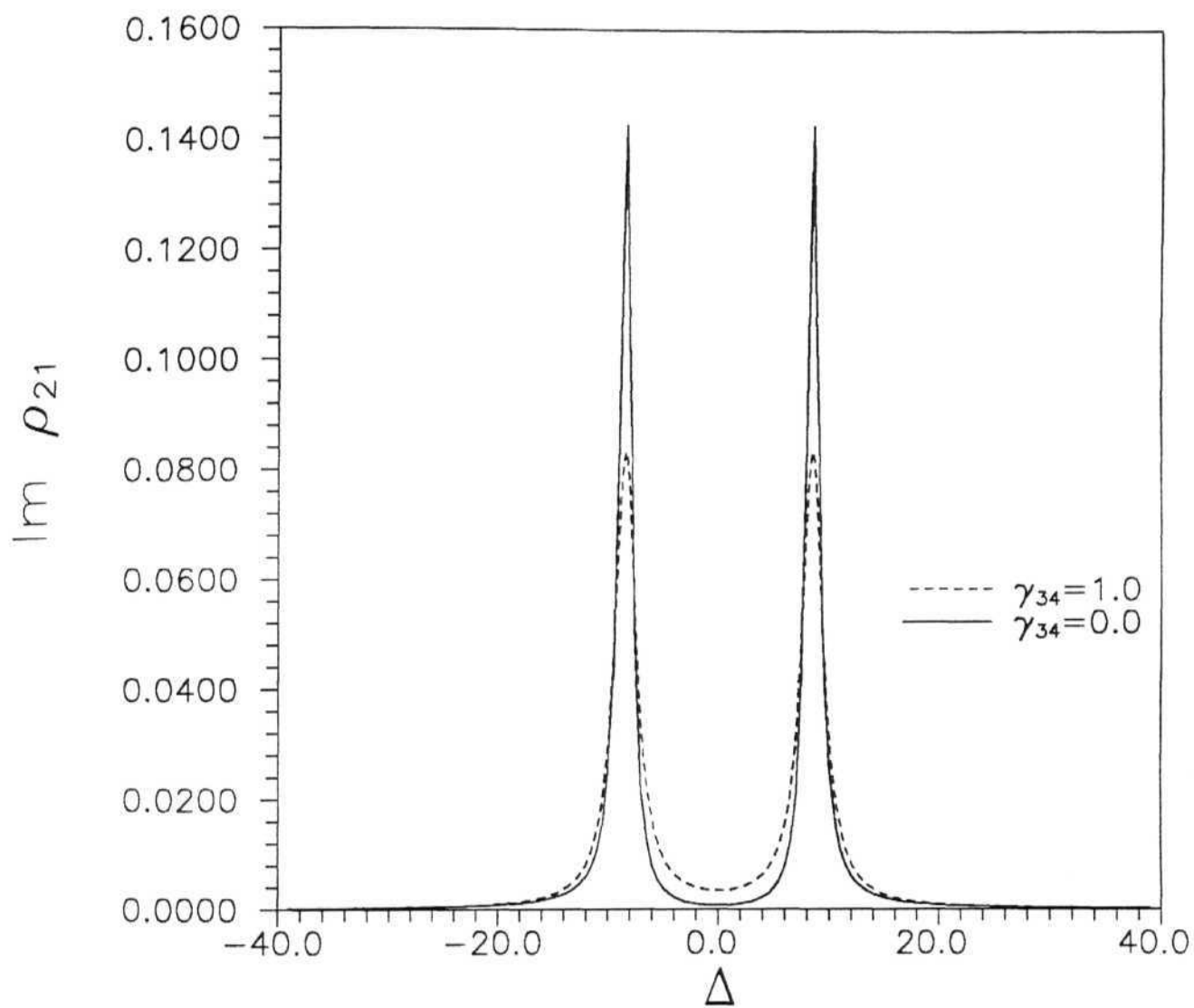


Fig. 2.3 (g): $\text{Im } \rho_{21}$ for $\Omega_s=0.2$; $\Omega_p=6.0$, at different γ_{34} values. The transparency is finite when γ_{34} is nonzero.

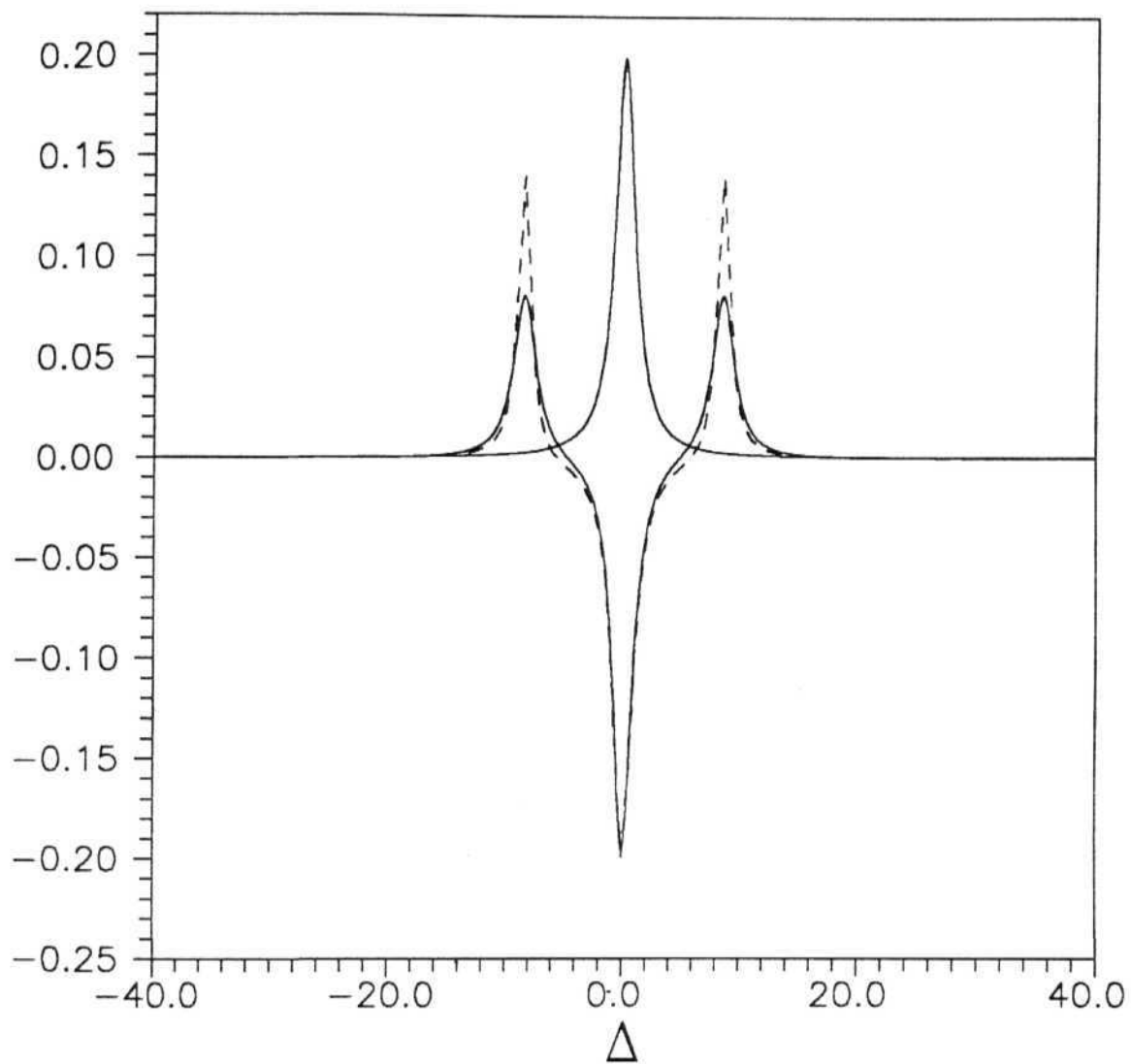


Fig.2.3 (h): Factors A and B (See text for explanation) for $\Omega_s=0.2$ and $\Omega_p=6.0.$, Two B lines correspond to $\gamma_{34}=1.0$ (dashed) and $\gamma_{34}=0.0$ (solid).

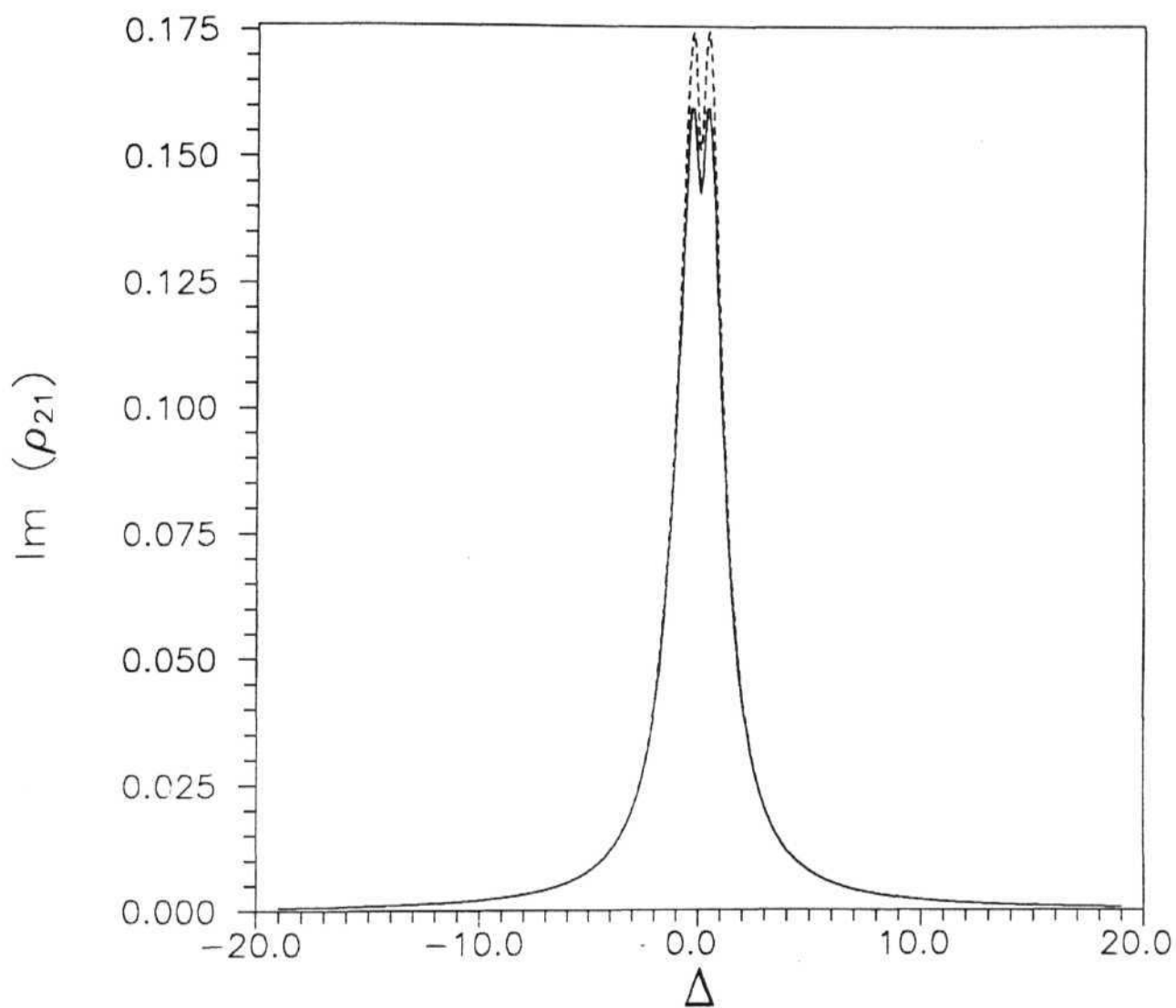


Fig. 2.4 : Analytical solution (dashes) compared with numerical result (solid) for $\Omega_s=0.2$, $\Omega_p=0.2$

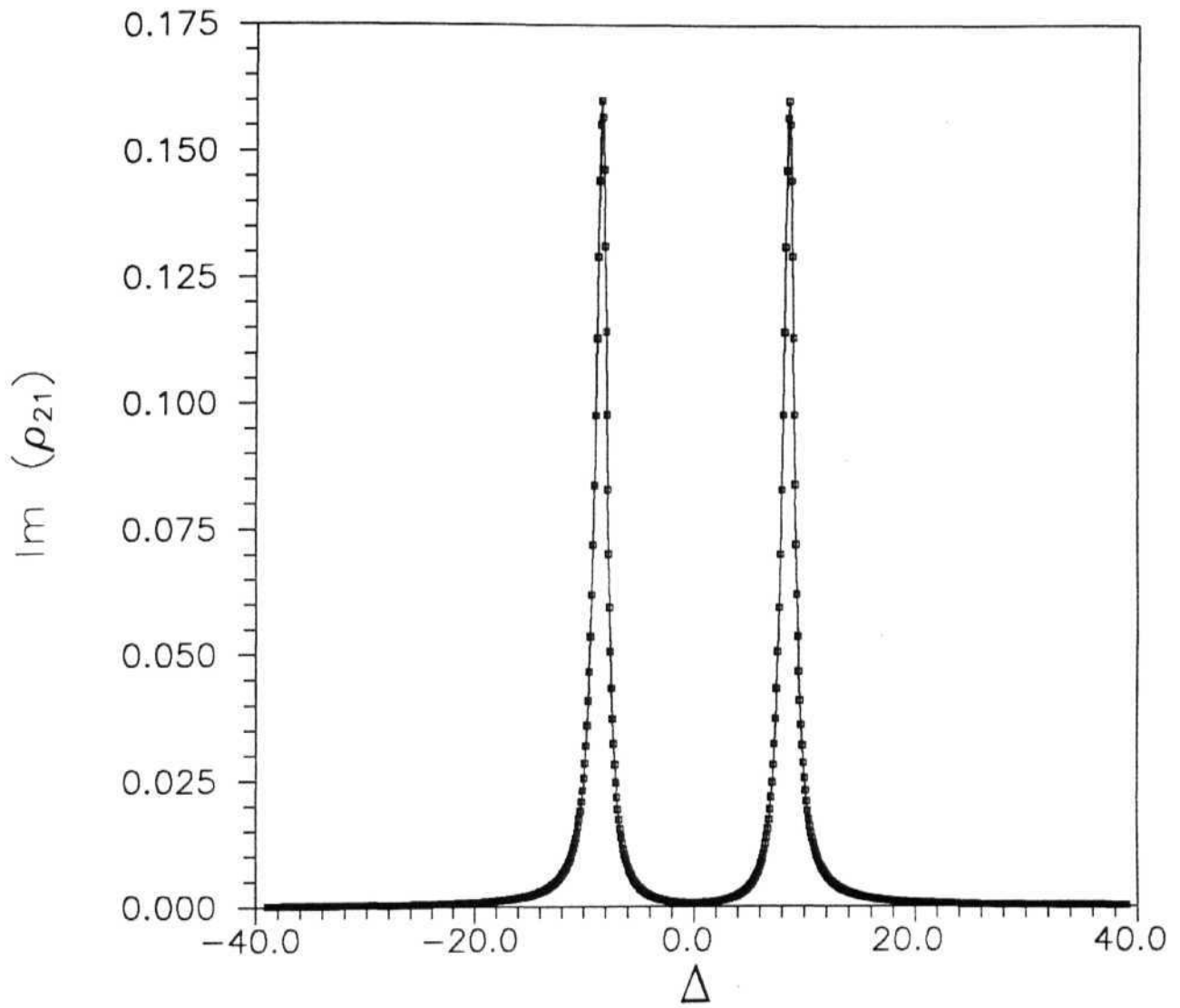


Fig. 2.5 : Analytical result (symbols) compared with numerical result (line) for $\Omega_s=0.2$, $\Omega_p=6.0$

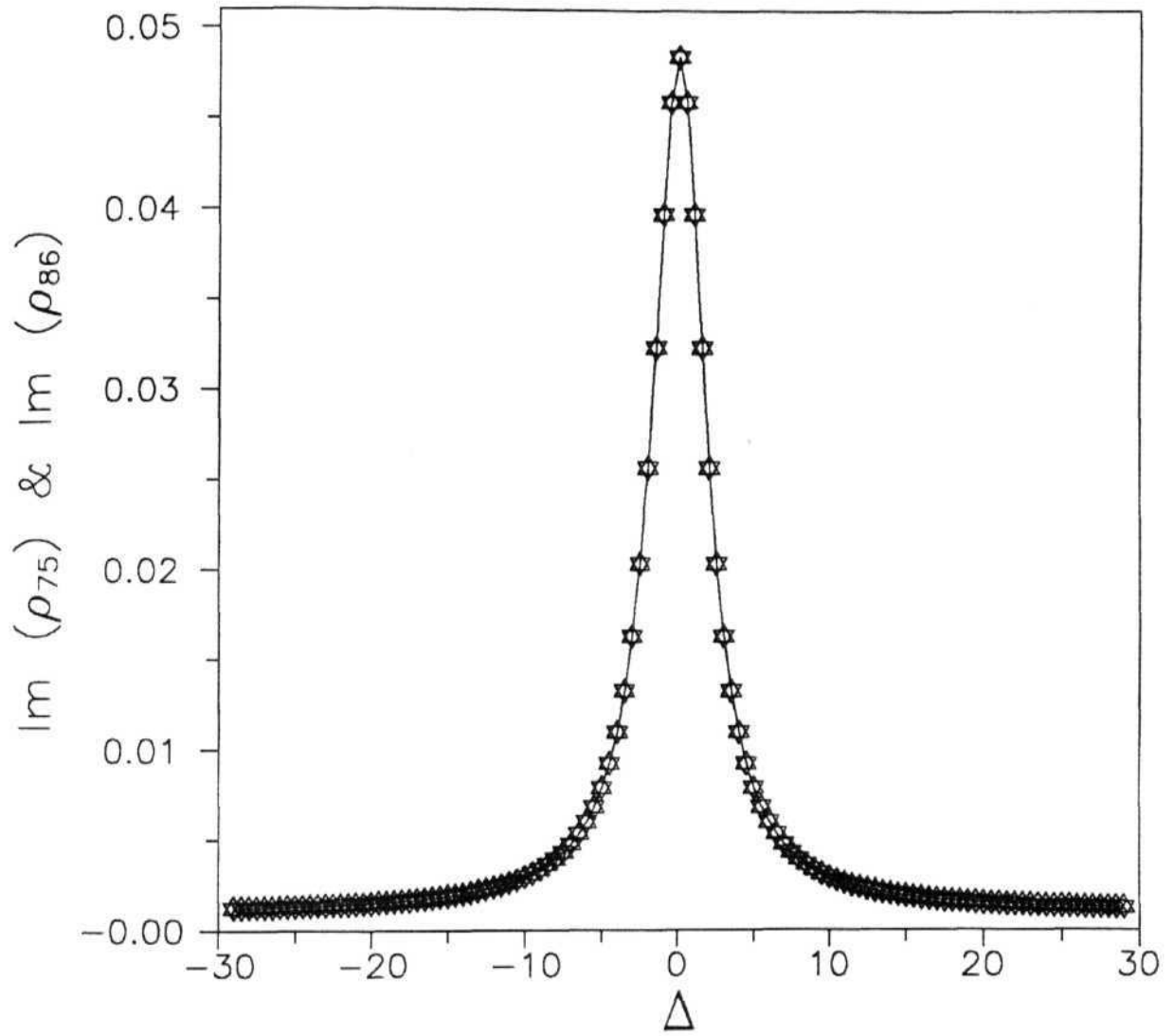


Fig. 2.7 (a): Absorption of probe $\text{Im } \rho_{75}$ (line) and $\text{Im } \rho_{86}$ (symbols) for $\Omega_s = \Omega_p = 0.2$ for Gate system.

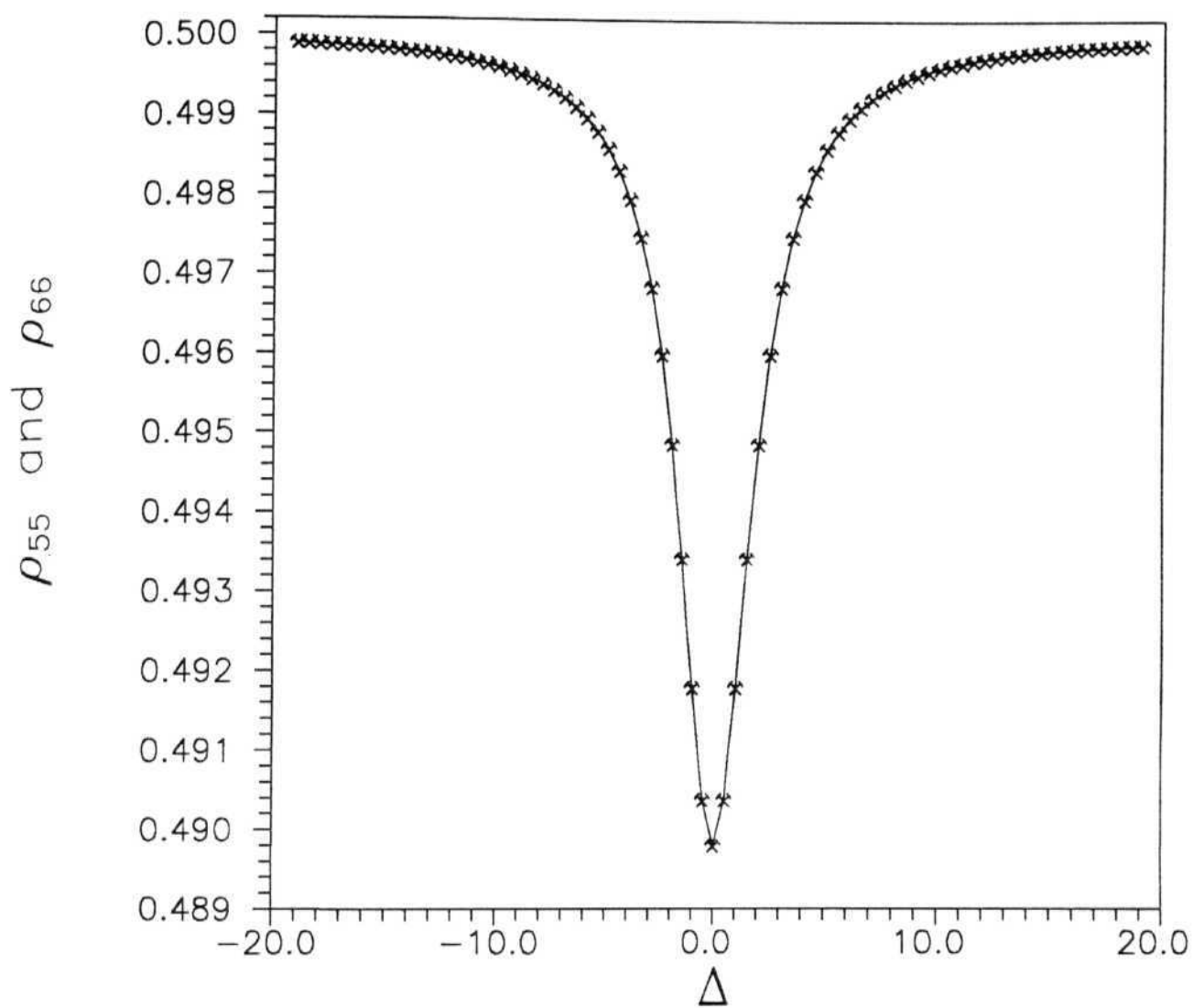


Fig. 2.7 (b): Population of levels 5 (line) and 6 (symbols), for $\Omega_s = \Omega_s = 0.2$.

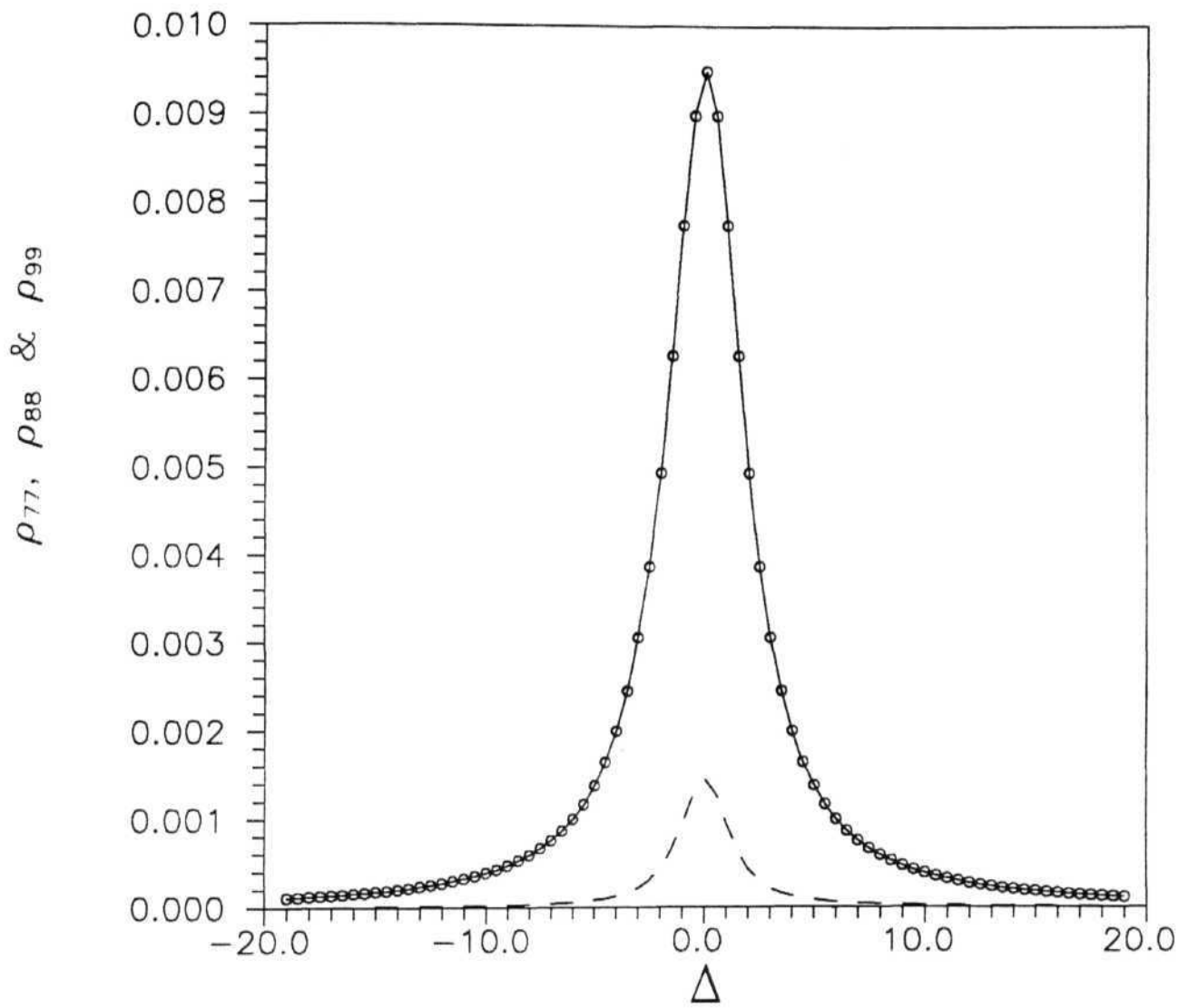


Fig. 2.7 (c): Populations for levels 7 (solid line), 8 (symbols) and 9 (dashed line) for $\Omega_s = \Omega_p = 0.2$.

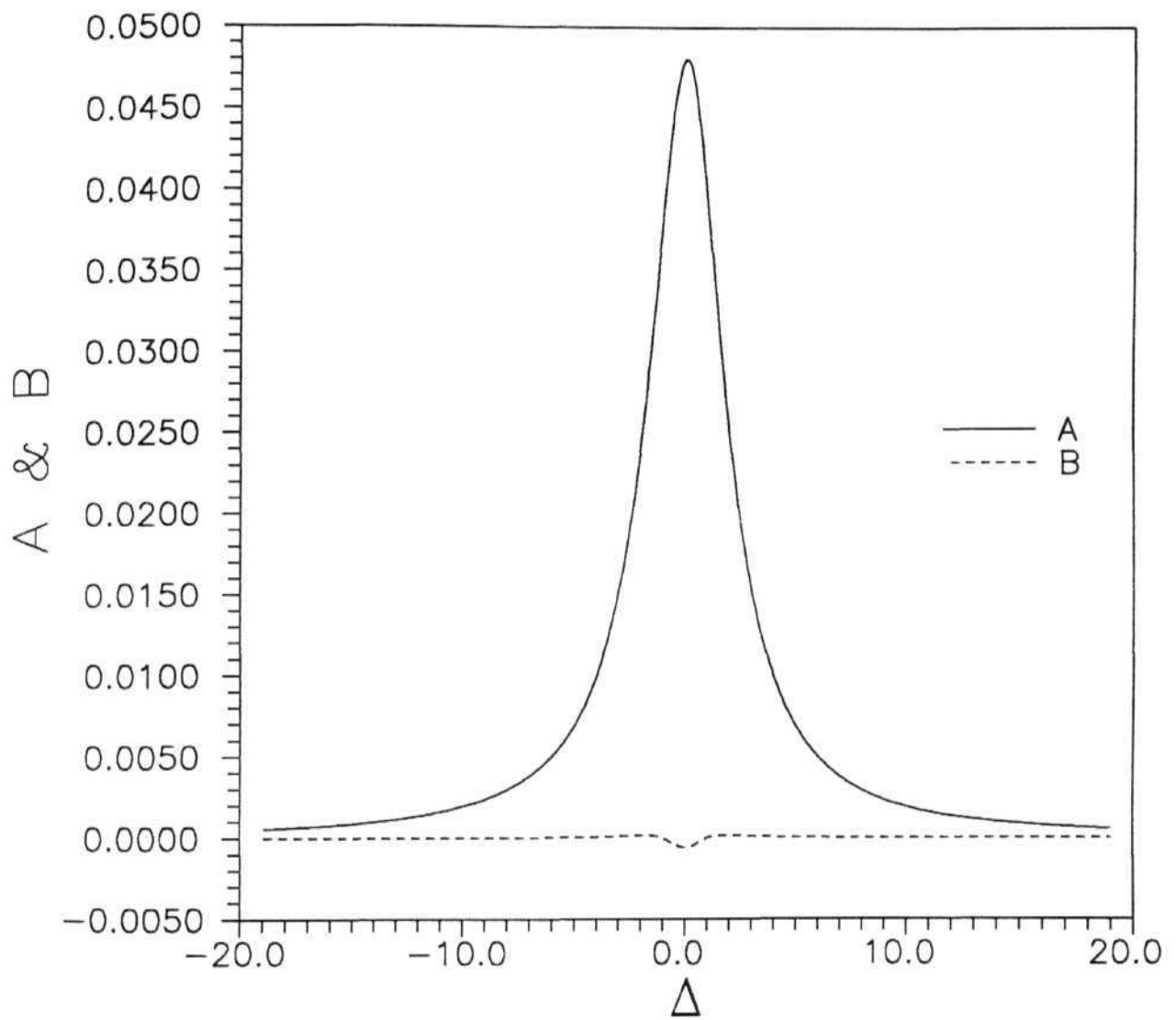


Fig. 2.7 (d): Factors A and B (See text for explanation)
for $\Omega_s=0.2$, $\Omega_p=0.2$

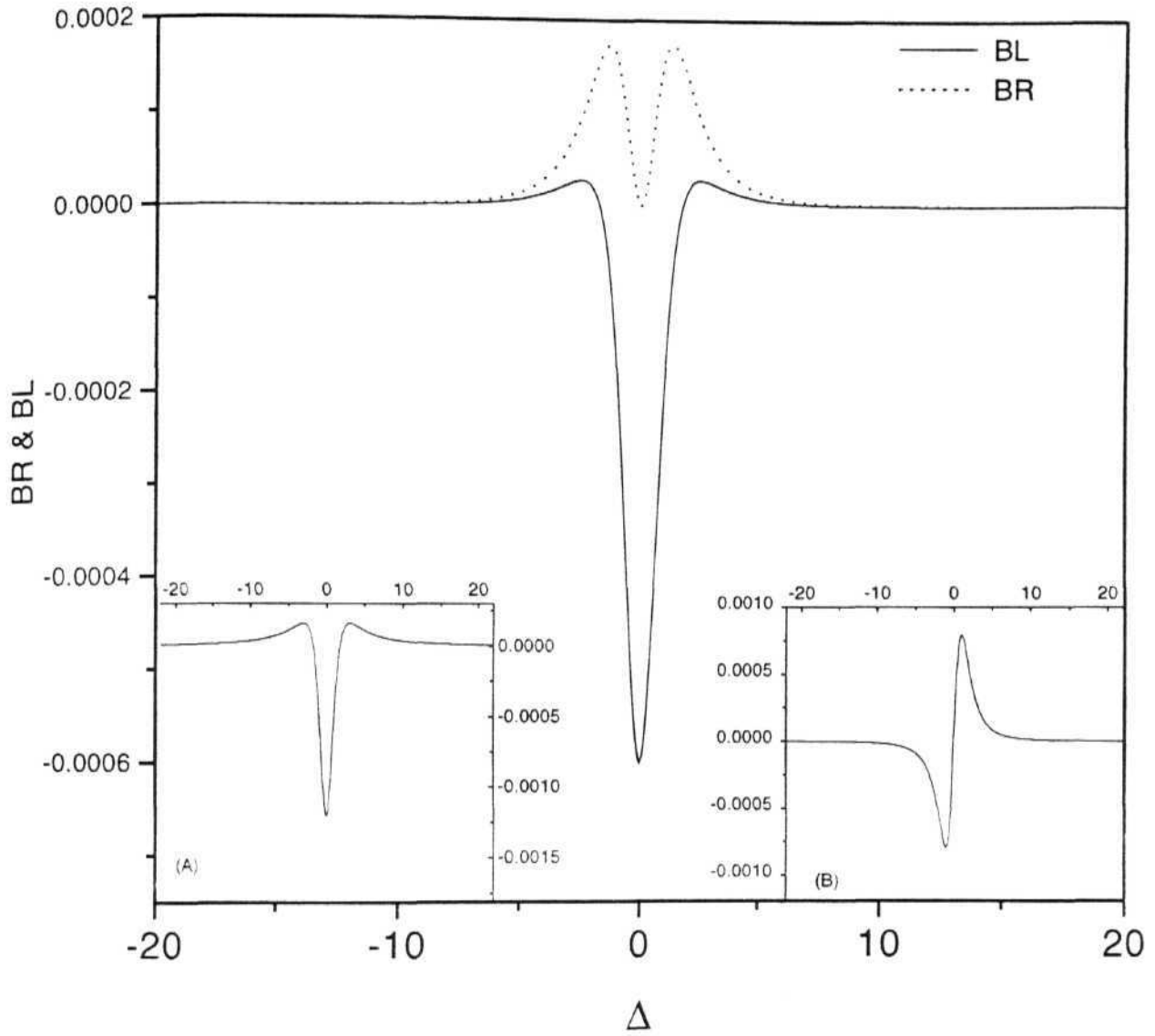


Fig. 2.7 (e): Factors BR and BL for $\Omega_s=0.2$ and $f_l=0.2$. Insets (A) and (B) show $\text{Re}(\rho_{95})$ and $\text{Im}(\rho_{95})$ respectively.

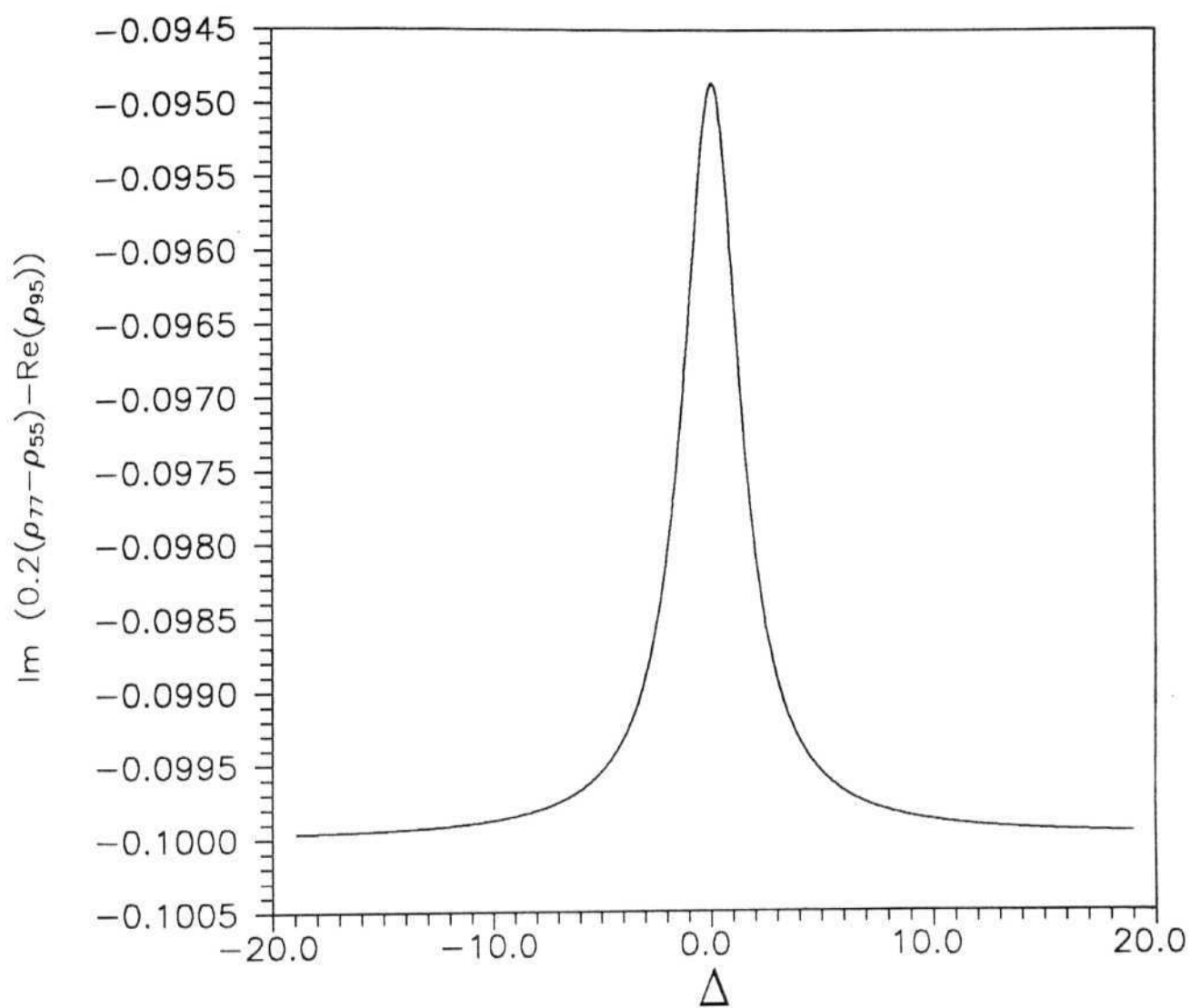


Fig. 2.7 (f): $\text{Im} (0.2(\rho_{77} - \rho_{55}) - \text{Re}(\rho_{95}))$ for $\Omega_s=0.2$ and $\Omega_p=0.2$.

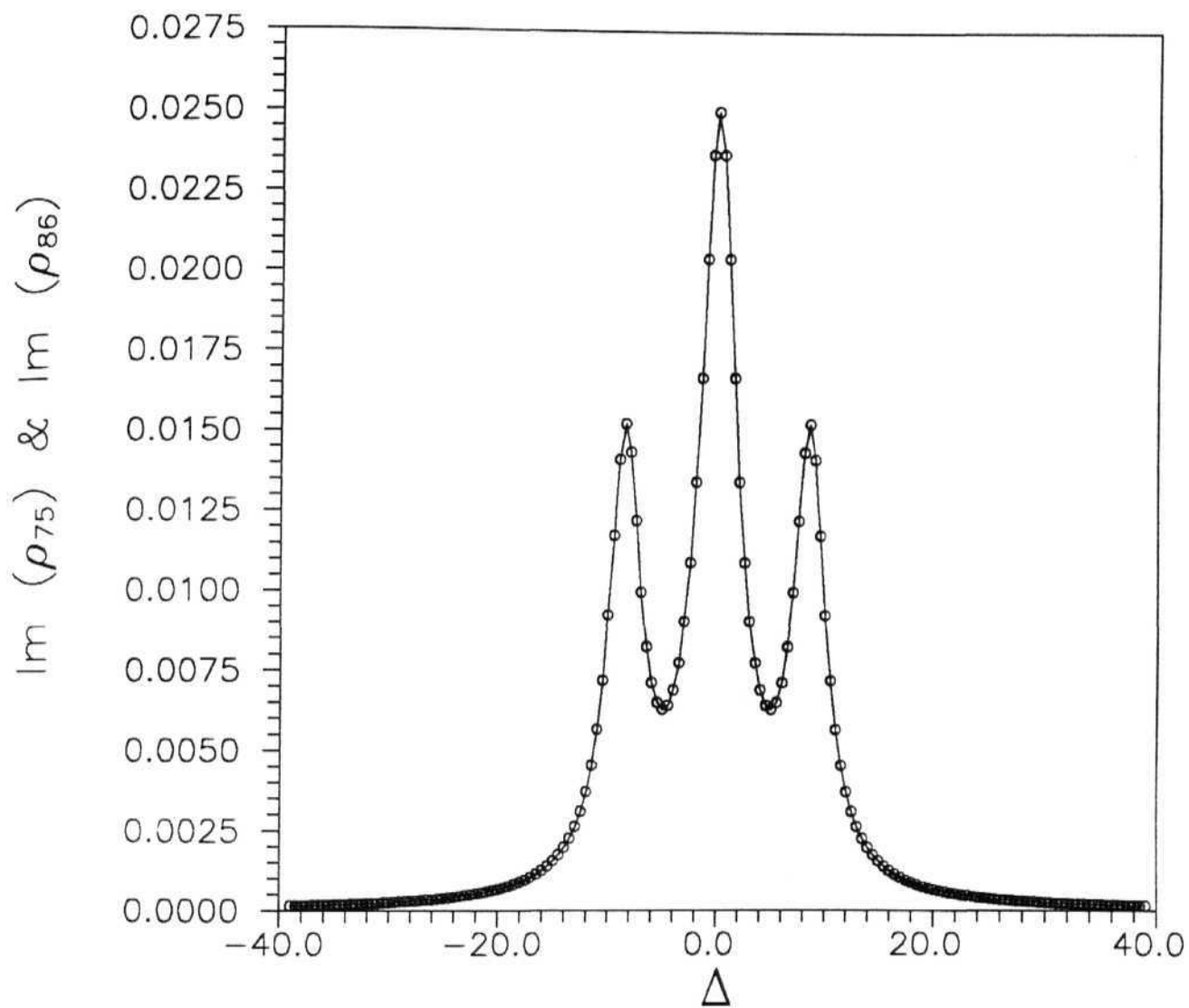


Fig. 2.8 (a): Probe absorption for $\Omega_s=0.2$ and $\Omega_p=6.0$.
solid line for $\text{Im}(\rho_{75})$, symbols for $\text{Im}(\rho_{86})$

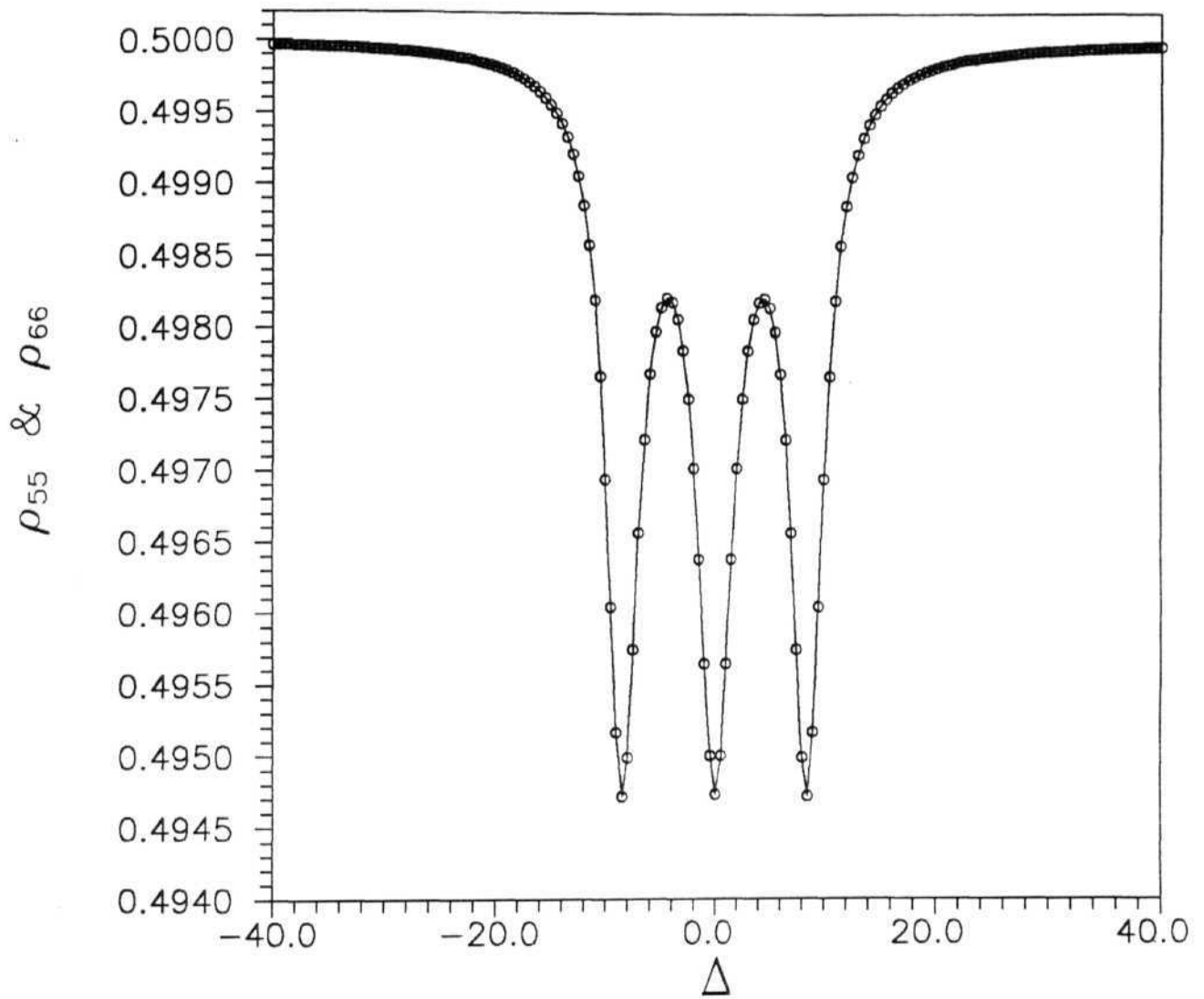


Fig. 2.8 (b): Population of levels 5 (line) and 6 (symbols) for $\Omega_s=0.2$ and $\Omega_p=6.0$.

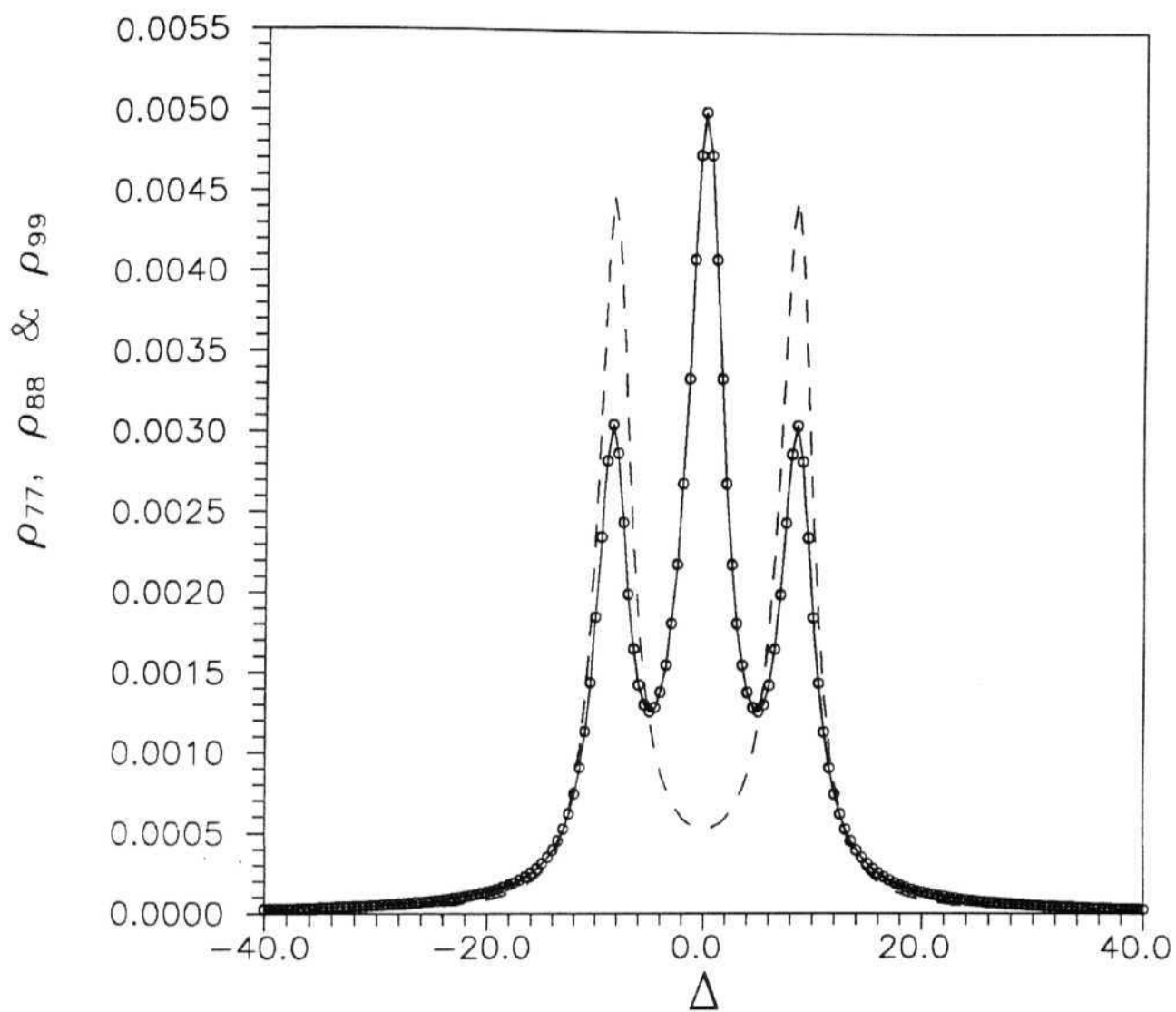


Fig. 2.8 (c): Population of levels 7 (solid line), 8 (symbols) and 9 (dashed line) for $\Omega_s=0.2$ and $\Omega_p=6.0$.

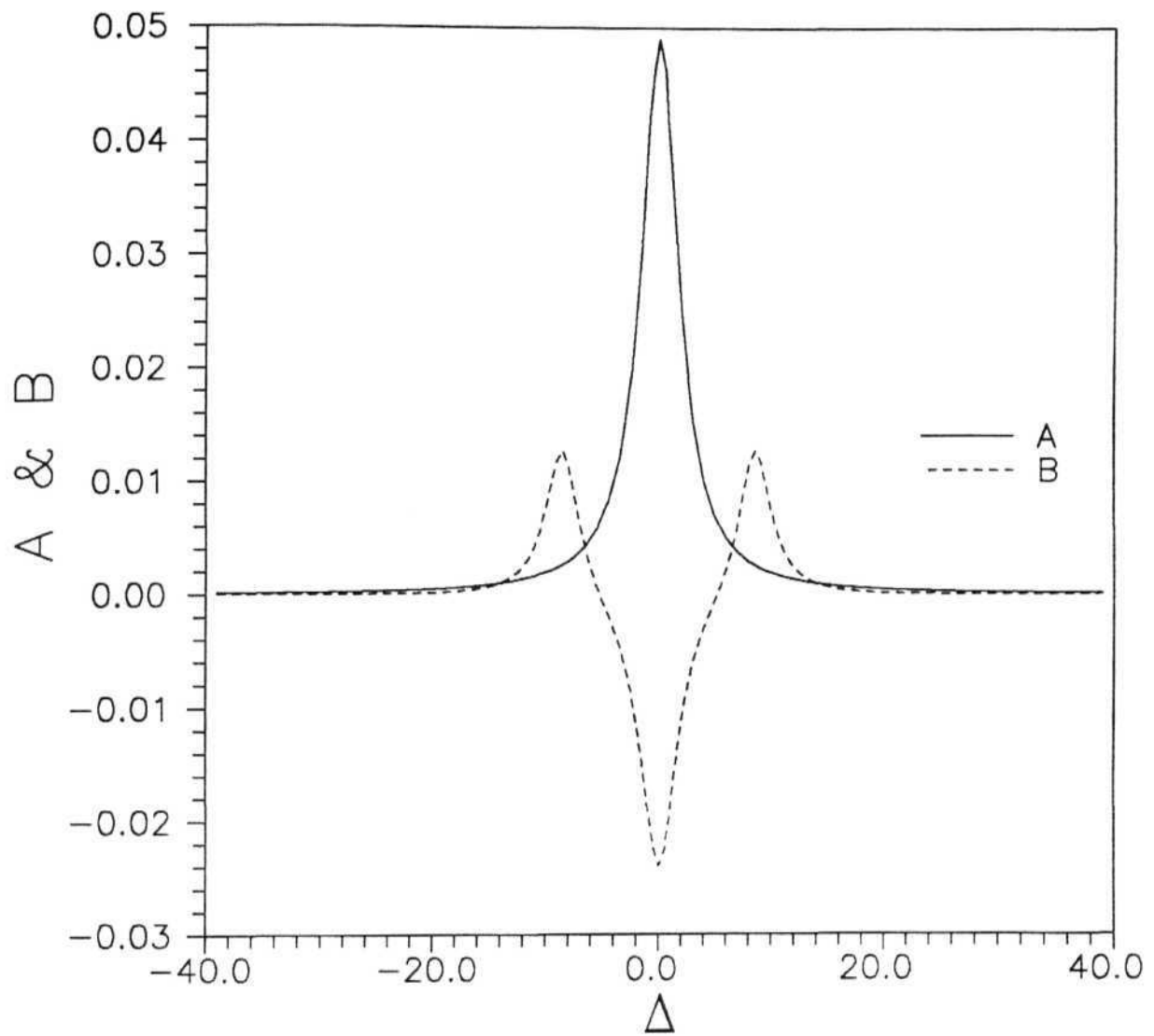


Fig. 2.8 (d): Factors A and B (See text for explanation)
for $\Omega_s=0.2$, $\Omega_p=6.0$

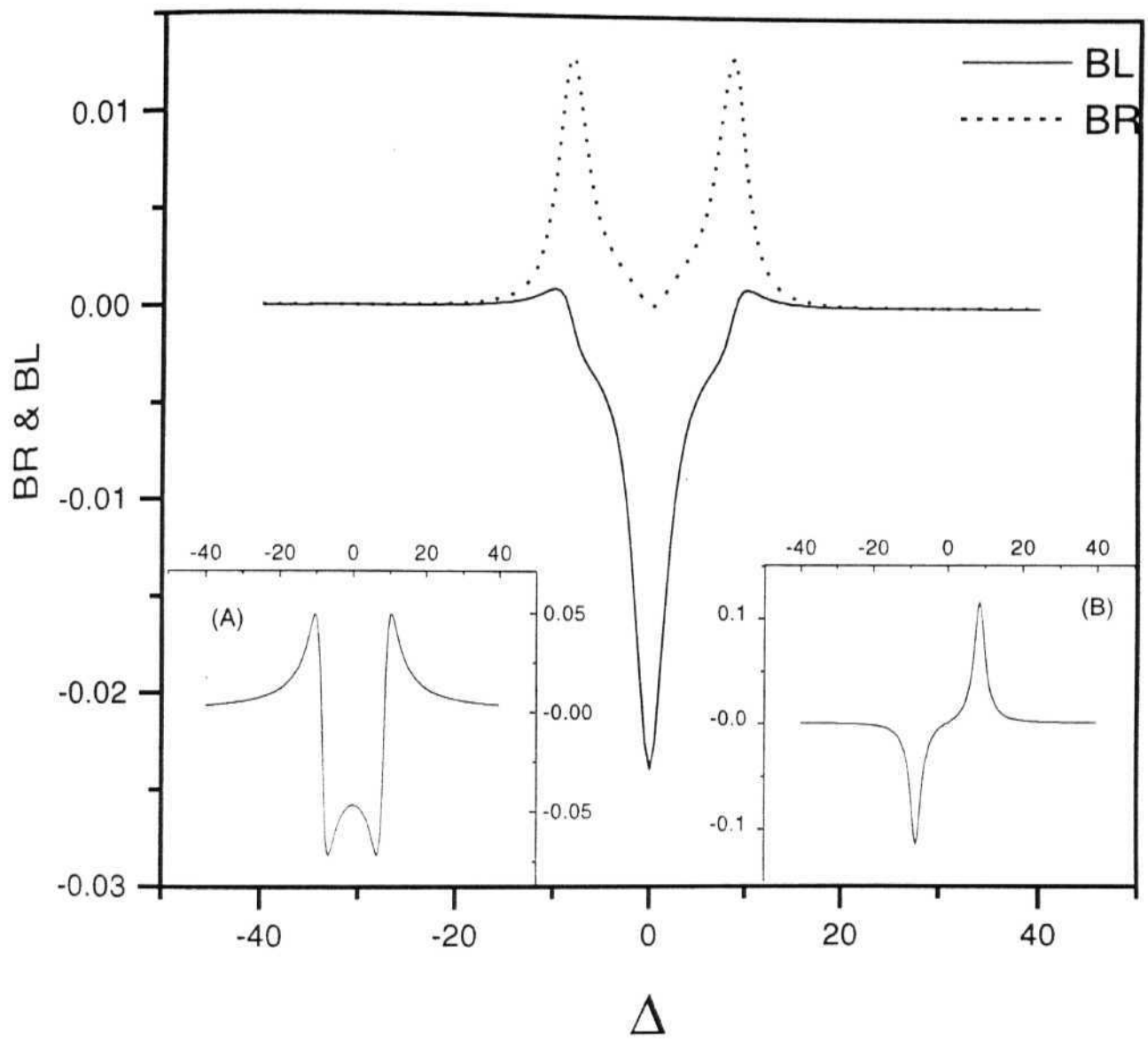


Fig. 2.8 (e): Factors BR and BL for $ft_s=0.2$ and $\Omega_p=6.0$. Insets (A) and (B) show $\text{Re}(\rho_{95})$ and $\text{Im}(\rho_{95})$ respectively.

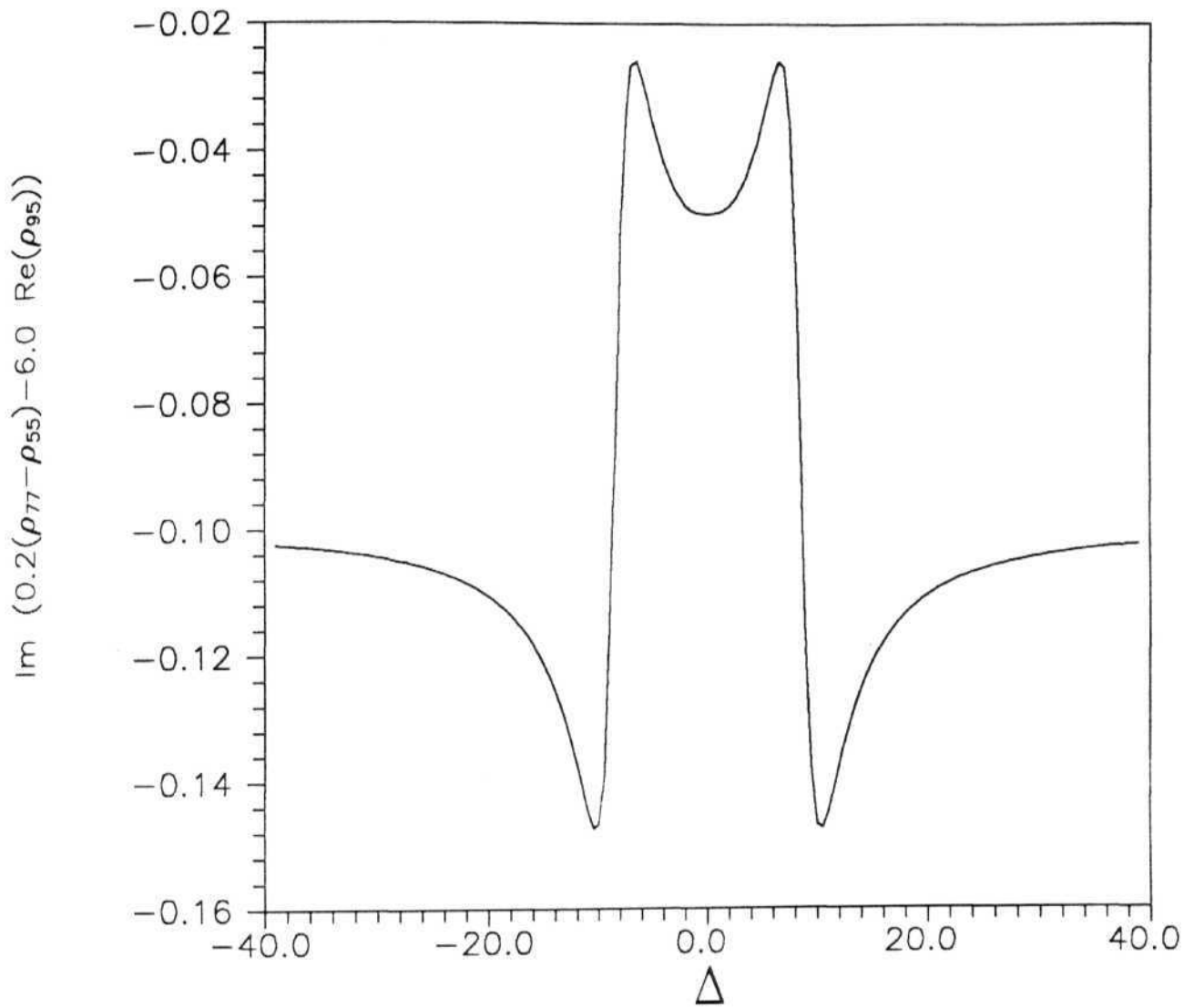


Fig. 2.8 (f): $\text{Im} (0.2(\rho_{77}-\rho_{55})-6.0 \text{Re}(\rho_{95}))$ for $\Omega_s=0.2$
and $\Omega_p=6.0$.

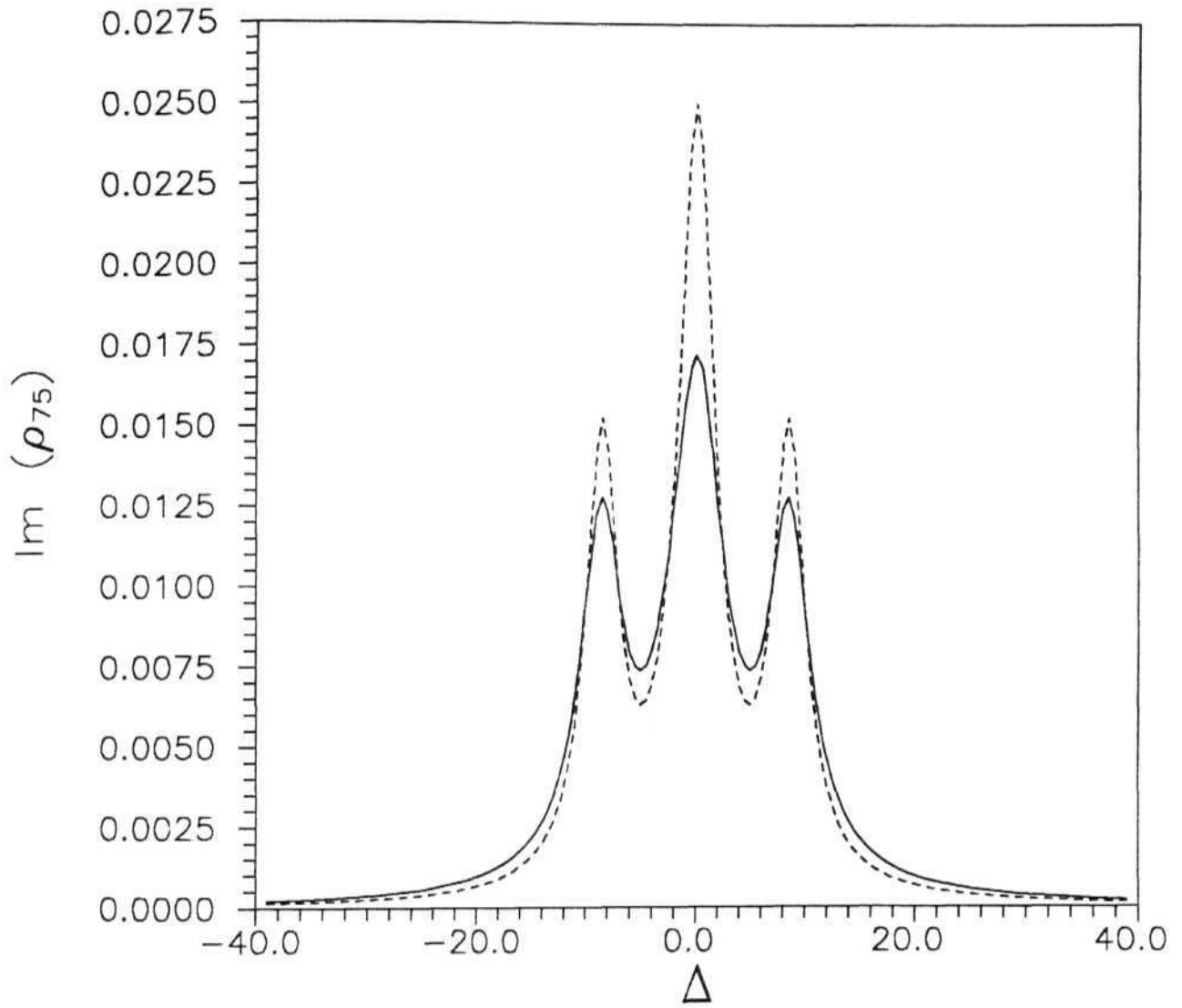


Fig. 2.8(g): Probe absorption for $\gamma_{78}=0.0$ (dashed line) and $\gamma_{78}=1.0$ (solid line) for $\Omega_s=0.2$, $\Omega_p=6.0$

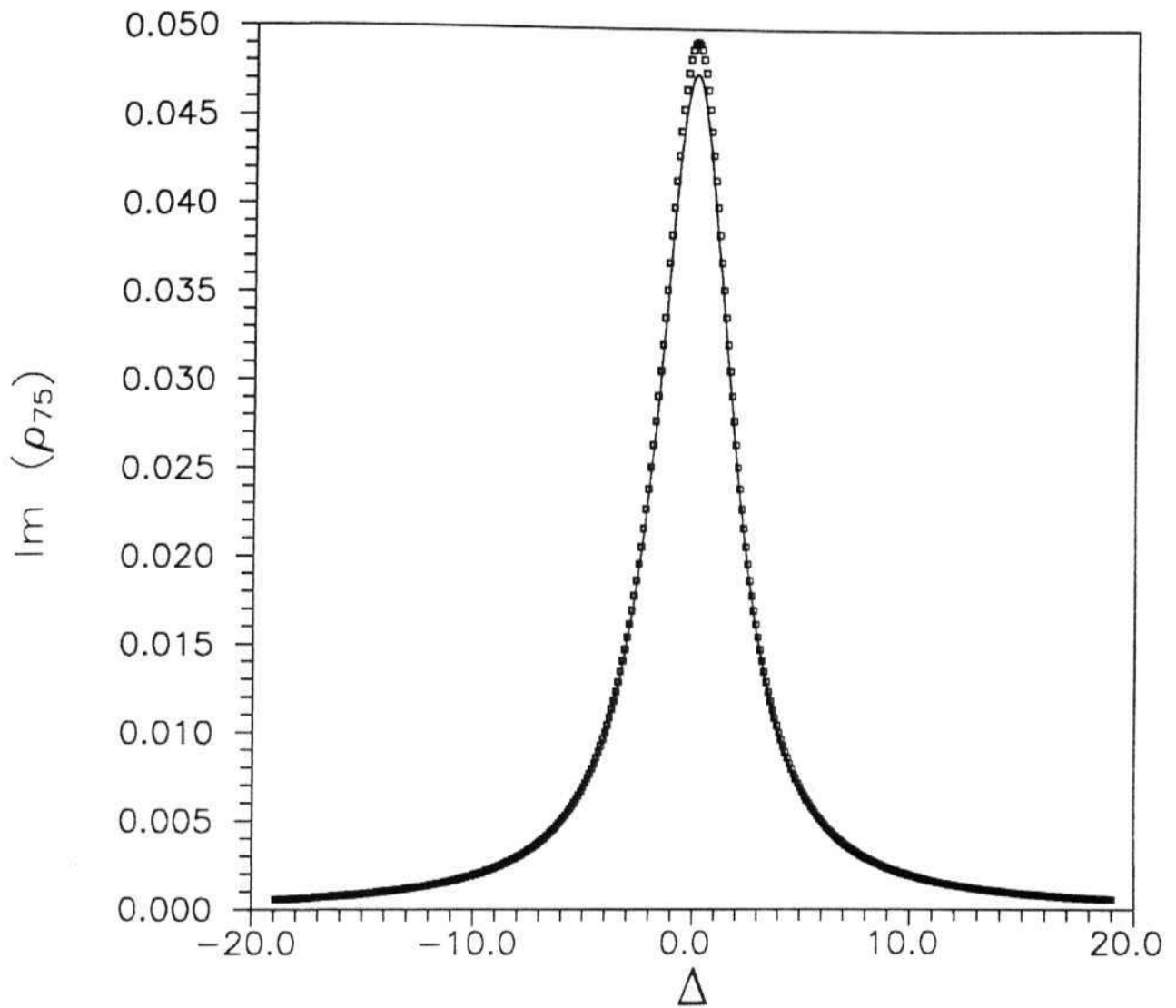


Fig. 2.9 (a): Analytical solution (symbols) compared with numerical solutions (line) for $\Omega_s=0.2$, $\Omega_p=6.0$

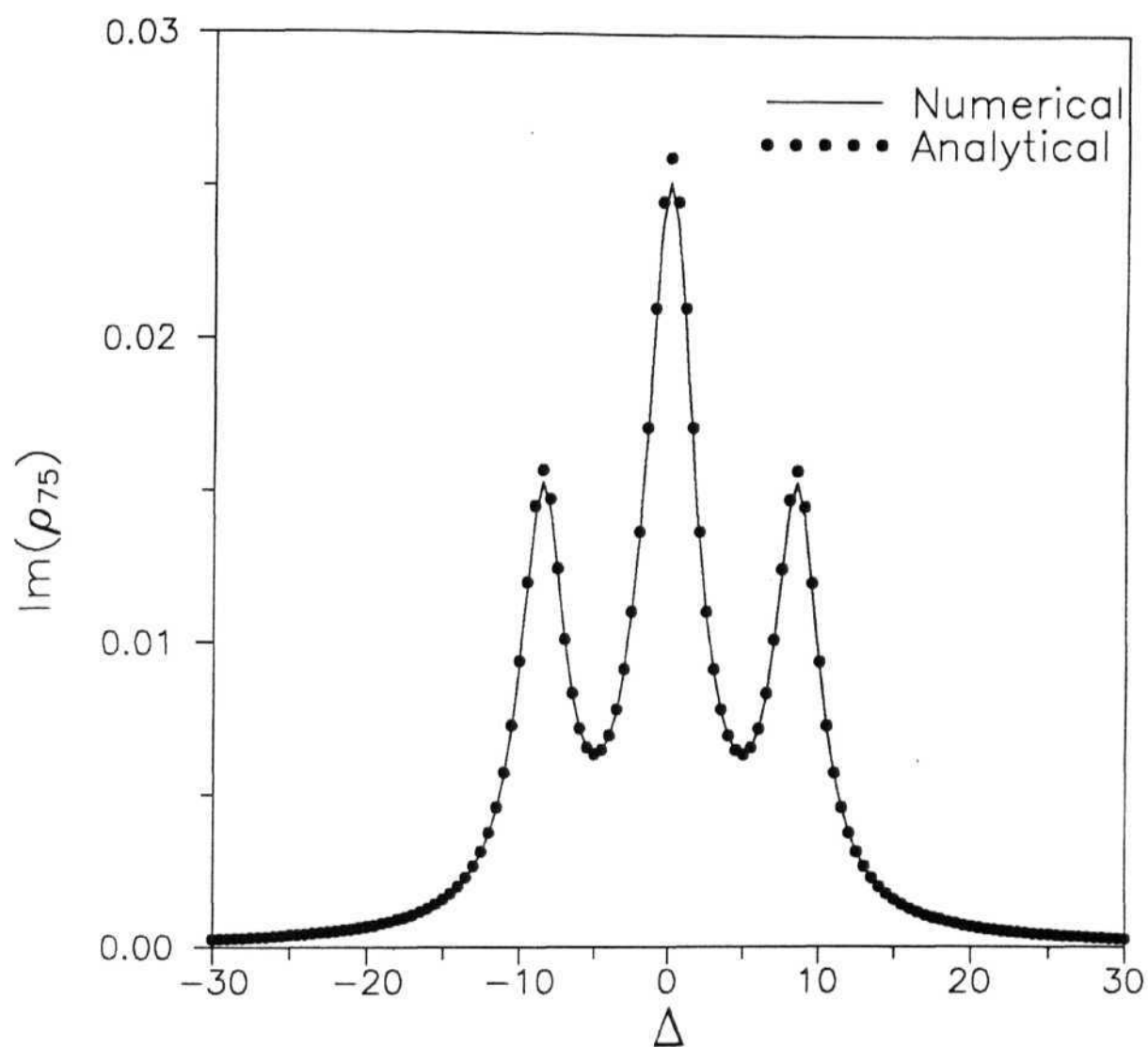


Fig. 2.9(b): Comparison of analytical solution (symbols) with the numerical solution (solid line) for $\Omega_s=0.2$ and $\Omega_p=6.0$

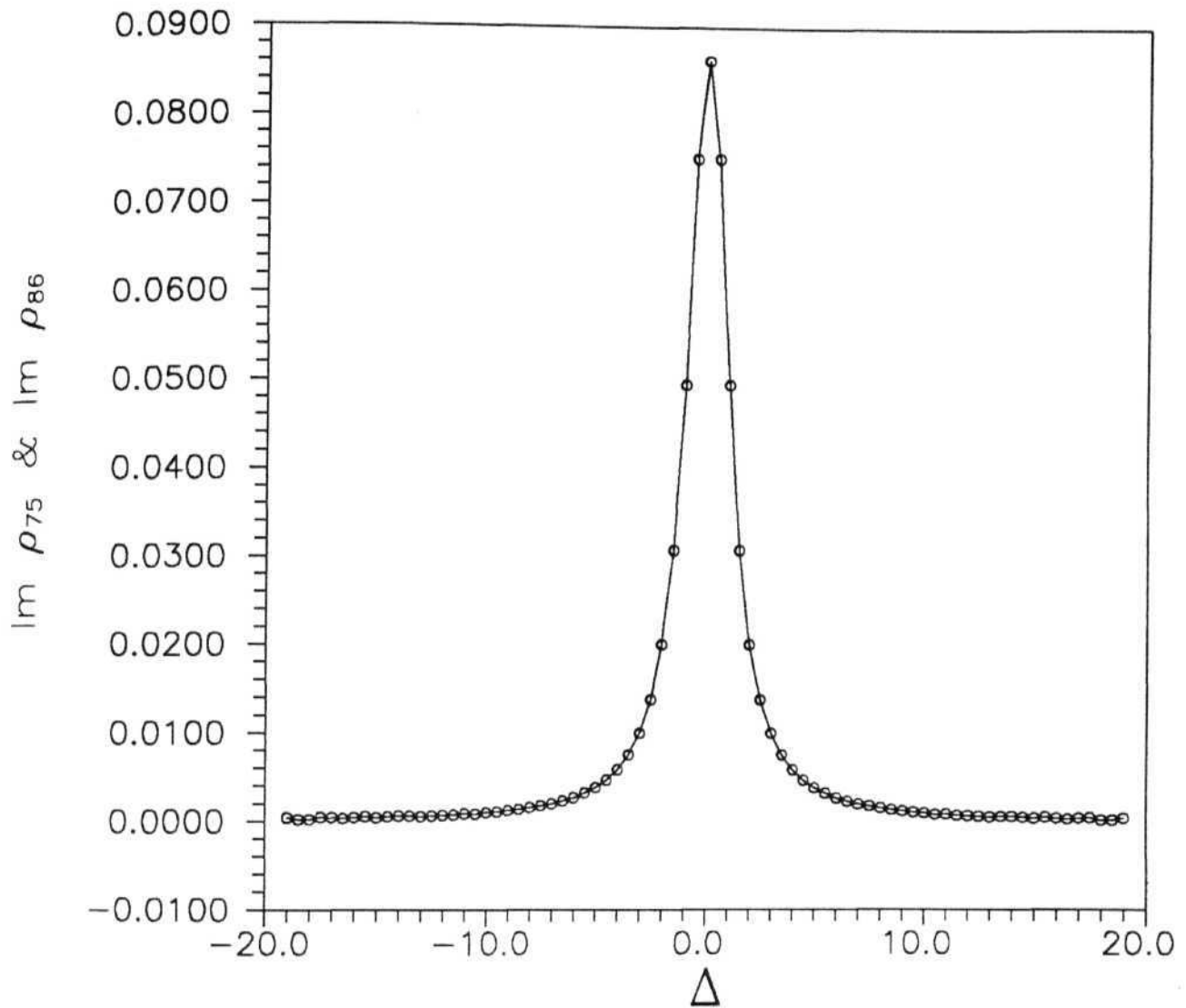


Fig. 2.10: Probe absorption, $\text{Im } (\rho_{75})$ (line), $\text{Im } (\rho_{86})$ (symbols) for $\Omega_s = \Omega_p = 0.2$, $\gamma_{56} = \gamma_{65} = 0.0$. It shows very little variation from $\gamma_{56} = \gamma_{65} = 1.0$ case (figure 2.7 a).

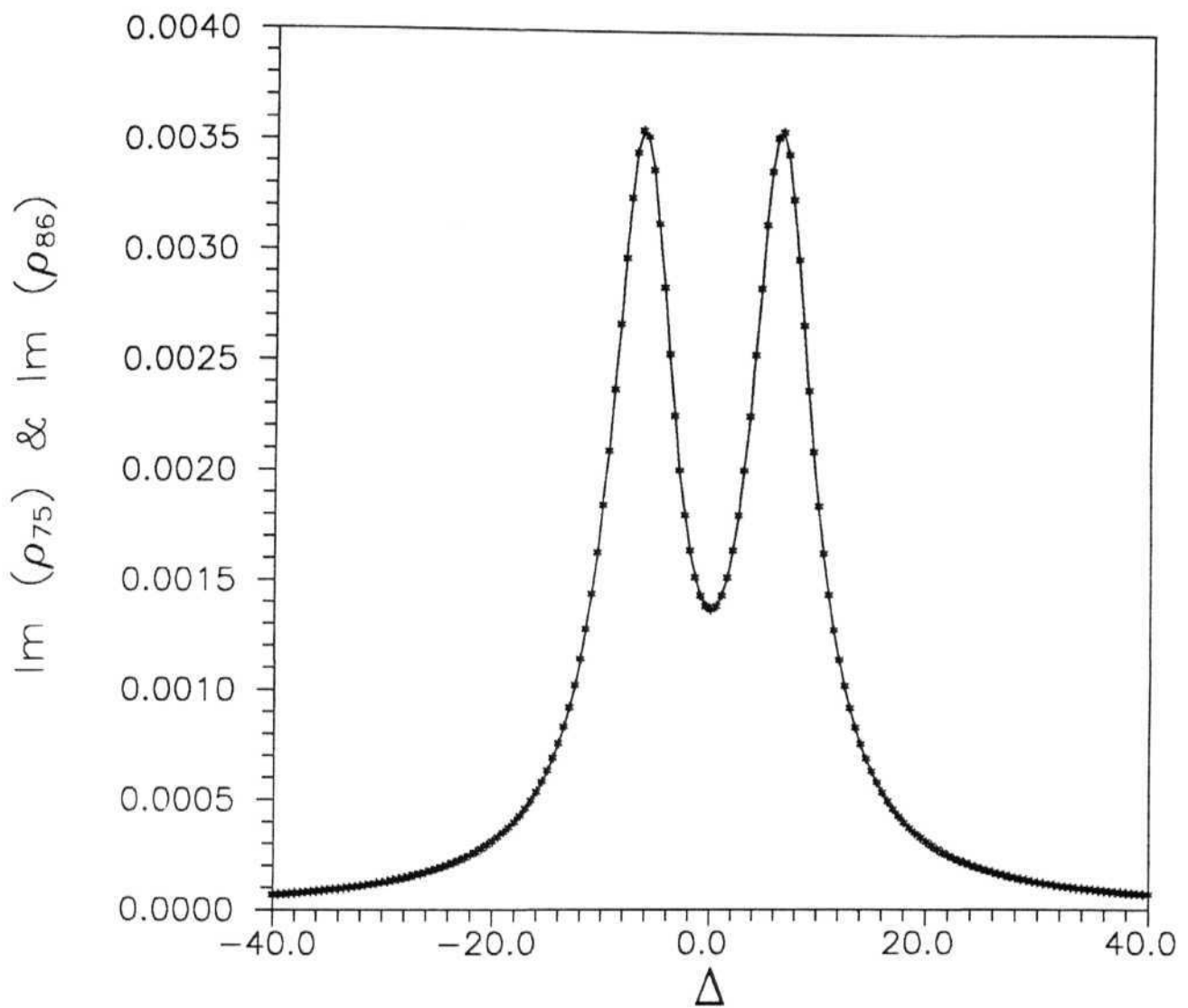


Fig. 2.11: Probe absorption for $\Omega_s=0.2$ and $\Omega_p=6.0$. solid line for $\text{Im}(\rho_{75})$, symbols for $\text{Im}(\rho_{86})$ for $\gamma_{56}=\gamma_{65}=0.0$. Note that the central peak of figure 2.8 a is absent.

References

- [1] A. S. Zibrov, M. D. Lukin, D. E. Nikonov, L. Holleberg, M. O. Scully, V. L. Velichansky and H. G. Robinson, *Phys. Rev. Lett.* 75, 1499 (1995)
- [2] J. Gao, C. Guo, X. Guo, G. Jin, P. Wang, J. Zho, H. Zhang, Y. Jiang, D. Waig, D. Jiang, *Opt. Comm.* 93, 323 (1992)
- [3] M. Fleischhauer, C. H. Keitel, L. M. Narducci, M. O. Scully, S. -Y. Zhu and M. S. Zubairy, *Opt. Comm.* 94, 599 (1992)
- [4] G. S. Agarwal *Springer Tracts in Modern Physics* 70, Springer Verlag, Berlin (1974)
- [5] R. M. Whitely, C. R. Stroud Jr. *Phys. Rev. A* 14, 1498 (1976)
- [6] Y-q Li and M. Xiao, *Phys. Rev. A* 51, 4959 (1995)
- [7] Alan Corney, *"Atomic and Laser Spectroscopy"*, Clarendon, Oxford 1977, pp 107
- [8] Martin, C.E. & Sandeman, R.J., *Phys. Scripta*, 22, 373 (1980)
- [9] C. Cohen-Tannoudji and S. Reynaud, *J. Phys. B* 10 345, (1976)

Chapter III

Dressed state analysis

*A study of **Y** and **Gate** is presented in the wave function approach. Diagonalization of **the** interaction Hamiltonian leads to 'Dressed States'. Results for probe absorption in the long-time limit are obtained in both 'Bare states' and 'Dressed States'. These two solutions are shown to match with each other for both **Y** and **Gate** cases. Also, they match with the results of density matrix solutions obtained in previous chapter. A straightforward description for the behaviour of **Y** and **Gate** schemes is evident in the dressed state picture.*

3.1 Semiclassical Dressed States

A 'Dressed State' approach to solving light-atom interaction involves using eigenstates of the complete Hamiltonian which contains both bare atom and the interaction terms with the dressing field. The new eigenstates thus obtained are termed 'Dressed states' and the atom is visualized to be *dressed* by the surrounding photons [1]. Eigenstates of the atomic hamiltonian in absence of 'dressing' field are termed 'Bare States'. 'Semiclassical Dressed States' are those dressed states obtained by using a Semiclassical picture of light-atom interaction [2]. These new states are coherent superposition of bare states. Their energies are Stark shifted from those of the bare states by an amount proportional to Rabi frequencies of the interaction. This new energy structure becomes

relevant when the dressed states are shifted beyond the linewidths of bare states. Therefore, 'Dressed State' picture is appropriate when strong 'dressing' fields are involved. In this case, Rabi frequency Ω of the interaction is larger than the decay constant γ , which determines the linewidth.

Analysis of **Y** and **Gate** configurations in this chapter are presented as follows. At first the behaviour of Y configuration is studied in the wavefunction picture without resorting to the dressed states. The probe absorption behaviour is shown to be equivalent to the results from density matrix formalism. Dressed states formed by the pump beam are obtained and the interaction of probe beam between these states and the ground states are analysed. Effect of Quantum Interference between spontaneous emission pathways is investigated. The study of Gate system is then presented in the same manner.

3.2 Y configuration

3.2.1 Bare state analysis

The state vector in the four-dimensional Hilbert space for the Y system is written as

$$|\psi\rangle = C_1|1\rangle + C_2|2\rangle + C_3|3\rangle + C_4|4\rangle$$

The Hamiltonian of the system is the same as the one used in previous chapter,

which, in $\hbar = 1$ units, is

$$\mathcal{H} = \begin{pmatrix} \omega_1 & -d_{21} \cdot E_s & 0 & 0 \\ -d_{21} \cdot E_s & \omega_2 & -d_{32} \cdot E_p & -d_{42} \cdot E_p \\ 0 & -d_{32} \cdot E_p & \omega_3 & 0 \\ 0 & -d_{42} \cdot E_p & 0 & \omega_4 \end{pmatrix}$$

where, d_{ij} is the the dipole moment of the transition between i and j and ω_i is the energy eigenvalue of the i^{th} level in radian frequency.

Using them in Schrödinger equation $i\partial_t|\psi\rangle = \mathcal{H}|\psi\rangle$, and after suitable transformations the equations for the probability amplitudes are obtained as

$$\partial_t C_4 = [i(\Delta_{42} + \Delta_{21}) - \gamma_{42}]C_4 + id_{42} \cdot \mathcal{E}_p^- C_2, \quad (3.1)$$

$$\partial_t C_3 = [i(\Delta_{32} + \Delta_{21}) - \gamma_{32}]C_3 + id_{32} \cdot \mathcal{E}_p^+ C_2, \quad (3.2)$$

$$\partial_t C_2 = (i\Delta_{21} - \gamma_{21})C_2 + id_{42}^* \cdot \mathcal{E}_p^- C_4 + id_{32}^* \cdot \mathcal{E}_p^+ C_3 + id_{21} \cdot \mathcal{E}_s C_1, \quad (3.3)$$

$$\partial_t C_1 = id_{21}^* \cdot \mathcal{E}_s^* C_2. \quad (3.4)$$

The detunings are defined as

$$\Delta_{21} = \omega_2 - \omega_1 - \omega_s,$$

$$\Delta_{32} = \omega_3 - \omega_2 - \omega_p,$$

and

$$\Delta_{42} = \omega_4 - \omega_2 - \omega_p$$

γ_{ij} are the rates of decay from level j to level i **which are** added here in a manner

following Harris and coworkers [5, 6] §,

For a large value of $i\Delta_{21} - \gamma_{42}$ and $i\Delta_{21} - \gamma_{32}$, the time derivatives on the LHS of 3.1 and 3.2 can be assumed negligible and hence set to zero. Solutions of C_3 and C_4 obtained from such a procedure is substituted into equation 3.3. By setting the LHS of 3.3 also equal to zero, the solution for C_2 is obtained in the form

$$C_2 = \frac{-id_{21} \cdot \mathcal{E}_s C_1}{[i\Delta_{21} - \gamma_{12}] + \frac{|d_{42} \cdot \mathcal{E}_p^-|^2}{i(\Delta_{42} + \Delta_{21}) - \gamma_{24}} + \frac{|d_{32} \cdot \mathcal{E}_p^-|^2}{i(\Delta_{32} + \Delta_{21}) - \gamma_{23}}}.$$

Substituting this in equation 3.4

$$\partial_t C_1 = - \frac{|d_{21} \cdot \mathcal{E}_s|^2}{[i\Delta_{21} - \gamma_{12}] + \frac{|d_{42} \cdot \mathcal{E}_p^-|^2}{i(\Delta_{42} + \Delta_{21}) - \gamma_{24}} + \frac{|d_{32} \cdot \mathcal{E}_p^-|^2}{i(\Delta_{32} + \Delta_{21}) - \gamma_{23}}} C_1. \quad (3.5)$$

This shows that the time evolution of the amplitude C_1 is governed by the probe beam coupling $|d_{21} \cdot \mathcal{E}_s|^2$. The time evolution of population in levels $|1\rangle$ is then given by

$$\begin{aligned} \partial_t |C_1|^2 &= C_1 \partial_t C_1^* + \partial_t C_1 C_1^* \\ &= -|d_{21} \cdot \mathcal{E}_s|^2 \left[\frac{1}{D} + \frac{1}{D^*} \right] |C_1|^2 \end{aligned} \quad (3.6)$$

Where,

$$D = [i\Delta_{21} - \gamma_{12}] + \frac{|d_{42} \cdot \mathcal{E}_p^-|^2}{i(\Delta_{42} + \Delta_{21}) - \gamma_{24}} + \frac{|d_{32} \cdot \mathcal{E}_p^-|^2}{i(\Delta_{32} + \Delta_{21}) - \gamma_{23}}$$

and D^* is its complex conjugate.

§A detailed derivation of spontaneous emission decay is discussed in a later section.

It is seen that **population** loss from level $|1\rangle$ is only due the coherent process involving probe beam. Therefore, **the** probe beam absorption can be assumed equivalent to loss of population of level $|1\rangle$. It can also be noted that the denominator D is identical to the denominator of the analytical solution of $\rho_{21}^{(1)}$ which is obtained in Chapter II.

Solution of 3.6 is then

$$|C_1|^2(t) = \exp \left\{ -|d_{21} \cdot \mathcal{E}_s|^2 \left[\frac{1}{D} + \frac{1}{D^*} \right] t \right\} |C_1|^2(0) \quad (3.7)$$

Where $|C_1|^2(0)$ is the population of level $|1\rangle$ at initial time $t = 0$. The absorption coefficient $\beta = |d_{21} \cdot \mathcal{E}_s|^2 \left[\frac{1}{D} + \frac{1}{D^*} \right]$ is plotted in figure 3.1 as a function of detuning Δ_{21} for the same parameters used in Chapter II. i.e., $f_{21} = 0.2$ and $\Omega_{32} = \Omega_{42} = 6.0$. The profile of this factor is identical to the probe absorption behaviour obtained in Chapter II for the Y system.

3.2.2 Dressed State picture

Grouping the equations 3.1-3.4 in the form

$$\begin{aligned} \partial_t \begin{pmatrix} C_4 \\ C_3 \\ C_2 \end{pmatrix} = i \begin{pmatrix} \Delta_{42} + \Delta_{21} & 0 & d_{42} \cdot \mathcal{E}_p^- \\ 0 & \Delta_{32} + \Delta_{21} & d_{32} \cdot \mathcal{E}_p^+ \\ d_{42} \cdot \mathcal{E}_p^- & d_{32} \cdot \mathcal{E}_p^+ & 0 \end{pmatrix} \cdot \begin{pmatrix} C_4 \\ C_3 \\ C_2 \end{pmatrix} - \begin{pmatrix} \gamma_{24} & 0 & 0 \\ 0 & \gamma_{23} & 0 \\ 0 & 0 & \gamma_{12} \end{pmatrix} \cdot \begin{pmatrix} C_4 \\ C_3 \\ C_2 \end{pmatrix} \\ + \begin{pmatrix} 0 \\ 0 \\ id_{21} \cdot \mathcal{E}_s C_1 \end{pmatrix} \quad (3.8) \end{aligned}$$

and

$$\partial_t C_1 = id_{21} \cdot \mathcal{E}_s C_2.$$

Operating a transformation $\bar{C}_j = C_j \exp(-i \Delta_{21} t)$ for $j = 1, 2, 3, 4$ and setting $A_{42} = 0 = \Delta_{32}$ for simplicity, equations 3.1 - 3.4 become

$$\partial_t \begin{pmatrix} \bar{C}_4 \\ \bar{C}_3 \\ \bar{C}_2 \end{pmatrix} = i \begin{pmatrix} 0 & 0 & d_{42} \mathcal{E}_p^- \\ 0 & 0 & d_{32} \mathcal{E}_p^+ \\ d_{42} \mathcal{E}_p^- & d_{32} \mathcal{E}_p^+ & 0 \end{pmatrix} \cdot \begin{pmatrix} \bar{C}_4 \\ \bar{C}_3 \\ \bar{C}_2 \end{pmatrix} - \begin{pmatrix} \gamma_{24} & 0 & 0 \\ 0 & \gamma_{23} & 0 \\ 0 & 0 & \gamma_{12} \end{pmatrix} \cdot \begin{pmatrix} \bar{C}_4 \\ \bar{C}_3 \\ \bar{C}_2 \end{pmatrix} + \begin{pmatrix} 0 \\ 0 \\ id_{21} \mathcal{E}_s \bar{C}_1 \end{pmatrix} \quad (3.9)$$

and

$$\partial_t \bar{C}_1 = -i \Delta_{21} \bar{C}_1 + id_{21} \mathcal{E}_s \bar{C}_2$$

The above equations in the matrix notation are

$$\partial_t \bar{C} = iM\bar{C} - \gamma\bar{C} + \bar{D} \quad (3.10)$$

$$\partial_t \bar{C}_1 = -i \Delta_{21} \bar{C}_1 + id_{21} \mathcal{E}_s \bar{C}_2 \quad (3.11)$$

Where \bar{C} is the column matrix $(C_4 \ C_3 \ C_2)$ and M is the 3×3 matrix containing the $d \mathcal{E}_p^\pm$ terms. γ is the 3×3 matrix containing the decay terms and D is the column matrix consisting of the C_1 coupling term. Solving characteristic equation for the matrix M , the eigenvalues obtained are, $A = 0, \pm \alpha$, where $\alpha^2 = |d_{32} \mathcal{E}_p^+|^2 + |d_{42} \mathcal{E}_p^-|^2$

Denoting $g_{32} = d_{32} \mathcal{E}_p^+$ and $g_{42} = d_{42} \mathcal{E}_p^-$, the diagonalizing matrix S is obtained by arranging normalized eigenvectors,

$$S = \frac{1}{\alpha\sqrt{2}} \begin{pmatrix} ig_{24} & g_{23}^* \sqrt{2} & -ig_{24} \\ ig_{23} & -g_{24}^* \sqrt{2} & -ig_{23} \\ \alpha & 0 & \alpha \end{pmatrix}.$$

Carrying out the unitary transformation using S and S^\dagger ,

$$\partial_t(S^\dagger \bar{C}) = iS^\dagger M S S^\dagger \bar{C} - S^\dagger \gamma S S^\dagger \bar{C} + S^\dagger D$$

gives

$$\partial_t \Psi_D = iM_D \Psi_D - \Gamma_D \Psi_D + D_D, \quad (3.12)$$

where

$$\Psi_D = \begin{pmatrix} \Psi_1 \\ \Psi_2 \\ \Psi_3 \end{pmatrix} = S^\dagger \cdot \begin{pmatrix} \bar{C}_4 \\ \bar{C}_3 \\ \bar{C}_2 \end{pmatrix}, \quad M_D = \begin{pmatrix} -\alpha & 0 & 0 \\ 0 & 0 & 0 \\ 0 & 0 & \alpha \end{pmatrix},$$

and

$$\Gamma_D = \begin{pmatrix} \Gamma_1 & 0 & \Gamma_3 \\ 0 & \Gamma_2 & 0 \\ \Gamma_3 & 0 & \Gamma_1 \end{pmatrix}, \quad D_D = \begin{pmatrix} \alpha g_{12} \bar{C}_1 \\ 0 \\ \alpha g_{12} \bar{C}_1 \end{pmatrix}$$

$$\Gamma_1 = \frac{|g_{24}|^2 \gamma_{24} + |g_{23}|^2 \gamma_{23} + \alpha^2 \gamma_{21}}{2\alpha^2}$$

$$\Gamma_2 = \frac{|g_{24}|^2 \gamma_4 + |g_{23}|^2 \gamma_3}{\alpha^2}$$

$$\Gamma_3 = \frac{-|g_{24}|^2 \gamma_4 - |g_{23}|^2 \gamma_3 + \alpha^2 \gamma_{21}}{2\alpha^2}$$

Where it is assumed that $\gamma_{23} = \gamma_{24}$

The individual dressed states are given by

$$\Psi_1 = \frac{1}{\alpha\sqrt{2}}(-ig_{24}^* \bar{C}_4|4\rangle - ig_{23}^* \bar{C}_3|3\rangle + \alpha \bar{C}_2|2\rangle)$$

$$\begin{aligned}
\Psi_2 &= \frac{1}{\alpha}(g_{23}\bar{C}_4|4\rangle - g_{24}\bar{C}_3|3\rangle) \\
\Psi_3 &= \frac{1}{\alpha\sqrt{2}}(ig_{24}^*\bar{C}_4|4\rangle + ig_{23}^*\bar{C}_3|3\rangle + \alpha\bar{C}_2|2\rangle)
\end{aligned} \tag{3.13}$$

Substituting them into equation for \bar{C}_1 ,

$$\partial_t \bar{C}_1 = -i\Delta_{21}\bar{C}_1 - d_{21}\mathcal{E}_s \left[\frac{\Psi_1 + \Psi_3}{\sqrt{2}} \right]$$

Equation (3.12) shows that the 'Dressed States' Ψ_1, Ψ_2 and Ψ_3 have energy eigenvalues $+\alpha, 0$ and $-\alpha$ respectively. The probe laser is then resonant with levels Ψ_1, Ψ_2 and Ψ_3 for the detunings $\Delta_{21} = +\alpha, 0$ and $-\alpha$ respectively. The eigenstate associated with $\Delta_{21} = 0$ is $\Psi_2 = (g_{23}\bar{C}_4|4\rangle - g_{24}\bar{C}_3|3\rangle)/\alpha$, which does not contain any contribution from the state $|2\rangle$. Therefore, transition probability $\langle 1|d.E|\Psi_2\rangle = 0$, which means that the probe absorption at zero detuning is zero. The manner in which this zero coupling at $\Delta_{21} = 0$ is obtained is different from the conventional zero coupling of the CPT case. In well known CPT mechanisms, the transition probability due to individual components that make up the superposition state interfere with each other and the total transition probability is therefore a zero [4]. Whereas in the Y system, the superposition state which interacts with the ground state at $\Delta_{21} = 0$ is made up of only those components which individually are uncoupled to state $|1\rangle$ by the probe transition. Therefore the total transition probability is a sum of zeros.

Carrying out a transformation, $\Psi_j = \bar{\Psi}_j \cdot \exp(-i\Delta_{21}t)$ for $j = 1, 2, 3$ the equations 3.12 become

$$\partial_t \bar{\Psi}_1 = [i(\Delta_{21} - \alpha) - \Gamma_1] \bar{\Psi}_1 - \Gamma_3 \bar{\Psi}_3 + i \frac{g_{12}}{\sqrt{2}} \bar{C}_1 \quad (3.14)$$

$$\partial_t \bar{\Psi}_2 = (i\Delta_{21} - \Gamma_2) \bar{\Psi}_2 \quad (3.15)$$

$$\partial_t \bar{\Psi}_3 = [i(\Delta_{21} + \alpha) - \Gamma_1] \bar{\Psi}_3 - \Gamma_3 \bar{\Psi}_1 + i \frac{g_{12}}{\sqrt{2}} \bar{C}_1 \quad (3.16)$$

where $g_{12} = d_{21} \mathcal{E}_s$.

The time derivatives on the LHS of equations 3.14 and 3.16 can again be set to zero when the term $i\Delta_{21} \pm \alpha - \Gamma_1$ is large, and the two equations can be written in the form,

$$\begin{aligned} [i(\Delta_{21} - \alpha) - \Gamma_1] \bar{\Psi}_1 - \Gamma_3 \bar{\Psi}_3 &= -i \frac{g_{12}}{\sqrt{2}} \bar{C}_1 \\ -\Gamma_3 \bar{\Psi}_1 + [i(\Delta_{21} + \alpha) - \Gamma_1] \bar{\Psi}_3 &= -i \frac{g_{12}}{\sqrt{2}} \bar{C}_1 \end{aligned} \quad (3.17)$$

Solving these two equations simultaneously,

$$\bar{\Psi}_3 = -\frac{[i(\Delta_{21} - \alpha) - \Gamma_1 + \Gamma_3]}{(i\Delta_{21} - \Gamma_1)^2 + \alpha^2 - \Gamma_3^2} i \frac{g_{12}}{\sqrt{2}} \bar{C}_1 \quad (3.18)$$

$$\bar{\Psi}_1 = -\frac{[i(\Delta_{21} + \alpha) - \Gamma_1 + \Gamma_3]}{(i\Delta_{21} - \Gamma_1)^2 + \alpha^2 - \Gamma_3^2} i \frac{g_{12}}{\sqrt{2}} \bar{C}_1 \quad (3.19)$$

Using an inverse transformation $\bar{C} = S \cdot \Psi_D$, the amplitude C_2 in terms of dressed states is obtained as

$$\begin{aligned} \bar{C}_2 &= \frac{\bar{\Psi}_1 + \bar{\Psi}_3}{\sqrt{2}} \\ &= \frac{-2i\Delta_{21} + 2\Gamma_1 - 2\Gamma_3}{(i\Delta_{21} - \Gamma_1)^2 + \alpha^2 - \Gamma_3^2} i \frac{g_{12}}{2} \bar{C}_1 \end{aligned}$$

Substituting this into equation for C_1 gives

$$\partial_t \bar{C}_1 = -i\Delta_{21} \bar{C}_1 + \left[\frac{i\Delta_{21} - \Gamma_1 + \Gamma_3}{(i\Delta_{21} - \Gamma_1)^2 + \alpha^2 - \Gamma_3^2} \right] |g_{12}|^2 \bar{C}_1 \quad (3.20)$$

Rewriting the above equation as

$$\partial_t \bar{C}_1 = D' \bar{C}_1$$

and hence,

$$\partial_t |\bar{C}_1|^2 = 2 \text{Re}(D') |\bar{C}_1|^2. \quad (3.21(6))$$

where $D' = -i\Delta_{21} + \left[\frac{i\Delta_{21} - \Gamma_1 + \Gamma_3}{(i\Delta_{21} - \Gamma_1)^2 + \alpha^2 - \Gamma_3^2} \right] |g_{12}|^2$.

The symbols in Fig. 3.1 shows the behaviour of $2 \text{Re}(D')$ for detuning Δ_{21} , which matches with the solid line representing the absorption factor from 3.7.

3.2.3 Interference between spontaneous emission pathways

Quantum Interference between spontaneous emission channels can lead to a modification of absorption and emission profiles. It has been shown that this effect will manifest as coupling between the decay terms in the wavefunction equation [5, 6, 7]. Such coupling was absent in the equations for the Y system of previous section, where the form of decay terms **had** been adopted following references [5, 6]. To verify the absence of such an interference, a detailed analysis of the form of these decay terms is necessary. Such calculation is presented for the Y system in this section. The form of decay terms is derived in the Weisskopf-Wigner formalism [8, 9]. Each state is represented by $|i, n_L, n_{k,\sigma}\rangle$, where $|i\rangle$ is the bare atomic state, with n_L photons of laser **and** $n_{k,\sigma}$ number of spontaneous emission photons in mode k and polarization σ [1]. The quantised

electromagnetic field is represented by $\hat{E} = i\sqrt{\left(\frac{\hbar\omega_k}{2\epsilon_0 V}\right)}[a_{k_L} \exp(i\omega_k t) - a_{k_L}^\dagger \exp(i\omega_k t)]$ [10].

The total Hamiltonian will then contain atomic, photon and interaction terms, as

$$\begin{aligned} \mathcal{H} = & \omega_1|1\rangle\langle 1| + \omega_2|2\rangle\langle 2| + \omega_3|3\rangle\langle 3| + \omega_4|4\rangle\langle 4| \\ & + ig_{24}|4\rangle\langle 2|a_{k_L} - ig_{24}^*|2\rangle\langle 4|a_{k_L}^\dagger \\ & + ig_{23}|3\rangle\langle 2|a_{k_L} - ig_{23}^*|2\rangle\langle 3|a_{k_L}^\dagger \\ & + ig_{12}^{\omega_p}|2\rangle\langle 1|a_{k_p} - ig_{12}^{\omega_p*}|1\rangle\langle 2|a_{k_p}^\dagger \\ & + \sum_{k\sigma} ig_{24}^{k_1\sigma_1}|4\rangle\langle 2|a_{k_1\sigma_1} + ig_{23}^{k_2\sigma_2}|3\rangle\langle 2|a_{k_2\sigma_2} + ig_{12}^{k_3\sigma_3}|2\rangle\langle 1|a_{k_3\sigma_3} + C.C. \\ & + \omega_L a_{k_L}^\dagger a_{k_L} + \omega_p a_{k_p}^\dagger a_{k_p} + \omega_{k_1\sigma_1} a_{k_1\sigma_1}^\dagger a_{k_1\sigma_1} + \omega_{k_2\sigma_2} a_{k_2\sigma_2}^\dagger a_{k_2\sigma_2} + \omega_{k_3\sigma_3} a_{k_3\sigma_3}^\dagger a_{k_3\sigma_3} \quad (3.21) \end{aligned}$$

where ω_i is the energy of the i^{th} state in angular frequencies, $a_{k_i\sigma_i}$ denotes annihilation operator for spontaneous emission photon of i^{th} mode and $a_{k_i\sigma_i}^\dagger$, its creation operator. $a_{k_L}^\dagger$ and a_{k_L} are creation and annihilation operator for the strong laser and subscript k_p denote the same for the probe beam. The factor g_{ij} are given by the relation[6],

$$g_{ijk\sigma} = i q \left(\frac{\omega_k}{2\epsilon_0 \hbar V} \right)^{1/2} \langle i | \hat{\epsilon}_{k\sigma} \cdot \vec{r} | j \rangle$$

Where, $\hat{\epsilon}_{k\sigma}$ is the polarization vector of photon $k\sigma$, V is the normalization volume, ϵ_0 is the permittivity of free space. C. C. denotes complex conjugate.

A closed family of essential states is considered, which are coupled by the interaction Hamiltonian. They form a wavefunction,

$$\begin{aligned} |\psi\rangle = & C_4|4, (n_L + 1)\omega_L, n_p\omega_p\rangle + C_3|3, (n_L + 1)\omega_L, n_p\omega_p\rangle + C_2|2, (n_L + 2)\omega_L, n_p\omega_p\rangle \\ & + C_1^{\omega_p}|1, (n_L + 2)\omega_L, (n_p + 1)\omega_p\rangle + C_2^{k_1\sigma_1}|2, (n_L + 1)\omega_L, n_p\omega_p, k_1, \sigma_1\rangle \\ & + C_1^{k_3\sigma_3}|1, (n_L + 2)\omega_L, n_p\omega_p, k_3\sigma_3\rangle \end{aligned}$$

$(n_L + 1)\omega_L$ refers to $n_L + 1$ photons of the laser at frequency ω_L and n_p is the number of photons of probe laser at frequency ω_p . $\sigma_i k_i$ is the spontaneous emission photon in the i^{th} mode with a wavevector k and a polarization σ .

The Schrödinger equation, $i\partial_t|\psi\rangle = \mathcal{H}|\psi\rangle$ gives an equation for each probability amplitude as

$$\begin{aligned}
\partial_t C_1 &= -\sqrt{n_p} g_{12}^{\omega_p*} C_2 \\
\partial_t C_2 &= i\Delta_{21} C_2 - \sqrt{n_L+1} g_{24}^* C_4 - \sqrt{n_L+1} g_{23}^* C_3 + \sqrt{n_p} g_{12}^{\omega_p} C_1 + \sum_{k\sigma} g_{12}^{k_3\sigma_3} C_1^{k_3\sigma_3} \\
\partial_t C_3 &= i[\Delta_{32} + \Delta_{21}] C_3 + \sqrt{n_L+1} g_{23} C_2 + \sum_{\sigma k} g_{23}^{k_2\sigma_2} C_2^{k_2\sigma_2} \\
\partial_t C_4 &= i[\Delta_{42} + \Delta_{21}] C_3 + \sqrt{n_L+1} g_{24} C_2 + \sum_{\sigma k} g_{23}^{k_1\sigma_1} C_2^{k_1\sigma_1}
\end{aligned} \tag{3.22}$$

and for each $k\sigma$ mode

$$\begin{aligned}
\partial_t C_2^{k_1\sigma_1} &= i\Delta_{21} C_2^{k_1\sigma_1} - i g_{24}^{k_1\sigma_1*} C_4 \\
\partial_t C_2^{k_2\sigma_2} &= i\Delta_{21}^{k_2\sigma_2} C_2^{k_2\sigma_2} - i g_{23}^{k_2\sigma_2*} C_3 \\
\partial_t C_1^{k_3\sigma_3} &= i\Delta_1^{k_3\sigma_3} C_1^{k_3\sigma_3} - i g_{12}^{k_3\sigma_3} C_2
\end{aligned} \tag{3.23}$$

Where, the detunings are defined as

$$\begin{aligned}
\Delta_{21}^{k_i\sigma_i} &= \omega_2 - \omega_1 - \omega_{k_i\sigma_i} \\
&\text{and} \\
\Delta_1^{k_3\sigma_3} &= \omega_1 - \omega_{k_3\sigma_3}
\end{aligned} \tag{3.24}$$

Solving equation 3.23 for long-time-limit as $t \rightarrow \infty$

$$\begin{aligned}
C_1^{k_3\sigma_3} &= \lim_{t \rightarrow \infty} - \int_0^t g_{12}^{k_3\sigma_3*} C_2 \exp(i\Delta_1^{k_3\sigma_3} . t') dt' \\
&= \lim_{t \rightarrow \infty} - g_{12}^{k_3\sigma_3*} C_2 \int_0^t \exp(i\Delta_1^{k_3\sigma_3} . t') dt'
\end{aligned} \tag{3.25}$$

C_2 is assumed to be a slowly varying quantity when compared to the exponential terms in the integrand.

Solving this integral, [8],

$$\begin{aligned}
 &= \lim_{t \rightarrow \infty} -g_{12}^{k_3\sigma_3*} C_2 \left[\frac{\exp(i\Delta_1^{k_3\sigma_3} t) - 1}{-i\Delta_1^{k_3\sigma_3}} \right] \\
 &= i g_{12}^{k_3\sigma_3*} C_2 \left[\frac{\wp}{\Delta_1^{k_3\sigma_3}} + i\pi\delta(\Delta_1^{k_3\sigma_3}) \right]
 \end{aligned} \tag{3.26}$$

Where $\wp/\Delta_1^{k_3\sigma_3}$ is the Principal value of $\Delta_1^{k_3\sigma_3}$ and $\delta(\Delta_1^{k_3\sigma_3})$ is the Dirac delta function centered at $\Delta_1^{k_3\sigma_3}$. The Principal value terms give the energy shifts induced by the vacuum fluctuations[6]. Assuming that the basis set is already in such a form that these shifting terms are included in the energy eigenvalue terms,

$$C_1^{k_3\sigma_3} = -g_{12}^{k_3\sigma_3*} C_2 \pi \delta(\Delta_1^{k_3\sigma_3}) \tag{3.27}$$

On similar lines,

$$\begin{aligned}
 C_2^{k_2\sigma_2} &= i g_{23}^{k_2\sigma_2*} C_3 \pi \delta(\Delta_{21}^{k_2\sigma_2}) \\
 C_2^{k_1\sigma_1} &= i g_{21}^{k_1\sigma_1*} C_4 \pi \delta(\Delta_{21}^{k_1\sigma_1})
 \end{aligned} \tag{3.28}$$

Substituting these in equation 3.22, we get

$$\begin{aligned}
 \partial_t C_4 &= i[\Delta_{42} + \Delta_{21}] C_4 + g_{24} C_2 - \int_{k\sigma} |g_{24}^{k_1\sigma_1}|^2 C_4 \pi \delta(\Delta_{21}^{k_1\sigma_1}) \\
 &= i[\Delta_{42} + \Delta_{21}] C_4 + g_{24} C_2 - |g_{24}^{k_1\sigma_1}|^2 \pi C_4
 \end{aligned} \tag{3.29}$$

Where, due to high density of modes, the summation over $k\sigma$ has been converted into an integration. Further, denoting $|g_{24}^{k_1\sigma_1}|^2 \pi = \gamma_4$,

$$\partial_t C_4 = [i(\Delta_{42} + \Delta_{21}) - \gamma_4] C_4 + g_{24} C_2 \tag{3.30}$$

On similar lines,

$$\begin{aligned}
\partial_t C_3 &= [i(\Delta_{32} + \Delta_{21})]C_3 + g_{23}C_2 - |g_{23}^{k_2\sigma_2}|^2\pi C_3 \\
&= [i(\Delta_{32} + \Delta_{21}) - \gamma_3]C_3 + g_{23}C_2 \\
\partial_t C_2 &= i\Delta_{21}C_2 - g_{24}^*C_4 - g_{23}^*C_3 + g_{12}^{\omega_p}C_1 - |g_{12}^{k_3\sigma_3}|^2\pi C_2 \\
&= [i\Delta_{21} - \gamma_2]C_2 - g_{24}^*C_4 - g_{23}^*C_3 + g_{12}^{\omega_p}C_1
\end{aligned} \tag{3.31}$$

where, $\gamma_2 = |g_{12}^{k_3\sigma_3}|^2\pi$ and $\gamma_3 = |g_{23}^{k_2\sigma_2}|^2\pi$.

This returns equations identical to the equations 3.1-3.4, which have been already solved. As expected, there is no coupling between the decay terms, which would have indicated an interference between the spontaneous emission modes. In other words Harris-Imamoğlu type of interference effects are absent in the Y system.

In conclusion, the pump field E_p interacts with levels $|2\rangle$, $|3\rangle$ and $|4\rangle$ to form dressed states $|\Psi_1\rangle$, $|\Psi_2\rangle$ and $|\Psi_3\rangle$ with eigenenergies $-a$, 0 and α respectively. The probe beam is resonant with transitions between level $|1\rangle$ and the states $|\Psi_1\rangle$, $|\Psi_2\rangle$ and $|\Psi_3\rangle$ for detunings $A = -a$, 0 and a in that order. For such a situation, equation (3.13) leads to

$$\begin{aligned}
\langle \Psi_1 | d.E | 1 \rangle &\neq 0 \\
\langle \Psi_3 | d.E | 1 \rangle &\neq 0 \\
&\text{whereas} \\
\langle \Psi_2 | d.E | 1 \rangle &= 0
\end{aligned} \tag{3.32}$$

The first two relations of 3.32 give rise to two resonant absorption bands at $\Delta_{21} = \pm\alpha$. The third relation implies a zero absorption at $\Delta_{21} = 0$. Unlike the earlier QI

effects leading to transparency [7, 11, 12], transparency in **Y** is induced due to absence of the coupling level $|2\rangle$ in the superposition state $|\Psi_2\rangle$.

3.3 The Gate System

3.3.1 The Bare state picture

Calculation similar to that used for **Y** system are obtained for the **Gate** system. The Hamiltonian 2.11 from Chapter II is used again which, in $\hbar = 1$ units, is

$$\mathcal{H} = \begin{pmatrix} \omega_5 & 0 & -d_{75}^* E_s^* & 0 & 0 \\ 0 & \omega_6 & 0 & -d_{86}^* E_s^* & 0 \\ -d_{75} E_s & 0 & \omega_7 & 0 & -d_{97}^* E_p^{*-} \\ 0 & -d_{86} E_s & 0 & \omega_8 & -d_{98}^* E_p^{+*} \\ 0 & 0 & -d_{97} E_p^- & -d_{98} E_p^+ & \omega_9 \end{pmatrix} \quad (3.33)$$

ω_j is the energy of the j^{th} level in terms of angular frequency.

The state vector in the 5-dimensional Hilbert space for the **Gate** configuration is $|\psi\rangle = C_9|9\rangle + |C_8|8\rangle + C_7|7\rangle + C_6|6\rangle + C_5|5\rangle$

Using these two in the Schrödinger equation $i\partial_t\psi = \mathcal{H}\psi$, equations for the probability amplitudes are obtained as

$$\partial_t C_9 = [i(\Delta_p + \Delta_s) - (\gamma_{79} + \gamma_{89})]C_9 + id_{97} \mathcal{E}_p^+ C_7 + id_{98} \mathcal{E}_p^- C_8 \quad (3.34)$$

$$\partial_t C_8 = [i\Delta_s - \gamma_{68}]C_8 + id_{98}^* \mathcal{E}_p^{+*} C_9 + id_{86} \mathcal{E}_s C_6 \quad (3.35)$$

$$\partial_t C_7 = [i\Delta_s - \gamma_{57}]C_7 + id_{97}^* \mathcal{E}_p^{+*} C_9 + id_{75} \mathcal{E}_s C_5 \quad (3.36)$$

$$\partial_t C_5 = +id_{75}^* \mathcal{E}_s^* C_7 \quad (3.37)$$

$$\partial_t C_6 = +id_{86}^* \mathcal{E}_s^* C_8 \quad (3.38)$$

γ_{ij} are the decay rates from level j to i , introduced following reference [5, 6].

Equations 3.34 and 3.35 are solved by setting the time derivatives on the LHS to zero, under the assumption that the variation is negligible compared to large $i\Delta_s - \gamma_{68}$ and $i\Delta_s - \gamma_{57}$ factors. The solutions for C_8 and C_7 are

$$C_8 = -i \frac{d_{98} \mathcal{E}_p^- C_9 + d_{86} \mathcal{E}_s C_6}{i\Delta_s - \gamma_{68}} \quad (3.39)$$

$$C_7 = -i \frac{d_{97} \mathcal{E}_p^+ C_9 + d_{75} \mathcal{E}_s C_5}{i\Delta_s - \gamma_{57}} \quad (3.40)$$

These are substituted in 3.34, and then the time derivative of C_9 is set to zero under the same arguments, which gives

$$C_9 = \frac{1}{F} \left[\frac{d_{97} \mathcal{E}_p^+ d_{75} \mathcal{E}_s C_5}{i\Delta_s - \gamma_{57}} + \frac{d_{98} \mathcal{E}_p^- d_{86} \mathcal{E}_s C_6}{i\Delta_s - \gamma_{68}} \right] \quad (3.41)$$

Where

$$F = \left[i(\Delta_p + \Delta_s) - (\gamma_{79} + \gamma_{89}) + \frac{|d_{97} \mathcal{E}_p^+|^2}{i\Delta_s - \gamma_{57}} + \frac{|d_{98} \mathcal{E}_p^-|^2}{i\Delta_s - \gamma_{68}} \right]$$

Substituting this into equations 3.39 and 3.40 gives

$$C_8 = -i \frac{1}{F} \left[\frac{d_{98}^* \mathcal{E}_p^- d_{97} \mathcal{E}_p^+ d_{75} \mathcal{E}_s C_5}{(i\Delta_s - \gamma_{57})(i\Delta_s - \gamma_{68})} + \frac{|d_{98} \mathcal{E}_p^-|^2 d_{86} \mathcal{E}_s C_6}{(i\Delta_s - \gamma_{68})^2} \right] \quad (3.42)$$

$$C_7 = -i \frac{1}{F} \left[\frac{|d_{97} \mathcal{E}_p^+|^2 d_{75} \mathcal{E}_s C_5}{(i\Delta_s - \gamma_{57})^2} + \frac{d_{97}^* \mathcal{E}_p^+ d_{98} \mathcal{E}_p^- d_{86} \mathcal{E}_s C_6}{(i\Delta_s - \gamma_{57})(i\Delta_s - \gamma_{68})^2} \right] \quad (3.43)$$

Substituting these into equation 3.37 and 3.38,

$$\partial_t C_5 = \left[\frac{i\Delta_9 - \gamma_9 + F_2}{i\Delta_9 - \gamma_9 + F_1 + F_2} \right] \frac{|d_{75} \cdot \mathcal{E}_s|^2 C_5}{i\Delta_s - \gamma_{57}} + \frac{d_{75}^* \cdot \mathcal{E}_s^* d_{97}^* \cdot \mathcal{E}_p^+ d_{98} \cdot \mathcal{E}_p^- d_{86} \cdot \mathcal{E}_s C_6}{(i\Delta_9 - \gamma_9 + F_1 + F_2)(i\Delta_s - \gamma_{57})(i\Delta_s - \gamma_{68})} \quad (3.44)$$

$$\partial_t C_6 = \left[\frac{i\Delta_9 - \gamma_9 + F_1}{i\Delta_9 - \gamma_9 + F_1 + F_2} \right] \frac{|d_{86} \cdot \mathcal{E}_s|^2 C_6}{i\Delta_s - \gamma_{68}} + \frac{d_{86}^* \cdot \mathcal{E}_s^* d_{98}^* \cdot \mathcal{E}_p^+ d_{97} \cdot \mathcal{E}_p^- d_{75} \cdot \mathcal{E}_s C_5}{(i\Delta_9 - \gamma_9 + F_1 + F_2)(i\Delta_s - \gamma_{57})(i\Delta_s - \gamma_{68})} \quad (3.45)$$

where

$$F_1 = \frac{|d_{97} \cdot \mathcal{E}_p^+|^2}{i\Delta_s - \gamma_{59}} \quad \text{and} \quad F_2 = \frac{|d_{98} \cdot \mathcal{E}_p^-|^2}{i\Delta_s - \gamma_{68}}$$

and $\Delta_9 = \Delta_s + \Delta_p$, and $\gamma_9 = \gamma_{79} = \gamma_{89}$

Equations 3.44 and 3.45 are rewritten as

$$\begin{aligned} \partial_t C_5 &= \phi_5 C_5 + \phi_{56} C_6 \\ \partial_t C_5^* &= \phi_5^* C_5^* + \phi_{56}^* C_6^* \\ \partial_t C_6 &= \phi_6 C_6 + \phi_{65} C_5 \\ \partial_t C_6^* &= \phi_6^* C_6^* + \phi_{65}^* C_5^* \end{aligned}$$

where ϕ_5 and ϕ_{65} represent the coefficients of C_5 , C_6 in 3.44 and ϕ_6 and ϕ_{65} represent the coefficients of C_6 and C_5 in 3.45 respectively

The time evolution of populations will then be

$$\begin{aligned} \partial_t |C_5|^2 &= 2\text{Real}(\phi_5) |C_5|^2 + \phi_{56} C_6 C_5^* + \phi_{56}^* C_6^* C_5 \\ \partial_t |C_6|^2 &= 2\text{Real}(\phi_6) |C_6|^2 + \phi_{65} C_5 C_6^* + \phi_{65}^* C_5^* C_6 \end{aligned} \quad (3.46)$$

and that for the coherence terms are

$$\begin{aligned}\partial_t C_5 C_6^* &= (\phi_5 + \phi_6^*) C_5 C_6^* + \phi_{56} |C_6|^2 + \phi_{56}^* |C_5|^2 \\ C_6 C_5^* &= (C_5 C_6^*)^*\end{aligned}$$

Equations 3.44, 3.45 show that the time evolution of amplitudes C_5 and C_6 are coupled to each other. The population terms in turn (3.46) are coupled to the cross coherences $C_5 C_6^*$ and $C_6 C_5^*$. Since loss of population is assumed to be only due to the interaction of probe beam, equations 3.46 represent the probe absorption behaviour. Which means that the absorption of probe between levels $|5\rangle \leftrightarrow |7\rangle$ and $|6\rangle \leftrightarrow |8\rangle$ are affected by the coherence between the ground states $|5\rangle$ and $|6\rangle$. Such a coupling of coherences was not seen in the approximate analytical solution of the density matrix for probe absorption which was obtained in previous chapter. This is due to the fact that the zeroth order coherence ρ_{56} there is assumed to be zero and the probe absorption is calculated only upto first order in probe beam amplitude.

Effect of this coherence revealed in 3.46 on the probe absorption is a subject of study of the next chapter. For the present, such coherences are assumed zero and only the factors ϕ_5 and ϕ_6 are taken into account. Under such assumption, the probe absorption, which is equivalent to loss of population from ground states is given by the equations

$$\begin{aligned}\partial_t |C_5|^2 &= 2\text{Real}(\phi_5) |C_5|^2 \\ \partial_t |C_6|^2 &= 2\text{Real}(\phi_6) |C_6|^2\end{aligned}\tag{3.47}$$

which leads to

$$|C_5(t)|^2 = \exp[2\text{Re}(\phi_5)t] |C_5(0)|^2$$

$$|C_6(t)|^2 = \exp[2\text{Re}(\phi_6)t]|C_6(0)|^2 \quad (3.48)$$

where, $|C_5(0)|^2$ and $|C_6(0)|^2$ denote the initial populations at $t=0$. Figure 3.2 shows the absorption factors ϕ_5 and ϕ_6 as a function of probe detuning Δ_s . The profile of this curve is identical to the one obtained by density matrix solutions, showing a resonant absorption peak at $\Delta_s = 0$ and two side bands at $\Delta_s = \sqrt{|\Omega_{97}|^2 + |\Omega_{98}|^2}$. A better understanding of this behaviour is obtained in the dressed state picture which is presented in the following section.

3.3.2 Dressed State picture

Operating a transformation on all the factors as $C_j = \bar{C}_j \exp(i\Delta_s t)$; $j = 5, 6, 7, 8, 9$, the equations 3.34-3.38 become,

$$\partial_t \begin{pmatrix} \bar{C}_9 \\ \bar{C}_8 \\ \bar{C}_7 \end{pmatrix} = i \begin{pmatrix} \Delta_p & g_{89} & g_{79} \\ g_{89}^* & 0 & 0 \\ g_{79}^* & 0 & 0 \end{pmatrix} \cdot \begin{pmatrix} \bar{C}_9 \\ \bar{C}_8 \\ \bar{C}_7 \end{pmatrix} - \begin{pmatrix} \gamma_9 & 0 & 0 \\ 0 & \gamma_{68} & 0 \\ 0 & 0 & \gamma_{57} \end{pmatrix} \cdot \begin{pmatrix} \bar{C}_9 \\ \bar{C}_8 \\ \bar{C}_7 \end{pmatrix} + \begin{pmatrix} 0 \\ ig_{68} \cdot C_6 e^{(i\Delta_s t)} \\ ig_{57} \cdot C_5 e^{(i\Delta_s t)} \end{pmatrix} \quad (3.49)$$

and

$$\begin{aligned} \partial_t C_5 \exp(i\Delta_s t) &= ig_{57}^* \bar{C}_7 \\ \partial_t C_6 \exp(i\Delta_s t) &= ig_{68}^* \bar{C}_8 \end{aligned} \quad (3.50)$$

$$g_{79} = d_{97} \mathcal{E}_p^+, g_{89} = d_{98} \mathcal{E}_p^-, g_{57} = d_{75} \mathcal{E}_s \text{ and } g_{68} = d_{86} \mathcal{E}_s.$$

Equation 3.49 is written in the form,

$$\partial_t \bar{C} = iM\bar{C} - \gamma\bar{C} + \bar{D}$$

and at $\Delta_p = 0$, the eigenvalues of matrix M are $\lambda = 0, \pm\alpha$, where $\alpha^2 = |g_{79}|^2 + g_{89}^2$.

The diagonalizing matrix S^\dagger is obtained by arranging normalized eigenvectors as

$$S^\dagger = \frac{1}{\alpha\sqrt{2}} \begin{pmatrix} \alpha & ig_{89} & ig_{79} \\ 0 & \sqrt{2}g_{79}^* & -\sqrt{2}g_{89}^* \\ \alpha & -ig_{89} & -ig_{79} \end{pmatrix}$$

and Carrying out the unitary transformation,

$$\partial_t(S^\dagger \bar{C}) = iS^\dagger M S S^\dagger \bar{C} - S^\dagger \gamma S S^\dagger \bar{C} + S^\dagger \bar{D}$$

gives

$$\partial_t \begin{pmatrix} \Psi_I \\ \Psi_{II} \\ \Psi_{III} \end{pmatrix} = i \left[\begin{pmatrix} -\alpha & 0 & 0 \\ 0 & 0 & 0 \\ 0 & 0 & \alpha \end{pmatrix} - \begin{pmatrix} \Gamma_1 & 0 & \Gamma_3 \\ 0 & \Gamma_2 & 0 \\ \Gamma_3 & 0 & \Gamma_1 \end{pmatrix} \right] \cdot \begin{pmatrix} \Psi_I \\ \Psi_{II} \\ \Psi_{III} \end{pmatrix} + \begin{pmatrix} D_1 \\ D_2 \\ D_3 \end{pmatrix} \quad (3.51)$$

Where,

$$\begin{aligned} D_1 &= i[g_{89}g_{68}C_6 + g_{79}g_{57}C_5] \exp(-i\Delta_s t) \\ D_2 &= \sqrt{2}[g_{79}^*g_{68}C_6 - g_{89}^*g_{57}C_5] \exp(-i\Delta_s t) \\ D_3 &= -i[g_{89}g_{68}C_6 + g_{79}g_{57}C_5] \exp(-i\Delta_s t) \end{aligned}$$

and

$$\begin{aligned} \Gamma_1 &= \frac{1}{2\alpha^2} [\alpha^2\gamma_9 + |g_{89}|^2\gamma_{68} + |g_{79}|^2\gamma_{57}] \\ \Gamma_2 &= \frac{1}{\alpha^2} [|g_{79}|^2\gamma_{68} + |g_{89}|^2\gamma_{57}] \end{aligned}$$

$$\Gamma_3 = \frac{1}{2\alpha^2} [\alpha^2 \gamma_9 - |g_{89}|^2 \gamma_{68} - |g_{79}|^2 \gamma_{57}]$$

where it is assumed that $\gamma_{57} = \gamma_{68}$. The new states are related to Bare states by

$$\begin{aligned}\Psi_I &= \frac{1}{\sqrt{2}\alpha} [\alpha \bar{C}_9 + i g_{89} \bar{C}_8 + i g_{79} \bar{C}_7] \\ \Psi_{II} &= \frac{1}{\alpha} [g_{79}^* \bar{C}_8 - g_{89}^* \bar{C}_7] \\ \Psi_{III} &= \frac{1}{\sqrt{2}\alpha} [\alpha \bar{C}_9 - i g_{89} \bar{C}_8 - i g_{79} \bar{C}_7]\end{aligned}\tag{3.52}$$

operating a transformation $\Psi_j = \bar{\Psi}_j \exp(-i\Delta_s t)$, the equations become,

$$\begin{aligned}\partial_t \bar{\Psi}_I &= (i\Delta_s - i\alpha - \Gamma_1) \bar{\Psi}_I - \Gamma_3 \bar{\Psi}_{III} + iG \\ \partial_t \bar{\Psi}_{II} &= (i\Delta_s - \Gamma_2) \bar{\Psi}_{II} + \sqrt{2} [g_{79}^* g_{68} C_6 - g_{89}^* g_{57} C_5] \\ \partial_t \bar{\Psi}_{III} &= (i\Delta_s + i\alpha - \Gamma_1) \bar{\Psi}_{III} - iG\end{aligned}\tag{3.53}$$

Where, $G = g_{89} g_{68} C_6 + g_{79} g_{57} C_5$.

Assuming the derivatives on the LHS are negligible when $i\Delta_s - \Gamma$ terms are large, the solutions for $\bar{\Psi}$ become

$$\bar{\Psi}_{II} = \frac{-\sqrt{2} [g_{79}^* g_{68} C_6 - g_{89}^* g_{57} C_5]}{i\Delta_s - \Gamma_2}\tag{3.54}$$

and

$$\begin{aligned}0 &= (i\Delta_s - i\alpha - \Gamma_1) \bar{\Psi}_I - \Gamma_3 \bar{\Psi}_{III} + iG \\ 0 &= (i\Delta_s + i\alpha - \Gamma_1) \bar{\Psi}_{III} - \Gamma_3 \bar{\Psi}_I - iG\end{aligned}\tag{3.55}$$

Solving the two equations of 3.55 simultaneously,

$$\begin{aligned}\bar{\Psi}_{III} &= \frac{(i\Delta_s - i\alpha - \Gamma_1 - \Gamma_3) iG}{(i\Delta_s - \Gamma_1)^2 + \alpha^2 - \Gamma_3^2} \\ \bar{\Psi}_I &= \frac{-(i\Delta_s + i\alpha - \Gamma_1 - \Gamma_3) iG}{(i\Delta_s - \Gamma_1)^2 + \alpha^2 - \Gamma_3^2}\end{aligned}\quad (3.56)$$

Substituting in equation 3.50,

$$\begin{aligned}\partial_t C_6 &= i\Delta_s C_6 - i \frac{g_{68} g_{89}^*}{\sqrt{2}\alpha} (\bar{\Psi}_I - \bar{\Psi}_{III}) - \frac{g_{68} g_{79}^*}{\alpha} \bar{\Psi}_{II} \\ \partial_t C_5 &= i\Delta_s C_5 + i \frac{g_{57} g_{79}^*}{\sqrt{2}\alpha} (\bar{\Psi}_I - \bar{\Psi}_{III}) + g_{57}^* g_{89} \bar{\Psi}_{II}\end{aligned}\quad (3.57)$$

From 3.56

$$\bar{\Psi}_I - \bar{\Psi}_{III} = \frac{-2 [i\Delta_s - \Gamma_1 - \Gamma_3] iG}{(i\Delta_s - \Gamma_1)^2 + \alpha^2 - \Gamma_3^2}\quad (3.58)$$

Substituting this into 3.57 and writing in matrix form,

$$\partial_t \begin{pmatrix} C_6 \\ C_5 \end{pmatrix} = \begin{pmatrix} i\Delta_s + \frac{\sqrt{2}}{\alpha} |g_{68}|^2 \bar{B} & \frac{\sqrt{2}}{\alpha} g_{68}^* g_{89} g_{79} (B_1 - B_2) \\ \frac{\sqrt{2}}{\alpha} g_{79}^* g_{57} g_{68} g_{89} (B_1 - B_2) & i\Delta_s + \frac{\sqrt{2}}{\alpha} |g_{57}|^2 \bar{B} \end{pmatrix} \cdot \begin{pmatrix} C_6 \\ C_5 \end{pmatrix}\quad (3.59)$$

Where

$$B_1 = \frac{i\Delta_s - \Gamma_1 - \Gamma_3}{(i\Delta_s - \Gamma_1)^2 + \alpha^2 - \Gamma_3^2} \quad \text{and} \quad B_2 = \frac{1}{i\Delta_s - \Gamma_2}$$

and

$$\bar{B} = (B_1 |g_{89}|^2 + B_2 |g_{79}|^2)$$

Denoting equation 3.57 as

$$\begin{aligned}\partial_t C_5 &= \Theta_5 C_5 + \Theta_{56} C_6 \\ \partial_t C_6 &= \Theta_6 C_6 + \Theta_{65} C_5\end{aligned}$$

These two equations are similar to those of 3.46. The evolutions of populations of ground states are then given by two equations, using,

$$\partial_t |C_5|^2 = C_5^* \partial_t C_5 + \partial_t C_5^* C_5$$

and

$$\partial_t |C_6|^2 = C_6^* \partial_t C_6 + \partial_t C_6^* C_6,$$

$$\partial_t |C_5|^2 = 2 \text{Real} (\Theta_5) |C_5|^2 + \Theta_{56} C_6 C_5^* + \Theta_{56}^* C_6^* C_5$$

and

$$\partial_t |C_6|^2 = 2 \text{Real} (\Theta_6) |C_6|^2 + \Theta_{65} C_5 C_6^* + \Theta_{65}^* C_5^* C_6 \quad (3.60)$$

which are similar to those of 3.46, but with coefficients Θ which appear to be different from the coefficients ϕ of 3.46. But a numerical plot of the coefficients Θ with respect to the detuning Δ shows that they are identical. These values are plotted in figure 3.2 along with the plots of ϕ_5 and ϕ_6 , which overlap perfectly.

3.3.3 Interference between Spontaneous emission pathways

As in the case of Y system, interference between spontaneous emission modes is investigated for the **Gate** system also. State vectors are taken to be combination of bare atomic states and associated photon modes. A closed set of degenerate states are considered,

$$\begin{aligned} |\psi\rangle &= C_5^{\omega_p} |5, (n_L + 2)\omega_L, (n_p + 1)\omega_p\rangle + C_6^{\omega_p} |6, (n_L + 2)\omega_L, (n_p + 1)\omega_p\rangle \\ &+ C_7 |7, (n_L + 2)\omega_L, n_p\omega_p\rangle + C_8 |8, (n_L + 2)\omega_L, n_p\omega_p\rangle + C_9 |9, (n_L + 1)\omega_L, n_p\omega_p\rangle \\ &+ C_5^{k_3} \sigma_3 |5, (n_L + 2)\omega_L, n_p\omega_p, k_3\sigma_3\rangle + C_6^{k_3} \sigma_3 |6, (n_L + 2)\omega_L, n_p\omega_p, k_3\sigma_3\rangle \\ &+ C_7^{k_4} \sigma_4 |7, (n_L + 1)\omega_L, n_p\omega_p, k_4\sigma_4\rangle + C_8^{k_5} \sigma_5 |8, (n_L + 1)\omega_L, n_p\omega_p, k_5\sigma_5\rangle + \dots \end{aligned}$$

The Hamiltonian is written as

$$\begin{aligned}
\mathcal{H} = & \omega_5|5\rangle\langle 5| + \omega_6|6\rangle\langle 6| + \omega_7|7\rangle\langle 7| + \omega_8|8\rangle\langle 8| + \omega_9|9\rangle\langle 9| \\
& + ig_{57}^{\omega_p}|7\rangle\langle 5|a_{k_p} - ig_{57}^{\omega_p*}|5\rangle\langle 7|a_{k_p}^\dagger + ig_{68}^{\omega_p}|8\rangle\langle 6|a_{k_p} - ig_{68}^{\omega_p*}|6\rangle\langle 8|a_{k_p}^\dagger \\
& + \sum_{k\sigma} ig_{57}^{k_3\sigma_3}|7\rangle\langle 5|a_{k_3\sigma_3} - ig_{57}^{k_3\sigma_3*}|5\rangle\langle 7|a_{k_3\sigma_3}^\dagger + ig_{68}^{k_3\sigma_3}|8\rangle\langle 6|a_{k_3\sigma_3} - ig_{68}^{k_3\sigma_3*}|6\rangle\langle 8|a_{k_3\sigma_3}^\dagger \\
& + \sum_{k\sigma} ig_{79}^{k_4\sigma_4}|9\rangle\langle 7|a_{k_4\sigma_4} - ig_{79}^{k_4\sigma_4*}|7\rangle\langle 9|a_{k_4\sigma_4}^\dagger + g_{89}^{k_5\sigma_5}|9\rangle\langle 8|a_{k_5\sigma_5} - ig_{89}^{k_5\sigma_5*}|8\rangle\langle 9|a_{k_5\sigma_5}^\dagger \\
& + \omega_{k_L}a_{k_L}a_{k_L}^\dagger + \omega_p a_{k_p}a_{k_p}^\dagger + \omega_{k_3\sigma_3}a_{k_3\sigma_3}a_{k_3\sigma_3}^\dagger + \omega_{k_4\sigma_4}a_{k_4\sigma_4}a_{k_4\sigma_4}^\dagger + \omega_{k_5\sigma_5}a_{k_5\sigma_5}a_{k_5\sigma_5}^\dagger \quad (3.61)
\end{aligned}$$

ω_j is the energy eigenvalue of j^{th} level in angular frequency. $k_i\sigma_i$ denote the spontaneous emission photon of the i^{th} mode, with momentum k_i and polarity σ_i . $k_4\sigma_4$ and $k_5\sigma_5$ are of different polarization states. $a_{k_i\sigma_i}$ denotes annihilation operator for spontaneous emission photon of i^{th} mode and $a_{k_i\sigma_i}^\dagger$ its creation operator. $a_{k_L}^\dagger$ and a_{k_L} are creation and annihilation operator for the strong laser and subscript k_p denote the same for the probe beam. The factor g_{ij} are given by the relation[10],

$$g_{ijk\sigma} = i q \left(\frac{\omega_k}{2\epsilon_0 \hbar V} \right)^{1/2} \langle i | \hat{\epsilon}_{k\sigma} \cdot \vec{r} | j \rangle$$

Where, $\hat{\epsilon}_{k\sigma}$ is the polarization vector of photon $k\sigma$, V is the normalization volume, ϵ_0 is the permittivity of free space. q is the electronic charge.

The equations after the unitary transformations are

$$\begin{aligned}
\partial_t C_9 &= i(\Delta_{97} + \Delta_{75})C_9 + g'_{79}C_7 + g'_{89}C_8 + \sum_{\sigma k} g_{79}^{d_4\sigma_4} C_7^{d_4\sigma_4} + g_{89}^{k_5\sigma_5} \\
\partial_t C_8 &= i\Delta_{86}C_8 + g_{68}^{\omega_p} C_6^{\omega_p} - g_{89}^{\omega_p*} C_9 + \sum_{\sigma k} g_{68}^{k_3\sigma_3} C_6^{k_3\sigma_3} \\
\partial_t C_7 &= i\Delta_{57}C_7 + g_{57}^{\omega_p} C_5^{\omega_p} - g_{79}^{\omega_p*} C_9 + \sum_{\sigma k} g_{57}^{k_3\sigma_3} C_5^{k_3\sigma_3} \\
\partial_t C_5^{\omega_p} &= -g_{57}^{\omega_p} C_7 \\
\partial_t C_6^{\omega_p} &= -g_{68}^{\omega_p} C_8
\end{aligned} \quad (3.62)$$

And for each mode $k_i\sigma_{i,j}$

$$\begin{aligned}
 \partial_t C_5^{k_3\sigma_3} &= i\Delta_{75}^{k_3\sigma_3} C_5^{k_3\sigma_3} - g_{57}^{k_3\sigma_3} C_7 \\
 \partial_t C_6^{k_3\sigma_3} &= i\Delta_{86}^{k_3\sigma_3} C_6^{k_3\sigma_3} - g_{68}^{k_3\sigma_3} C_8 \\
 \partial_t C_7^{k_4\sigma_4} &= i\Delta_{97}^{k_4\sigma_4} C_7^{k_4\sigma_4} - g_{79}^{k_4\sigma_4} C_9 \\
 \partial_t C_8^{k_5\sigma_5} &= i\Delta_{98}^{k_5\sigma_5} C_8^{k_5\sigma_5} - g_{89}^{k_5\sigma_5} C_9
 \end{aligned} \tag{3.63}$$

where

$$\begin{aligned}
 g_{57}^{\omega_{p'}} &= \sqrt{n_P} g_{57}^{\omega_p} \quad , \quad g_{68}^{\omega_{p'}} = \sqrt{n_P} g_{68}^{\omega_p} \\
 g_{79}' &= \sqrt{n_L + 1} g_{79} \quad \text{and} \quad g_{89}' = \sqrt{n_L + 1} g_{79}
 \end{aligned}$$

Solving for each ak equation in the long time limit[8],

$$\begin{aligned}
 C_7^{k_4\sigma_4} &= -g_{79}^{k_4\sigma_4} C_9 \lim_{t \rightarrow \infty} \int_0^t \exp(i\Delta_{97}^{k_4\sigma_4} t') dt' \\
 &= -g_{79}^{k_4\sigma_4} C_9 \lim_{t \rightarrow \infty} \left[\frac{e^{-i\Delta_{97}^{k_4\sigma_4} t} - 1}{\Delta_{97}^{k_4\sigma_4}} \right] \\
 &= -g_{79}^{k_4\sigma_4} C_9 \left[i \frac{\wp}{\Delta_{97}^{k_4\sigma_4}} + \pi \delta(\Delta_{97}) \right]
 \end{aligned} \tag{3.64}$$

The amplitude C_9 is assumed to vary slowly within the time scale considered. On similar lines, the other equations lead to

$$\begin{aligned}
 C_8^{k_5\sigma_5} &= -g_{89}^{k_5\sigma_5} C_9 \left[\frac{i\wp}{\Delta_{98}^{k_5\sigma_5}} + \pi \delta(\Delta_{98}^{k_5\sigma_5}) \right] \\
 C_5^{k_3\sigma_3} &= -g_{75}^{k_3\sigma_3} C_7 \left[\frac{i\wp}{\Delta_{75}^{k_3\sigma_3}} + \pi \delta(\Delta_{75}^{k_3\sigma_3}) \right] \\
 C_6^{k_3\sigma_3} &= -g_{86}^{k_3\sigma_3} C_8 \left[\frac{i\wp}{\Delta_{86}^{k_3\sigma_3}} + \pi \delta(\Delta_{86}^{k_3\sigma_3}) \right]
 \end{aligned} \tag{3.65}$$

Assuming the shift due to fluctuations $i\varphi/\Delta_{ij}$ are already included in the energy eigenvalues, and denoting

$$\gamma_{ij} = \int_{k_n \sigma_n} |g_{ij}| \pi \delta(\Delta_{ij}^{k_n \sigma_n}),$$

for $n = 3, 4, 5$ and $i, j = 5, 6, 7, 8, 9$, the equations 3.62 become

$$\partial_t C_9 = [i(\Delta_p + \Delta_s) - (\gamma_{79} + \gamma_{89})]C_9 + g'_{79}C_7 + g'_{89}C_8 \quad (3.66)$$

$$\partial_t C_8 = [i\Delta_s - \gamma_{68}]C_8 + g'_{68}C_6 \quad (3.67)$$

$$\partial_t C_7 = [i\Delta_s - \gamma_{57}]C_7 + g'_{57}C_5 \quad (3.68)$$

$$\partial_t C_5 = -g'^*_{57}C_7 \quad (3.69)$$

$$\partial_t C_6 = -g'^*_{68}C_8 \quad (3.70)$$

These equations are identical to equations 3.34-3.38, whose solutions have already been presented. There is no coherence coupling generated by vacuum fields between the decay terms. This shows that there are no Harris-Imamoğlu type of interference effects in **Gate** system.

Summarizing the results of **Gate** system, the pump beam forms 'Dressed states' out of levels $|7\rangle$, $|9\rangle$ and $|8\rangle$ in the form shown in (3.52). The new levels Ψ_I , Ψ_{II} , and Ψ_{III} are shifted from their original energy levels by amount $-a$, 0 and α respectively. The probe beam connects both $|5\rangle$ and $|6\rangle$ to levels Ψ_I , Ψ_{II} and Ψ_{III} respectively for detunings $A = -a$, 0 and α . Since $|7\rangle$ and $|8\rangle$ have components in all the three dressed states, the transition probability for all three states from $|5\rangle$ and $|6\rangle$ is nonzero, in other words,

$$\langle \Psi_{I,II,III} | d.E | 5, 6 \rangle \neq 0.$$

Therefore, all the three peaks are present and there is no transparency at zero detuning. Even though the coherence between $|7\rangle$ and $|8\rangle$ is that of a typical CPT situation, it does not cancel the absorption. This is due to the fact that levels $|5\rangle$ and $|6\rangle$ independently interact with levels $|7\rangle$ and $|8\rangle$ via the probe beam. Also, the quantum interference between spontaneous emission photons requires a condition that the two decaying levels should have the same J and m_J values [6, 5]. Dressed states had provided such a condition in the earlier studies [7, 13]. But, two decay channels $|7\rangle \rightarrow |5\rangle$ and $|8\rangle \rightarrow |6\rangle$ do not interfere destructively, and this mechanism of EIT does not exist for the **Gate** system. But there is an effect on probe absorption due to the coherence between the two ground states $|5\rangle$ and $|6\rangle$. In the subsequent chapters, the effect of this coherence on probe absorption is investigated in detail.

3.4 Conclusion

There are two main drawbacks of the wavefunction approach, because of which density matrix formalism is usually considered a preferred method of calculation. Firstly, in the density matrix formalism, decay of coherence is incorporated in a more straightforward way, as damping rates of off-diagonal elements. These dampings consist of both natural decay of phase and decoherence due to collision. Decoherence decays are not incorporated in the calculations of this chapter. Secondly, a completeness condition is easily imposed on a density matrix system by setting the sum of all the diagonal elements of density matrix equal to one at all times. Such representation of a closed system is not mathematically clear in wavefunction approach. Further, using this completeness condition, one of the diagonal terms of density matrix can be eliminated and hence the

equations can be solved for 'steady state' in the strict sense of the term. However, wavefunction approach results in simpler solutions and lesser number of equations to solve. Solutions for long-time limit can be a good substitute for 'steady-state solutions'. The advantage of wavefunction solutions lies in the 'Dressed state' analysis which clearly depicts the superposition states formed and their interactions. For both **Y** and **Gate** schemes, the wavefunction solutions match the density matrix solutions showing that either approach can be employed for these two systems.

Summing up the results of this chapter, the **Y** and **Gate** systems are analysed in the wavefunction approach and the results are compared with those obtained in density matrix formalism. The results are found to agree with each other. The Dressed states formed in both cases are determined and the cause of transparency in case of **Y** and lack of a complete transparency in case of **Gate** is clearly shown. At zero detuning, the **Y** system shows a transparency because the dressed state involved is made up of two bare states that do not connect to the ground state via the probe beam. In the **Gate** system, the dressed state involved consists of two states, such that they connect to two different ground states and hence a cancellation of absorption does not take place. A rigorous derivation of spontaneous emission decay shows that Quantum Interference between spontaneous emission pathways is not observed in either **Y** or **Gate** system. The coherences between ground states is seen to significantly affect the behaviour of system in the **Gate** system, which will be discussed in detail in the next chapter. The validity of different approximations used is established by the fact that the three approaches, viz, density matrix, bare state wavefunctions and the dressed states show exactly identical behaviour.

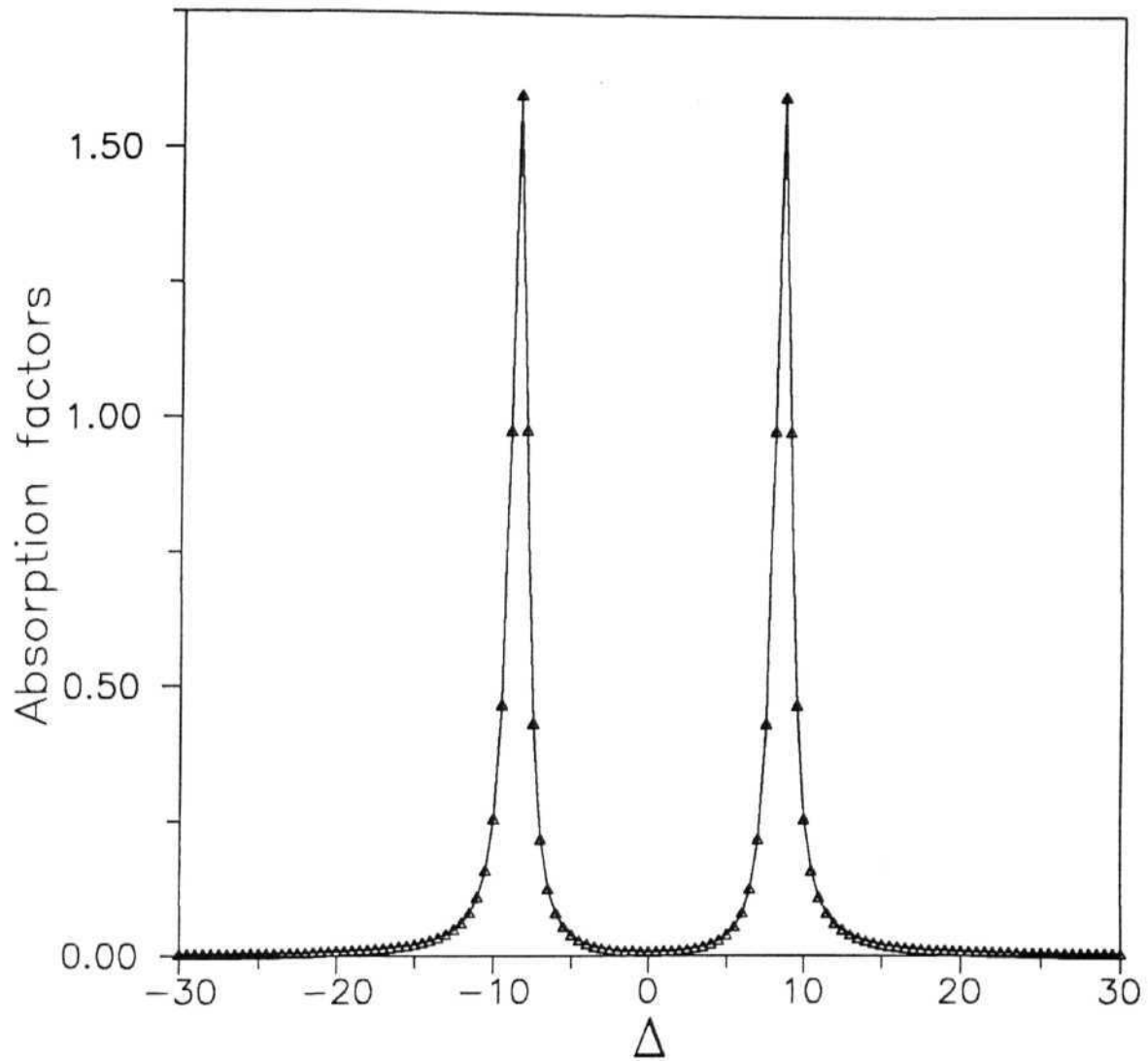


Fig. 3.1: Two absorption factors are plotted against probe detuning. Solid line is the factor in equation 3.6. Symbols are for factor in equation 3.20(b).

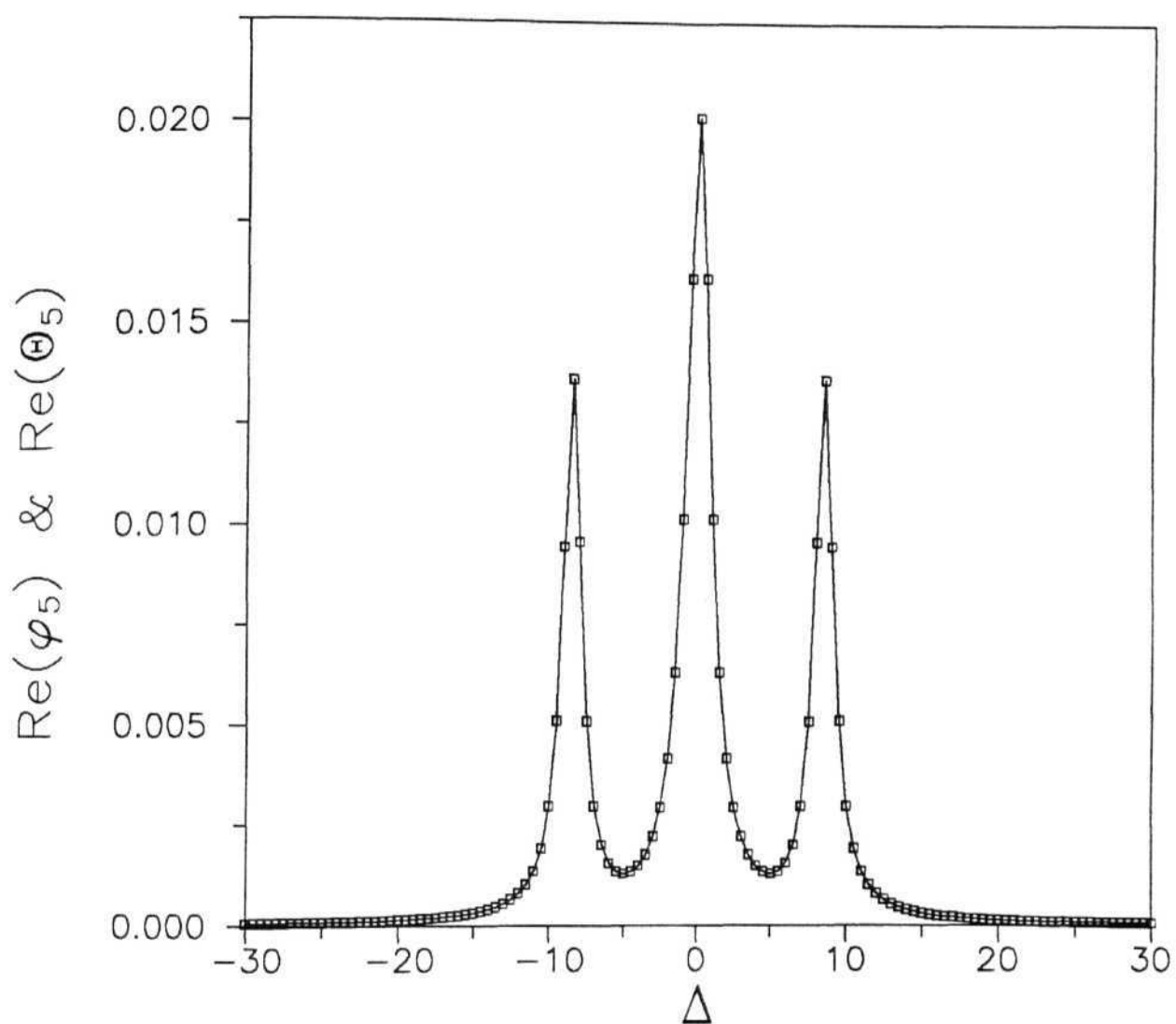


Fig. 3.2 : $\text{Re}(\varphi_5)$ (solid line) and $\text{Re}(\Theta_5)$ (symbols).
 $\text{Re}(\varphi_6)$ and $\text{Re}(\Theta_6)$ are identical.

References

- [1] C. Cohen-Tannoudji, *Frontiers in Laser Spectroscopy*, Vol I , ed:-R. Balian, S. Haroche and S. Liberman, North Holland, pp 17 (1977); R. M. Whitely and C. R. Sroud Jr. Phys. Rev. A 14, 1498 (1976); C. Cohen-Tannoudji and S. Reynaud. J. Phys. B 10, 345 (1977)
- [2] P. R. Berman, Phys. Rev. A 53, 2627. (1996); P. R. Berman and R. Salomaa, Phys. Rev. A 25, 2667 (1982)
- [3] M. Sargent III, M. O. Scully and W. E. Lamb Jr. *Laser Physics*, Addison Wesley, Mass. (1974) pp 23.
- [4] E. Arimondo, *Progress in Optics*, XXXV, ed: E. Wolf, Elsevier 1996. pp 259
- [5] S. E. Harris, Phys. Rev. Lett. 62, 1033(1989)
- [6] A. Imamoglu Phys. Rev. A 40, 2835 (1989)
- [7] Y-q Li and M. Xiao, Phys. Rev. A 51, 4959 (1995)
- [8] W. Heitler, *The Quantum Theory of Radiation*, Clarendon, Oxford, (1954), pp 68
- [9] M. O. Scully and M. S. Zubairy *Quantum Optics*, Cambridge Univeristy Press (1997), pp 206
- [10] R. Loudon, *The Quantum Theory of Light*, Clarendon, Oxford, (1988) pp 174
- [11] A. S. Zibrov, M. D. Lukin, D. E. Nikonov, L. Holleberg, M. O. Scully, V. L. Velichansky and H. G. Robinson, Phys. Rev. Lett. 75, 1499 (1995)
- [12] P. T. H. Fisk, H. -A. Bachor and R. J. Sandeman Phys. Rev A 33 2418 (1986); ibid 2424; ibid A 34 4762 (1986)
- [13] M. Fleischhauer, C. H. Keitel, L. M. Narducci, M. O. Scully, S. -Y. Zhu, M. S. Zubairy, Opt. Comm 94, 599 (1992)

References

- [1] C. Cohen-Tannoudji, *Frontiers in Laser Spectroscopy*, Vol I , ed:-R. Balian, S. Haroche and S. Liberman, North Holland, pp 17 (1977); R. M. Whitely and C. R. Stroud Jr. Phys. Rev. A 14, 1498 (1976); C. Cohen-Tannoudji and S. Reynaud, J. Phys. B 10, 345 (1977)
- [2] P. R. Berman, Phys. Rev. A 53, 2627, (1996); P. R. Berman and R. Salomaa, Phys. Rev. A **25**, 2667 (1982)
- [3] M. Sargent III, M. O. Scully and W. E. Lamb Jr. *Laser Physics*, Addison Wesley, Mass. (1974) pp 23.
- [4] E. Arimondo, *Progress in Optics* XXXV, ed: E. Wolf, Elsevier 1996, pp 259
- [5] S. E. Harris, Phys. Rev. Lett. 62, 1033(1989)
- [6] A. Imamoglu Phys. Rev. A 40, 2835 (1989)
- [7] Y-q Li and M. Xiao, Phys. Rev. A 51, 4959 (1995)
- [8] W. Heitler, *The Quantum Theory of Radiation*, Clarendon, Oxford, (1954), pp 68
- [9] M. O. Scully and M. S. Zubairy *Quantum Optics*, Cambridge University Press (1997), pp 206
- [10] R. Loudon, *The Quantum Theory of Light*, Clarendon, Oxford, (1988) pp 174
- [11] A. S. Zibrov, M. D. Lukin, D. E. Nikonov, L. Holleberg, M. O. Scully, V. L. Velichansky and H. G. Robinson, Phys. Rev. Lett. 75, 1499 (1995)
- [12] P. T. H. Fisk, H. -A. Bachor and R. J. Sandeman Phys. Rev A 33 2418 (1986); ibid 2424; ibid A 34 4762 (1986)
- [13] M. Fleischhauer, C. H. Keitel, L. M. Narducci, M. O. Scully, S. -Y. Zhu, M. S. Zubairy, Opt. Comm 94, 599 (1992)

Chapter IV

Groundstate Coherences

*The effect of injected atomic ground state coherences in **Gate** system on the probe absorption is discussed. The coherence is created externally between two ground states of **Gate**, $|5\rangle$ and $|6\rangle$, and its effect on probe absorption is studied. At the limiting values, the maximum positive coherence is seen to enhance the transparency while the negative coherence annuls the effect of transparency. The concept of Coherent Population Trapped (CPT) states is discussed in view of this result and an interaction between the two CPT states is shown to be possible.*

In previous chapters, the coherences that modify the probe absorption were constantly created by the strong laser beam. Instead, the atomic system can be prepared with a definite coherence and the probe laser interacts with such atoms [1, 2]. On similar lines, we present a study of **Gate** configuration, where the two ground states $|5\rangle$ and $|6\rangle$ are prepared in a superposition state prior to the interaction with the pump and the probe beam. Effect of such 'injected coherence', which acts in addition to the coherence generated by the pump beams is analysed in this chapter. It is assumed that the injected coherence is not destroyed during the interaction with the probe and pump beams. This additional coherence is seen to either enhance or destroy the transparency. In Chapter V, such coherences are seen to result from a detuned interaction of the pump beam on the probe transition. The results of this chapter form a basis on

which the results of Chapter V can be easily understood.

From the previous chapter, the probe absorption for the **Gate** system is obtained from,

$$\partial_t C_5 = \left[\frac{i\Delta_9 - \gamma_9 + F_2}{i\Delta_9 - \gamma_9 + F_1 + F_2} \right] \frac{|g_{57}|^2 C_5}{i\Delta_s - \gamma_{57}} + \frac{g_{57}^* g_{79}^* g_{89} g_{68} C_6}{(i\Delta_9 - \gamma_9 + F_1 + F_2)(i\Delta_s - \gamma_{57})(i\Delta_s - \gamma_{68})} \quad (4.1)$$

$$\partial_t C_6 = \left[\frac{i\Delta_9 - \gamma_9 + F_1}{i\Delta_9 - \gamma_9 + F_1 + F_2} \right] \frac{|g_{68}|^2 C_6}{i\Delta_s - \gamma_{68}} + \frac{g_{68}^* g_{89}^* g_{79} g_{57} C_5}{(i\Delta_9 - \gamma_9 + F_1 + F_2)(i\Delta_s - \gamma_{57})(i\Delta_s - \gamma_{68})} \quad (4.2)$$

where

$$F_1 = \frac{|g_{79}|^2}{i\Delta_s - \gamma_{59}} \quad \text{and} \quad F_2 = \frac{|g_{89}|^2}{i\Delta_s - \gamma_{68}}$$

also $\Delta_9 = \Delta_s + \Delta_p$, and $\gamma_9 = \gamma_{79} = \gamma_{89}$

$$\partial_t |C_5|^2 = 2 \text{Real}(\phi_5) |C_5|^2 + \phi_{56} C_6 C_5^* + \phi_{56}^* C_6^* C_5 \quad (4.3)$$

$$\partial_t |C_6|^2 = 2 \text{Real}(\phi_6) |C_6|^2 + \phi_{65} C_5 C_6^* + \phi_{65}^* C_5^* C_6 \quad (4.4)$$

If population is equally distributed between levels $|5\rangle$ and $|6\rangle$, then, $|C_5|^2 = |C_6|^2 = 1/2$ and hence, $C_5 = C_6 = \sqrt{1/2}$. Therefore, the maximum value of the coherence that can develop between levels $|5\rangle$ and $|6\rangle$ is $|\rho_{56}| = |C_5 C_6^*| = 0.5$. Depending upon the phase of the wave functions $|5\rangle$ and $|6\rangle$, the coherence can be either $+0.5$ or -0.5 . In other words, a superposition state is created which consists of $|5\rangle + |6\rangle$ for a $+0.5$ coherence or $|5\rangle - |6\rangle$ for a -0.5 coherence[§]. Assuming that (i) the atomic system is prepared in either one of these states and (ii) such a superposition is not destroyed due

[§]In this and subsequent chapters, the complete, normalized superposition state of which $|5\rangle \pm |6\rangle$ is a part is referred to, for the ease of readability, simply as the $|5\rangle \pm |6\rangle$. Similarly the state which consists $|7\rangle \pm |8\rangle$ is referred to as the $|7\rangle \pm |8\rangle$ state.

to collisions or the action of pump and probe beams, equations 4.3 and 4.4 reduce to,

$$\begin{aligned}\partial_t |C_5(t)|^2 &= 2 \operatorname{Real} (\phi_5 \pm \phi_{56}) \cdot (1/2) \\ \partial_t |C_6(t)|^2 &= 2 \operatorname{Real} (\phi_6 \pm \phi_{65}) \cdot (1/2)\end{aligned}\tag{4.5}$$

Figures 4.1, 4.2 and 4.3 show the behaviour of $\phi_5 \pm \phi_{56}$ for three values of coherences, viz, 0 and $\pm 1/2$. Figure 4.1 shows the absorption profile for the case when coherence is zero, which is a triplet structure obtained in the previous two chapters. The sidebands are at $\Delta_s = \pm \sqrt{|g_{79}|^2 + |g_{89}|^2}$.

For coherence $\rho_{56} = -0.5$, the two sidebands disappear and only the central peak exists, as shown in figure 4.2. This profile is a Lorentzian which is a typical absorption profile for a two level system [4]. In absence of the pump beam the Gate system would have been a system of two two-level configurations made up of $|5\rangle \leftrightarrow |7\rangle$ and $|6\rangle \leftrightarrow |8\rangle$. Each of these two would have a Lorentzian absorption profile and the total absorption would be a sum of these two Lorentzians. A coherence of $C_5 C_6^* = -0.5$ give this profile in spite of the pump beams creating a superposition state of excited states $|7\rangle$ and $|8\rangle$.

Figure 4.3 shows the probe absorption profile when the coherence $\rho_{56} = +0.5$. The central peak is absent now and only the sidebands are present. The system achieves a complete EIT, as in case of the Y system. It can also be seen that in all these cases the area under the curves for all the three profiles are same. The absorption is getting redistributed into sidebands.

A straightforward explanation for this effect can be found in the 'Dressed state' picture. It was seen in Chapter III, that the strong laser creates the 'Dressed states'

out of levels $|7\rangle$, $|8\rangle$ and $|9\rangle$, and that these states have eigenenergy values $0, \pm\alpha$. The new eigenstates are related to Bare states by

$$\begin{aligned} |\Psi_+\rangle &= \frac{1}{\sqrt{2}\alpha} \left[\alpha \bar{C}_9 |9\rangle + i g_{89} \bar{C}_8 |8\rangle + i g_{79} \bar{C}_7 |7\rangle \right] \\ |\Psi_0\rangle &= \frac{1}{\alpha} \left[g_{79}^* \bar{C}_8 |8\rangle - g_{89}^* \bar{C}_7 |7\rangle \right] \\ |\Psi_-\rangle &= \frac{1}{\sqrt{2}\alpha} \left[\alpha \bar{C}_9 |9\rangle - i g_{89} \bar{C}_8 |8\rangle - i g_{79} \bar{C}_7 |7\rangle \right] \end{aligned} \quad (4.6)$$

where $a^2 = |g_{79}|^2 + |g_{89}|^2$.

On resonance, when $\Delta_s = 0$, the probe beam interacts with Ψ_0 . When coherence $\rho_{56} = 0$, the two ground states $|5\rangle$ and $|6\rangle$ are independent. Therefore the absorption is proportional to the transition probability

$$|\langle \Psi_0 | d \cdot \mathcal{E} | 5 \rangle|^2 + |\langle \Psi_0 | d \cdot \mathcal{E} | 6 \rangle|^2.$$

which reduces to

$$\frac{1}{\alpha} |g_2|^2 \left[|\langle 7 | d \cdot \mathcal{E} | 5 \rangle|^2 + |\langle 8 | d \cdot \mathcal{E} | 6 \rangle|^2 \right] \quad (4.7)$$

Where, $g_2 = g_{79} = g_{89}$

At detuning $\Delta_s = \pm\alpha$, the probe interacts with the states Ψ_{\pm} and the absorption is proportional to transition probability

$$|\langle \Psi_{+,-} | d \cdot \mathcal{E} | 5 \rangle|^2 + |\langle \Psi_{+,-} | d \cdot \mathcal{E} | 6 \rangle|^2.$$

which reduces to

$$\frac{1}{\sqrt{2}\alpha} |g_2|^2 \left[|\langle 7 | d \cdot \mathcal{E} | 5 \rangle|^2 + |\langle 8 | d \cdot \mathcal{E} | 6 \rangle|^2 \right] \quad (4.8)$$

Equation (4.7) shows the origin of the central peak leading to a nonzero absorption,

while equation (4.8) **shows** the origin of the sidebands. These equations also show **that** the ratio between the heights of central peak and sidebands is $1/\sqrt{2}$.

A nonzero coherence $C_5 C_6^*$ is equivalent to a superposition of ground states in the form $|5 \pm 6\rangle$. The interaction of this state with $\Psi_{0,\pm}$ will be governed by the probabilities $|\langle \Psi_{0,\pm} | d.\mathcal{E} | 5 \pm 6 \rangle|^2$. When the coherence is positive, with $C_5 C_6^* = +0.5$, the state formed is $|5 + 6\rangle$ and transition probability of its interaction with Ψ_{\pm} is given by

$$\begin{aligned} |\langle \Psi_{+,-} | d.\mathcal{E} | 5 + 6 \rangle|^2 &= |\langle \Psi_{+,-} | d.\mathcal{E} | 5 \rangle + \langle \Psi_{+,-} | d.\mathcal{E} | 6 \rangle|^2 \\ &= \frac{1}{2} \alpha^2 [|\langle 7 | d.\mathcal{E} | 5 \rangle + \langle 8 | d.\mathcal{E} | 6 \rangle|^2] \neq 0 \end{aligned} \quad (4.9)$$

$$\begin{aligned} |\langle \Psi_0 | d.\mathcal{E} | 5 + 6 \rangle|^2 &= [|\langle \Psi_0 | d.\mathcal{E} | 5 \rangle + \langle \Psi_0 | d.\mathcal{E} | 6 \rangle|^2] \\ &= \frac{1}{2} [|\langle 7 | d.\mathcal{E} | 5 \rangle - \langle 8 | d.\mathcal{E} | 6 \rangle|^2] = 0 \end{aligned} \quad (4.10)$$

Equation (4.10) shows that the central peak is absent, while (4.9) indicates the presence of two sidebands of equal height.

When the coherence $C_5 C_6^* = -0.5$ the superposition state formed is $|5\rangle - |6\rangle$. Transition probability for this state interacting with the Ψ states are

$$\begin{aligned} |\langle \Psi_{+,-} | d.\mathcal{E} | 5 - 6 \rangle|^2 &= |\langle \Psi_{+,-} | d.\mathcal{E} | 5 \rangle - \langle \Psi_{+,-} | d.\mathcal{E} | 6 \rangle|^2 \\ &= \frac{1}{2} \alpha^2 [|\langle 7 | d.\mathcal{E} | 5 \rangle - \langle 8 | d.\mathcal{E} | 6 \rangle|^2] = 0 \end{aligned} \quad (4.11)$$

$$\begin{aligned} |\langle \Psi_0 | d.\mathcal{E} | 5 - 6 \rangle|^2 &= [|\langle \Psi_0 | d.\mathcal{E} | 5 \rangle - \langle \Psi_0 | d.\mathcal{E} | 6 \rangle|^2] \\ &= \frac{1}{2} [|\langle 7 | d.\mathcal{E} | 5 \rangle + \langle 8 | d.\mathcal{E} | 6 \rangle|^2] \neq 0 \end{aligned} \quad (4.12)$$

Equation (4.11) shows a zero transition probability with Ψ_{\pm} which denotes absence

of the sidebands. A non-zero probability with Ψ_0 in (4.12) is an indication of the central peak.

4.1 Coupling of Non-Coupling States

This leads to the discussion on the Coherent Population Trapped (CPT) states. CPT states are obtained when two ground states form a non-coupling superposition state where population get trapped [5, 6, 21, 8]. In a typical A configuration two degenerate lower states $|a\rangle$ and $|b\rangle$ interact with an upper state $|c\rangle$ via an EM field with equal transition probability $\langle a|d.E|c\rangle = \langle b|d.E|c\rangle$. d is the dipole moment of the transition and E is the amplitude of the EM field that is involved. The steady state situation of this system is a superposition state $P_- = \frac{1}{\sqrt{2}}(|a\rangle - |b\rangle)$. This is a noncoupling state because the transition probability

$$\begin{aligned} |\langle c|d.E|a\rangle - \langle c|d.E|b\rangle|^2 &= |\langle c|d.E|a\rangle - \langle c|d.E|b\rangle|^2 \\ &= |\langle a|d.E|c\rangle|^2 + |\langle b|d.E|c\rangle|^2 - 2\langle a|d.E|c\rangle \cdot \langle b|d.E|c\rangle = 0 \end{aligned} \quad (4.13)$$

A superposition of the form $Q_+ = |a + b\rangle$ will be a coupled state since the transition probability is

$$\begin{aligned} |\langle c|d.E|a + b\rangle|^2 &= |\langle c|d.E|a\rangle + \langle c|d.E|b\rangle|^2 \\ &= |\langle a|d.E|c\rangle|^2 + |\langle b|d.E|c\rangle|^2 + 2\langle a|d.E|c\rangle \cdot \langle b|d.E|c\rangle \neq 0 \end{aligned} \quad (4.14)$$

A similar cancellation occurs in a V system, where two upper states $|p\rangle$ and $|q\rangle$ form a superposition state $|Q_- \rangle = \frac{1}{\sqrt{2}}|p - q\rangle$ and a cancellation of transition probability occurs when this state interacts with a ground state $|r\rangle$. Unlike the CPT condition, the population is trapped in state $|r\rangle$ and not in the coherent superposition state Q_- .

Though situations containing V and A have been encountered [9, 10], the interaction between these two configurations have not been analyzed. Interaction of two superposition states thus formed can be generalized in following way.

Considering the set of superposition states formed

$$|P_+\rangle = \frac{1}{\sqrt{2}}|a\rangle + |b\rangle$$

$$|P_-\rangle = \frac{1}{\sqrt{2}}|a\rangle - |b\rangle$$

$$|Q_+\rangle = \frac{1}{\sqrt{2}}|p\rangle + |q\rangle$$

$$|Q_-\rangle = \frac{1}{\sqrt{2}}|p\rangle - |q\rangle$$

wherein the individual bare states interact via a dipole transition as

$$\langle a|d.E|p\rangle = \langle b|d.E|q\rangle$$

and

$$\langle a|d.E|q\rangle = 0 = \langle b|d.E|p\rangle$$

Then the superposition states obey dipole allowed transitions in the form

$$\langle P_+|d.E|Q_+\rangle = \langle a|d.E|p\rangle + \langle b|d.E|q\rangle \neq 0$$

$$\langle P_-|d.E|Q_-\rangle = \langle a|d.E|p\rangle + \langle b|d.E|q\rangle \neq 0$$

$$\langle P_+|d.E|Q_-\rangle = \langle a|d.E|p\rangle - \langle b|d.E|q\rangle = 0$$

and

$$\langle P_- | d.E | Q_+ \rangle = -\langle a | d.E | p \rangle + \langle b | d.E | q \rangle = 0 \quad (4.15)$$

In short form

$$\langle P_{\pm} | d.E | Q_{\pm} \rangle = \delta_{\pm,\pm} \quad (4.16)$$

In other words, two Non-Coupling states interact with each other with complete transition. The term Non-Coupling is therefore relative, defined with respect to the level with which the probe is trying to couple. And equations 4.15 and 4.16 define a set of rules for quantum interference between states which are intrinsically superposition of basis states. This property has to be incorporated while calculating the selection rules between complex atomic or molecular states.

A naturally occurring phenomena is an example of this effect. Clebsch-Gordon coefficient for a transition between $m_F=0$ of $S_{1/2}$ and $m_F=0$ of $P_{1/2}$ is zero[†]. A dipole transition of the form $m_F = 0 \leftrightarrow m_F = 0$ is therefore forbidden [19]. It is seen that state $|F = 1, m_F = 0\rangle$ of $S_{1/2}$ is $|F = 1, m_F = 0\rangle = -\sqrt{\frac{1}{2}}|\frac{3}{2}, -\frac{1}{2}\rangle |0, 0\rangle |\frac{1}{2}, \frac{1}{2}\rangle + \sqrt{\frac{1}{2}}|\frac{3}{2}, \frac{1}{2}\rangle |0, 0\rangle |\frac{1}{2}, -\frac{1}{2}\rangle$, which is a Q_- state. State $|F = 1, m_F = 0\rangle$ of $P_{1/2}$ is $|F = 1, m_F = 0\rangle = \sqrt{\frac{1}{6}}|\frac{3}{2}, -\frac{1}{2}\rangle |1, 0\rangle |\frac{1}{2}, \frac{1}{2}\rangle - \sqrt{\frac{1}{3}}|\frac{3}{2}, -\frac{1}{2}\rangle |1, 1\rangle |\frac{1}{2}, -\frac{1}{2}\rangle - \sqrt{\frac{1}{3}}|\frac{3}{2}, \frac{1}{2}\rangle |1, -1\rangle |\frac{1}{2}, \frac{1}{2}\rangle + \sqrt{\frac{1}{6}}|\frac{3}{2}, \frac{1}{2}\rangle |1, 0\rangle |\frac{1}{2}, -\frac{1}{2}\rangle$ which is a Q_+ state. Therefore, from 4.15, the transition probability between these two states is zero. Whereas, the $|F=2, m_F = 0\rangle$ level of $P_{1/2}$ is a Q_- state and the transition $|S_{1/2} F=1, m_F = 0\rangle \rightarrow |P_{1/2} F=1, m_F = 0\rangle \neq 0$. $|P_{3/2} F=1, m_F = 0\rangle$ level is also a Q_+ state and the transition probability is zero here also. On similar arguments, $|S_{1/2} F=2, m_F = 0\rangle$ level of has a nonzero transition probability with $|P_{1/2} F=1, m_F = 0\rangle$ level of and $|S_{1/2} F=2, m_F = 0\rangle$ level has a zero transition probability with $|P_{1/2} F=2, m_F = 0\rangle$.

[†]See appendix C for Clebsch-Gordon coefficients

If in an experiment, a π polarized light is shone onto Sodium vapour, which connects $|F \approx 1\rangle$ to $|F=1\rangle$ state, it brings about a $\Delta m_F = 0$ transition. Then, the population from $m_F = +1$ of $S_{1/2}$ is pumped to $m_F = +1$ of $P_{1/2}$ and that from $m_F = -1$ to $m_F = -1$. A fraction of this population that decays due to spontaneous emission to state $m_F = 0$ of $S_{1/2}$ gets trapped and eventually, all the population is optically pumped into this state and trapped. State $m_F = 0$ is a natural trapped state of the atom.

4.2 Density matrix solutions

The effect of the coherence between the two ground states is evident even in the solutions obtained in density matrix solutions. While deriving the analytical expression for probe absorption in the density matrix formalism, the coherence $\rho_{56}^{(0)}$ was neglected, assuming that the zeroth order term will have an insignificant value. But, if this coherence is induced externally, and assuming that the collision rate is too small to destroy this coherence, then the effect of the coherence is seen to modify the probe absorption.

From equations 2.13-2.18

$$-i \partial_t \rho_{75}^{(1)} = (-\Delta_{75} + i \gamma_{57}) \rho_{75}^{(1)} + d_{75} \mathcal{E}_s^- (\rho_{55}^{(0)} - \rho_{77}^{(0)}) + d_{97}^* \mathcal{E}_p^+ \rho_{95}^{(1)} \quad (4.17)$$

$$\begin{aligned} -i \partial_t \rho_{95}^{(1)} &= [-(\Delta_{97} + \Delta_{75}) + i (\gamma_{79} + \gamma_{89})] \rho_{95}^{(1)} + d_{97} \mathcal{E}_p^+ \rho_{75}^{(1)} \\ &+ d_{98} \mathcal{E}_p^- \rho_{85}^{(1)} - d_{75} \mathcal{E}_s^- \rho_{97}^{(0)} \end{aligned} \quad (4.18)$$

$$-i \partial_t \rho_{85}^{(1)} = (-\Delta_{85} + i \gamma_{68}) \rho_{85}^{(1)} + d_{86} \mathcal{E}_s^- \rho_{65}^{(0)} + d_{98}^* \mathcal{E}_p^+ \rho_{95}^{(1)} - d_{75} \mathcal{E}_s^- \rho_{87}^{(0)} \quad (4.19)$$

$$-i \partial_t \rho_{86} = (-\Delta_{86} + 8i \gamma_{68}) \rho_{86}^{(1)} + d_{86} \mathcal{E}_s^- (\rho_{66}^{(0)} - \rho_{88}^{(20)}) + d_{98}^* \mathcal{E}_p^- \rho_{96}^{(1)} \quad (4.20)$$

$$-i \partial_t \rho_{96} = [-(\Delta_{98} + \Delta_{86}) + i (\gamma_{89} + \gamma_{79})] \rho_{96}^{(1)} + d_{98} \mathcal{E}_p^- \rho_{86}^{(1)}$$

$$+ d_{97}\mathcal{E}_p^+ \rho_{76}^{(1)} - d_{86}\mathcal{E}_s^- \rho_{98}^{(0)} \quad (4.21)$$

$$-i \partial_t \rho_{76}^{(1)} = (-\Delta_{76} + i \gamma_{57}) \rho_{76}^{(1)} + d_{86}\mathcal{E}_s^- \rho_{78}^{(0)} + d_{75}\mathcal{E}_s^- \rho_{56}^{(0)} - d_{97}^* \mathcal{E}_p^+ \rho_{96}^{(1)} \quad (4.22)$$

Again, $\rho_{77}^{(0)}$, $\rho_{78}^{(0)}$ and $\rho_{79}^{(0)}$ are neglected but $\rho_{56}^{(0)}$ is retained,

With the above assumptions, steady state solution of equation 4.19 is obtained as

$$\rho_{85} = \frac{d_{98}^* \mathcal{E}_p^- \rho_{95}^{(1)} + d_{86} \mathcal{E}_s^- \rho_{65}^{(0)}}{\Delta_{85} - i \gamma_{68}}$$

Plugging this into equation 4.18, the steady state solution for (4.18) is

$$\rho_{95} = \frac{d_{97} \mathcal{E}_p^+ \rho_{75}^{(1)}}{\Delta_{95} - i \gamma_9 - \frac{|g_{98}|^2}{\Delta_{85} - i \gamma_{68}}} + \frac{d_{98} \mathcal{E}_p^- d_{86} \mathcal{E}_s^- \rho_{65}^{(0)}}{\left[\Delta_{95} - i \gamma_9 - \frac{|g_{98}|^2}{\Delta_{85} - i \gamma_{68}} \right] [\Delta_{86} - i \gamma_{68}]}$$

Substituting this result into equation 4.17, we get at steady state,

$$\begin{aligned} \rho_{75} = & \frac{d_{75} \mathcal{E}_s^- \rho_{55}^{(0)}}{\Delta_{75} - i \gamma_{57} - \frac{|d_{97} \mathcal{E}_p^+|^2}{\Delta_{95} - i \gamma_9 - \frac{|d_{98} \mathcal{E}_p^-|^2}{\Delta_{85} - i \gamma_{68}}}} + \\ & \frac{d_{97}^* \mathcal{E}_p^+ d_{98} \mathcal{E}_p^- d_{86} \mathcal{E}_s^- \rho_{65}^{(0)}}{\left[\Delta_{75} - i \gamma_{57} - \frac{|d_{97} \mathcal{E}_p^+|^2}{\Delta_{95} - i \gamma_9 - \frac{|d_{98} \mathcal{E}_p^-|^2}{\Delta_{85} - i \gamma_{68}}} \right] \left[\Delta_{95} - i \gamma_9 - \frac{|d_{98} \mathcal{E}_p^-|^2}{\Delta_{85} - i \gamma_{68}} \right] [\Delta_{85} - i \gamma_{68}]} \end{aligned} \quad (4.23)$$

The expression 4.23 is seen to contain two terms. The first term is same as that obtained in Chapter II, at equations 2.20 and 2.21. The second term contains the

dependency on coherence $\rho_{56}^{(0)}$ and $\rho_{65}^{(0)}$. Under the conditions that $\gamma_{57} = \gamma_{68} = \gamma$, $\Delta_{76} = \Delta_{86} = \Delta_{85} = \Delta_{75} = \Delta_s$, which is usually the case if the **Gate** system is symmetric, then the coherence ρ_{56} shows the same effect that is shown by $C_5 C_6^*$ for equations 4.3 and 4.4. That is, when $\rho_{56}^{(0)} = \rho_{65}^{(0)} = \rho_{55}^{(0)} = \rho_{66}^{(0)}$, then the probe absorption consists of only sidebands and the central peak is absent. If $\rho_{56}^{(0)} = \rho_{65}^{(0)} = -\rho_{55}^{(0)} = -\rho_{66}^{(0)}$, then the probe absorption consists of only central peak and the sidebands are absent. Complete cancellation of transparency effect by a coherence of -0.5 is shown by density matrix equations also. Rewriting equation 4.23

$$\rho_{75} = \frac{g_s \mathcal{E}_s^- \rho_{55}^{(0)}}{\left[F_{75} - \frac{|g_p|^2}{F_{95} - \frac{|g_p|^2}{F_{85}}} \right]} + \frac{g_p^* g_p d_s \rho_{65}^{(0)}}{\left[F_{75} - \frac{|g_p|^2}{F_{95} - \frac{|g_p|^2}{F_{85}}} \right] \left[F_{95} - \frac{|g_p|^2}{F_{85}} \right] F_{85}}$$

where, $g_{75} = g_{86} = g_s$, $g_{97} = g_{98} = g_p$ and $F_{ij} = \Delta_{ij} - \gamma_i$. Further, $\gamma_{57} = \gamma_{68} = \gamma_s$, and $\Delta_{85} = \Delta_{75} = \Delta_s$, where the equality arises out of the symmetry of the system. Therefore, $F_{75} = \Delta_{75} - i\gamma_{57} = F_{86} = \Delta_{85} - i\gamma_{68} = F_s$. When $\rho_{65}^{(0)} = \pm \rho_{55}^{(0)}$, taking the common terms, the equation can be rewritten as

$$\begin{aligned} \rho_{75} &= \frac{g_s \mathcal{E}_s^- \rho_{55}^{(0)}}{\left[F_s - \frac{|g_p|^2}{F_{95} - \frac{|g_p|^2}{F_s}} \right]} \left[1 - \frac{|g_p|^2}{\left(F_{95} - \frac{|g_p|^2}{F_s} \right) F_s} \right] \\ &= \frac{g_s \mathcal{E}_s^- \rho_{55}^{(0)}}{\left[F_s - \frac{|g_p|^2}{F_{95} - \frac{|g_p|^2}{F_s}} \right]} \left[F_s - \frac{|g_p|^2}{\left(F_{95} - \frac{|g_p|^2}{F_s} \right)} \right] \frac{1}{F_s} \end{aligned}$$

$$\begin{aligned}
&= \frac{g_s \mathcal{E}_s^- \rho_{55}^{(0)}}{F_s} \\
&= \frac{g_s \mathcal{E}_s^- \rho_{55}^{(0)}}{\Delta - i\gamma}
\end{aligned}$$

which is same as the probe absorption for a two-level atom interacting with the probe, which is a single peaked Lorentzian. The coherence $\rho_{56}^{(0)} = -\rho_{55}^{(0)}$ has completely cancelled the effect of strong laser.

A similar two-term expression for $\rho_{68}^{(1)}$ can be obtained as

$$\begin{aligned}
\rho_{86} &= \frac{d_{86} \mathcal{E}_s^- \rho_{66}^{(0)}}{\Delta_{86} - i\gamma_{68} - \frac{|d_{98} \mathcal{E}_p^-|^2}{\Delta_{96} - i\gamma_9 - \frac{|d_{97} \mathcal{E}_p^+|^2}{\Delta_{76} - i\gamma_{57}}}} + \\
&\quad \frac{d_{98}^* \mathcal{E}_p^- d_{97} \mathcal{E}_p^+ d_{75} \mathcal{E}_s^- \rho_{56}^{(0)}}{\left[\Delta_{86} - i\gamma_{68} - \frac{|d_{98} \mathcal{E}_p^-|^2}{\Delta_{96} - i\gamma_9 - \frac{|d_{97} \mathcal{E}_p^+|^2}{\Delta_{76} - i\gamma_{57}}} \right] \left[\Delta_{96} - i\gamma_9 - \frac{|d_{97} \mathcal{E}_p^+|^2}{\Delta_{76} - i\gamma_{57}} \right] [\Delta_{76} - i\gamma_{57}]}
\end{aligned}
\tag{4.24}$$

And when the coherence is negative and equal to population, the expression reduces to

$$\rho_{86} = \frac{d_{86} \mathcal{E}_s^- \rho_{66}^{(0)}}{\Delta_{86} - i\gamma_{68}}$$

which is the probe absorption for a two-level atom.

4.3 Stability of ground state coherence

A simple method of preparing the coherence between two ground states is to connect them with a third level by a laser beam, forming a conventional A system. Suppose the A is formed out of levels $|5\rangle$, $|6\rangle$ and $|2\rangle$. The laser creates a coherence $\rho_{56} = -0.5$, preparing the system in a superposition state $Q_- = (1/\sqrt{2})|5\rangle - |6\rangle$ which is generally termed a CPT state [6, 8, 21]. Collisions between atoms and the walls can destroy this coherence. A competing effect between coherence creation by the laser and a coherence destruction by collisional damping can be verified. Steady state value for the coherence ρ_{56} can be examined as a function of collisional damping. The relevant set of equations, in the matrix form is

$$\partial_t \rho = M \cdot \rho + B \quad (4.25)$$

Where,

$$\rho = (\rho_{52} \quad \rho_{62} \quad \rho_{25} \quad \rho_{26} \quad \rho_{55} \quad \rho_{66} \quad \rho_{56} \quad \rho_{65})$$

$$M = \begin{pmatrix} D_1 & 0 & 0 & 0 & -2ig_{25}^* & -ig_{25}^* & -ig_{26}^* & 0 \\ 0 & D_2 & 0 & 0 & -ig_{26}^* & -2ig_{26}^* & 0 & -ig_{26}^* \\ 0 & 0 & D_3 & 0 & 2ig_{25} & ig_{25} & 0 & ig_{26} \\ 0 & 0 & 0 & D_4 & ig_{26} & 2ig_{26} & ig_{25} & 0 \\ -ig_{25} & 0 & ig_{25}^* & 0 & -2(\gamma_{52} + \gamma_{65}) & -2(\gamma_{52} - \gamma_{56}) & 0 & 0 \\ 0 & -ig_{26} & 0 & ig_{26}^* & -2(\gamma_{62} - \gamma_{65}) & -2(\gamma_{62} + \gamma_{56}) & 0 & 0 \\ -ig_{26} & 0 & 0 & ig_{25}^* & 0 & 0 & -(\gamma_{56} + \gamma_{65}) & 0 \\ 0 & -ig_{25} & ig_{26}^* & 0 & 0 & 0 & 0 & -(\gamma_{56} + \gamma_{65}) \end{pmatrix}$$

and

$$B = (ig_{25}^* \quad ig_{26}^* \quad -ig_{25} \quad -ig_{26} \quad 2\gamma_{52} \quad 2\gamma_{62} \quad 0 \quad 0)$$

Where,

$$D_1 = i\Delta_{25} - (\gamma_2 + \gamma_{65}) \quad (4.26)$$

$$D_2 = i\Delta_{26} - (\gamma_2 + \gamma_{56}) \quad (4.27)$$

$$D_3 = -i\Delta_{25} - (\gamma_2 + \gamma_{65}) \quad (4.28)$$

$$D_4 = -i\Delta_{26} - (\gamma_2 + \gamma_{56}) \quad (4.29)$$

Solving equation (4.25) for steady state, the value of ρ_{56} can be obtained. γ_{65} is the collisional damping rate. This damping is caused either by collisions between two atoms of similar type or by collision with the wall. The rate can be controlled in a vapour cell. Atom-atom collisions are controlled by the density of atoms inside the cell and atom-wall collision can be controlled by introducing a buffer gas. Figures 4.4 and 4.5 show the variation of ρ_{56} with collisional damping. Real and imaginary part of ρ_{56} is plotted in figures 4.4 (a) and (b) respectively for a value of $g_{25} = g_{26} = 0.2$, which is a weak beam. Different curves correspond to different detunings. It is seen that as detuning increases, very small collisions destroy the coherence ρ_{56} and its value decreases to zero rapidly. Figure 4.5 (a) and 4.5 (b) show real and imaginary part of ρ_{56} for $g_{25} = g_{26} = 6.0$ which is a strong beam. Here, the collisions do not destroy the coherence so easily. It takes a stronger collisional damping or more collisions, to spoil the coherence. All parameters are normalized to spontaneous emission decay γ as in the previous cases.

4.4 Conclusion

Effect of coherences between ground states of the **Gate** system, viz., $|5\rangle$ and $|6\rangle$ on probe absorption is presented. It is seen that the for a maximum value, the coherence

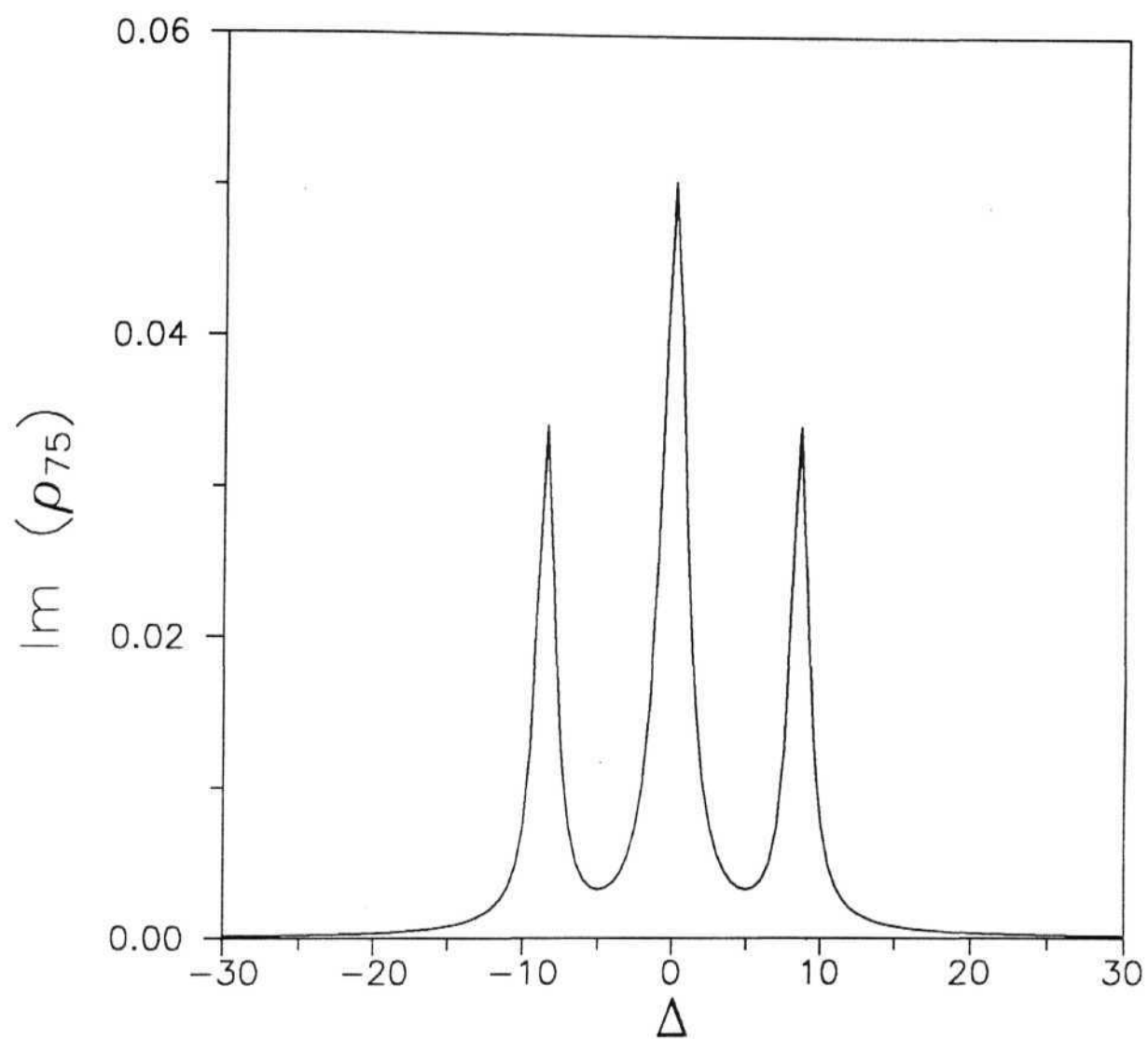


Fig. 4.1: Probe absorption for ground state coherence $\rho_{65}=0.0$

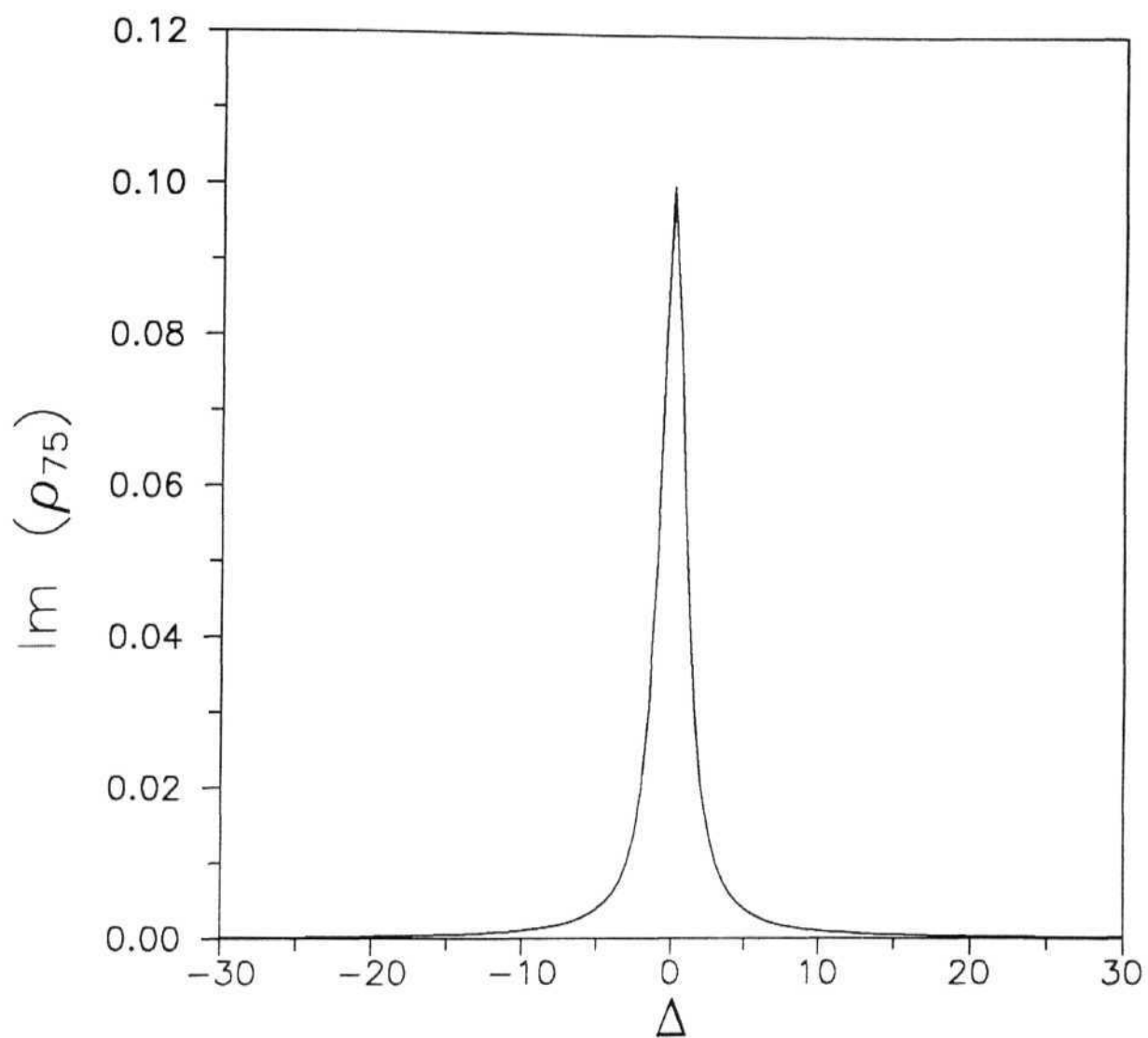


Fig. 4.2: Probe absorption for ground state coherence $\rho_{65} = -\rho_{55} = -\rho_{66}$

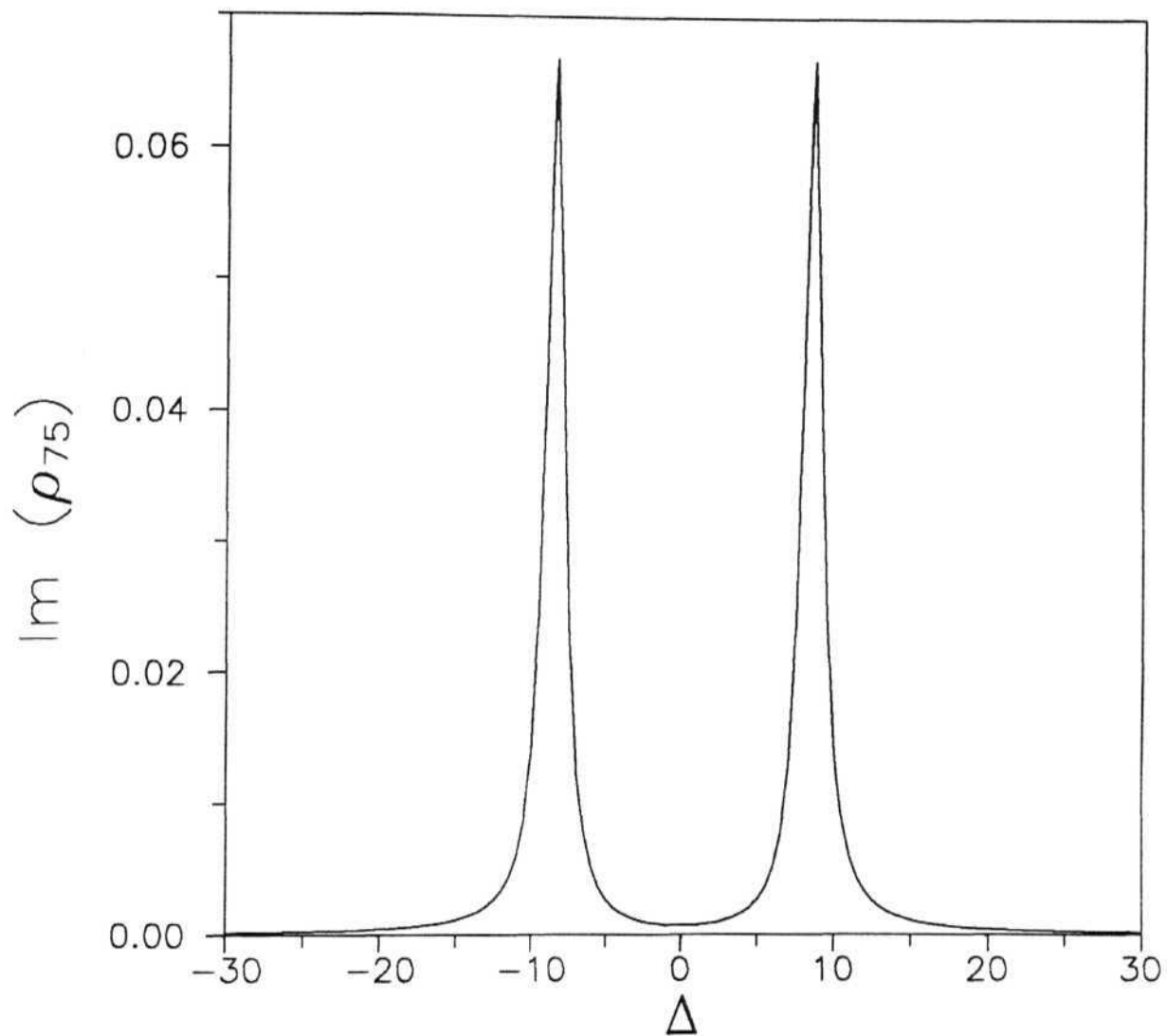


Fig. 4.3: Probe absorption for ground state coherence $\rho_{65}=\rho_{55}=\rho_{66}$.

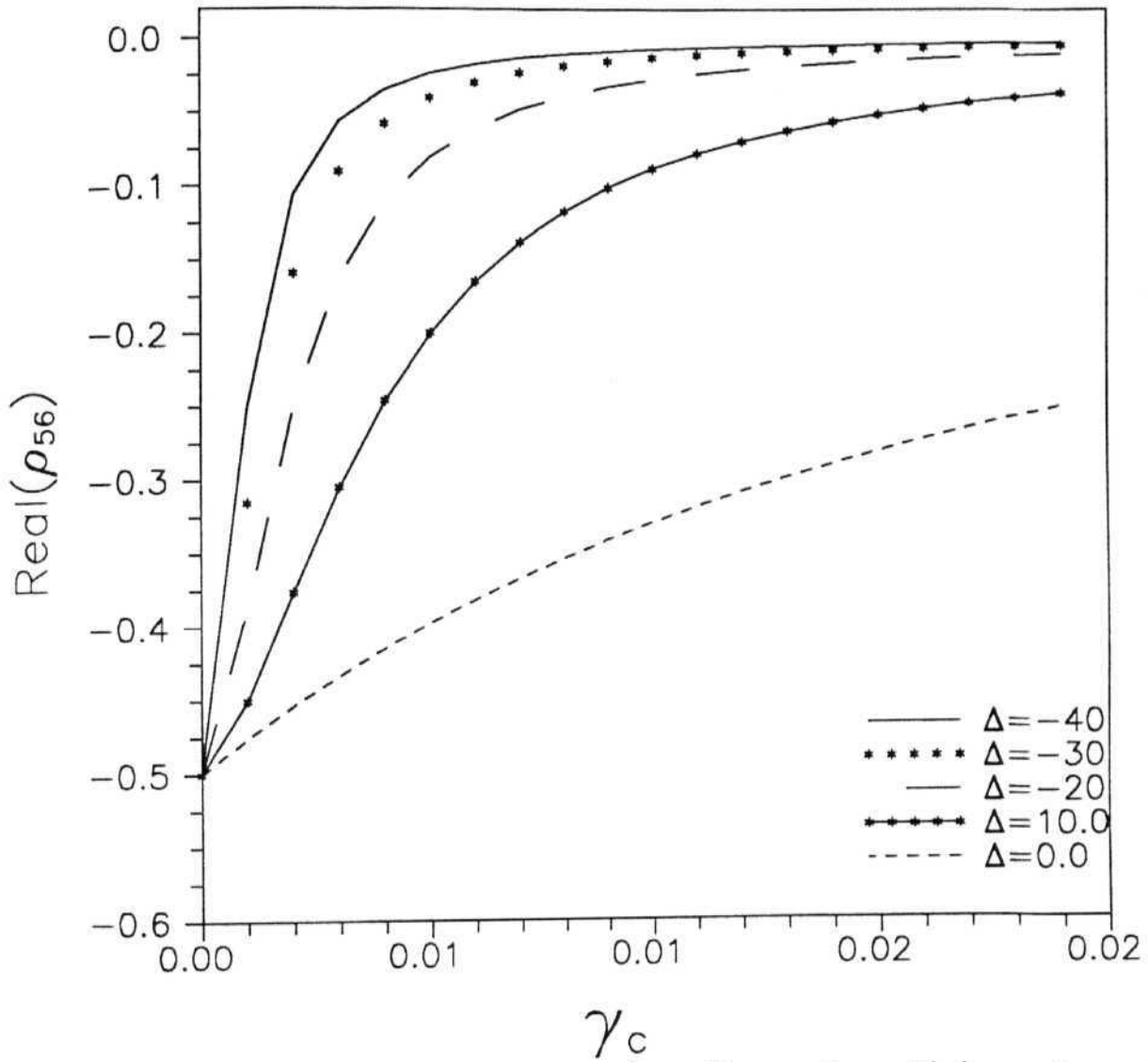


Fig. 4.4(a): Real ρ_{56} as a function of collision damping γ_c for $g_{25}=g_{26}=0.2$, for different detunings.

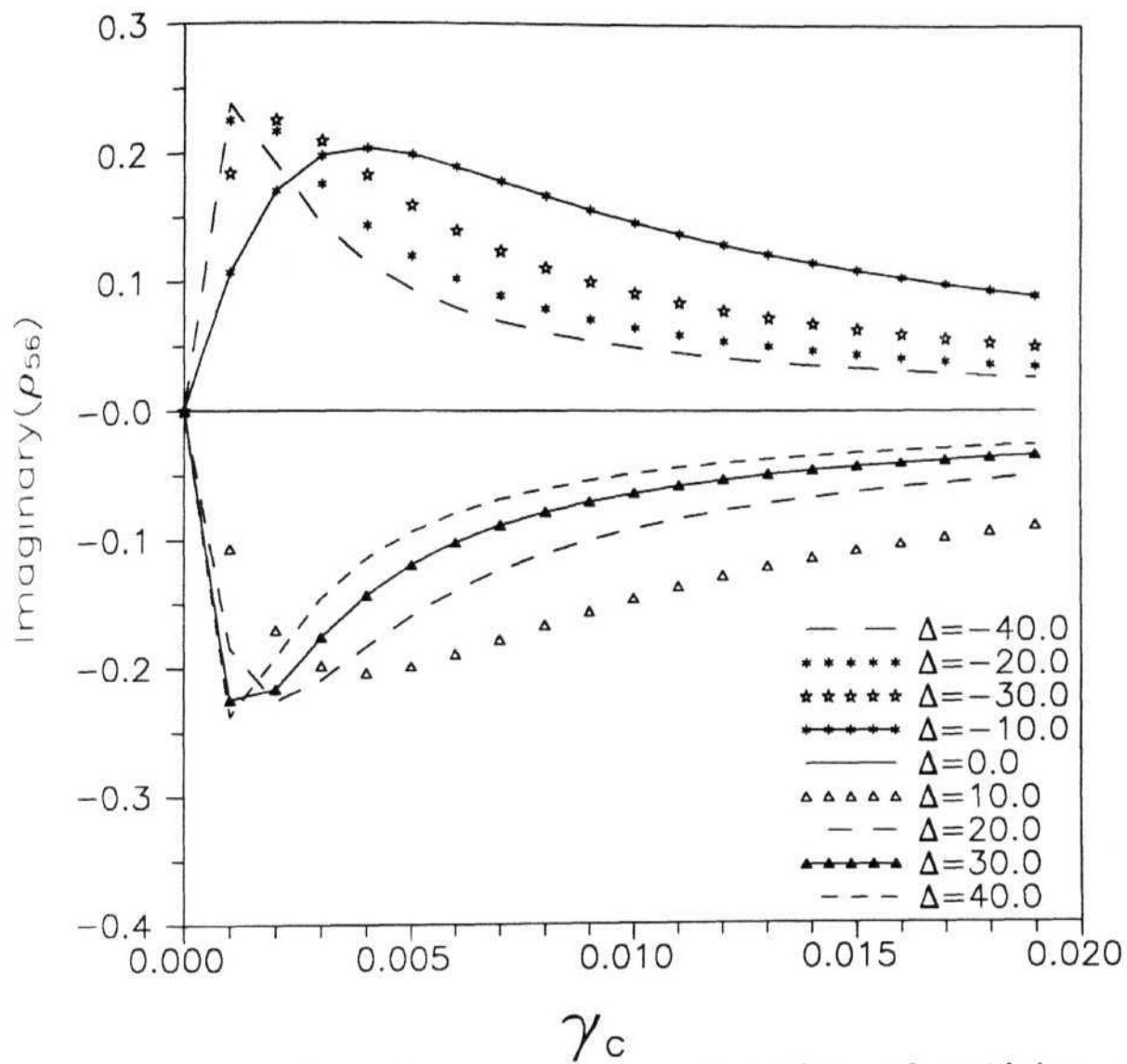


Fig. 4.4(b): Imaginary ρ_{56} as a function of collision damping γ_c for $g_{25}=g_{26}=0.2$, for different detunings.

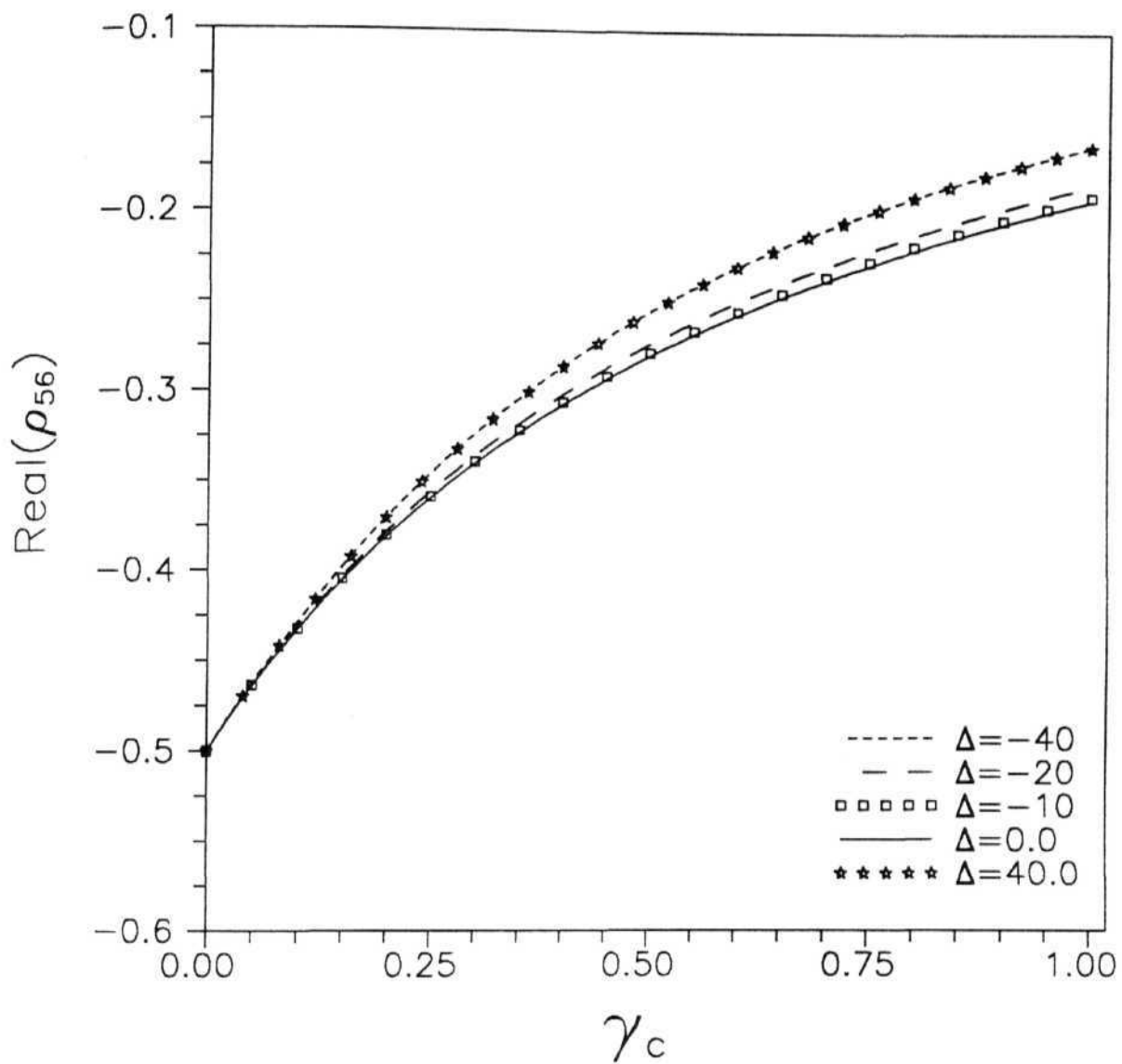


Fig. 4.5(a): Real ρ_{56} as a function of collision damping γ_c for $g_{25}=g_{26}=6.0$, for different detunings.

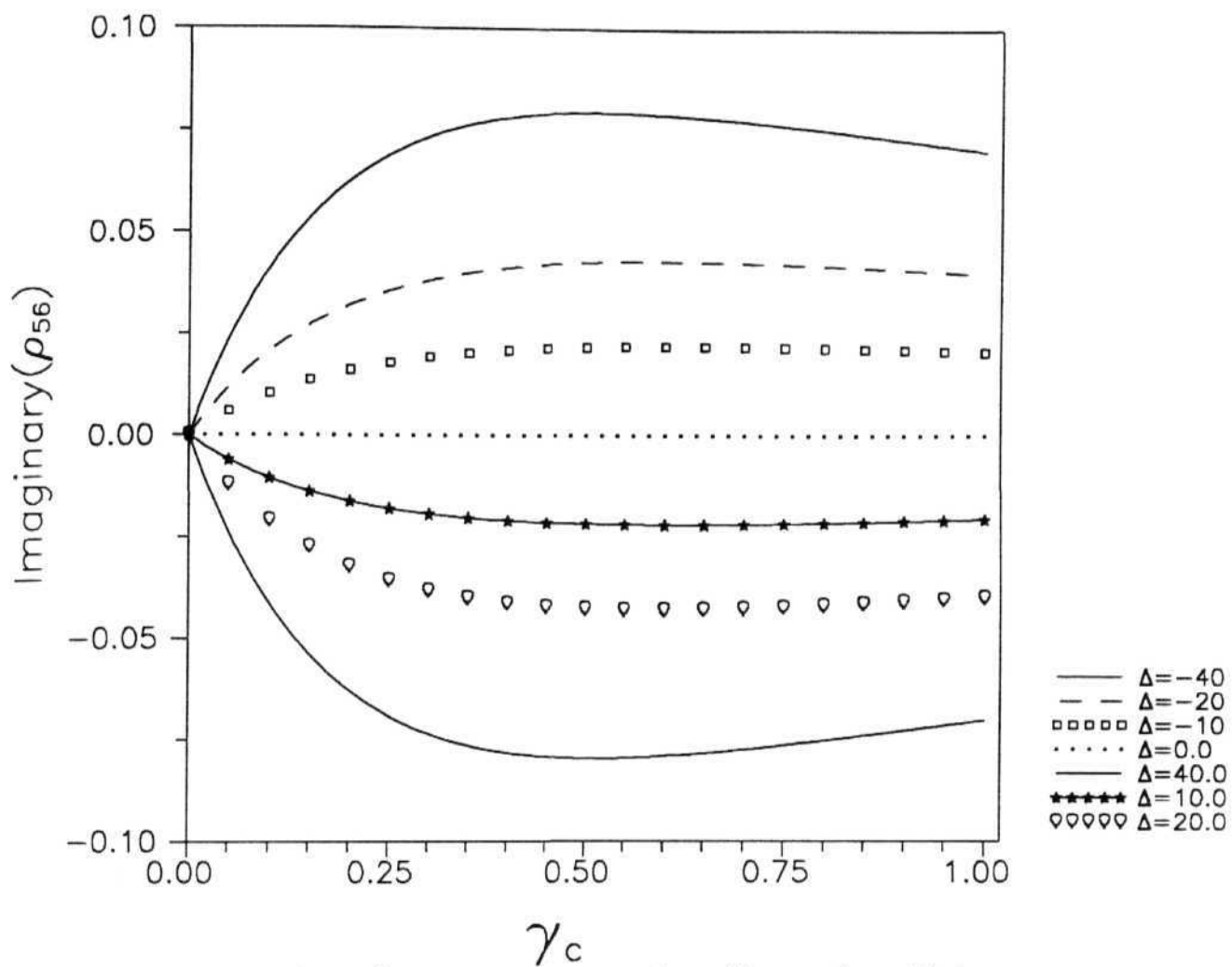


Fig. 4.5(b): Imaginary ρ_{56} as a function of collision damping γ_c for $g_{25}=g_{26}=6.0$

References

- [1] M.Fleischhauer, C. H. Keitel, M. O. Scully and C. Su, *Opt. Comm.* 87, 109 (1990)
- [2] J. A. Bergou, P. Bogár, *Phys. Rev. A* 43, 4889 (1991)
- [3] M. O. Scully, *Phys. Rev. Lett.* 67, 1855 (1991)
- [4] A. Yariv, *Quantum Electronics*, John Wiley, N.Y. (1989).
- [5] E. Arimondo, *Progress in Optics*, Vol. XXXV, Ed: E. Wolf, Elsevier, 1996, pp 259
- [6] H. R. Gray, R. M. Whitely and C. R. Stroud Jr., *Opt. Lett.* 3, 218 (1978)
- [7] G. Alzetta, A. Gozzini, L. Moi and G. Orriols *Nu.Cm* 36B, 5 (1976)
- [8] C. Cohen-Tannoudji and S. Reynaud, *J. Phys. B* 10 345, (1976)
- [9] F. Renzoni, W. Maichen, L. Windholz and E. Arimondo, *Phys. Rev. A* 55, 3710 (1997)
- [10] F. Papoff, F. Mauri and E. Arimondo, *J. of Opt. Soc. Am. B* 9, 321 (1992)
- [11] A. Imamoğlu, S. E. Harris, *Opt. Lett* 14, 134, (1989)
- [12] G. Orriols, *Nu. Cim. B* 53, 1 (1979)
- [13] A. S. Zibrov, M. D. Lukin, D. E. Nikonov, L. Holleberg, M. O. Scully, V. L. Velichansky and H. G. Robinson, *Phys. Rev. Lett.* 75, 1499 (1995)
- [14] J. Gao, C. Guo, X. Guo, G. Jin, P. Wang, J. Zho, H. Zhang, Y. Jiang, D. Waig, D. Jiang, *Opt. Comm.* 93, 323 (1992)
- [15] Narducci, H. M. Doss, P. Ru and M. O. Scully, *Opt. comm.* 81, 379 (1991)
- [16] A. Karawajczyk and J. Zakrzewski, *Phys. Rev. A* 51, 830 (1995)
- [17] Y-q Li and M. Xiao, *Phys. Rev. A* 51, 4959 (1995) and references therein.

- [18] E.Fry, X.Li, D.Nikonov, G.G.Padmabandu, M.O.Scully, A.V. Smith, F.K.Tittel, C.Wong, S.R.Wilkinson and S.Y.Zhu, Phys.Rev. Lett. 70, 3235 (1993)
- [19] V.I.Balykin, V. S. Letokhov, V. G. Minogin, Yu. V. Rozhdestvensky, and A. I. Sidorov, J. Opt. Soc. Am. B 2, 1776 (1985)
- [20] E. U. Condon and G. H. Shortley *The Theory of Atomic Spectra*, Cambridge, (1970). pp 76
- [21] S. Swain, J. Phys. B 10, 3405 (1982)
- [22] E. Arimondo, *Fundamentals of Quantum Optics III*, ed: F. Ehlotzky, (Lecture Notes in Physics Vol. 420), Springer Verlag, Berlin, 1993, pp 170.

Chapter V

Configurations in Real atomic systems

Examples of real atomic systems where Gate and Y configurations can be formed are presented. Three configurations using hyperfine atomic levels of Sodium are discussed; one configuration forms only a Gate system; another configuration is a combination of single Gate and a single Y and the third system invoicing many levels can be decomposed into combination of Gate-like and Y-like systems. The behaviour of these systems is shown to be similar to that of Gate and Y. A possibility is examined where the strong pump beam acting off-resonant on the probe transition creates additional coherences. The effect of such coherences on the probe absorption is presented. It is shown that such an effect leads to a complete transparency of the Gate system.

Experiments to achieve both EIT and LWI have been performed using atomic vapours of Sodium [1, 2, 3, 4], Rubidium [5, 6], Lead [7, 8] and Cesium [9]. In spite of complex energy levels of these atoms, the mechanism behind EIT and **LWI** in these systems are identified as identical to the mechanism in ladder, A and V configurations which in turn, have been well understood as model systems [10, 11, 12, 13]. The following configurations can similarly be decomposed into **Gate** and **Y**.

5.1 Case I: $F=1 \rightarrow F'=1 \rightarrow F''=1$

A simple ladder configuration involving multiple sublevels is an example to be examined (see figure 5.1 for notation and nomenclature). For definiteness, let the energy levels involved be $F=1$ of $S_{1/2}$, $F'=1$ of $P_{1/2}$ and $F''=1$ of $D_{1/2}$ of a Sodium atom, denoted as F , F' and F'' respectively. Each of these levels is a triplet made up of $m_F=-1, 0$ and $+1$. Considering the polarizations of the resonantly interacting radiations, a closer analysis brings out several possibilities in this level scheme. For example, it is well known that a TT polarized light will bring about a $\Delta m_F=0$ transition and σ_{\pm} light will bring about a $\Delta m_F=\pm 1$ transition among the atomic energy levels. Which means, that if an unpolarized radiation, which is a sum of all possible polarizations were to be used, at each stage, it will connect all transitions involving $\Delta m_F=-1, 0, +1$. Thus, all possible transitions will be connected between m_F sublevels of each stage of transition between $F=1 \leftrightarrow F'=1 \leftrightarrow F''=1$ levels shown in figure 5.1. This is a complicated situation and an analysis in terms of three level systems is not very illuminating.

Simplifying the analysis, let light of a definite polarizations be used. In particular the probe beam be assumed to be π polarized, which connects $\Delta m_F=0$ transition only. If the pump beam is also TT polarized then the configuration may be viewed as a set of two ladders (figure 5.2 (a)). On the other hand when the pump beam is plane polarized in xy plane, it can be analysed as a sum of σ_+ and σ_- beams, which causes a $\Delta m_F=\pm 1$ transition. The configuration now is as shown in figure 5.2 (b). Here, the energy levels are numbered 1,2,... 9 in the order shown for the sake of convenience. The probe beam connects transition $|5\rangle \leftrightarrow |7\rangle$ and $|6\rangle \leftrightarrow |8\rangle$. The transition between $|1\rangle$ and $|2\rangle$ is forbidden because of their $m_F=0$ values. This is now a **Gate** configuration made up of levels $|5\rangle \leftrightarrow |7\rangle \leftrightarrow |9\rangle \leftrightarrow |8\rangle \leftrightarrow |6\rangle$. Note that, the coherences between levels $|3\rangle, |4\rangle$

and $|2\rangle$ do not affect the coherences between levels $|7\rangle$, $|8\rangle$ and $|9\rangle$. Behaviour of this system can be taken to be same as that of the **Gate** configuration discussed in earlier chapters.

However, one problem that troubles a study of this nine level configuration is that the state $|1\rangle$ acquires population by spontaneous emission and it does not leak out. The π polarized probe beam does not transfer this population to other levels. As explained in the previous chapter, the state $|1\rangle$, with an $m_F=0$, is a natural trapping state of the system. Collisional processes can however transfer population from $|1\rangle$ to $|5\rangle$ and $|6\rangle$. Or an external pumping process, which can pump population out of level $|1\rangle$ and redistribute between levels $|5\rangle$ and $|6\rangle$ can be used. To ensure that this does not create any additional coherences, an incoherent beam can be used for such repumping processes.

Another point to be noted here is that the dipole matrix elements of the two legs of the Gate are of opposite signs. In other words, $\langle 5|d.\mathcal{E}|7\rangle = -\langle 6|d.\mathcal{E}|8\rangle$ [§]. This sign difference occurs due to the Clebsch-Gordon coefficients for the $m_F=\pm 1$ sublevels[¶]. In the model **Gate** configuration studied in earlier chapters, the two dipole transitions were assumed to be of the same sign. This difference does not alter the probe absorption behaviour when there does not exist any coherence between levels $|5\rangle$ and $|6\rangle$. In such situations, the levels $|5\rangle$ and $|6\rangle$ independently probe the coherence developed by the pump beam between levels $|7\rangle$ and $|8\rangle$. However, when a coherence exists between levels $|5\rangle$ and $|6\rangle$, as in the case of 'injected coherences' dealt in Chapter IV, the difference in the signs of dipole matrix elements does matter. For instance, the rules (4.17) of

[§]The complete, normalized superposition state of which $|5\rangle \pm |6\rangle$ and $|7\rangle \pm |8\rangle$ form a part are referred to as $|5\rangle \pm |6\rangle$ state and $|7\rangle \pm |8\rangle$ state.

[¶]See Appendix C

transition between superposition states, which were discussed in previous chapter, will be modified. The transition between a state of Q_- type to a state of P_- type will be an allowed transition but to a state of P_+ type will not be allowed as:

$$\begin{aligned} (\langle 5| - \langle 6|)d.\mathcal{E}(|7\rangle + |8\rangle) &= \langle 5|d.\mathcal{E}|7\rangle + \langle 6|d.\mathcal{E}|8\rangle = 0 \\ (\langle 5| - \langle 6|)d.\mathcal{E}(|7\rangle - |8\rangle) &= \langle 5|d.\mathcal{E}|7\rangle - \langle 6|d.\mathcal{E}|8\rangle \neq 0 \end{aligned} \quad (5.1)$$

This is because

$$\langle 5|d.\mathcal{E}|7\rangle = -\langle 6|d.\mathcal{E}|8\rangle$$

On similar lines the state $|5\rangle + |6\rangle$ has a nonzero transition probability for a transition to $|7\rangle + |8\rangle$ and a zero transition probability for a transition to $|7\rangle - |8\rangle$. The effect of this change becomes relevant in the section 5.4 of this chapter where the coherences between ground states created by the pump beam is taken into account.

5.2 Case II: $F=2 \rightarrow F'=1 \rightarrow F''=1$

Consider the situation when the ground level is an $F=2$ state of $S_{1/2}$ level, while the upper two levels are $F'=1$ states of $P_{1/2}$ and $F''=1$ of $D_{1/2}$ respectively. This configuration, which is shown in figure 5.2, consists of five ground state sublevels interacting with three sublevels of $F'=1$ of $P_{1/2}$ (See figure 5.2 for labeling of states). Here, $|1\rangle \leftrightarrow |2\rangle$ transition is allowed". Therefore, the Y configuration formed by $|1\rangle$, $|2\rangle$, $|3\rangle$ and $|4\rangle$ coexists with the Gate configuration formed by levels $|5\rangle$, $|6\rangle$, $|7\rangle$, $|8\rangle$ and $|9\rangle$. Levels $|5'\rangle$ and $|6'\rangle$ do not contribute to coherence developed in the system. Their participation in the dynamics is limited to their trapping the population which they receive by spontaneous emission processes. Therefore, this configuration is equivalent

See Appendix C

to strictly the Y configuration that was discussed in Chapters II and **III**. Further, the Gate and Y systems in Figure 5.2 are uncoupled by any coherent transition. The only coupling between these two configurations is by spontaneous emission channels which transfer population from levels of Gate to those of Y and vice versa. These transitions do not create any coherences in steady state between the levels of **Gate** and **Y**.

The population that gets trapped in states $|5'\rangle$ and $|6'\rangle$ or in the states of $F=1$ can be repumped back into the configuration using incoherent pumping processes.

5.3 Case **III**: $F=1$ and $F=2 \leftrightarrow F'=2 \leftrightarrow F''=1$

This configuration is a modification of an earlier study [3] wherein $F=1$ and $F=2$ of $S_{1/2}$ with $F'=2$ of $P_{1/2}$ were only involved. Here, $F''=2$ of $D_{1/2}$ is also used with a strong pump laser connecting transitions between m_F levels of $P_{1/2}$ and $D_{1/2}$. This pump beam is plane polarized in xy plane and hence connects $\Delta m_F = \pm 1$ transition. The probe beam is made up of σ^+ and σ^- lights as was the case in reference [3]. This configuration is shown in figure 5.3. From Schrödinger equation, $i\partial_t\psi = \mathcal{H}\psi$, equations are obtained for each coefficient 'C' as (See figure 5.3 for notations),

$$\begin{aligned}
 \partial_t C_{5_1} &= -g_{5_1 7_1} C_{7_1} \\
 \partial_t C_{5_2} &= -i\Delta_{5_2 5_1} C_{5_2} - g_{5_2 7_2}^* C_{7_2} \\
 \partial_t C_{5_3} &= -i\Delta_{5_3 5_1} C_{5_3} - g_{5_3 7_3}^* C_{7_3} \\
 \partial_t C_{6_1} &= -i\Delta_{6_1 5_1} C_{6_1} - g_{6_1 7_1}^* C_{7_1} \\
 \partial_t C_{6_2} &= -i\Delta_{6_2 5_1} C_{6_2} - g_{6_1 8_1}^* C_{8_1} \\
 \partial_t C_{6_3} &= -i\Delta_{6_3 5_1} C_{6_3} - g_{6_3 8_2}^* C_{8_2} \\
 \partial_t C_{6_4} &= -i\Delta_{6_4 5_1} C_{6_4} - g_{6_4 8_2}^* C_{8_2}
 \end{aligned}$$

$$\begin{aligned}
\partial_t C_{7_1} &= [-i\Delta_{7_1 5_1} - \gamma_{7_1}]C_{7_1} + g_{5_1 7_1} C_{5_1} - g_{7_1 9_1}^* C_{9_1} - g_{7_1 9_2}^* C_{9_2} + g_{6_2 7_1} C_{6_2} \\
\partial_t C_{7_2} &= [-i\Delta_{7_2 5_1} - \gamma_{7_2}]C_{7_2} + g_{5_2 7_2} C_{5_2} - g_{7_2 9_2}^* C_{9_2} \\
\partial_t C_{7_3} &= [-i\Delta_{7_3 5_1} - \gamma_{7_3}]C_{7_3} + g_{5_3 7_3} C_{5_3} + g_{7_3 9_3} C_{9_3} - g_{7_3 9_4}^* C_{9_4} \\
\partial_t C_{8_1} &= [-i\Delta_{8_1 5_1} - \gamma_{8_1}]C_{8_1} + g_{6_1 8_1} C_{6_1} - g_{8_1 9_1}^* C_{9_1} \\
\partial_t C_{8_2} &= [-i\Delta_{8_2 5_1} - \gamma_{8_2}]C_{8_2} + g_{6_3 8_2} C_{6_3} + g_{6_4 8_2} C_{6_4} - g_{8_2 9_3}^* C_{9_3} - g_{8_2 9_5}^* C_{9_5} \\
\partial_t C_{9_1} &= [-i\Delta_{9_1 5_1} - \gamma_{9_1}]C_{9_1} + g_{7_1 9_1} C_{7_1} + g_{8_1 9_1} C_{8_1} \\
\partial_t C_{9_2} &= [-i\Delta_{9_2 5_1} - \gamma_{9_2}]C_{9_2} + g_{7_1 9_2} C_{7_1} + g_{7_2 9_2} C_{7_2} \\
\partial_t C_{9_3} &= [-i\Delta_{9_3 5_1} - \gamma_{9_3}]C_{9_3} + g_{7_3 9_3} C_{7_3} + g_{8_2 9_3} C_{8_2} \\
\partial_t C_{9_4} &= [-i\Delta_{9_4 5_1} - \gamma_{9_4}]C_{9_4} + g_{7_3 9_4} C_{7_3} \\
\partial_t C_{9_5} &= [-i\Delta_{9_5 5_1} - \gamma_{9_5}]C_{9_5} + g_{8_2 9_5} C_{8_2}
\end{aligned} \tag{5.2}$$

Here, $g_{ij} = id_{ij} \cdot E$.

It can be seen that there are two uncoupled systems, one consisting of levels $|5_2\rangle$, $|7_2\rangle$, $|9_2\rangle$, $|7_1\rangle$, $|5_1\rangle$, $|6_2\rangle$, $|9_1\rangle$, $|8_1\rangle$, $|6_1\rangle$ and another of levels $|9_4\rangle$, $|7_3\rangle$, $|5_3\rangle$, $|9_3\rangle$, $|8_2\rangle$, $|6_3\rangle$, $|6_4\rangle$, $|9_5\rangle$. Using the method followed in Chapter II, the probe absorption is assumed equivalent to the loss of population from ground levels. It can thus be determined from

$$\begin{aligned}
\partial_t C_{6_1} &= \left[-i\Delta_{6_1 5_1} - \frac{|g_{6_1 8_1}|^2}{i\Delta_{8_1 5_1} + \gamma_{8_1} + \frac{|g_{8_1 9_1}|^2}{i\Delta_{d_4} + \gamma_{d_4}}} \right] C_{6_1} \\
&+ \frac{g_{6_1 8_1}^* g_{8_1 9_1}^* g_{7_1 9_1} g_{7_1 9_2} g_{5_2 7_2} C_{5_2}}{[i\Delta_{7_2 5_1} + \gamma_{7_2}][i\Delta_{d_2} + \gamma_{d_2}][i\Delta_{d_3} + \gamma_{d_3}][i\Delta_{d_4} + \gamma_{d_4}][i\Delta_{8_1 5_1} + \gamma_{8_1} + \frac{|g_{8_1 9_1}|^2}{i\Delta_{d_4} + \gamma_{d_4}}]} \\
&+ \frac{g_{6_1 8_1}^* g_{8_1 9_1}^* g_{7_1 9_1} g_{5_1 7_1} C_{5_1} + g_{6_1 8_1}^* g_{8_1 9_1}^* g_{7_1 9_1} g_{6_2 7_1} C_{6_2}}{[i\Delta_{d_3} + \gamma_{d_3}][i\Delta_{d_4} + \gamma_{d_4}][i\Delta_{8_1 5_1} + \gamma_{8_1} + \frac{|g_{8_1 9_1}|^2}{i\Delta_{d_4} + \gamma_{d_4}}]} \\
\partial_t C_{5_2} &= \left[-i\Delta_{5_2 5_1} - \frac{|g_{5_2 7_2}|^2}{i\Delta_{h_2} + \gamma_{h_2}} \right] C_{5_2}
\end{aligned} \tag{5.3}$$

$$\begin{aligned}
& + \frac{g_{5_2 7_2}^* g_{7_2 9_2}^* g_{7_1 9_1} g_{5_1 7_1} C_{5_1}}{[i\Delta_{h_2} + \gamma_{h_2}] [i\Delta_{h_1} + \gamma_{h_1}] [i\Delta_{g_1} + \gamma_{g_1}]} \\
& + \frac{g_{5_2 7_2}^* g_{7_2 9_2}^* g_{7_1 9_1} g_{6_2 7_1} C_{6_2}}{[i\Delta_{h_2} + \gamma_{h_2}] [i\Delta_{h_1} + \gamma_{h_1}] [i\Delta_{g_1} + \gamma_{g_1}]} \\
& - \frac{g_{5_2 7_2}^* g_{7_2 9_2} g_{7_1 9_1} g_{8_1 9_1} g_{8_1 9_1} g_{6_1 8_1} C_{6_1}}{[i\Delta_{h_2} + \gamma_{h_2}] [i\Delta_{h_1} + \gamma_{h_1}] [i\Delta_{g_1} + \gamma_{g_1}] [i\Delta_{e_1} + \gamma_{e_1}] [i\Delta_{8_1 5_1} + \gamma_{8_1}]} \quad (5.4)
\end{aligned}$$

$$\begin{aligned}
\partial_i C_{6_2} &= \left[i\Delta_{6_2 5_1} - \frac{|g_{6_2 7_1}|^2}{i\Delta_f + \gamma_f} \right] C_{6_2} - \frac{g_{6_1 7_1}^* g_{5_1 7_1} C_{5_1}}{i\Delta_f + \gamma_f} \\
&= \frac{g_{6_2 7_1}^* g_{7_1 9_1} g_{8_1 9_1} g_{6_1 8_1} C_{6_1}}{[i\Delta_f + \gamma_f] [i\Delta_{d_1} + \gamma_{d_1}] [i\Delta_{8_1 5_1} + \gamma_{8_1}]} \\
&+ \frac{g_{6_2 7_1}^* g_{7_1 9_2} g_{7_2 9_2} g_{5_2 7_2} C_{5_2}}{[i\Delta_f + \gamma_f] [i\Delta_{d_2} + \gamma_{d_2}] [i\Delta_{7_2 5_1} + \gamma_{7_2}]} \quad (5.5)
\end{aligned}$$

$$\begin{aligned}
\partial_i C_{5_1} &= -\frac{|g_{5_1 7_1}|^2}{i\Delta_f + \gamma_f} C_{5_1} - \frac{g_{5_1 7_1}^* g_{6_2 7_1} C_{6_2}}{i\Delta_f + \gamma_f} + \frac{g_{5_1 7_1}^* g_{7_1 9_1} g_{8_1 9_1} g_{6_1 8_1} C_{6_1}}{[i\Delta_f + \gamma_f] [i\Delta_{d_1} + \gamma_{d_1}] [i\Delta_{8_1 5_1} + \gamma_{8_1}]} \\
&+ \frac{g_{5_1 7_1}^* g_{7_1 9_2} g_{7_2 9_2} g_{5_2 7_2} C_{5_2}}{[i\Delta_f + \gamma_f] [i\Delta_{d_2} + \gamma_{d_2}] [i\Delta_{7_2 5_1} + \gamma_{7_2}]} \quad (5.6)
\end{aligned}$$

for the one set, where

$$\begin{aligned}
i\Delta_{d_1} + \gamma_{d_1} &= i\Delta_{9_1 5_1} + \gamma_{9_1} + \frac{|g_{8_1 9_1}|^2}{i\Delta_{8_1 5_1} + \gamma_{8_1}} \\
i\Delta_{d_2} + \gamma_{d_2} &= i\Delta_{9_2 5_1} + \gamma_{9_2} + \frac{|g_{7_2 9_2}|^2}{i\Delta_{7_2 5_1} + \gamma_{7_2}} \\
i\Delta_{d_3} + \gamma_{d_3} &= i\Delta_{7_1 5_1} + \gamma_{7_1} + \frac{|g_{7_1 9_2}|^2}{i\Delta_{d_2} + \gamma_{d_2}} \\
i\Delta_{d_4} + \gamma_{d_4} &= i\Delta_{9_1 5_1} + \gamma_{9_1} - \frac{|g_{7_1 9_1}|^2}{i\Delta_{d_3} + \gamma_{d_3}}
\end{aligned}$$

$$\begin{aligned}
i\Delta_f + \gamma_f &= i\Delta_{7_1 5_1} + \gamma_{7_1} + \frac{|g_{7_1 9_1}|^2}{i\Delta_{d_1} + \gamma_{d_1}} + \frac{|g_{7_1 9_2}|^2}{i\Delta_{d_2} + \gamma_{d_2}} \\
i\Delta_{e_1} + \gamma_{e_1} &= i\Delta_{9_1 5_1} + \gamma_{9_1} + \frac{|g_{8_1 9_1}|^2}{i\Delta_{8_1 5_1} + \gamma_{8_1}} \\
i\Delta_{g_1} + \gamma_{g_1} &= i\Delta_{7_1 5_1} + \gamma_{7_1} + \frac{|g_{7_1 9_1}|^2}{i\Delta_{e_1} + \gamma_{e_1}} \\
i\Delta_h + \gamma_h &= i\Delta_{9_2 5_1} + \gamma_{9_2} + \frac{|g_{7_1 9_2}|^2}{i\Delta_{g_1} + \gamma_{g_1}}
\end{aligned}$$

And for the other set absorption can be determined from the equations,

$$\begin{aligned}
\partial_t C_{6_3} &= \left[i\Delta_{6_3 5_1} - \frac{|g_{6_3 8_2}|^2}{i\Delta_c + \gamma_c} \right] C_{6_3} - \frac{g_{6_3 8_2}^* g_{6_4 8_2} C_{6_4}}{i\Delta_c + \gamma_c} \\
&\quad + \frac{g_{6_3 8_2}^* g_{8_2 9_3}^* g_{7_3 9_3} g_{5_3 7_3} C_{5_3}}{[i\Delta_a + \gamma_a] [i\Delta_b + \gamma_b] [i\Delta_c + \gamma_c]} \quad (5.7)
\end{aligned}$$

$$\begin{aligned}
\partial_t C_{6_4} &= \left[i\Delta_{6_4 5_1} - \frac{|g_{6_4 8_2}|^2}{i\Delta_c + \gamma_c} \right] C_{6_4} - \frac{g_{6_4 8_2}^* g_{6_3 8_2} C_{6_3}}{i\Delta_c + \gamma_c} \\
&\quad + \frac{g_{6_4 8_2}^* g_{8_2 9_3}^* g_{7_3 9_3} g_{5_3 7_3} C_{5_3}}{[i\Delta_a + \gamma_a] [i\Delta_b + \gamma_b] [i\Delta_c + \gamma_c]} \quad (5.8)
\end{aligned}$$

$$\begin{aligned}
\partial_t C_{5_3} &= \left[i\Delta_{5_3 5_1} - \frac{|g_{5_3 7_3}|^2}{i\Delta_c + \gamma_c} \right] C_{5_3} + \frac{g_{5_3 7_3}^* g_{7_3 9_3}^* g_{8_2 9_3} g_{6_3 8_2} C_{6_3} + g_{5_3 7_3}^* g_{7_3 9_3}^* g_{8_2 9_3} g_{6_4 8_2} C_{6_4}}{[i\Delta'_c + \gamma'_c] [i\Delta'_b + \gamma'_b] [i\Delta'_a + \gamma'_a]} \\
&\quad (5.9)
\end{aligned}$$

Where,

$$\begin{aligned}
i\Delta_a + \gamma_a &= i\Delta_{7_3 5_1} + \gamma_{7_3} + \frac{|g_{7_3 9_4}|^2}{i\Delta_{9_4 5_1} + \gamma_{9_1}} \\
i\Delta_b + \gamma_b &= i\Delta_{9_3 5_1} + \gamma_{9_3} + \frac{|g_{7_3 9_3}|^2}{i\Delta_a + \gamma_a}
\end{aligned}$$

$$\begin{aligned}
i\Delta_c + \gamma_c &= i\Delta_{8_2 5_1} + \gamma_{8_2} + \frac{|g_{8_2 9_3}|^2}{i\Delta_b + \gamma_b} + \frac{|g_{8_2 9_5}|^2}{i\Delta_{9_5 5_1} + \gamma_{9_5}} \\
i\Delta'_a + \gamma'_a &= i\Delta_{8_2 5_1} + \gamma_{8_2} + \frac{|g_{8_2 9_5}|^2}{\Delta_{9_5 5_1} + \gamma_{9_5}} \\
i\Delta'_b + \gamma'_b &= i\Delta_{9_3 5_1} + \gamma_{9_3} + \frac{|g_{8_2 9_3}|^2}{i\Delta'_a + \gamma'_a} \\
i\Delta'_c + \gamma'_c &= i\Delta_{7_3 5_1} + \gamma_{7_3} + \frac{|g_{7_3 9_3}|^2}{i\Delta'_b + \gamma'_b} + \frac{|g_{7_3 9_4}|^2}{i\Delta_{9_3 5_1} + \gamma_{9_3}}
\end{aligned}$$

Figure 5.4 shows the behaviour of absorption determined from the coefficients of equations $\partial_t |C_i|^2 = f(\Delta) |C_i|^2$, for variation of detuning Δ . Δ here denotes the probe detuning involving all the probe transitions. Since multiple, degenerate levels will have the same detuning with the probe beam, the subscripts of Δ are dropped in this notation. In equations 5.3-5.6 and 5.7-5.9, the adiabatic elimination similar to the one used in Chapter III is used. The cross coherence factors which affect these absorption profiles are assumed to be zero for the present. The figure 5.4a shows the loss of population from levels $|6_3\rangle$ and $|6_4\rangle$. It indicates presence of two sets of sidebands with a zero absorption at the line center. Population loss from state $|5_3\rangle$ shows a similar behaviour (figure 5.4 b). Population loss from states $|5_1\rangle$ and $|6_2\rangle$ (figure 5.4 c) and, $|6_1\rangle$ and $|5_2\rangle$ (figure 5.4 d) on the other hand shows a central absorption band along with the four sidebands. Figure 5.4e shows total absorption, which is a sum of all these absorptions.

Without going deeper into the discussion of these results one observes from these graphs that the configuration in figure 5.3 can be broken into **Gate** like and **Y** like subconfigurations. Results from Chapters II and III show that a **Y** system has a

transparent window at $A = 0$, while a **Gate** configuration shows a reduced but finite absorption for $A = 0$. Extending that argument, the configuration formed by the levels $|6_3\rangle$, $|6_4\rangle$ and $|5_3\rangle$ can be judged as a combination of Y systems and the configuration formed by levels $|5_1\rangle$, $|5_2\rangle$, $|6_1\rangle$ and $|6_2\rangle$ can be judged a combination of **Gate** systems. From the figures in 5.4, all the coupled Y systems having a zero absorption at $A = 0$, while the coupled **Gates** have an absorption peak at $A = 0$.

The fact to be noted is that, the configuration $|5_3\rangle - |7_3\rangle - |9_3\rangle - |8_2\rangle - |6_1\rangle$ appears to be a candidate for a **Gate**. But, it is a combination of two Y systems formed out of $|9_4\rangle - |7_3\rangle - |5_3\rangle - |9_3\rangle$ and $|9_5\rangle - |8_2\rangle - (|6_3\rangle, |6_4\rangle) - |9_5\rangle$, coupled at $|9_3\rangle$. This leads to an absorption profile which has a zero at resonance. Similarly, $|9_2\rangle - |7_1\rangle - |6_2\rangle - |9_1\rangle$ does not form a Y configuration. It consists of two **Gates** $|5_2\rangle - |7_2\rangle - |9_2\rangle - (|5_1\rangle, |6_2\rangle)$ and $(|5_1\rangle, |6_2\rangle) - |7_1\rangle - |9_1\rangle - |8_1\rangle - |6_1\rangle$. Thus, it gives a profile which has a nonzero absorption on resonance. Also, absorption from levels $|6_3\rangle$ and $|6_4\rangle$ are identical (figure 5.4 (a)). Absorption from levels $|5_1\rangle$ and $|6_2\rangle$ are identical and so are absorption from levels $|6_1\rangle$ and $|5_2\rangle$. This shows that the coherence effect affecting these absorption profiles are identical. This identity is obviously lost if the difference in oscillator strengths between these transitions are taken into account. Because the values of oscillator strengths between $F=1 \leftrightarrow F=1$ transitions are different from those for $F=2 \leftrightarrow F=1$ transition, the absorption profiles will numerically be different. But the modifications to absorption profiles are caused by similar configurations for both levels of a pair. Therefore, the profiles should differ only numerically while the shape remains identical.

Summing up the above discussion, it can be stated that configurations which appear to be **Gate**-like and Y-like, behave like **Gate** and Y. All Y-like systems show a complete transparency at resonance, while all **Gate**-like systems show a reduced

but nonzero absorption on resonance. In either cases, sidebands of absorption profiles show the eigenenergies of the Dressed states. Effect of externally caused coherence between different levels will be identical to the effects discussed in previous chapter. But as the equations show, there are more than one set of levels interconnected and the coherence between all of them have to be prepared before any significant difference to the absorption profile is achieved.

5.4.1 Bichromatic approach

While analyzing a multi-level atomic system interacting with more than one field, it is usually assumed that each field interacts only with resonant transition. In other words, the pump beam is assumed to act only on pump transition and the probe beam only on probe transition. For a transition between levels $|a\rangle$ and $|b\rangle$ in an atom brought about by an electromagnetic field, the effective coupling factor with electromagnetic field is $|d_{ab} \cdot E|^2 / \Delta_{ab}$, where d_{ab} is the dipole moment of the transition and Δ_{ab} , the detuning. When the detuning Δ_{ab} is large, this factor becomes negligibly small for weak fields. In a far detuned situation, the action of an electromagnetic can be neglected [14]. If the beam is strong, the factor $|d_{ab} \cdot E|^2 / \Delta_{ab}$ can be significant even for large detunings and its effect has to be considered. In particular the action of the strong pump beam even when off-resonance on the probe beam transition can create additional coherences which can modify the probe absorption behaviour. A study of such action is particularly valid for atomic systems where the pump and probe beams are not very different in their frequencies. In the example of Sodium, which is considered here, the probe beam is of 5986 Å and the pump beam is of a frequency of 5960 Å and hence

the contribution of the pump beam on the probe beam transition (and vice versa) can be very significant. In this section an example of such an analysis is presented for the $F=1 \leftrightarrow F'=1 \leftrightarrow F''=1$ case where the off resonant action of the pump beam on probe transition and that of probe beam on pump transition is also taken into account to solve for the probe absorption. We will see that the contribution of probe beam action on the pump transition is very small since it is a weak field. But the pump beam creates additional coherences on probe transitions which lead to the modifications of the probe absorption. However, the action of two electromagnetic fields of different frequencies on same transition leads to a modification of the mathematical procedure in applying the rotating wave approximation. This modification is required as operating the rotation transformation in either of the frequency frames will not completely render the hamiltonian time independent. A bichromatic field approach is used in the following which is a non-perturbative analysis to obtain solutions for the probe absorption. We also analyse the dressed states of the system and show that the results obtained are in agreement with the results of Chapter IV, where the effect of additional coherences were discussed.

Figure 5.5 shows the configuration where both the pump and the probe beams are interacting simultaneously with both types of transitions. The thick lines represent interaction of the pump beams and the thin lines are for interaction of probe beams. The total Hamiltonian for this system, in $\hbar = 1$ units is taken to be

$$\begin{aligned}
 \mathcal{H} = & \sum_i \omega_i |i\rangle\langle i| \\
 & - g_{17}^* e^{i\omega_L t} |1\rangle\langle 7| - g_{18}^* e^{i\omega_L t} |1\rangle\langle 8| \\
 & - g_{25} e^{-i\omega_L t} |2\rangle\langle 5| - g_{26} e^{-i\omega_L t} |2\rangle\langle 6| - g_{32}^* e^{i\omega_L t} |2\rangle\langle 3| - g_{42}^* e^{i\omega_L t} |2\rangle\langle 4| \\
 & - g_{32} e^{-i\omega_L t} |3\rangle\langle 2| - g_{37} e^{-i\omega_p t} |3\rangle\langle 7| - g_{42} e^{-i\omega_L t} |4\rangle\langle 2| - g_{48} e^{-i\omega_p t} |4\rangle\langle 8|
 \end{aligned}$$

$$\begin{aligned}
& - g_{52}^* e^{i\omega_L t} |5\rangle\langle 2| - g_{57}^* e^{i\omega_p t} |5\rangle\langle 7| - g_{62}^* e^{i\omega_L t} |6\rangle\langle 2| - g_{68}^* e^{i\omega_p t} |6\rangle\langle 8| \\
& - g_{71} e^{-i\omega_L t} |7\rangle\langle 1| - g_{73}^* e^{i\omega_p t} |7\rangle\langle 3| - g_{75} e^{-i\omega_p t} |7\rangle\langle 5| - g_{97}^* e^{i\omega_L t} |7\rangle\langle 9| \\
& - g_{81} e^{-i\omega_L t} |8\rangle\langle 1| - g_{84}^* e^{i\omega_p t} |8\rangle\langle 4| - g_{86} e^{-i\omega_p t} |8\rangle\langle 6| - g_{98}^* e^{i\omega_L t} |8\rangle\langle 9| \\
& - g_{97} e^{-i\omega_L t} |9\rangle\langle 7| - g_{98} e^{-i\omega_L t} |9\rangle\langle 8|
\end{aligned}$$

ω_i , $i = 1, 2, \dots, 9$ are the energy values of level i , in angular frequencies. Note in this configuration the level $|1\rangle$ does not behave as a trapping state as the population in it can leak out due to the pump beam.

The Liouville equation for the dynamics of the density matrix is written in the usual manner as

$$\partial_t \rho = -i[\mathcal{H}, \rho] - \mathcal{L}\rho.$$

\mathcal{A}_p contains the decay terms that follow the master equation

$$[\mathcal{L}\rho]_{ij} = -\delta_{ij} \sum_{k \neq i} 2\gamma_{ik} \rho_{kk} + \left(\sum_{k \neq i} \gamma_{ki} + \sum_{k \neq j} \gamma_{kj} \right) \rho_{ij}.$$

The Rotating Wave Transformation (RWT) is operated on the resulting equations by denoting

$$\begin{aligned}
\tilde{\rho}_{ij} &= \rho_{ij} \exp(-i\omega_p t); \quad \text{for } i = 5, 6, 1; j = 7, 2, 8 \\
\tilde{\rho}_{ij} &= \rho_{ij} \exp(-i\omega_L t); \quad \text{for } i = 7, 2, 8; j = 3, 4, 9 \\
\tilde{\rho}_{ij} &= \rho_{ij} \exp(-i(\omega_L + \omega_p)t); \quad \text{for } i = 5, 6, 1; j = 3, 4, 9
\end{aligned} \tag{5.10}$$

Physically, this corresponds to the lower transitions of $|7\rangle$, $|8\rangle$ and $|2\rangle$ with $|5\rangle$, $|6\rangle$ and $|1\rangle$ being resonant with the probe beam at frequency ω_p , and the upper transitions

of |3) , |4) and |9) with |7) ,|8) and |2) being resonant with the pump beam at frequency ω_L . The detunings are denoted as

$$\begin{aligned}\Delta_p &= (\omega_{7,8,2} - \omega_{5,6,1}) - \omega_p \\ \Delta_u &= (\omega_{3,4,9} - \omega_{7,8,2}) - \omega_L \\ \Delta_L &= (\omega_{7,8,2} - \omega_{5,6,1}) - \omega_L.\end{aligned}$$

Δ_L is the detuning between the pump beam and the lower transitions. Notations of detunings are changed here from previous chapters for the sake of convinience. Δ_p is the detuning of the probe beam and Δ_u is the detuning of the pump beam with $F'=1 \leftrightarrow F''=1$ transitions.

The difference between the pump and probe laser frequencies is denoted by $\omega_{Lp} = \omega_L - \omega_p$. The relation between Δ_p and Δ_L is then obtained as

$$\begin{aligned}\Delta_p &= (\omega_{7,8,2} - \omega_{5,6,1}) - \omega_p \\ &= (\omega_{7,8,2} - \omega_{5,6,1}) - \omega_p - \omega_L + \omega_L \\ &= (\omega_{7,8,2} - \omega_{5,6,1}) - \omega_L - \omega_p + \omega_L \\ &= \Delta_L + \omega_{Lp}.\end{aligned}\tag{5.11}$$

The resulting density matrix equation for the slowly varying time dependant parts can then be cast as

$$\partial_t \tilde{\rho} = A \tilde{\rho} + e^{i(\omega_L - \omega_p)t} M_+ \tilde{\rho} + e^{-i(\omega_L - \omega_p)t} M_- \tilde{\rho} + I_0 \tag{5.12}$$

Here, I_0 is a (80 x 1) column vector containing the inhomogeneous terms which arise out of eliminating ρ_{11} using the closedness condition $\rho_{11} = 1 - (\rho_{22} + \rho_{33} + \rho_{44} + \rho_{55} + \rho_{66} + \rho_{77} + \rho_{88} + \rho_{99})$. A is a (80 x 80) square matrix containing coupling terms which are time independent after RWT and M_{\pm} are two (80 x 80) square matrices containing coupling terms related to probe absorption.

Now setting the time derivative to zero for calculating the steady state solution of 5.12 is invalid since the right hand side contains time dependent terms. In the modified picture, the vector $\tilde{\rho}$ is written as a series,

$$\tilde{\rho} = \sum e^{iN(\omega_L - \omega_p)t} \tilde{\rho}^N; \quad N = 0, \pm 1, \pm 2, \pm 3, \dots \quad (5.13)$$

Differentiating this with respect to time and substituting in 5.12,

$$\partial_t \tilde{\rho}^N = (A - iN(\omega_L - \omega_p)) \tilde{\rho}^N + M_+ \tilde{\rho}^{N-1} + M_- \tilde{\rho}^{N+1} + I_0 \delta_{N0} \quad (5.14)$$

Equating terms with the same power of $\exp(i(\omega_L - \omega_p)t)$, and then setting the time derivative zero, the steady state results are obtained as

$$\begin{aligned} A\tilde{\rho}^0 + M_- \tilde{\rho}^{-1} + M_+ \tilde{\rho}^1 &= -I_0 & \text{for } N = 0 \\ [A - i(\omega_L - \omega_p)] \tilde{\rho}^1 + M_+ \tilde{\rho}^0 + M_- \tilde{\rho}^2 &= 0 & \text{for } N = 1 \\ [A - 2i(\omega_L - \omega_p)] \tilde{\rho}^2 + M_+ \tilde{\rho}^1 + M_- \tilde{\rho}^3 &= 0 & \text{for } N = 2 \\ &\text{and so on} & (5.15) \end{aligned}$$

A general recurrence rule can be written for $N > 0$

$$[A - iN(\omega_L - \omega_p)] + M_+ X_N^{-1} + M_- X^{N+1} = 0 \quad (5.16)$$

where,

$$X_N = \tilde{\rho}^N (\tilde{\rho}^{N-1})^{-1}$$

and

$$X_N^{-1} = \tilde{\rho}^{N-1} (\tilde{\rho}^N)^{-1}$$

Which results in

$$X_N = -\frac{M_+}{A - i(\omega_L - \omega_p) + M_- X^{N+1}} \quad (5.17)$$

where $N = 0, 1, 2, 3, \dots$ Similarly, for $m < 0$,

$$[A + i m(\omega_L - \omega_p)] + M_+(X_{-m-1}) + M_-(X_{-m}) = 0 \quad (5.18)$$

Where

$$\begin{aligned} X_{-m} &= \tilde{\rho}^{-m}(\tilde{\rho}^{-m+1})^{-1} \\ X_{-m}^{-1} &= [\tilde{\rho}_{-m}(\tilde{\rho}_{-m+1})^{-1}]^{-1} \\ X_{-m-1} &= \tilde{\rho}_{-m-1}(\tilde{\rho}_{-m})^{-1} \end{aligned}$$

for $m = 0, 1, 2, 3$.

This gives the result,

$$X_{-m} = -\frac{M_-}{A + im(\omega_L - \omega_p) + m_+ X_{-m-1}} \quad (5.19)$$

From (5.15),

$$\tilde{\rho}^0 = -\frac{I_0}{A + M_+ X_{-1} + M_- X_{+1}} \quad (5.20)$$

Other results follow from,

$$\tilde{\rho}^N = X_N \tilde{\rho}^{N-1} \quad \text{For } N > 0 \quad (5.21)$$

$$\tilde{\rho}^{-m} = X_{-m} \tilde{\rho}^{-m+1} \quad \text{For } m < 0 \quad (5.22)$$

Using these equations, $\tilde{\rho}^N$ to any desired order N in the expression 5.13 can be obtained.

Using the inverse of the rotation transformation 5.10 one has,

$$\begin{aligned} \rho_{75} &= \exp(-i\omega_p t) \tilde{\rho}_{75} \\ &= \exp(-i\omega_p t) [\tilde{\rho}_{75}^{(0)} + \tilde{\rho}_{75}^{(+1)} e^{i(\omega_L - \omega_p t)} + \tilde{\rho}_{75}^{(+2)} e^{+2i(\omega_L - \omega_p t)} \dots] \end{aligned}$$

$$\tilde{\rho}_{75}^{(-1)} e^{-i(\omega_L - \omega_p t)} + \tilde{\rho}_{75}^{(-2)} e^{-2i(\omega_L - \omega_p t)} \dots]$$

Therefore, $\tilde{\rho}_{75}^{(0)} = \exp(-i\omega_p t) \tilde{\rho}_{75}^{(0)}$ is the term which is related to the probe absorption.

On similar lines the other terms of probe absorption are obtained

$$\begin{aligned} \rho_{86} &= \exp(-i\omega_p t) \tilde{\rho}_{86} \\ &= \exp(-i\omega_p t) \left[\tilde{\rho}_{86}^{(0)} + \tilde{\rho}_{86}^{(+1)} e^{i(\omega_L - \omega_p t)} + \tilde{\rho}_{86}^{(+2)} e^{+2i(\omega_L - \omega_p t)} \dots \right. \\ &\quad \left. \tilde{\rho}_{86}^{(-1)} e^{-i(\omega_L - \omega_p t)} + \tilde{\rho}_{86}^{(-2)} e^{-2i(\omega_L - \omega_p t)} \dots \right] \\ \rho_{37} &= \exp(-i\omega_L t) \tilde{\rho}_{37} \\ &= \exp(-i\omega_L t) \left[\tilde{\rho}_{37}^{(0)} + \tilde{\rho}_{37}^{(+1)} e^{i(\omega_L - \omega_p t)} + \tilde{\rho}_{37}^{(+2)} e^{+2i(\omega_L - \omega_p t)} \dots \right. \\ &\quad \left. \tilde{\rho}_{37}^{(-1)} e^{-i(\omega_L - \omega_p t)} + \tilde{\rho}_{37}^{(-2)} e^{-2i(\omega_L - \omega_p t)} \dots \right] \\ \rho_{48} &= \exp(-i\omega_L t) \tilde{\rho}_{48} \\ &= \exp(-i\omega_L t) \left[\tilde{\rho}_{48}^{(0)} + \tilde{\rho}_{48}^{(+1)} e^{i(\omega_L - \omega_p t)} + \tilde{\rho}_{48}^{(+2)} e^{+2i(\omega_L - \omega_p t)} \dots \right. \\ &\quad \left. \tilde{\rho}_{48}^{(-1)} e^{-i(\omega_L - \omega_p t)} + \tilde{\rho}_{48}^{(-2)} e^{-2i(\omega_L - \omega_p t)} \dots \right] \end{aligned}$$

The total time-averaged probe absorption for ω_p field is then given by

$$d_{75} \tilde{\rho}_{75}^{(0)} + d_{86} \tilde{\rho}_{86}^{(0)} + d_{37} \tilde{\rho}_{37}^{(+1)} + d_{48} \tilde{\rho}_{48}^{(+1)}.$$

The numerical results obtained using the above procedure are presented in Figures 5.6 and 5.7. All the parameters are normalized to the coherence decays $\gamma_{57} = \gamma_{68} = \gamma_{25} = \gamma_{26} = \gamma_{71} = \gamma_{81}$. The coherence decays $\gamma_{97} = \gamma_{98} = \gamma_{37} = \gamma_{48} = \gamma_{42} = \gamma_{32}$ are assumed to be 0.25. The probe beam Rabi frequency is 0.2 and the pump beam Rabi frequency is 10.0. The pump laser is assumed to be resonant with the $|3\rangle \leftrightarrow |2\rangle \leftrightarrow |4\rangle$ and $|7\rangle \leftrightarrow |9\rangle \leftrightarrow |8\rangle$ transitions. Therefore $\Delta_u = 0$. The probe beam is scanned varying Δ_p . Different values of Δ_L , which is the detuning of the pump laser beam with

respect to the probe transition, are used for these calculations. The pump beam which is resonant with $F'=1 \leftrightarrow F''=1$ transition can not be in resonance with the $F=1 \leftrightarrow F'=1$ transition also because the energy level structure in normal atoms is not equidistant. Conforming to normal atomic energy structure, $\Delta_L = 0$ case is not considered. The numerical results are thus obtained for values $A/\omega = 10, 50, 100, 150, 200$ and 500 in that order. The plots in Figure 5.6 are for zero collision damping. Plots in Figure 5.7 are for a collision damping rate of 0.5 .

Figures 5.6 (a) and (b) show three absorption peaks for all these values of Δ_L . The peaks are labeled I, II and III. The peak spectrum is asymmetric, but as the detuning A/ω is increased, the peaks labeled I and II approach a symmetric position about $\Delta_p = 0$ point as seen in figure 5.6 (b). There is a clear transparency at $\Delta_p = 0$ for larger detunings though, as seen in figure 5.6 (a), an absorption peak II is just off the $\Delta_p = 0$ point. In section 5.1 of this chapter, the case $F=1 \leftrightarrow F'=1 \leftrightarrow F''=1$ was shown to be a **Gate** system. This configuration then should have shown a three peaked absorption spectrum with an absorption peak at the line center as discussed in Chapter II. But this absorption peak is missing in figure 5.6. As the detailed analysis presented in rest of this chapter shows, the absence of the central peak is due to additional coherences generated by the pump beam on $F=1 \leftrightarrow F'=1$ transition.

Figures 5.7 (a) and (b) reiterate the results of figure 5.6. The effect of a finite collision damping rate is clearly seen as an increase in the width of all absorption peaks. The peaks labeled I, II and III occupy the same frequency position as in figure 5.6 but a new peak of sufficiently high magnitude is seen here which is labeled 'C'. The source of this peak is better explained in the dressed atom picture, which is discussed in the section 5.4.2 of this chapter.

Extending the arguments followed in Chapter II for the transparency effect induced by the coherences, the dynamical equation for $\tilde{\rho}_{75}$ is written as

$$\begin{aligned} i \partial_t \tilde{\rho}_{75} = & [\Delta_{75} - i (\gamma_7 + \gamma_5)] \tilde{\rho}_{75} - d_{71} \mathcal{E}_{71} \tilde{\rho}_{15} e^{-i(\omega_L - \omega_p)t} - d_{37}^* \mathcal{E}_{37}^* \tilde{\rho}_{35} e^{-i(\omega_L - \omega_p)t} \\ & - d_{75} \mathcal{E}_{75} (\tilde{\rho}_{55} - \tilde{\rho}_{77}) - d_{97}^* \mathcal{E}_{97}^* \tilde{\rho}_{95} + d_{25} \mathcal{E}_{25} \tilde{\rho}_{72} e^{-i(\omega_L - \omega_p)t}. \end{aligned} \quad (5.23)$$

The corresponding equation for $\tilde{\rho}_{75}^{(0)}$ term from above equation is

$$\begin{aligned} i \partial_t \tilde{\rho}_{75}^{(0)} = & [\Delta_{75} - i (\gamma_7 + \gamma_5)] \tilde{\rho}_{75}^{(0)} - d_{71} \mathcal{E}_{71} \tilde{\rho}_{15}^{(+1)} - d_{37}^* \mathcal{E}_{37}^* \tilde{\rho}_{35}^{(+1)} - d_{75} \mathcal{E}_{75} (\tilde{\rho}_{55}^{(0)} - \tilde{\rho}_{77}^{(0)}) \\ & - d_{97}^* \mathcal{E}_{97}^* \tilde{\rho}_{95}^{(0)} + d_{25} \mathcal{E}_{25} \tilde{\rho}_{72}^{(+1)}. \end{aligned} \quad (5.24)$$

Consequently the steady state value of $\tilde{\rho}_{75}^{(0)}$ can be written as

$$\tilde{\rho}_{75}^{(0)} = \frac{d_{71} \mathcal{E}_{71} \tilde{\rho}_{15}^{(+1)} + d_{37}^* \mathcal{E}_{37}^* \tilde{\rho}_{35}^{(+1)} + d_{75} \mathcal{E}_{75} (\tilde{\rho}_{55}^{(0)} - \tilde{\rho}_{77}^{(0)}) + d_{97}^* \mathcal{E}_{97}^* \tilde{\rho}_{95}^{(0)} - d_{25} \mathcal{E}_{25} \tilde{\rho}_{72}^{(+1)}}{[\Delta_{75} - i (\gamma_7 + \gamma_5)] \tilde{\rho}_{75}^{(0)}}. \quad (5.25)$$

It was shown in the analysis of the **Gate** system in chapter II, that the steady state value of probe absorption ρ_{75} is governed by the equation

$$\tilde{\rho}_{75} = \frac{d_{75} \mathcal{E}_{75} (\tilde{\rho}_{55} - \tilde{\rho}_{77})}{[\Delta_{75} - i (\gamma_7 + \gamma_5)]} + \frac{d_{97}^* \mathcal{E}_{97}^* \tilde{\rho}_{95}}{[\Delta_{75} - i (\gamma_7 + \gamma_5)]}. \quad (5.26)$$

The first term on the RHS of the above equation represents the purely two-level atom behaviour, controlled only by the population in the levels $|5\rangle$ and $|7\rangle$. The second term is the effect of the coherence with a third level $|9\rangle$, which, under suitable conditions cancels the effect of the first term leading to a transparency. But for the **Gate** system, it was shown in Chapter II, that this term is of a magnitude less than the magnitude required to cancel the central absorption peak. Therefore, the residual absorption in line center had resulted in a three peaked absorption profile (See figure 2.8d).

Equation 5.25 is similar to 5.26 but shows additional coherence terms that modify the Lorentzian profile of $\rho_{77} - \rho_{55}$. In all there are four such coherence terms, viz, ρ_{95}

which was present in the **Gate** configuration and the three new terms ρ_{15} , ρ_{35} and ρ_{72} . These terms are readily seen as contributions from various three level configurations that the pump and probe beams form in connection with the two **level** transition $|5\rangle \leftrightarrow |7\rangle$. That is, the term ρ_{15} is the coherence term of the A system formed with $|5\rangle$, $|7\rangle$ and $|1\rangle$; ρ_{35} is the contribution of the ladder $|5\rangle \leftrightarrow |7\rangle \leftrightarrow |3\rangle$; ρ_{95} is the coherence term of the ladder $|5\rangle \leftrightarrow |7\rangle \leftrightarrow |9\rangle$ and finally ρ_{72} is the coherence term of the V system formed from $|5\rangle$, $|7\rangle$ and $|2\rangle$. The three level configurations of A, ladder (E) and V, which were studied in the past in the context of EIT, are present in this configuration simultaneously.

On similar lines, the other leg of the probe absorption ρ_{86} can be shown to follow equation

$$\tilde{\rho}_{86}^{(0)} = \frac{d_{81}\mathcal{E}_{81}\tilde{\rho}_{16}^{(-1)} + d_{48}^*\mathcal{E}_{48}^*\tilde{\rho}_{46}^{(+1)} + d_{86}\mathcal{E}_{86}(\tilde{\rho}_{66}^{(0)} - \tilde{\rho}_{88}^{(0)}) + d_{98}^*\mathcal{E}_{98}^*\tilde{\rho}_{96}^{(0)} - d_{26}\mathcal{E}_{26}\tilde{\rho}_{82}^{(+1)}}{[\Delta_{86} - i(\gamma_6 + \gamma_8)]}. \quad (5.27)$$

This shows that the absorption of probe between levels $|6\rangle$ and $|8\rangle$ is modified by four coherence terms, viz., ρ_{16} , which is a coherence due to the A configuration formed out of $|6\rangle$, $|8\rangle$ and $|1\rangle$, ρ_{46} , which is a coherence term of the ladder $|6\rangle \leftrightarrow |8\rangle \leftrightarrow |4\rangle$, ρ_{96} of the ladder of $|6\rangle$, $|8\rangle$ and $|9\rangle$ and ρ_{82} , which is the coherence term of the V system of $|6\rangle$, $|8\rangle$ and $|2\rangle$.

Figure 5.6.1 shows individual factors that make up the ρ_{75} leg of the probe absorption. The plots marked a, b, c, d and e show respectively

$$A = \text{Im} \left[\frac{\rho_{15}^{(+1)}}{[\Delta_{75} - i(\gamma_7 + \gamma_5)]} \right],$$

$$B = \text{Im} \left[\frac{\rho_{35}^{(+1)}}{[\Delta_{75} - i(\gamma_7 + \gamma_5)]} \right],$$

$$\begin{aligned}
 C &= \text{Im} \left[\frac{(\rho_{55}^{(0)} - \rho_{77}^{(0)})}{[\Delta_{75} - i(\gamma_7 + \gamma_5)]} \right], \\
 D &= \text{Im} \left[\frac{\rho_{95}^{(0)}}{[\Delta_{75} - i(\gamma_7 + \gamma_5)]} \right], \\
 E &= \text{Im} \left[\frac{\rho_{72}^{(+1)}}{[\Delta_{75} - i(\gamma_7 + \gamma_5)]} \right]
 \end{aligned}$$

Plot f shows the sum of all these factors at $\Delta_L = 10.0$. Figure 5.6.2 show behaviour of these factors for $\Delta_L = 50.0$. Figures 5.6.3, figure 5.6.4, figure 5.6.5 and figure 5.6.6 show the variation of these factors for $\Delta_L = 100, 150, 200$ and 500 respectively.

Factor C is a contribution from the population difference $pn - \rho_{55}$ which results in the absorption peak at the line center $\Delta_p \approx 0$. The central peak of the factor $D = \text{Im} \left[\frac{\rho_{95}^{(0)}}{[\Delta_{75} - i(\gamma_7 + \gamma_5)]} \right]$ is equal to and opposite in sign to the peak of C and thus cancels it. This is in contrast to the case of isolated **Gate** system where the $\text{Im} \left[\frac{\rho_{95}^{(0)}}{[\Delta_{75} - i(\gamma_7 + \gamma_5)]} \right]$ factor was not of sufficient magnitude to cancel the central absorption peak completely (See figure 2.8 d). The remaining two sidebands coming from factor D can be identified as the peaks numbered I and II of figure 5.6 (a). Peak number **III** is a contribution from the coherence $A = \text{Im} \left[\frac{\rho_{15}^{(+1)}}{[\Delta_{75} - i(\gamma_7 + \gamma_5)]} \right]$. Factors B and E are very small in magnitude to affect the values of other factors in any way. The behaviour of the ρ_{86} part of the absorption can be understood in an identical fashion.

A further breakup of factors A, B, D and E into its constituent parts shows the structure of these factors. Contributions from their Real parts and Imaginary parts can separately be looked into. Figure 5.6.A shows these factors for an example case of $\Delta_L = 100.0$. For other detunings, these factors show a similar behaviour.

The figure 5.6.A.a shows

$$AR = \frac{\Delta_{75}}{\Delta_{75}^2 + \gamma^2} \text{Im } \rho_{15}^{(+1)} \quad \text{and} \quad AL \approx \frac{\gamma}{\Delta_{75}^2 + \gamma^2} \text{Im } \rho_{15}^{(+1)}.$$

Figure 5.6.A.b shows

$$BR = \frac{\Delta_{75}}{\Delta_{75}^2 + \gamma^2} \text{Im } \rho_{35}^{(+1)} \quad \text{and} \quad BL = \frac{\gamma}{\Delta_{75}^2 + \gamma^2} \text{Im } \rho_{35}^{(+1)}.$$

While figure 5.6.c shows

$$DR = \frac{\Delta_{75}}{\Delta_{75}^2 + \gamma^2} \text{Im } \rho_{95}^{(0)} \quad \text{and} \quad DL = \frac{\gamma}{\Delta_{75}^2 + \gamma^2} \text{Im } \rho_{95}^{(0)}.$$

and factors plotted in figure 5.6.A.d are

$$ER = \frac{\Delta_{75}}{\Delta_{75}^2 + \gamma^2} \text{Im } \rho_{72}^{(+1)} \quad \text{and} \quad EL \approx \frac{\gamma}{\Delta_{75}^2 + \gamma^2} \text{Im } \rho_{72}^{(+1)}.$$

$\gamma = \gamma_7 + \gamma_5$ is the decay term of the coherence ρ_{75} . Figure 5.6.a shows that the peak III is a result of factors AR and BR. The factor DL cancels the absorption due to factor C. The peaks I and II are result of factor DR. The peak number III on the other hand, which is at $\Delta_p = \Delta_L$ position is a result of ρ_{15} and ρ_{16} affecting the absorption of $\rho_{76}^{(0)} + \rho_{86}^{(0)}$.

At the position $\Delta_p = \Delta_L$, both the probe and pump beams are detuned equally from the $F=1 \leftrightarrow F'=1$ transition. Since both beams are detuned the population is distributed mostly in the three ground states $|5\rangle$, $|6\rangle$ and $|1\rangle$. As the population in states of $F'=1$ is very negligible, the transition $F'=1 \leftrightarrow F''=1$ can be neglected. The configuration can then be seen as a sixlevel configuration involving only $F=1 \leftrightarrow F'=1$ transition. The solutions for this configuration show that the pump and probe beam together develop coherences between the ground states to form a three-component superposition state, which leads to a very narrow absorption peak. This has been identified as a three component trapped state [15].

To analyse the nature of the superposition states that are formed due to the pump beam, the dressed state picture is next made use of.

5.4.2 Dressed State analysis

For a further understanding of the coherence developed by the pump beams, an analysis is presented in the dressed state picture, where the pump beam creates the coherent superposition states. All transitions connected by the pump beam are considered including the off-resonant coupling of the lower transitions. Figure 5.8 shows the configuration with only the pump beams which resonantly interact with upper six levels and act off-resonant on lower six levels. This system can be decoupled into two sub-configurations named X and Diamond after their shapes. Figure 5.9(a) shows the X configuration and figure 5.9 (b) shows the Diamond configuration. It is seen that the probe beam connects levels of X to levels of Diamond and vice versa. Therefore, the probe absorption behaviour is determined by the allowed transitions between the states of X and Diamond. On the other hand, the total configuration can also be analysed as a combination of a double A and a double V, where the A formed out of levels $|5\rangle$, $|2\rangle$ and $|6\rangle$ interacts with the A $|7\rangle$, $|9\rangle$ and $|8\rangle$ through the probe beams and the V system of $|7\rangle$, $|1\rangle$ and $|8\rangle$ interact with that of $|3\rangle$, $|2\rangle$ and $|4\rangle$ through probe beams. It is shown here that as Δ_L is increased, the X and Diamond picture goes closer to double A and double V picture.

The Hamiltonian for the X- configuration is

$$\mathcal{H}_X = \begin{pmatrix} \Delta_2 & -g_{25} & -g_{26} & -g_{32}^* & g_{42}^* \\ -g_{25}^* & 0 & 0 & 0 & 0 \\ -g_{26}^* & 0 & 0 & 0 & 0 \\ -g_{32} & 0 & 0 & \Delta_3 & 0 \\ -g_{42} & 0 & 0 & 0 & \Delta_4 \end{pmatrix}$$

The detunings are defined as $\Delta_i = \omega_i - \omega_1 - \omega_L$, where ω_i are the angular frequency energy value of level $|i\rangle$ for $i = 2, 3, 4, 5, 6$ and ω_L is the frequency of the pump laser. The coupling coefficients are defined $g_{ij} = d_{ij} \cdot \mathcal{E}_{ij}$.

Figure 5.10 (a) shows numerical eigenvalue of this hamiltonian for a variation in Δ_L . A value $g_{ij} = 10.0$ is used. $\Delta_3 = \Delta_4$ are detuning between the pump beam and $F'=1 \leftrightarrow F''=1$ transition. Since the pump beam is assumed resonant with this transition, their value is set to $\Delta_3 = \Delta_4 = 0$. The detuning between the pump beam and $F \approx 1 \leftrightarrow F'=1$ transition is $\Delta_2 = \Delta_L$. The numerical results show that of the five eigenvalues, two of the eigenvalues are 0 and Δ_L . The other three eigenvalues are determined by function of Δ_L and $|g|^2$. The inset shows that of these three eigenvalues, two reach an asymptotic limit of $\Delta_L \pm \sqrt{2}|g|$ as Δ_L increases.

The diamond system has a hamiltonian

$$\mathcal{H}_D = \begin{pmatrix} 0 & -g_{71} & -g_{81} & 0 \\ -g_{71} & \Delta_7 & 0 & -g_{97} \\ -g_{81} & 0 & \Delta_8 & -g_{98} \\ 0 & -g_{97} & -g_{98} & \Delta_9 \end{pmatrix}$$

Numerical values of eigenenergies of this hamiltonian is shown in figure 5.10 (b) for

a variation of Δ_L . The values $G_{71} = g_{81} = g_{98} = g_{97} = 10.0$, $\Delta_9 = 0$ and $\Delta_7 = \Delta_8 = \Delta_L$ are used. Of the four eigenvalues, one has a value equal to Δ_L and the other three are functions of Δ_L and $|g|^2$. Again, the inset shows that two of the eigenvalues approach $\Delta_L \pm \sqrt{2}|g| = \Delta_L \pm 14.141$ for large Δ_L . Further, the four eigenvalues of Diamond are degenerate with four eigenvalues of X.

The set of five eigenvalues of X configuration form a ladder, each set of five separated by energy of a single photon of pump beam. Similar ladder is formed by the set of four eigenvalues of Diamond configuration. Figure 5.11 (a) shows such a set at same photon number value; where the four eigenvalues of diamond, named D_1 , D_2 , D_3 and D_4 are degenerate with four of the X - eigenvalues, X_1 , X_2 , X_3 and X_5 . The eigenstate corresponding to $(1/\sqrt{2})(|5\rangle - |6\rangle)$ does not have a corresponding state in the Diamond system. The probe beam now connects states of X configuration from one such set to those of Diamond configuration of the set with higher energy as shown in figure 5.11 (b). Then, the absorption peaks should occur whenever $\omega_p = D_i + \omega_L - X_j$, where $i = 1, 2, 3, 4$ and $j = 1, \dots, 5$. Rewritten,

$$\begin{aligned}\omega_p &= D_i + \omega_L - X_j \\ \omega_p - \omega_L &= D_i - X_j \\ \omega_{Lp} &= D_i - X_j\end{aligned}\tag{5.28}$$

Substituting from equation (5.11), absorption peaks should occur at

$$\Delta_p = \Delta_L - (D_i - X_j).\tag{5.29}$$

But their appearance also depends on the nonzero values of the dipole transitions between the corresponding dressed eigenstates.

From the numerical values, the eigenvectors of X and Diamond configurations can be constructed as

$$\begin{aligned}
X_1 &= -x_{11}|2\rangle + x_{12}(|3\rangle + |4\rangle) + x_{13}(|5\rangle + |6\rangle) \\
X_2 &= 0.707|3\rangle - 0.707|4\rangle \\
X_3 &= x_{31}|2\rangle + x_{32}(|3\rangle + |4\rangle) - x_{33}(|5\rangle + |6\rangle) \\
X_4 &= 0.707|5\rangle - 0.707|6\rangle \\
X_5 &= x_{51}|2\rangle + x_{52}(|3\rangle + |4\rangle) + x_{53}(|5\rangle + |6\rangle) \\
\\
D_1 &= d_{11}|1\rangle - d_{12}(|7\rangle + |8\rangle) + d_{13}|9\rangle \\
D_2 &= 0.707|7\rangle - 0.707|8\rangle \\
D_3 &= -d_{31}|1\rangle + d_{32}(|7\rangle + |8\rangle) + d_{33}|9\rangle \\
D_4 &= -d_{41}|1\rangle - d_{42}(|7\rangle + |8\rangle) - d_{43}|9\rangle
\end{aligned} \tag{5.30}$$

where x_{ij} and d_{ij} are coefficients whose value depends upon Δ_L and the pump beam intensity.

Extending the selection rules for transitions between superposition states (4.17) of Chapter IV, and its modification due to signs of dipole matrix elements (5.1), the allowed transitions for the probe beam for the full nine-level system can be represented as

$$\begin{aligned}
|5\rangle - |6\rangle &\leftrightarrow |7\rangle + |8\rangle \\
|5\rangle + |6\rangle &\leftrightarrow |7\rangle - |8\rangle \\
|7\rangle - |8\rangle &\leftrightarrow |3\rangle + |4\rangle \\
|7\rangle + |8\rangle &\leftrightarrow |3\rangle - |4\rangle
\end{aligned} \tag{5.31}$$

where each side of double arrow represents a part of the superposition that occurs in the eigenvalues of X and Diamond.

From the rules (5.31), the nonzero transitions are found to be $X_4 \leftrightarrow D_{1,3,4}$ and $X_{1,2,3,5} \leftrightarrow D_2$. All other transitions have a zero transition probability. The state X_4 is a state of the form $|5\rangle - |6\rangle$ state. This is a trapping state and in the absence of the probe beam, all the population is trapped in this state. Collisions transfer population from this to other ground states, notable to X_5 which is a state of lower energy [16]. For a zero collision condition, which is shown in figure 5.6 (a) and (b), the strong absorption signals then are for transitions between $X_4 \leftrightarrow D_{1,3,4}$. The three absorption peaks shown in figure 5.6 (a) and (b) should then correspond to three transitions $X_4 \leftrightarrow D_1$, $X_4 \leftrightarrow D_3$ and $X_4 \leftrightarrow D_4$. Table 5.1 shows the Δ_p values corresponding to each $X_4 \leftrightarrow D_i$ transition, according to (5.29) where $i = 1, 3, 4$. The absorption peaks numbered I, II and III in figure 5.6 (a) and (b) are seen to exactly match these frequencies. This leads to the conclusion that the three peaks correspond to the transitions

$$\begin{aligned} X_4 \leftrightarrow D_1 &\implies I \\ X_4 \leftrightarrow D_3 &\implies II \\ X_4 \leftrightarrow D_4 &\implies III \end{aligned}$$

In presence of collisions, population is transferred to other lower states from X_4 , and the probe beam absorption should show transitions from these states of X to allowed states of D. Absorption profiles in presence of a collisional damping $\gamma_c = 0.5$ is shown in figures 5.7 (a) and (b) for the same values of Δ_L that was used for figures 5.6. But this

| Δ_L | D_1 | I | D_3 | II | D_4 | III |
|------------|---------|----------|---------|--------|---------|---------|
| 10.0 | 28.136 | -18.136 | 5.29 | 4.706 | -13.429 | 23.429 |
| 50.0 | 65.744 | -15.744 | 38.23 | 11.767 | 3.97 | 53.97 |
| 100.0 | 115.038 | -15.0381 | 86.9611 | 13.038 | -1.99 | 101.99 |
| 150.0 | 164.76 | -14.76 | 136.57 | 13.43 | -1.33 | 151.33 |
| 200.0 | 214.61 | -14.615 | 186.38 | 13.62 | -0.999 | -200.99 |
| 500.0 | 514.338 | -14.338 | 486.062 | 13.938 | -0.4 | 500.4 |

Table 5.1:

| Δ_L | X_5 | D_2 | c |
|------------|----------|-------|---------|
| 10.0 | -13.42 | 10.0 | 13.42 |
| 50.0 | -3.97827 | 50.0 | 3.97827 |
| 100.0 | -1.999 | 100.0 | 1.999 |
| 150.0 | -1.333 | 150.0 | 1.3333 |
| 200.0 | -0.998 | 200.0 | 0.998 |
| 500.0 | -0.088 | 500.0 | 0.088 |

Table 5.2:

shows only one additional absorption peak which is labeled 'c'. This should then be due to the fact that the maximum transfer of population due to collision is to the state X_5 , which is of energy lower than that of X_4 . This additional line 'c' is then identified to correspond to transition $X_5 \leftrightarrow D_2$. Contributions from other levels are very little. The position of the peak labeled 'c' corresponds to the frequency of transition between X_5 and D_2 , which is shown in table 5.2.

Position of the peaks numbered I, II and **III** are the same as for zero collision.

5.4.3 Double A and Double V configurations

This nine level configuration can be analysed in a manner shown in figure 5.5 (b), taking note of the two-photon resonances between levels of $F=1$ and $F''=1$. This configuration can be divided into double A and double V subconfigurations. Levels $|5\rangle$, $|2\rangle$, $|6\rangle$ and levels $|7\rangle$, $|9\rangle$, $|8\rangle$ form the two A systems and levels $|1\rangle$, $|7\rangle$, $|8\rangle$ and levels $|3\rangle$, $|2\rangle$, $|4\rangle$ form the two V configurations. Levels $|7\rangle$ and $|8\rangle$ that take part in double V scheme and the level $|2\rangle$ that forms a part of double A scheme are virtual levels. It can be seen that as Δ_L increases, the distance between the real $|7\rangle$, $|8\rangle$ and $|2\rangle$ and their virtual counter parts increase and the double A and double V configurations become less and less coupled. Therefore, approximation of double A and double V picture is more appropriate in large Δ_L regime. It can be shown that this picture, in the large Δ_L domain gives the two symmetric peaks I and II.

For the double A case, the lower A forms three eigenstates,

$$\begin{aligned} &|5\rangle - |6\rangle \\ &|2\rangle + |5\rangle + |6\rangle \\ &\text{and} \\ &-|2\rangle + |5\rangle + |6\rangle \end{aligned}$$

With eigenvalues 0 and $\frac{\Delta_L \pm \sqrt{\Delta_L^2 + 4\alpha_1^2}}{2}$, respectively where $\alpha_1^2 = |g_{25}|^2 + |g_{26}|^2$. The upper A forms three eigenstates with

$$\begin{aligned} &|7\rangle - |8\rangle \\ &|9\rangle + |7\rangle + |8\rangle \\ &\text{and} \\ &-|9\rangle + |7\rangle + |8\rangle \end{aligned}$$

with eigenvalue 0, $\pm\alpha_2$, where $\alpha_2^2 = |g_{97}|^2 + |g_{98}|^2$.

For $g_{97} = g_{98} = 10.0$, which is used in the numerical calculation, the eigenvalue $\alpha = \sqrt{200} = \pm 14.141$. Figures 5.10 (a) and 5.10 (b) show that two eigenvalues asymptotically reach $\Delta_L \pm \alpha$. Such a system shows two absorption peaks at $\Delta_p = \pm\alpha_2$.

Similarly the lower V of the Double V system results in three eigenstates

$$|7\rangle - |8\rangle$$

$$|1\rangle + |7\rangle + |8\rangle$$

and

$$-|1\rangle + |7\rangle + |8\rangle$$

with energies values Δ_L and $\frac{\Delta_L \pm \sqrt{\Delta_L^2 + 4\alpha_3^2}}{2}$, respectively where $\alpha_3^2 = |g_{71}|^2 + |g_{81}|^2$, and the upper V gives three eigenstates

$$|3\rangle - |4\rangle$$

$$|2\rangle + |3\rangle + |4\rangle$$

and

$$-|2\rangle + |3\rangle + |4\rangle$$

with eigenvalues 0 and $\pm\alpha_4$, where $\alpha_4^2 = |g_{32}|^2 + |g_{42}|^2$, which will also result in resonance peaks at $\Delta_p = \pm\sqrt{\alpha}$.

Numerical values of x_{ij} and d_{ij} show that for larger Δ_L , the eigenstates of X and Diamond configuration slowly approach eigenvalues of A and V, and the absorption peaks, as shown for $\Delta_L = 500.0$, approach $\Delta_p = \pm a$. But the double A and double V picture does not explain the presence of peak III.

At $\Delta_p = 0$, the maximum contribution to absorption should have been from the resonant transition $X_4 = 0.707(|5\rangle - |6\rangle) \leftrightarrow D_2 = 0.707(|7\rangle - |8\rangle)$. From the transition rules 5.1 it can be seen that this transition probability is zero due to quantum interference. Therefore, this configuration shows a transparency at $\Delta_p = 0$. Since the detuned action of pump beam on the probe transition was neglected in obtaining the solutions of the model Gate system in the previous chapters, the cancellation of absorption which is shown here is not seen. Only the non-perturbative approach used here leads to the effect. The fact the transparency at line center is achieved due to formation of the coherence superposition of the ground states also is in accordance with the results of Chapter IV. Whereas the atoms were prepared in the required superposition state before they interacted with the pump and probe beams, the necessary coherence is created here by the action of the pump beam on the $F=1 \leftrightarrow F'=1$ transition. Since this coherence is destroyed by collisional dampings and therefore, a measure of transparency can be used to determine the collisional decay rates.

5.4.4 Conclusion

Three configurations in Sodium-like atomic systems are discussed where Y and Gate configurations can be realized. A complex configuration is seen to be made up of Gate-like and Y-like subsystems and the absorption behaviour of this system is seen to be a summation of individual Gate-like and Y-like subsystems. Off-resonant behaviour of the pump beam on the probe transition is studied using a continued fraction technique for $F=1 \leftrightarrow F'=1 \leftrightarrow F''=1$. The results show that the pump beam can create the coherence necessary to reduce the central absorption peak of the system which is otherwise

a **Gate** system. As collisions destroy the coherence created by the pump beam, the absorption profile is a three peaked signature of the **Gate** configuration.

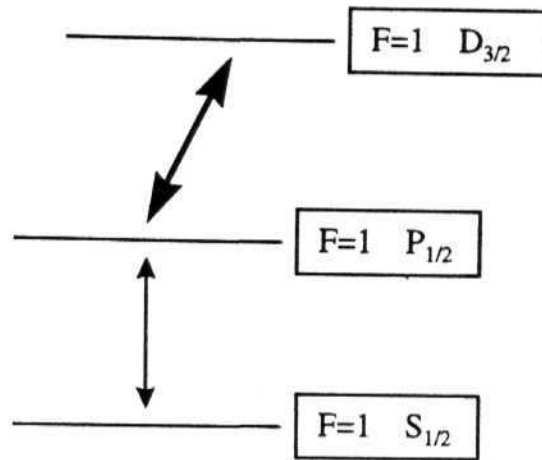


Fig 5.1 A simple 3 level configuration for EIT. The single line denotes probe and the double line is pump in all the figures.

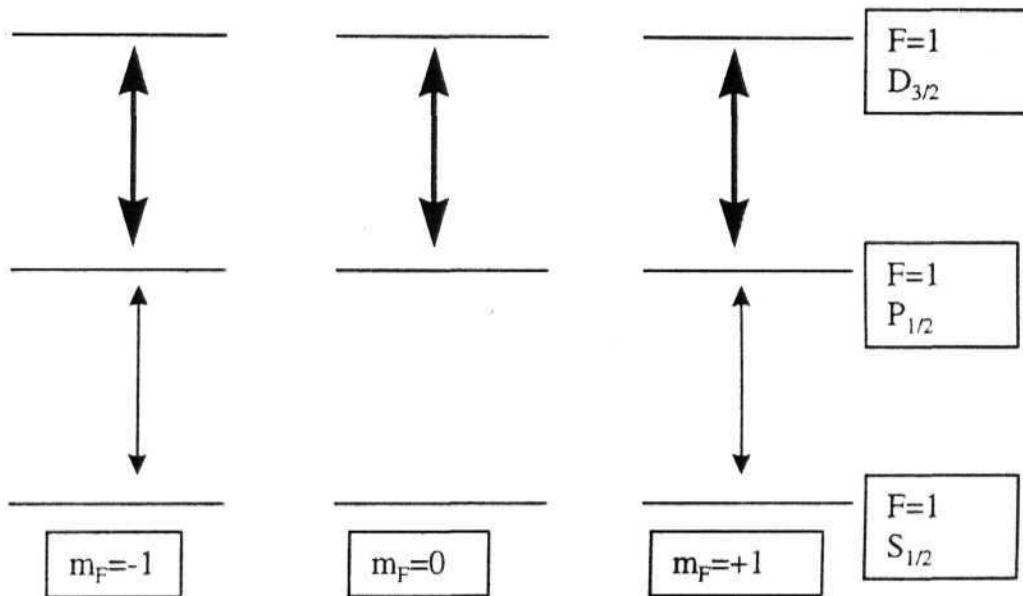


Fig. 5.2 (a): Figure showing the m_F sublevels of figure 5.1 and the dipole allowed transitions between them. For a π polarized strong beam, Fig. 5.1 reduces to a combination of two 'ladder's.

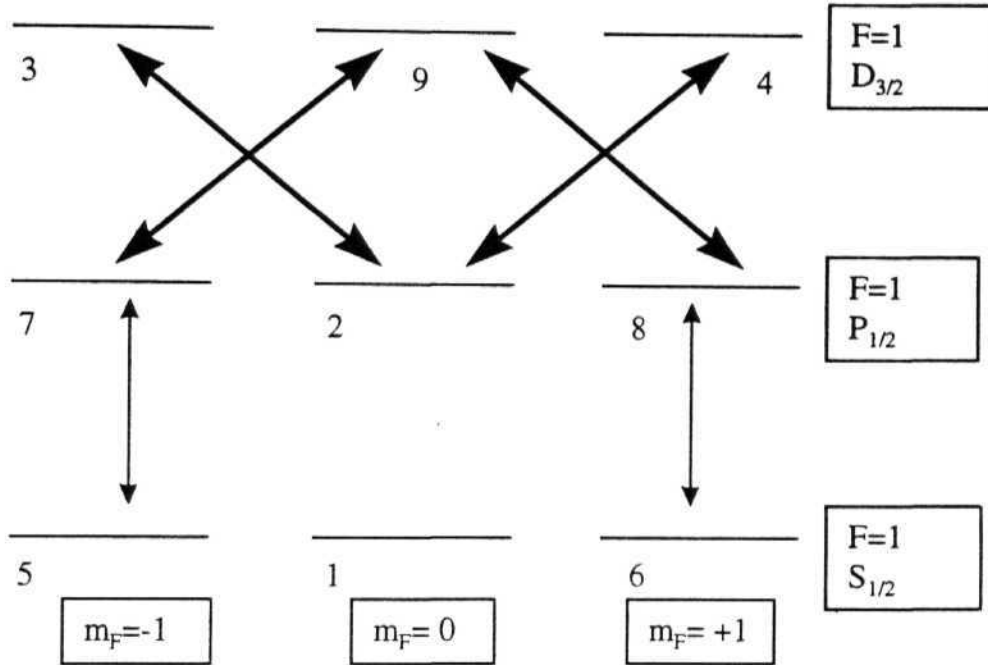


Fig. 5.2 (b): Figure showing the m_F sublevels of figure 5.1 and the dipole allowed transitions between them, for strong beam being plane polarized in xy plane. Scheme 5-7-9-8-6 forms a **Gate** configuration. Transition between 1-2 is not allowed.

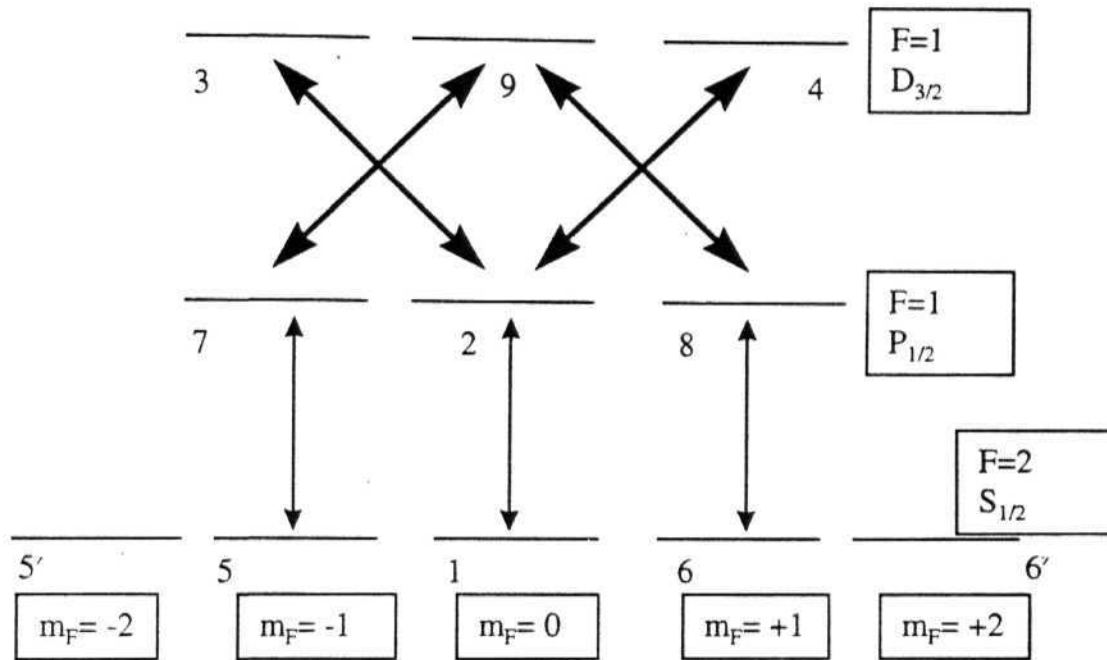


Fig. 5.2 (c) : Configuration using F=2 of ground level with F=1 of P_{1/2} and D_{3/2} levels. Polarization of beams is as in figure 5.2 (b). 1-2 transition is now allowed and therefore, scheme 5-7-9-8-6 forms a **Gate** and scheme 1-2-3-4 forms a Y system.

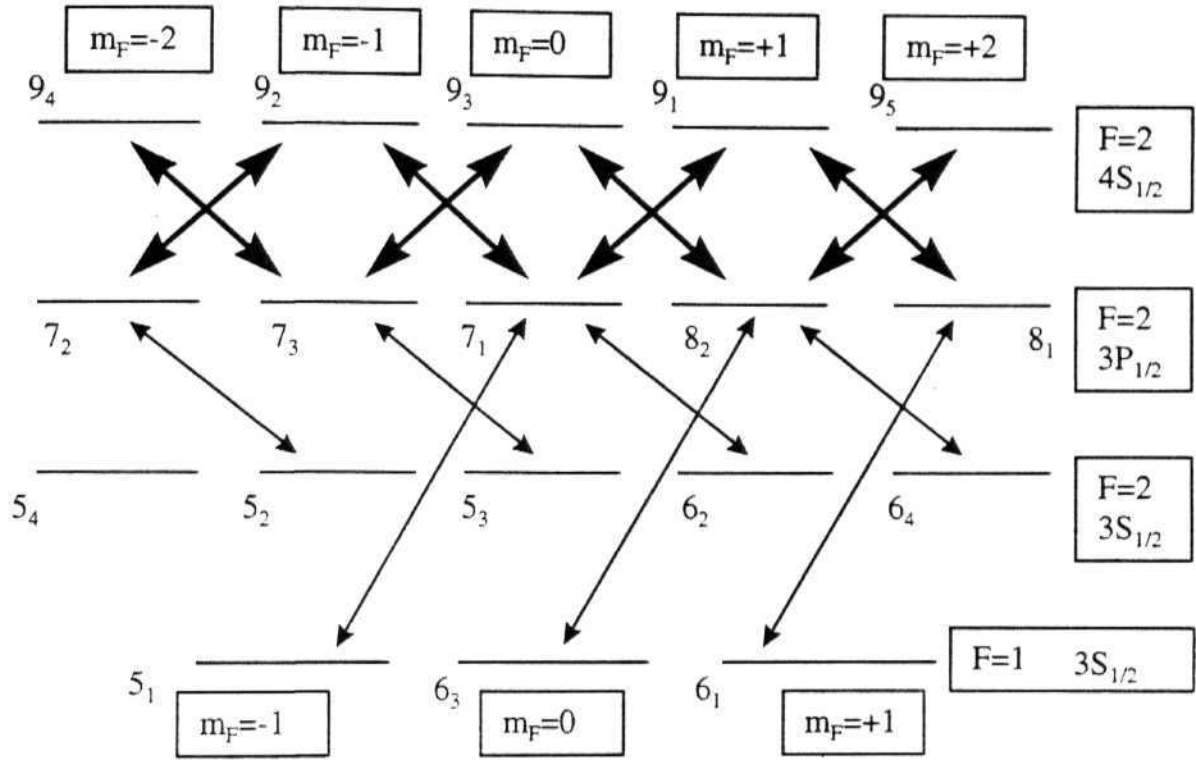


Fig. 5.3: Configuration for case III. Two lower levels are F=1 and F=2 of 3S_{1/2}. Upper levels are F=1 and F=2 levels of 3P_{1/2} and 4S_{1/2}. The probe beams are made up of two σ^+ and σ components resonant with the transition connecting.

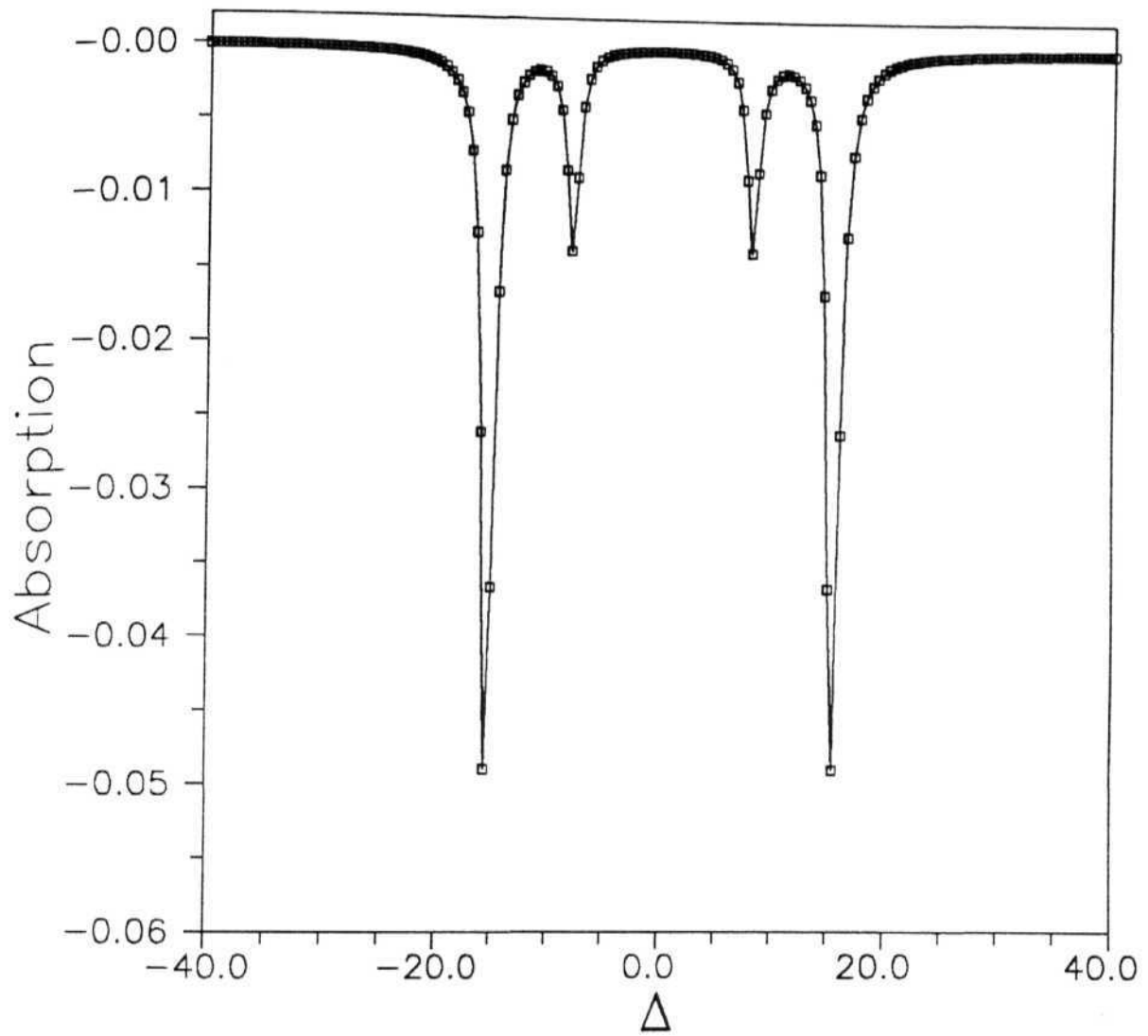


Fig. 5.4(a): Loss of population from 6_3 (solid line) and 6_4 (symbols). Equivalent to absorption of probe.

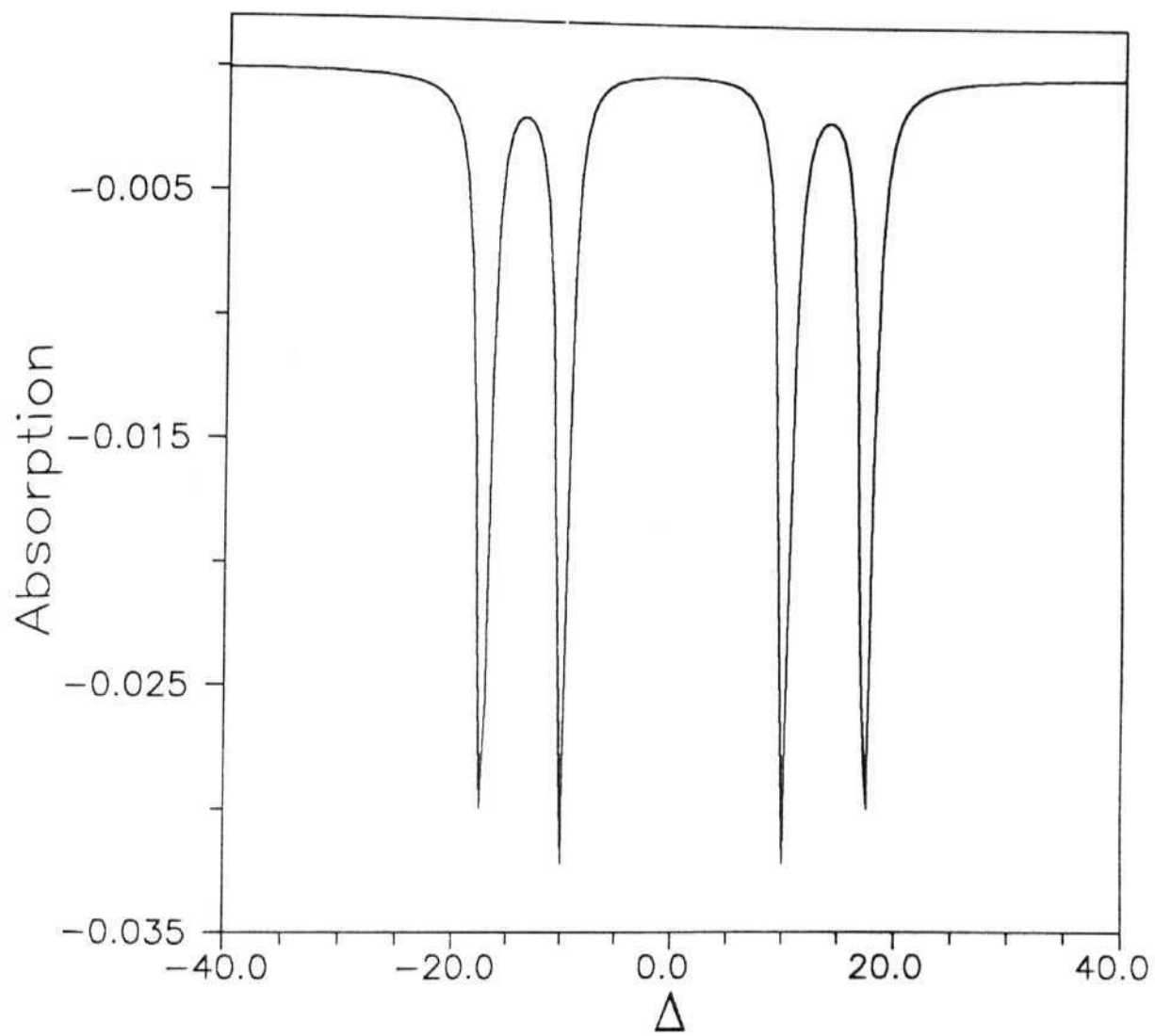


Fig. 5.4 (b): Loss of population from 5_3

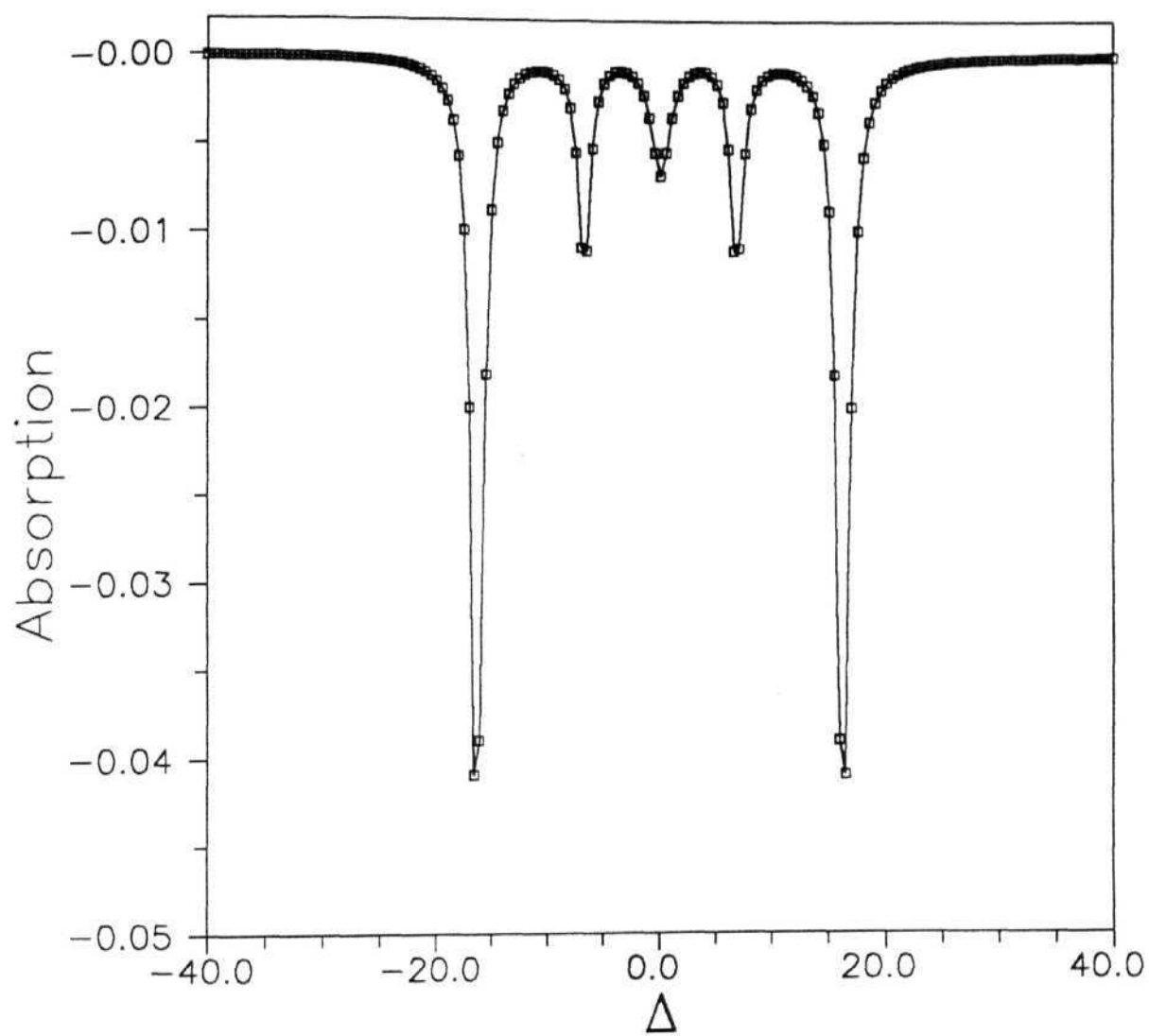


Fig. 5.4 (c): Loss of population from 5_1 (solid line) and 6_2 (symbols).

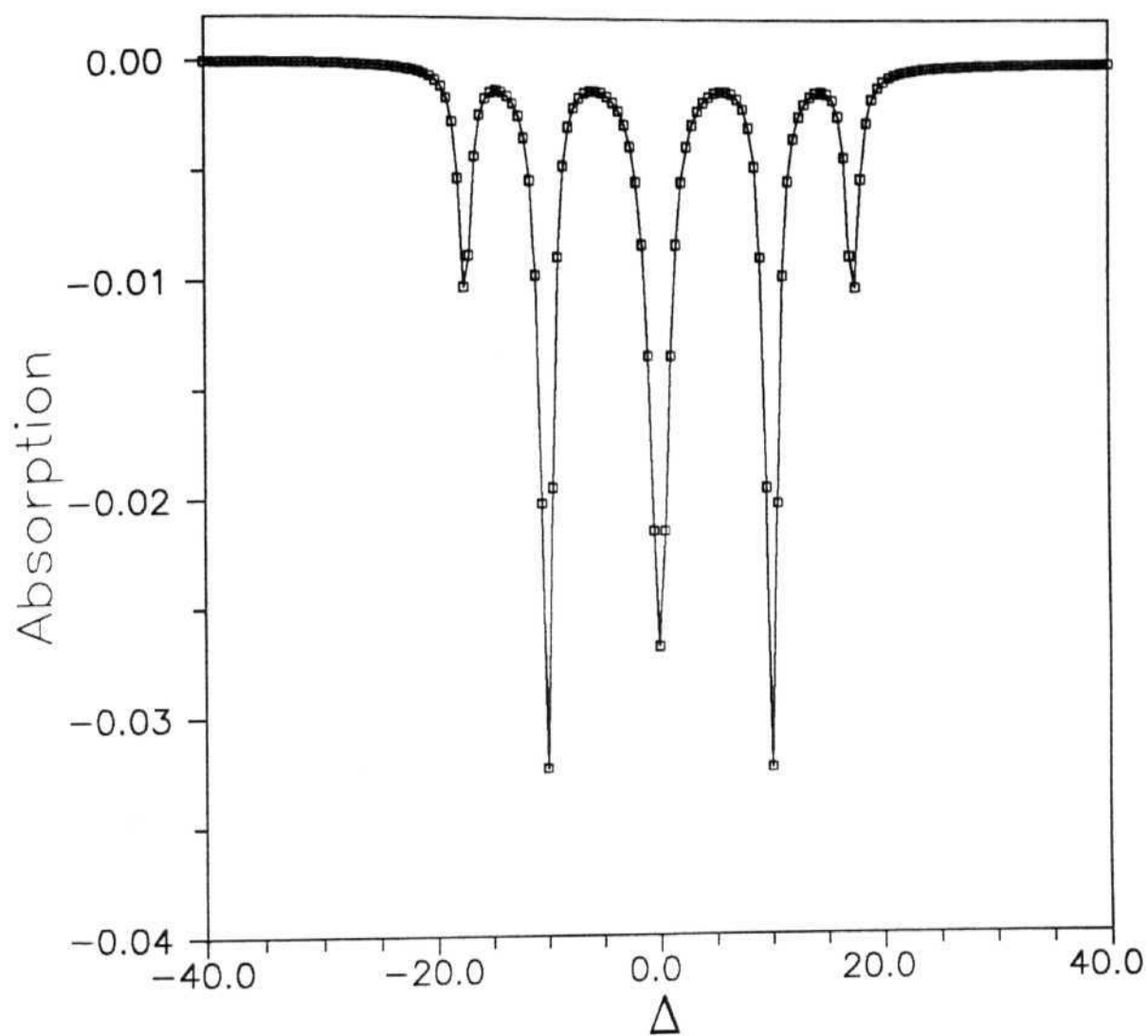


Fig. 5.4 (d): Loss of population from 6_1 (solid line) and 5_2 (symbols).

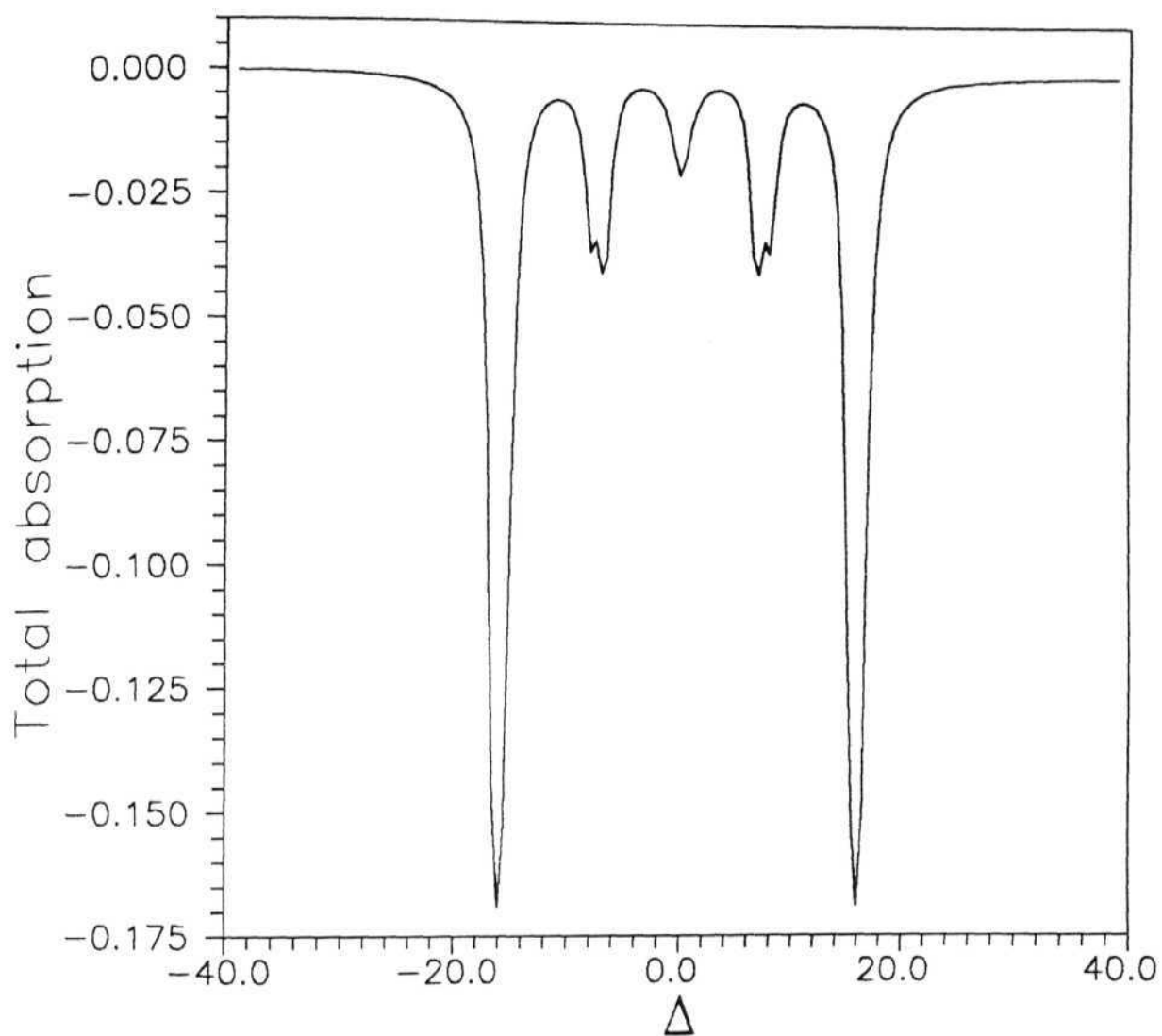


Fig. 5.4(e): Total absorption (total loss of population from all the ground levels).

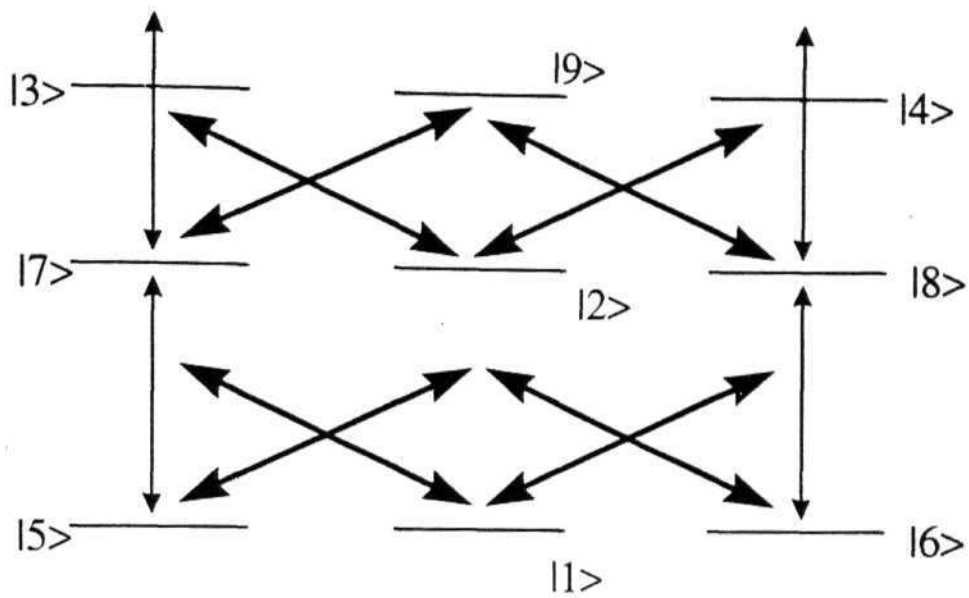


Fig. 5.5 (a): Complete configuration for $F=1 :F=1: F=1$ system. **Thick** lines represent Pump beams, and **thin lines** represent probe beams.

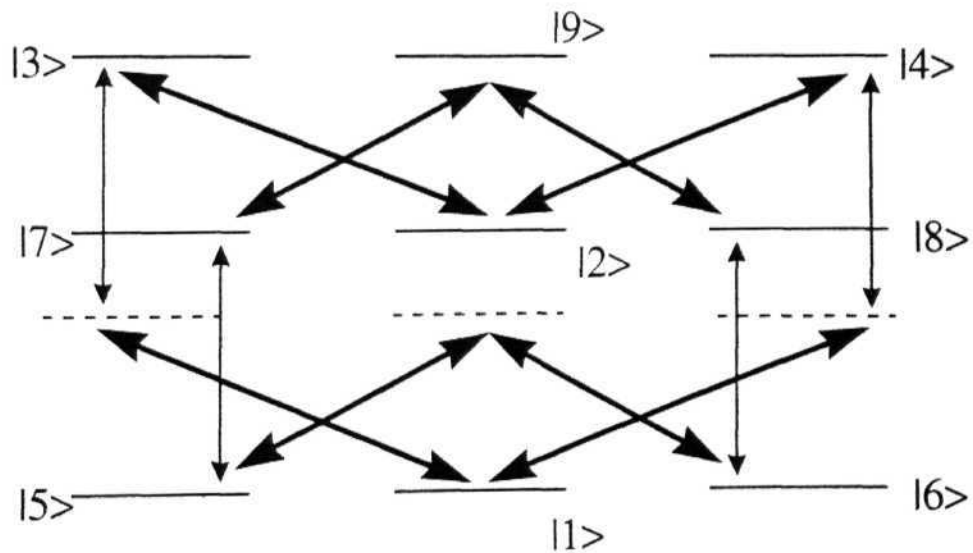


Fig. 5.5 (a): Complete configuration for $F=1 :F=1: F=1$ system, showing two-photon resonant transitions Double A and double V systems.

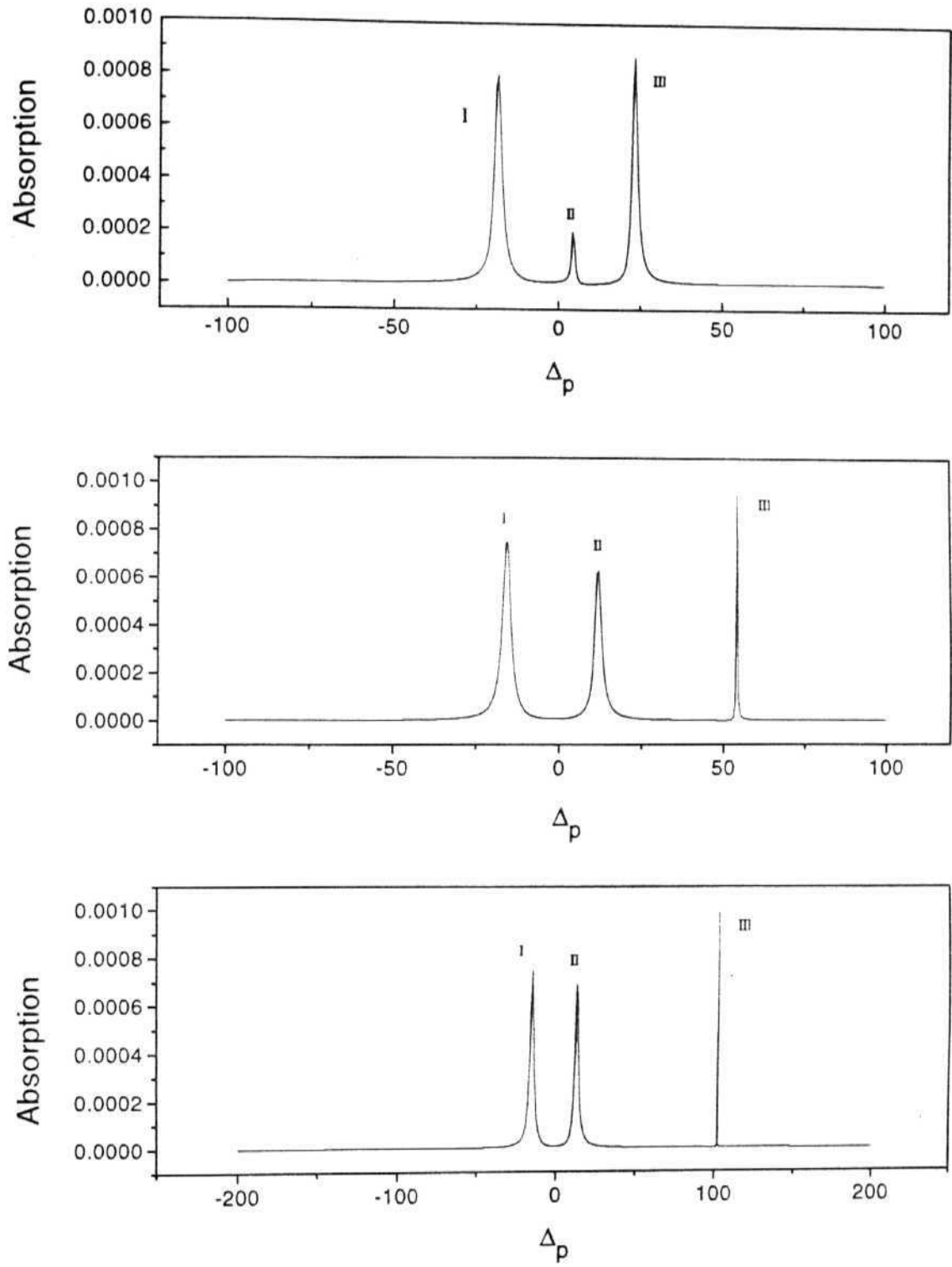


Fig. 5.6 (a): Probe absorption for $\Delta_L=10.0$, 50.0 and 100.0 .

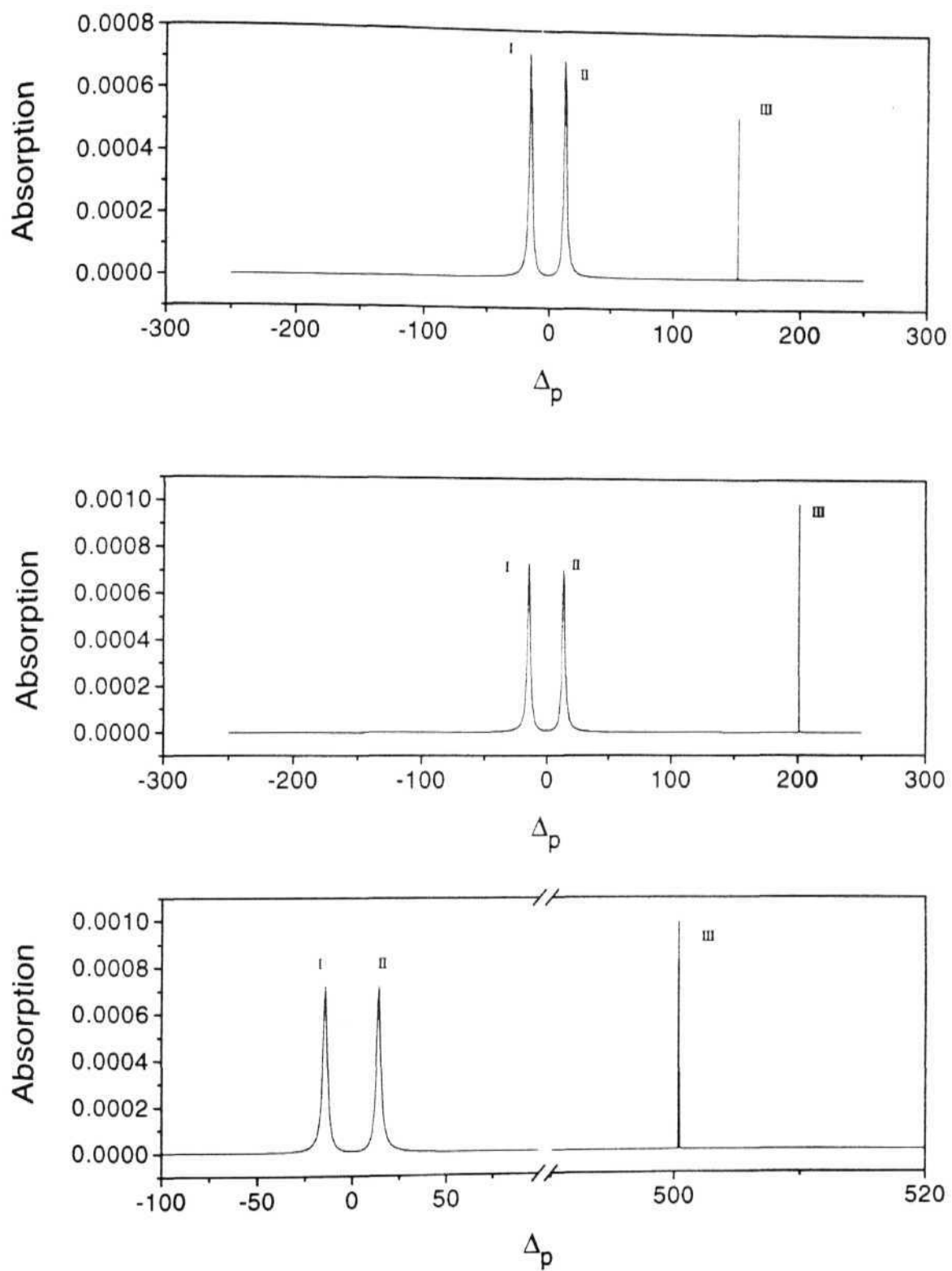


Fig. 5.6 (b): Probe absorption for $\Delta_L=150.0$, 200.0 and 500

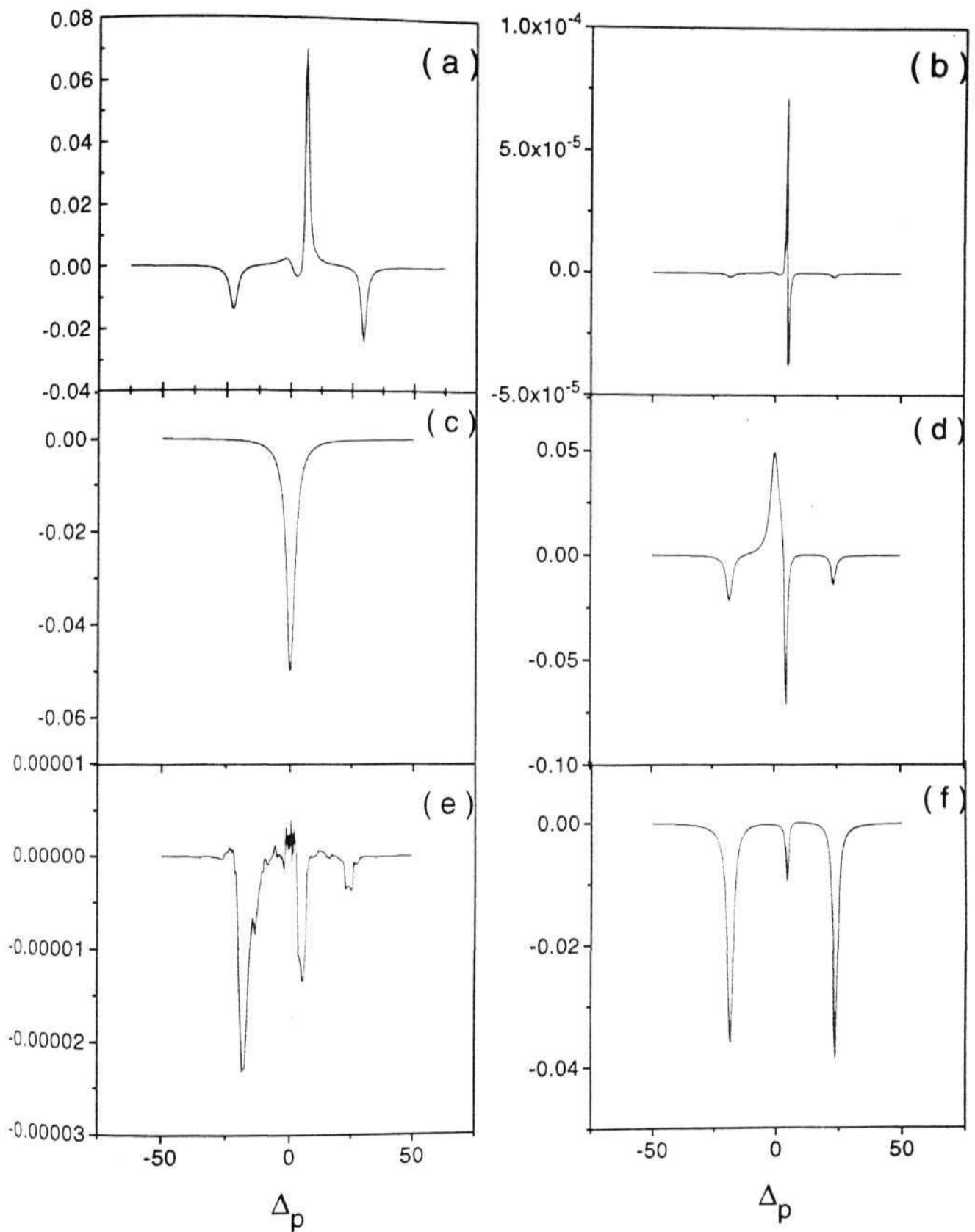


Fig. 5.6.1 Imaginary parts of ρ_{15} , ρ_{35} , $(\rho_{55} - \rho_{77})$, ρ_{95} , ρ_{72} and their sum respectively, divided by $[i \Delta_L - (\gamma_5 + \gamma_7)]$ for $\Delta_L = 10.0$

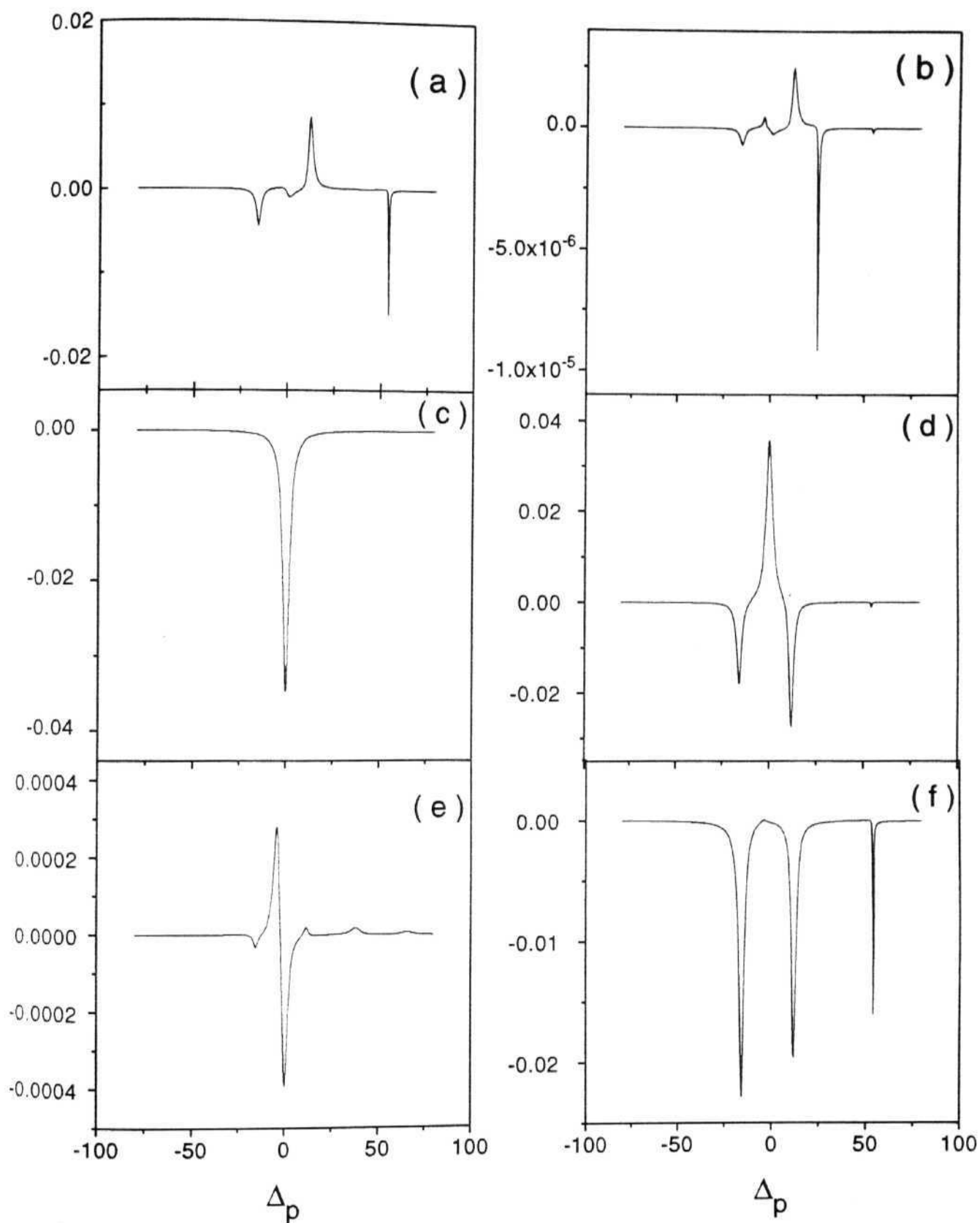


Fig. 5.6.2 : Imaginary parts of ρ_{15} , ρ_{35} , $(\rho_{55}-\rho_{77})$, ρ_{95} , ρ_{72} and their sum respectively, divided by $[i \Delta_L - (\gamma_5 + \gamma_7)]$ for $\Delta_L = 50.0$

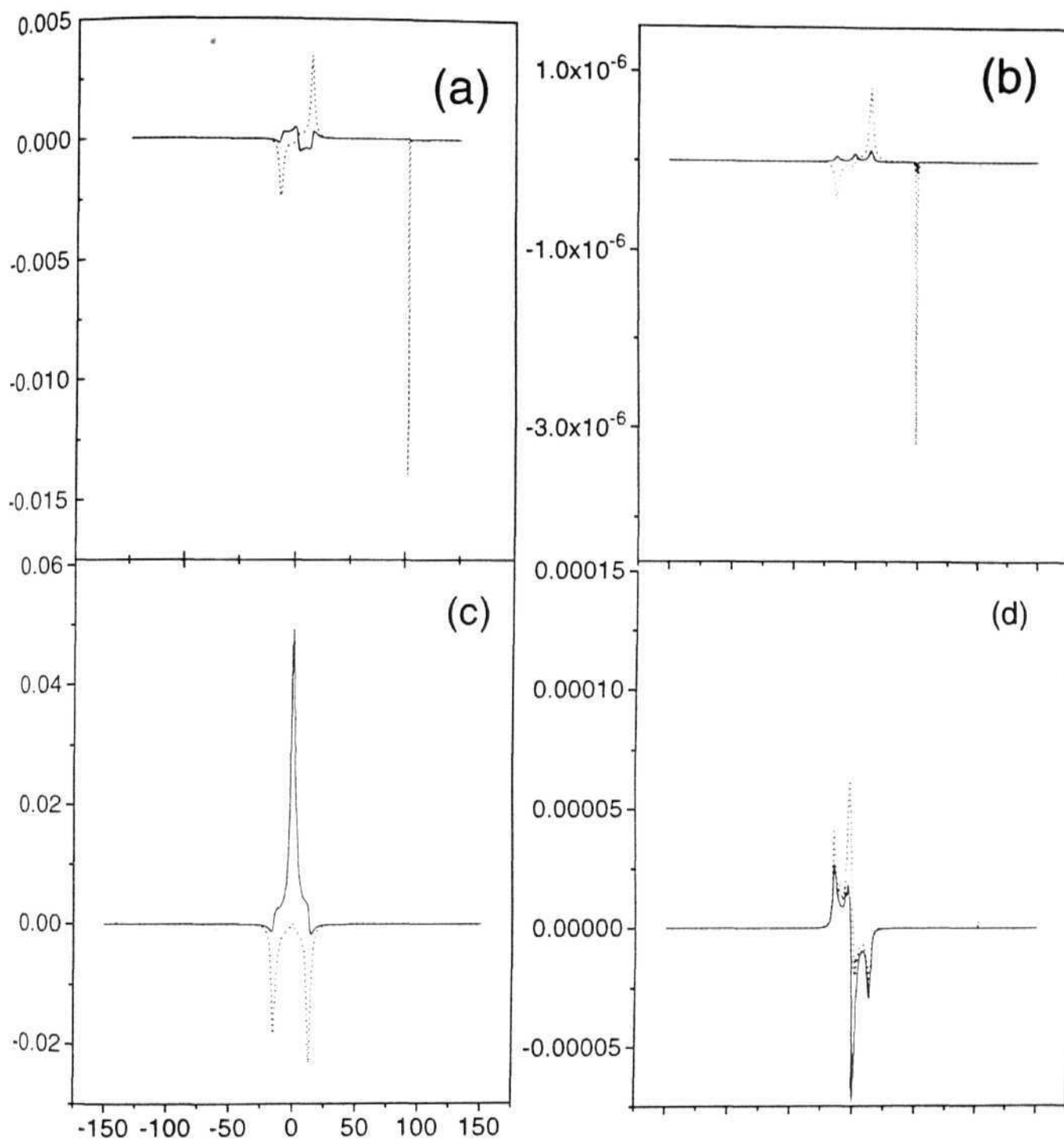


Fig. 5.6.2.A: Factors (a) AR (dashed lines), and (b) AL (solid lines), (b)BR (dashed) and BL (solid), (c) DR (dashed) and DL (solid) and (d) ER (dashed) and EL (solid). See text for details.

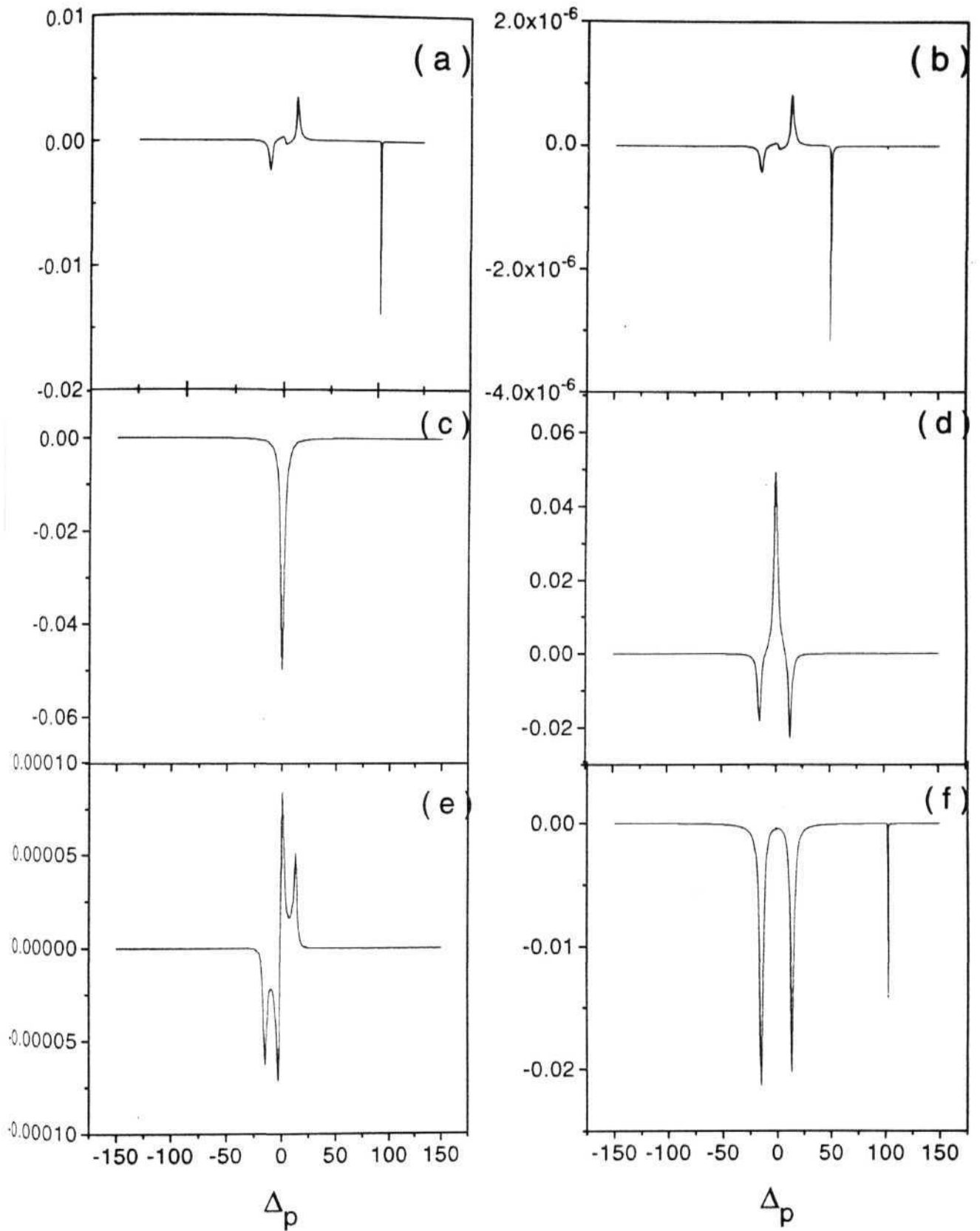


Fig. 5.6.3 Imaginary parts of ρ_{15} , ρ_{35} , $(\rho_{55} - \rho_{77})$, ρ_{95} , ρ_{72} and their sum respectively, divided by $[i \Delta_L - (\gamma_5 + \gamma_7)]$ for $\Delta_L = 100.0$

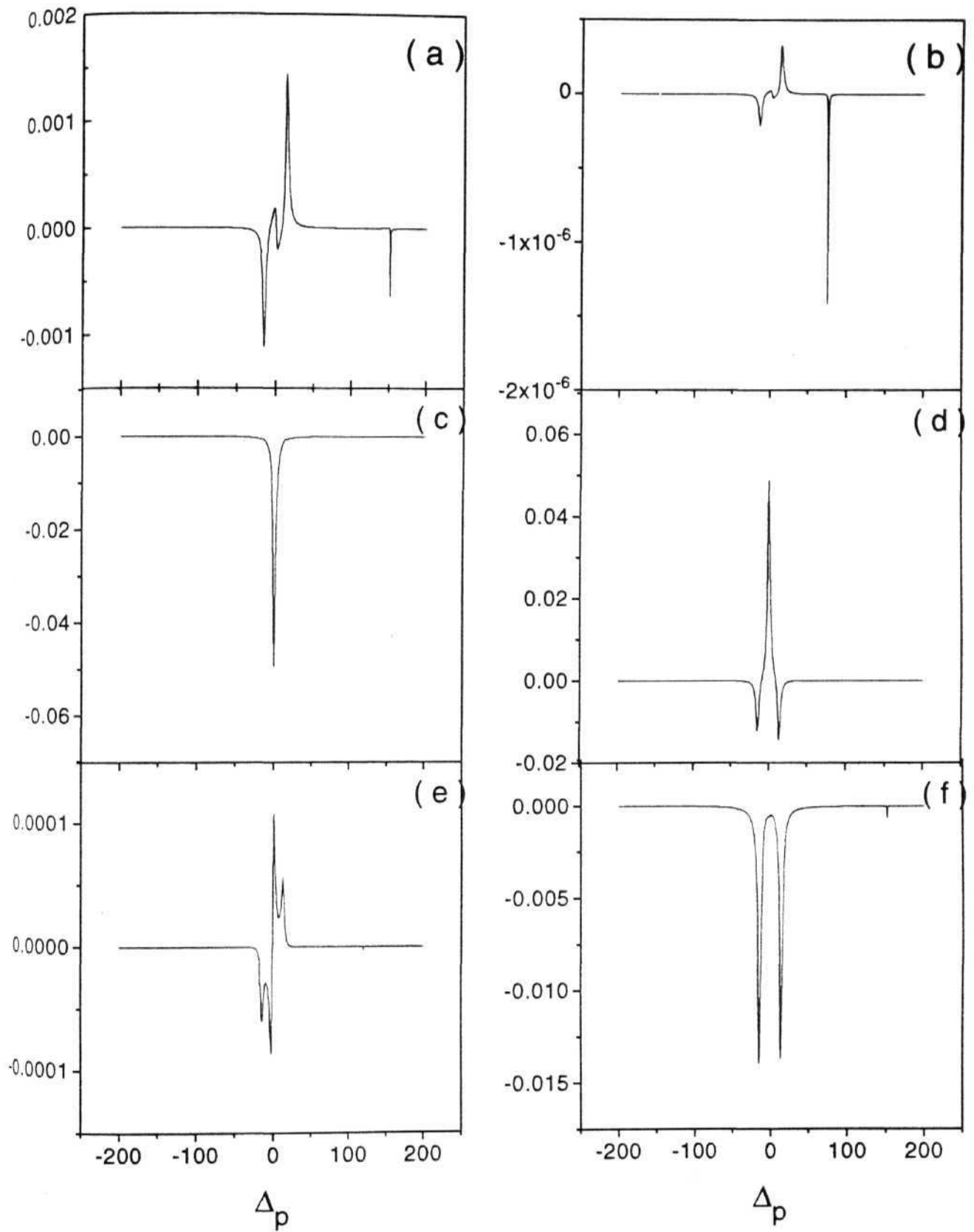


Fig. 5.6.4 : Imaginary parts of ρ_{15} , ρ_{35} , $(\rho_{55} - \rho_{77})$, ρ_{95} , ρ_{72} and their sum respectively, divided by $[i \Delta_L - (\gamma_5 + \gamma_7)]$ for $\Delta_L = 150.0$

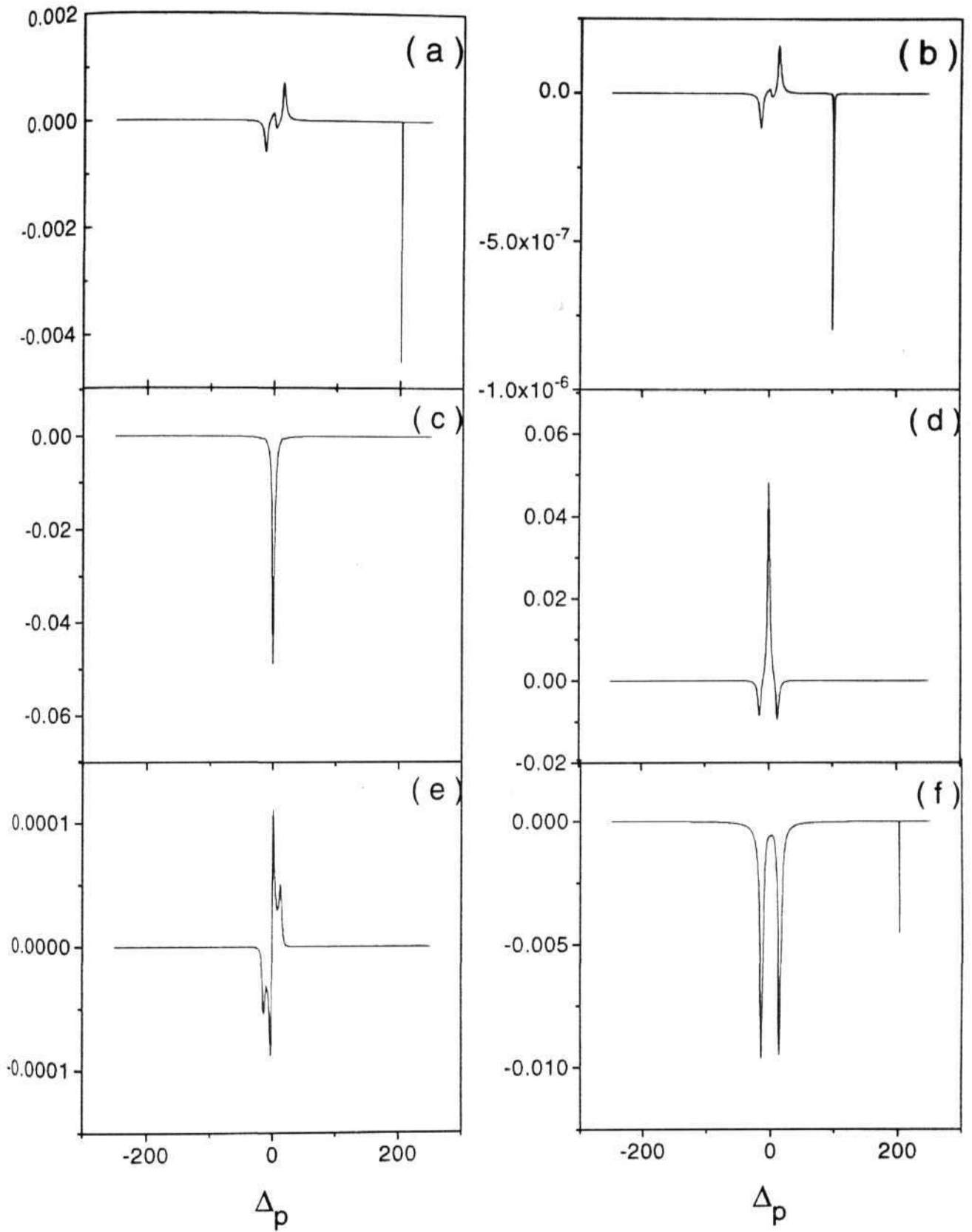


Fig. 5.6.5 : Imaginary parts of ρ_{15} , ρ_{35} , $(\rho_{55} - \rho_{77})$, ρ_{95} , ρ_{72} and their sum respectively, divided by $[i \Delta_L - (\gamma_5 + \gamma_7)]$ for $\Delta_L = 200.0$

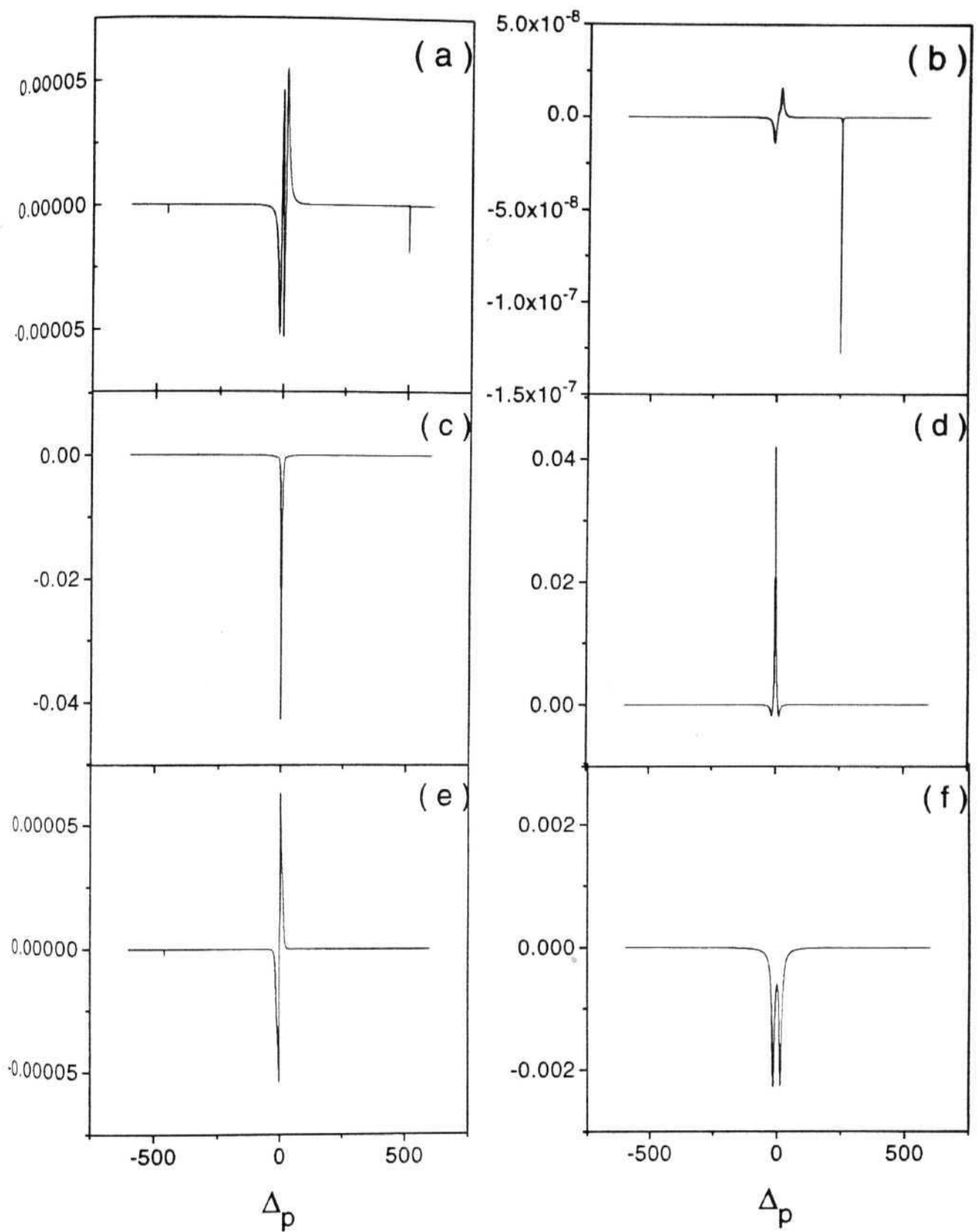


Fig. 5.6.6 Imaginary parts of ρ_{15} , ρ_{35} , $(\rho_{55} - \rho_{77})$, ρ_{95} , ρ_{72} and their sum respectively, divided by $[i \Delta_L - (\gamma_5 + \gamma_7)]$ for $\Delta_L = 500.0$

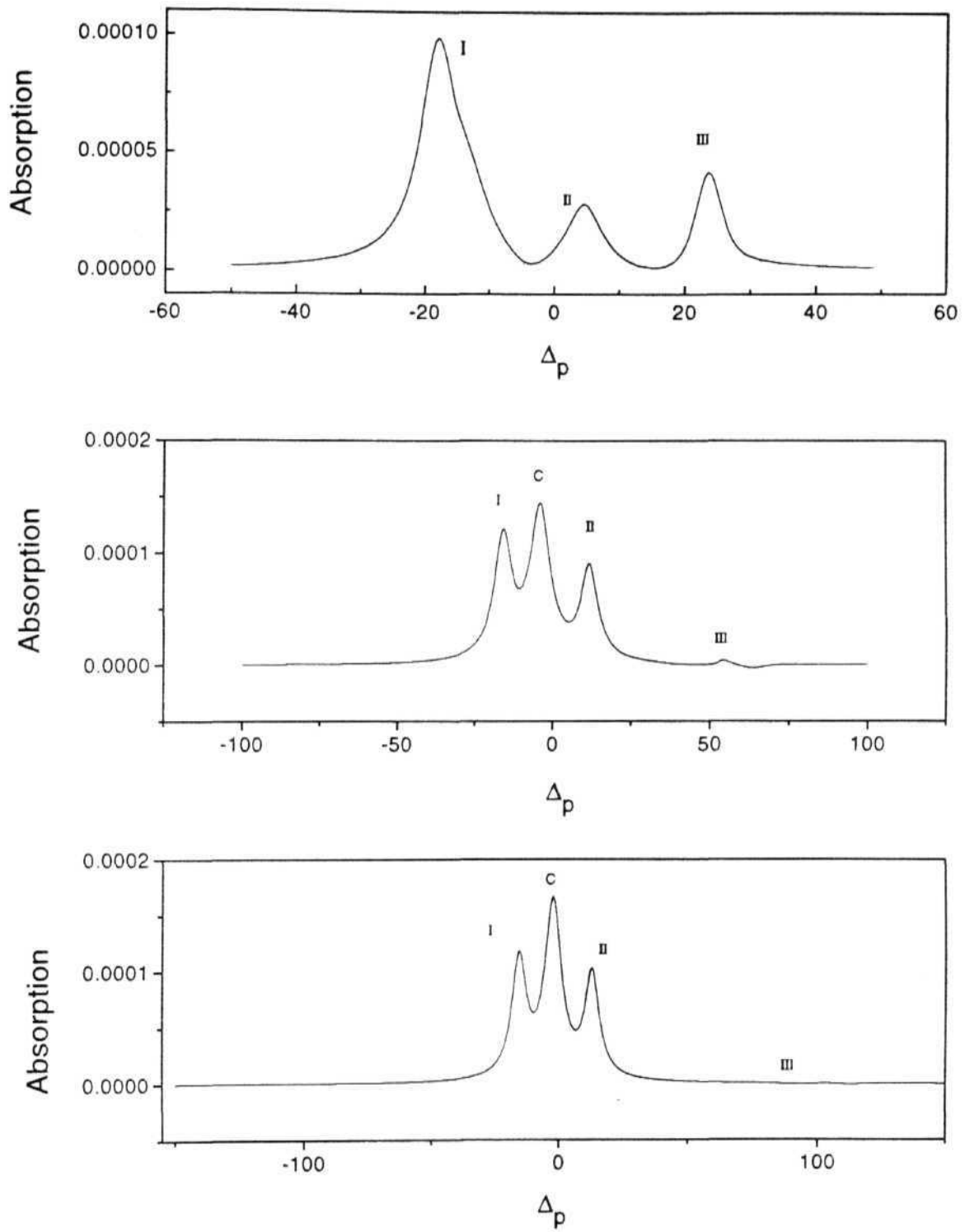


Fig. 5.7 (a): Probe absorption for $\Delta_L = 10.0, 50.0$ and 100.0 .

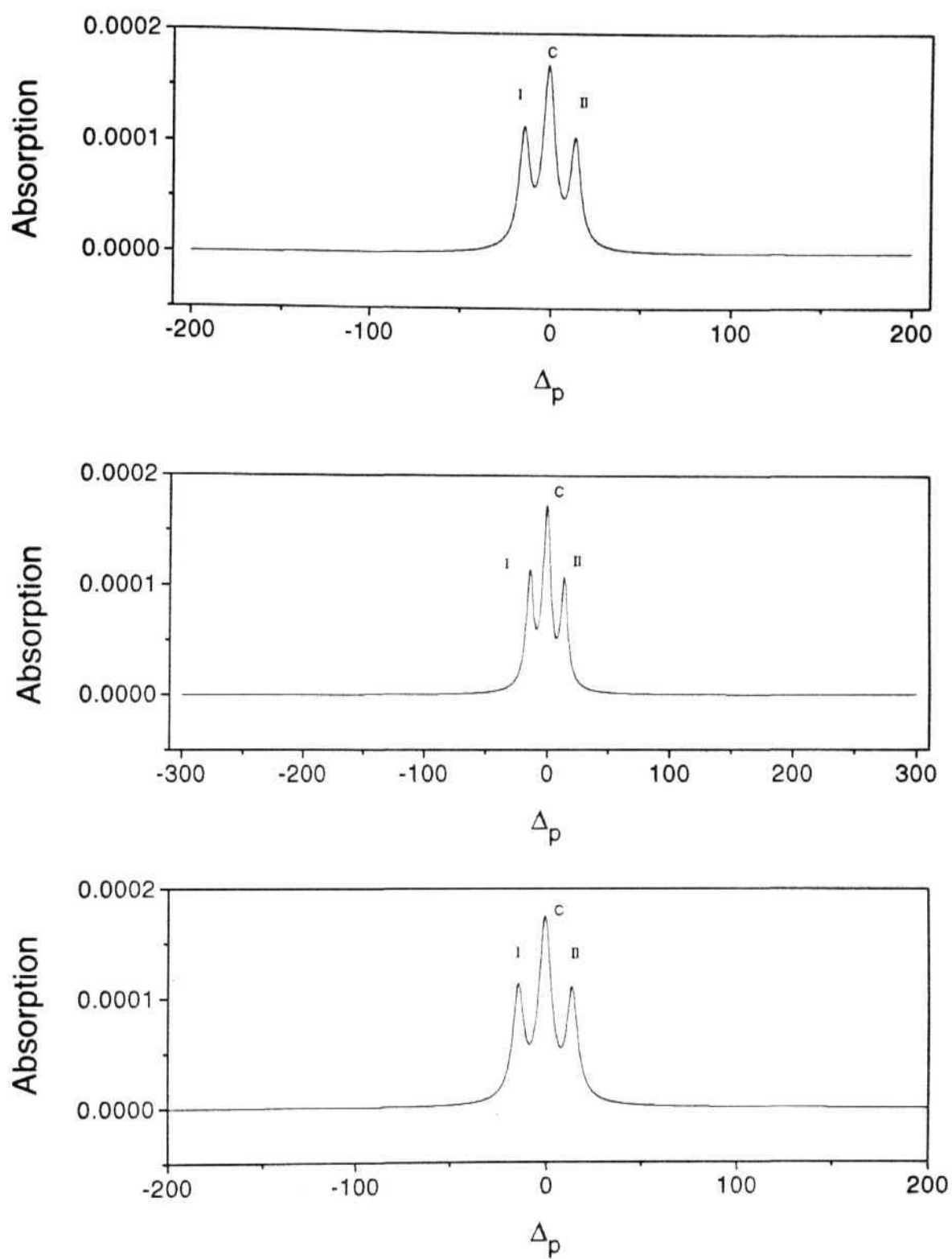


Fig. 5.7 (b): Probe absorption for $\Delta_L=150.0$, 200.0 and 500

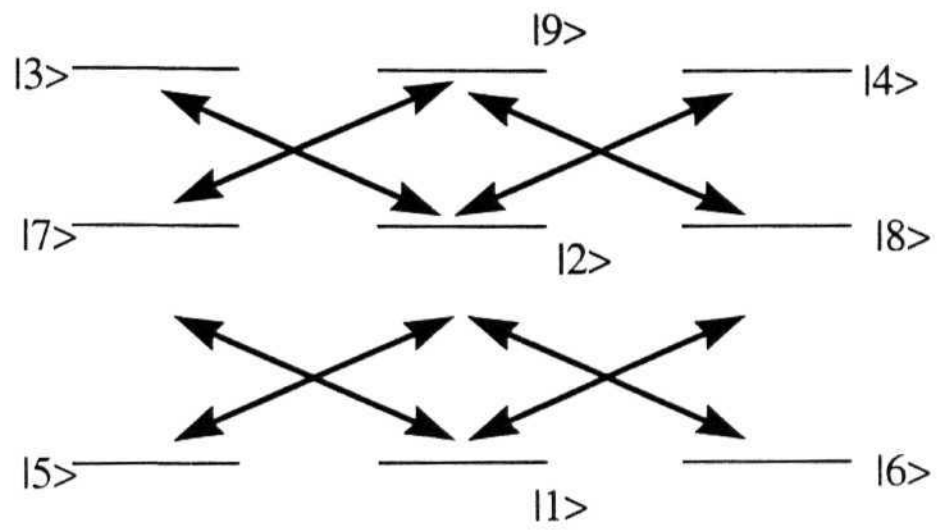


Fig. 5.8 : Only the pump beams

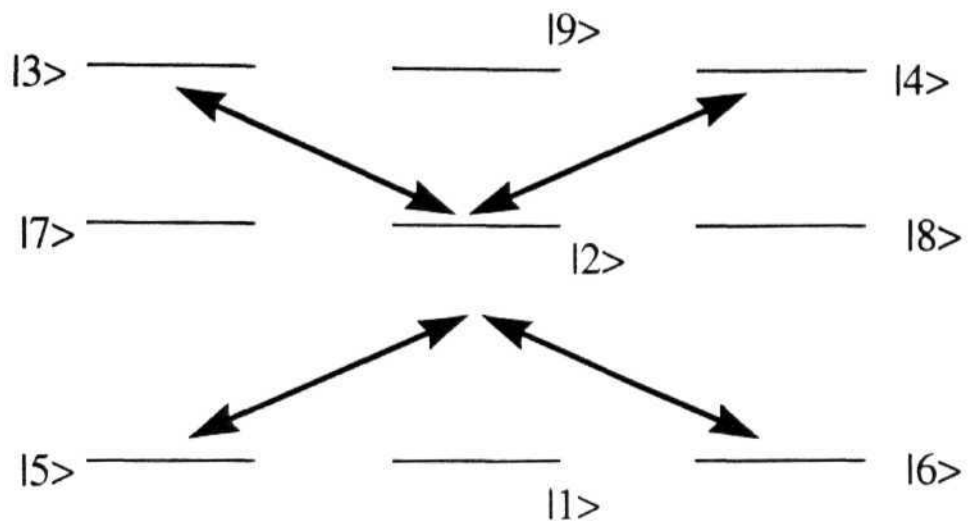


Fig. 5.9 (a): The X Configuration.

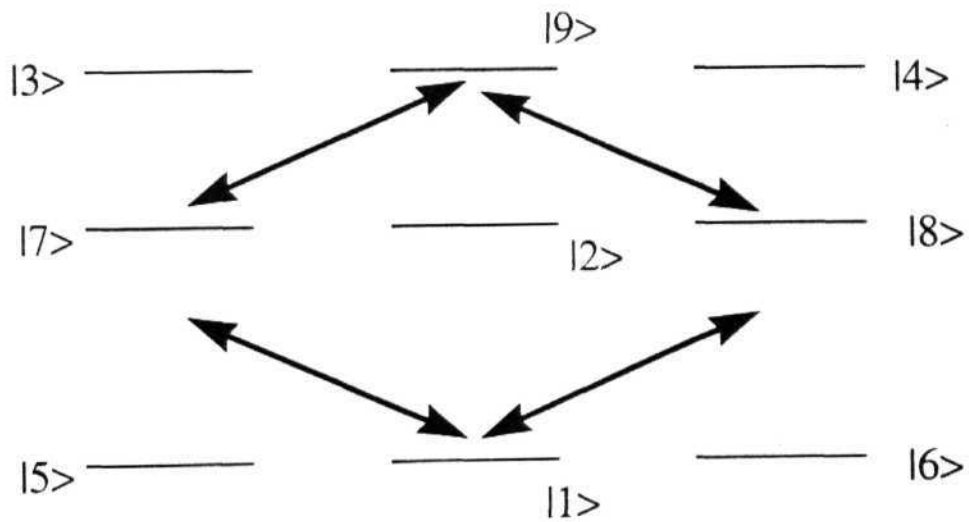


Fig. 5.9 (b): The Diamond Configuration.

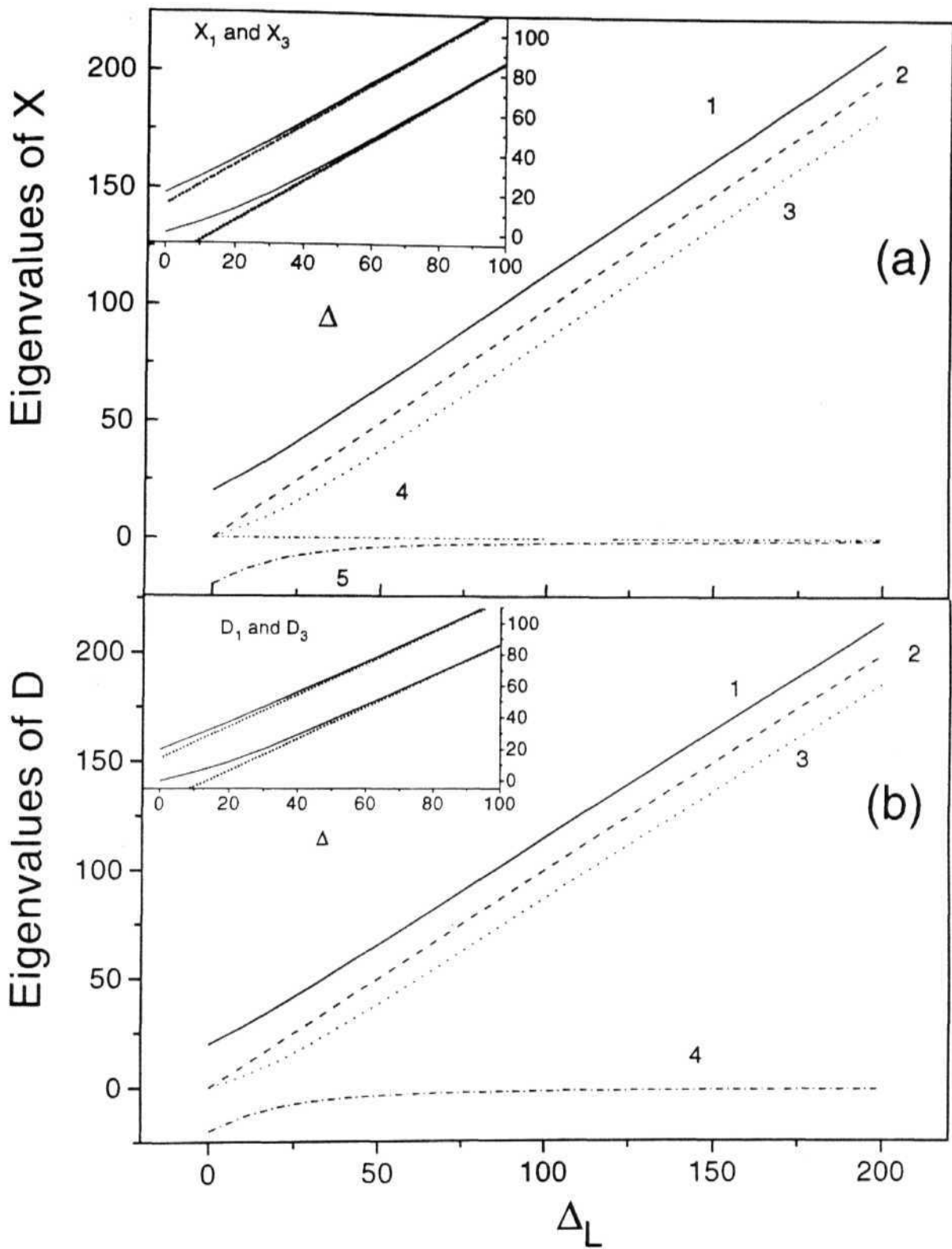


Fig. 5.10 : (a) Eigenvalues of X . Inset shows X_1 and X_3 reaching asymptotic values of $\Delta_L \pm 14.14$

(b) Eigenvalues of D . Inset shows D_1 and D_3 asymptotically reaching $\Delta_L \pm 14.14$.

References

- [1] J. Gao, C. Guo, X. Guo, G. Jin, P. Wang, J. Zho, H. Zhang, Y. Jiang, D. Waig, D. Jiang, Opt. Comm. 93, 323 (1992)
- [2] A. S. Zibrov, M. D. Lukin, D. E. Nikonov, L. Holleberg, M. O. Scully, V. L. Velichansky and H. G. Robinson, Phys. Rev. Lett. 75, 1499 (1995)
- [3] E.Fry, X.Li, D.Nikonov, G.G.Padmabandu, M.O.Scully, A.V. Smith, F.K.Tittel, C.Wong, S.R.Wilkinson and S.Y.Zhu, Phys.Rev. Lett. 70, 3235 (1993)
- [4] F. Renzoni, V. Maichen, L. Windholz and E. Arimondo, Phys. Rev. A 55, 3710 (1997)
- [5] J.Gea-Banacloche, Y. Li, S. Jin & M. Xian, Phys.Rev. A 51, 576 (1995)
- [6] Y -q Li and M. Xiao, Phys. Rev. A 51, 4959 (1995)
- [7] M. Jain, A. J. Merrin, A. Kasapi, G. V. Yin and S. E. Harris, Phys. Rev. Lett. 75, 4385 (1995)
- [8] A.Kasapi, Phys. Rev. Lett. 77, 1035 (1996)
- [9] C. Fort, F. S. Cataliotti, T. W. Hänsch, M. Inguscio, M. Prevedelii, Opt. Comm., 139 (1997)
- [10] M. O. Scully, S. -Y. Zhu and A. Gavrieldes, Phys. Rev. Lett. 62, 2813 (1989)
- [11] L. M. Narducci, H. M. Doss, P. Ru and M. O. Scully, Opt. Commun. 81, 379 (1991)
- [12] S. -Y. Zhu and M. O. Scully Phys. Rev. Lett. 76, 388 (1996)
- [13] A. Karawajczyk and J. Zakrzewski, Phys. Rev. A 51, 830 (1995)
- [14] L. Allen and J. H. Eberly, *Optical Resonance and Two-Level Atoms*, Wiley Interscience, New York 1975

- [15] S. P. Tewari **and** V. S. Ashok, submitted for publication.
- [16] E. Arimondo, *Progress in Optics*, **XXXV**, ed: E. Wolf, Elsevier 1996, pp 259;
E. Arimondo, *Fundamentals of Quantum Optics III*, Lecture Notes in Physics
420, ed: F. Ehlotzky, Springer -Verlag (1993) pp 170

Chapter VI

Gain without population inversion

*Lasing without inversion phenomenon in **Y** and **Gate** configurations is presented. In the **Y** configuration incoherent pumping of population can be used to achieve gain since it shows a complete transparency. This mechanism does not show a gain in the **Gate** system. Instead, injected atomic coherence is shown to exhibit gain in **Gate** system. A combined mechanism of injected coherence and incoherent pumping can also be used to obtain gain with the **Gate** configuration. It is shown that both of these mechanisms do not involve hidden inversion in the dressed states. Gain features of the **Gate** system in real atomic system, which was discussed in Chapter V is discussed. In this system, the additional coherences between ground states formed due to pump beam leads to a CPT state, which shows gain when an incoherent pumping of population is used.*

Population inversion which drives the conventional lasers requires (i) Suitable pumping mechanism to create inversion and (ii) states that maintain inversion till stimulated emission starts. These constraints restrict lasing action to a few frequencies and a few atomic/molecular media. Lasing without inversion schemes help overcome both of these barriers. Therefore, it has attracted considerable attention in the recent past and has been one of the extensively studied coherence induced phenomenon [1, 2, 3]

Three distinct mechanisms have been used in the past to achieve a lasing without

population inversion. 'Hidden Inversion' schemes follow a setup where a population inversion exists in the dressed state basis, though there is no inversion in the bare atomic basis [4, 5]. In another method, a CPT state is first created and then some population is pumped to excited state using an incoherent pump process. This excited population leads to a gain in the system [2, 3]. This process does not involve a 'Hidden inversion'. The third mechanism is a 'coherence induced gain' phenomenon. In a typical three level case, one of the relevant dynamic equation, recalled from equation 1.3 of Chapter I, is

$$\partial_t \rho_{eg} = [i(\omega - \omega_{eg}) - \gamma_{eg}] \rho_{eg} - i \frac{d_{eg} \cdot \mathcal{E}_1}{\hbar} (\rho_{ee} - \rho_{gg}) + i \frac{d_{em} \cdot \mathcal{E}_2}{\hbar} \rho_{mg}$$

Such system can show gain if contribution from from ρ_{mg} can exceed that from $\rho_{ee} - \rho_{gg}$ [1]. In this case, energy from the strong laser is transferred into the signal beam by the medium. This effect may manifest as either difference in emission and absorption profiles [6, 7] or as an increased susceptibility value for the signal beam [2, 8, 9].

The first two sections of this chapter present results of LWI for model cases of **Y** and **Gate** configurations. Incoherent pumping mechanism is used to obtain gain in **Y** system and Coherence Induced Gain method for the case of **Gate** system. The third section (6.3) presents a study of the real atomic system, where the pump beam acting off-resonant on the probe transition produces the necessary coherence to create CPT state. An incoherent population pumping produces gain in the system.

6.1 Y configuration: incoherent pumping

Since the Y configuration exhibits a transparency at zero detuning, the obvious method to obtain gain is to use an incoherent pumping mechanism. Rewriting the equations for only population terms in equation 2.2 of Chapter II,

$$\begin{aligned}
 \partial_t \rho_{11} &= -\Lambda_{12} \rho_{11} + 2\gamma_{12} \rho_{22} - i d_{21} \mathcal{E}_s^- \rho_{12} + i d_{21}^* \mathcal{E}_s^+ \rho_{21} \\
 \partial_t \rho_{22} &= \Lambda_{12} \rho_{11} - 2\gamma_{12} \rho_{22} + 2\gamma_{23} \rho_{33} + 2\gamma_{24} \rho_{44} + i d_{21} \mathcal{E}_s^- \rho_{12} - i d_{21}^* \mathcal{E}_s^+ \rho_{21} - i d_{32} \mathcal{E}_p^+ \rho_{23} \\
 &\quad + i d_{32}^* \mathcal{E}_p^- \rho_{32} - i d_{42} \mathcal{E}_p^- \rho_{24} + i d_{42}^* \mathcal{E}_p^+ \rho_{42} \\
 \partial_t \rho_{33} &= -2\gamma_{23} \rho_{33} + i d_{32} \mathcal{E}_p^+ \rho_{23} - i d_{32}^* \mathcal{E}_p^- \rho_{32} \\
 \partial_t \rho_{44} &= -2\gamma_{24} \rho_{44} + i d_{42} \mathcal{E}_p^- \rho_{24} - i d_{42}^* \mathcal{E}_p^+ \rho_{42}
 \end{aligned} \tag{6.1}$$

Rest of the equations for coherence terms remain unchanged, as

$$\begin{aligned}
 \partial_t \rho_{12} &= (i \Delta_s - \gamma_{12}) \rho_{12} - i d_{21}^* \mathcal{E}_s^+ (\rho_{11} - \rho_{22}) - i d_{32} \mathcal{E}_p^+ \rho_{13} - i d_{42} \mathcal{E}_p^- \rho_{14} \\
 \partial_t \rho_{13} &= [i (\Delta_s + \Delta_p) - \gamma_{23}] \rho_{13} + i d_{21}^* \mathcal{E}_s^+ \rho_{23} - i d_{32}^* \mathcal{E}_p^+ \rho_{12} \\
 \partial_t \rho_{14} &= [i (\Delta_s + \Delta_p) - \gamma_{24}] \rho_{14} + i d_{21}^* \mathcal{E}_s^+ \rho_{24} - i d_{42}^* \mathcal{E}_p^- \rho_{12} \\
 \partial_t \rho_{23} &= [i \Delta_p - (\gamma_{12} + \gamma_{23})] \rho_{23} + i d_{21} \mathcal{E}_s^- \rho_{13} - i d_{32}^* \mathcal{E}_p^+ (\rho_{22} - \rho_{33}) + i d_{42}^* \mathcal{E}_p^- \rho_{43} \\
 \partial_t \rho_{24} &= [i \Delta_p - (\gamma_{12} + \gamma_{24})] \rho_{24} + i d_{21} \mathcal{E}_s^- \rho_{14} - i d_{42}^* \mathcal{E}_p^- (\rho_{22} - \rho_{44}) + i d_{32}^* \mathcal{E}_p^+ \rho_{34} \\
 \partial_t \rho_{34} &= [i \Delta_{34} - (\gamma_{23} + \gamma_{24})] \rho_{34} + i d_{32} \mathcal{E}_p^+ \rho_{24} - i d_{42}^* \mathcal{E}_p^- \rho_{32}
 \end{aligned} \tag{6.2}$$

and their complex conjugates.

Λ_{ij} is the pumping term from level i to level j .

Equations (6.1) and (6.2) are solved for steady state as in chapter II. ρ_{11} is eliminated using the completeness condition $\rho_{11} = 1 - (\rho_{22} + \rho_{33} + \rho_{44})$ which leads to the equation

in matrix form

$$\partial_t \psi = M \cdot \psi + \phi$$

Steady state solutions of the above are obtained by setting $\partial_t \psi = 0$, and using the relation

$$\psi(\infty) = -M^{-1} \phi,$$

where M^{-1} denotes inverse of matrix M .

Figure 6.1 (a) shows imaginary part of ρ_{21} for an incoherent pumping parameter $\Lambda_{12} = 1.9$. Negative value of p_2 indicates gain. Figure 6.1 (b) shows corresponding population for levels $|2\rangle$ (dashed line) and $|1\rangle$ (solid line). It is seen that the population of level $|2\rangle$ is less than that of level $|1\rangle$.

To analyse the results, the dressed states of the system formed are looked into. From equation 3.13 of Chapter III, the dressed states are given by

$$\begin{pmatrix} \Psi_1 \\ \Psi_2 \\ \Psi_3 \end{pmatrix} = \frac{1}{\alpha\sqrt{2}} \begin{pmatrix} \alpha & g_{32} & g_{42} \\ 0 & -g_{42} & g_{32} \\ -\alpha & g_{32} & g_{42} \end{pmatrix} \begin{pmatrix} |2\rangle \\ |3\rangle \\ |4\rangle \end{pmatrix} \quad (6.3)$$

It can be seen that the level $|2\rangle$ forms a part of only Ψ_1 and Ψ_3 . Therefore the position of gain seen in figure 6.1 (a) can immediately be attributed to the transition from the dressed states Ψ_1 and Ψ_2 to level $|1\rangle$.

Further, equation 6.3 can be written in as

$$|\bar{\Psi}\rangle = S^\dagger |\Psi\rangle$$

and its conjugate as

$$\langle \bar{\Psi} | = \langle \Psi | S$$

where $|\bar{\Psi}\rangle = (|\Psi_1\rangle \quad |\Psi_2\rangle \quad |\Psi_3\rangle)$, $|\Psi\rangle = (|2\rangle \quad |3\rangle \quad |4\rangle)$ and the diagonalizing matrix is

$$S^\dagger = \frac{1}{\alpha\sqrt{2}} \begin{pmatrix} \alpha & g_{32} & g_{42} \\ 0 & -g_{42} & g_{32} \\ -\alpha & g_{32} & g_{42} \end{pmatrix}.$$

S is the hermitian conjugate of S^\dagger .

This equation leads to

$$|\bar{\Psi}\rangle\langle\bar{\Psi}| = S^\dagger |\Psi\rangle\langle\Psi| S$$

$$\bar{\rho} = S^\dagger \rho S$$

where the diagonal elements of the density matrix of the dressed atom $\bar{\rho}$ denote the population of the dressed states. These populations are plotted in Figure 6.1 (c). Population of Ψ_2 is zero. Populations of both Ψ_1 and Ψ_3 are less than population of level $|1\rangle$, showing that there is no inversion in the dressed state basis either.

Figure 6.2 (a) shows the gain profile for $\Lambda_{12} = 2.0$. Figure 6.2 (b) shows the corresponding populations in levels $|2\rangle$ and $|1\rangle$. Though the populations cross over at certain points, inversion does not exist for those detunings at which lasing can take place. Population of Ψ_1 and Ψ_3 for this case are shown in figure 6.2 (c). Population of Ψ_2 is zero for this case as well.

6.2 Gate configuration: injected atomic coherence

Coherence driven lasing without inversion schemes where the required coherence has been externally achieved has been studied earlier [11]. A similar scheme can be used to achieve gain in the **Gate** system, by controlling the coherence between levels |5) and |6). Since the **Gate** configuration shows a finite absorption at zero detuning, incoherent pumping mechanism will not show gain.

Probe absorption for the **Gate** system is given by equation 4.23 from Chapter IV as,

$$\begin{aligned}\rho_{75} &= \frac{d_{75}\mathcal{E}_s^-\rho_{55}^{(0)}}{F_{75}} + \frac{d_{97}^*\mathcal{E}_p^+d_{98}\mathcal{E}_p^-d_{86}\mathcal{E}_s^-\rho_{65}^{(0)}}{F_{75}F_{95}F_{85}} \\ \text{where} \\ F_{75} &= \Delta_{75} - i\gamma_{57} - \frac{|d_{97}\mathcal{E}_p^+|^2}{F_{95}} \\ F_{95} &= \Delta_{95} - i\gamma_{9} - \frac{|d_{98}\mathcal{E}_p^-|^2}{F_{85}} \\ F_{85} &= \Delta_{85} - i\gamma_{68}\end{aligned}\tag{6.4}$$

and

$$\begin{aligned}\rho_{86} &= \frac{d_{86}\mathcal{E}_s^-\rho_{66}^{(0)}}{F_{86}} + \frac{d_{98}^*\mathcal{E}_p^+d_{97}\mathcal{E}_p^-d_{86}\mathcal{E}_s^-\rho_{56}^{(0)}}{F_{86}F_{96}F_{76}} \\ \text{where} \\ F_{86} &= \Delta_{86} - i\gamma_{68} - \frac{|d_{98}\mathcal{E}_p^-|^2}{F_{96}} \\ F_{96} &= \Delta_{96} - i\gamma_{9} - \frac{|d_{97}\mathcal{E}_p^+|^2}{F_{76}}\end{aligned}$$

$$F_{76} = \Delta_{76} - i\gamma_{57} \quad (6.5)$$

Effect of $\rho_{56} = \pm 0.5$ was shown in Chapter IV where $\rho_{56} = 0.5$ resulted in a complete transparency and $\rho_{56} = -0.5$ resulted in a complete absorption. Since ρ_{56} is a complex quantity, its phase and amplitude can be varied independently. Figures 6.3 (a) and 6.3 (b) show effect of a complex ρ_{56} . Figure 6.3 (a) shows imaginary ρ_{75} for $\rho_{56} = 0.3 + i 0.3$ as a function of probe detuning. Figure 6.3 (b) shows imaginary ρ_{86} for the same. Figure 6.3 (c) shows total absorption which is the sum Imaginary $(\rho_{75} + \rho_{86})$. It is seen that, since the two absorption profiles are symmetric about zero, gain in one of the arm is cancelled by absorption in the other, and there is no net gain.

6.3 Bichromatic approach

It was shown in Chapter V that the pump beam acting off-resonant on the probe transition creates additional coherences which cancels the central absorption peak of the Gate configuration and lead to a complete transparency. This was shown to be due to the population being trapped in the superposition state $X_4 = 0.707(|5\rangle - |7\rangle)$. An incoherent pumping process can then be adopted to achieve gain in the system. Such a pumping can be achieved by either a π polarized light, which pumps population from $|5\rangle$ and $|6\rangle$ to $|7\rangle$ and $|8\rangle$, or by σ_{\pm} light which pumps population from $|1\rangle$ to $|7\rangle$ and $|8\rangle$, as well as from $|5\rangle$ and $|6\rangle$ to $|2\rangle$. Since two trapping states, $|5-6\rangle$ and $|1\rangle$, exist in the system, both pumping schemes have to be simultaneously used to prevent accumulation of population in either one of them. These pumping terms are included

in the density matrix equations and the equations are solved in the non-perturbative limit using Bichromatic solution technique which was discussed in Chapter V. The parameters used are same as in Chapter V with all the parameters being scaled to the coherence decay γ_{57} . The pump Rabi frequency of 10 and the probe Rabi frequency of 0.2 are used. The detuning between pump beam and $F=1 \leftrightarrow F'$ is chosen to be $\Delta_L = 100$. The incoherent pumping parameter $A = A_{57} = \Lambda_{68} = \Lambda_{12}$ is scanned from 0 to 2.0. The probe absorption obtained for these values are plotted in figures 6.5 (a) and (b).

Figure 6.4 shows the absorption profile as the pump parameter A increases from 0 to 1.5. $\Delta_L = 500.0$ is used for this calculation. Figure 6.5 shows an expanded part of this graph, showing the gain feature. It is clearly seen that a small absorption peak at $\Delta_p = -0.45$ develops into a gain peak as A increases. Comparing with the absorption spectrum obtained in Chapter V in absence of incoherent pumping, the position of the gain peak is seen to be corresponding to the peak labeled C in figure 5.7. This peak was identified to correspond to a $D_2 \leftrightarrow X_5$ transition, which is seen in figure 6.5 (b) as developing into a gain profile. It can be inferred from this that the incoherent pumping process transfers population predominantly into $D_2 = 0.707(|7\rangle - |8\rangle)$. This decays to the state X_5 showing up as gain in the probe beam.

Figure 6.6 shows the bare state populations for a particular value of pump parameter $A = 0.5$, for which the gain exists. Figure 6.6 (a) shows populations of ground levels $|5\rangle$, $|6\rangle$ and $|1\rangle$ and figure 6.6 (b) shows those of the excited state $|7\rangle$, $|8\rangle$ and $|9\rangle$. It is seen that population of ground states are more than those of excited states, showing that there is no population inversion. Figure 6.6 (c) shows populations of the two dressed states which are involved in the transition. Population of X_5 is plotted

with respect to left y-axis shown as a solid line and the population of D_2 is plotted with respect to the right y-axis by the dashed line. Population of D_2 is seen to be lesser than that of X_5 , showing that there is no inversion of population even in the dressed state.

Figures 6.7 show the behaviour of this gain with respect to the pump parameter A , at $\Delta_p = -0.45$, which is the point within the gain profile. Figure 6.7 (a) shows the probe absorption as a function of A . The absorption becomes negative valued, which is an indication of gain at $A = 0.4$, and stays negative as A is increased. But as Figure 6.7 (b) shows that the population of D_2 (dashed line) exceeds that of X_5 (solid line) at $A = 1.5$. However, the gain is achieved much before this value of A indicating absence of 'hidden inversion' between the two dressed states involved.

Figure 6.7 (c) shows the population of bare states $|5\rangle$, $|6\rangle$ and $|1\rangle$ while figure 6.7 (d) shows the population of excited states $|7\rangle$, $|8\rangle$ and $|2\rangle$, showing the absence of inversion among the bare states. In conclusion, a gain without population inversion can be achieved in the real atomic system of $F=1 \leftrightarrow F' \leftrightarrow F''$ by use of an incoherent population pumping method. The strong pump beam which acts off-resonant on the probe transition creates coherences which will trap the population in a Coherent Population Trapped state. Since the absorption profile at the line center is cancelled due to quantum interference, the transition of population from D_2 to X_5 results in gain in the probe beam.

Conclusion

Methods of achieving gain in model configurations of **Y** and **Gate** have been shown. Since **Y** configuration shows a complete transparency at zero detuning, method of incoherent population pumping. **Gate** system shows gain in individual arms if a coherence is externally imposed on ρ_{56} . But the total gain when absorption from both arms are added, cancel each other to give a zero absorption. In the real atomic system, the pump beam can act nonresonantly on the probe transition as well. This creates an additional coherence which cancels the central absorption peak of the **Gate** system. An incoherent pumping process can then be used to obtain gain in the system. This configuration shows gain without a population inversion either in the bare state basis or in the dressed state basis.

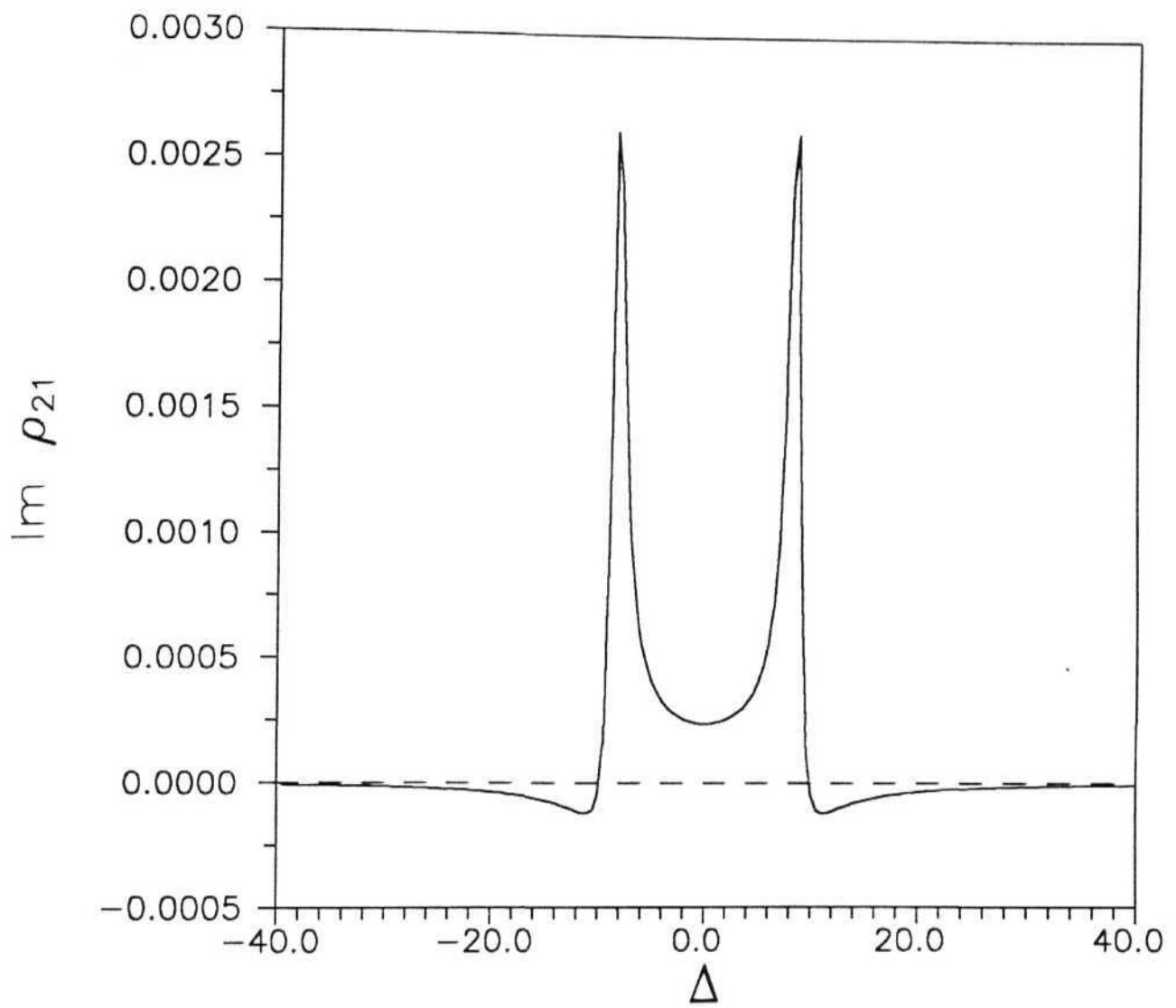


Fig. 6.1 (a): Probe absorption for $\Lambda_{12}=1.9$.

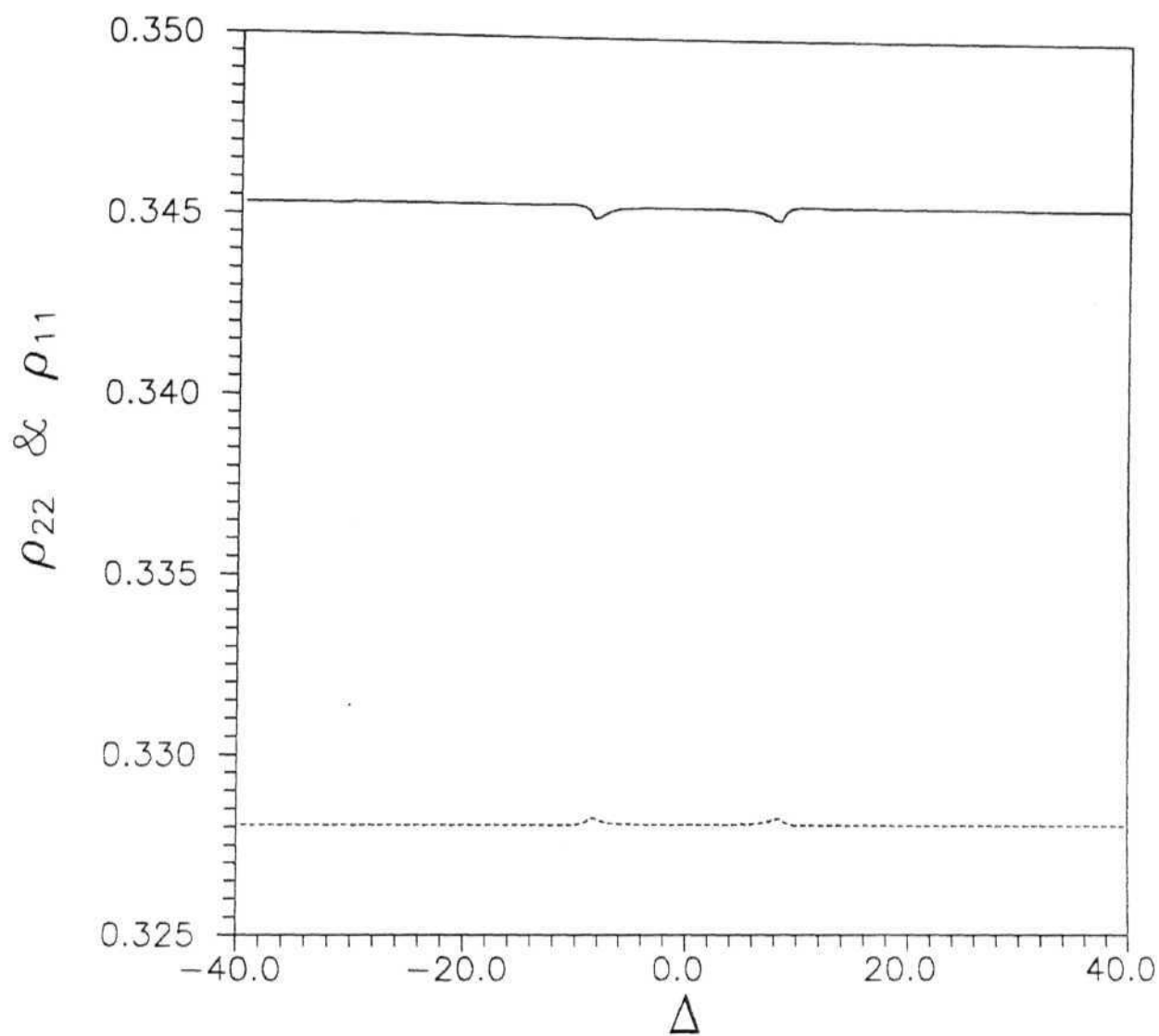


Fig. 6.1(b): Population of level 1 (solid line) and 2 (dashed line) for $\Delta_{12}=1.9$. Population of level 1 is more than that of level 2.

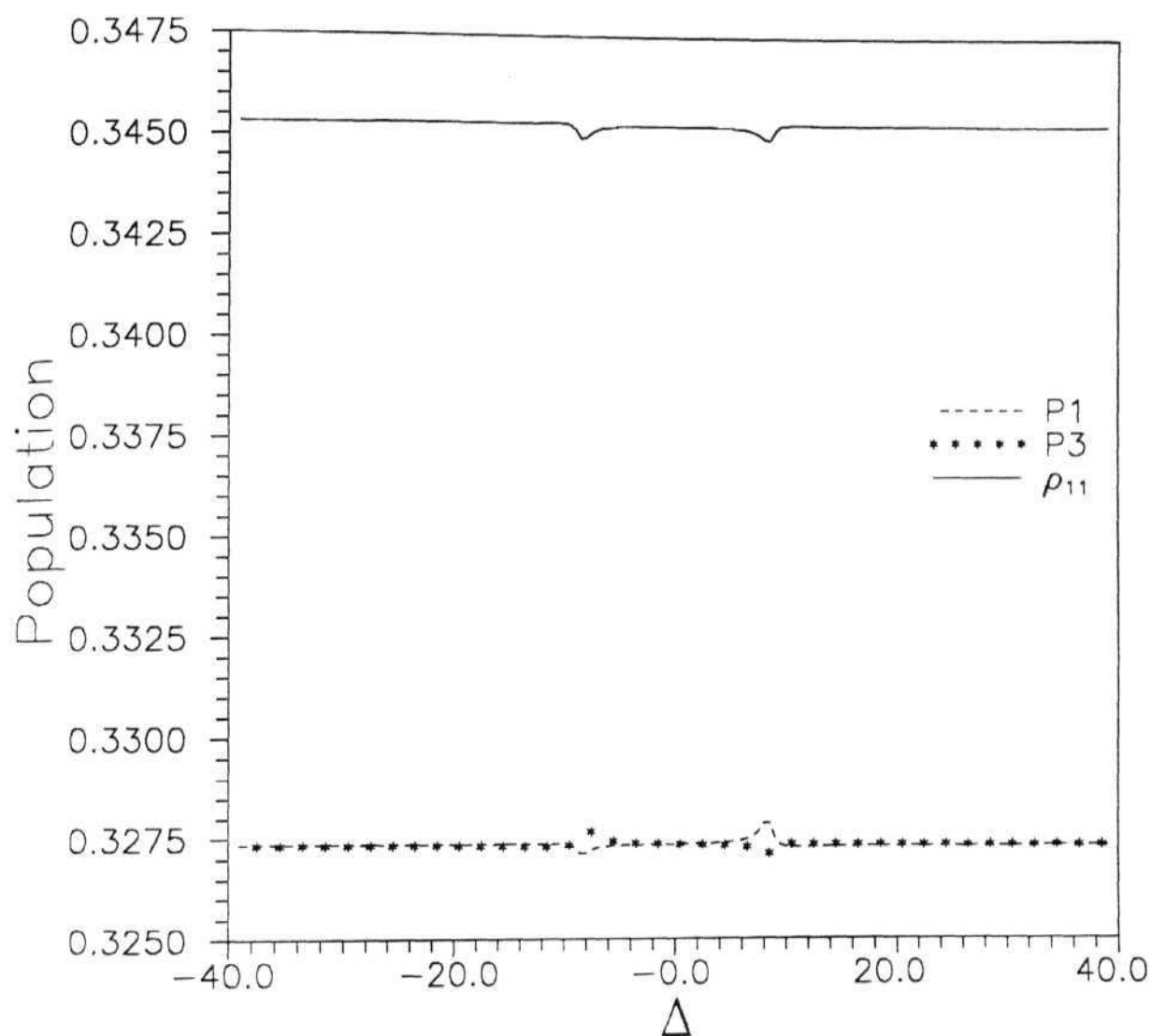


Fig.6.1(c): Population of dressed states Ψ_1 and Ψ_3 which are lower than that of level 1. (ρ_{11}). Population of Ψ_2 is zero.

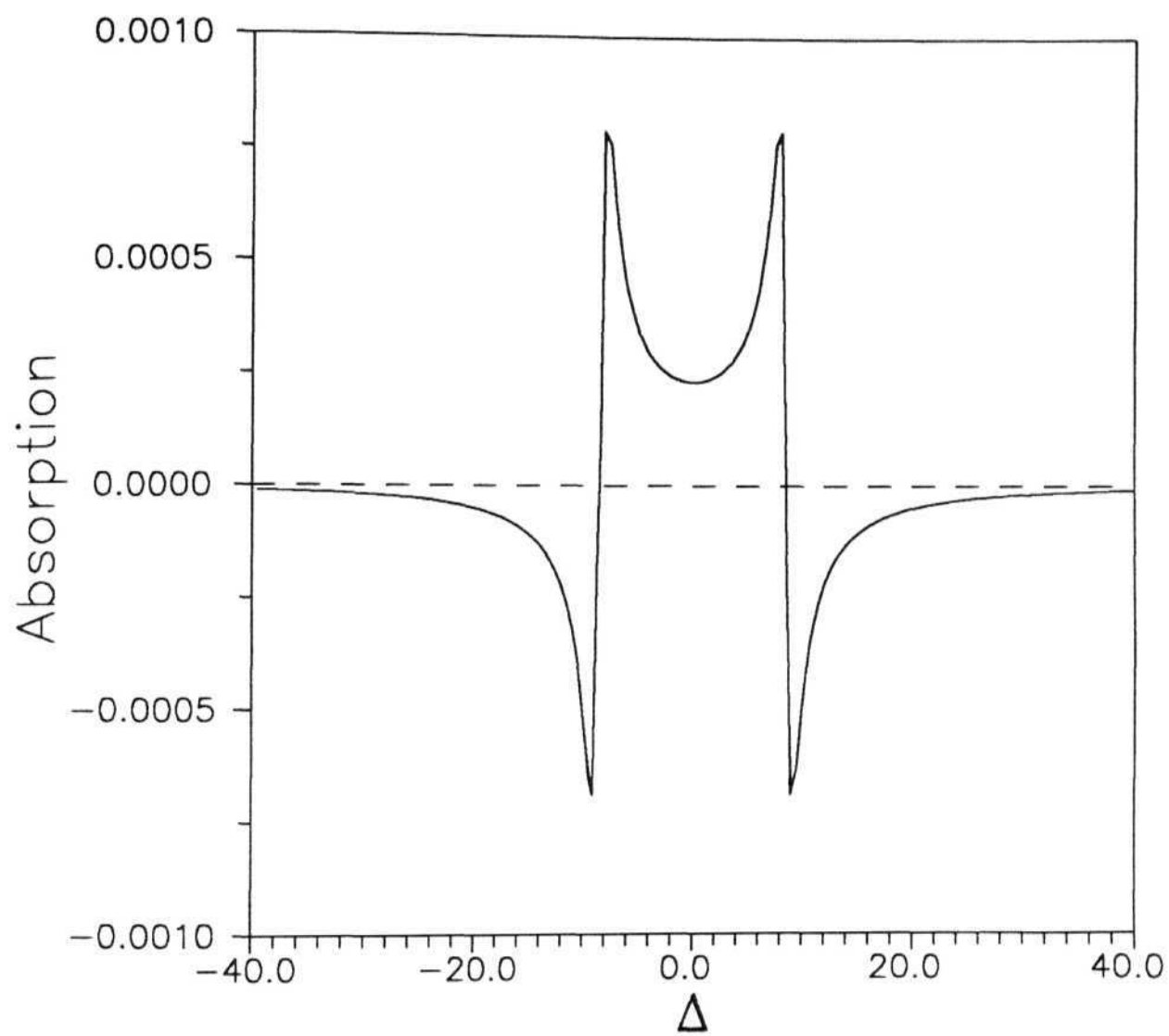


Fig. 6.2 (a): Probe absorption for $\Lambda_{12}=2.0$

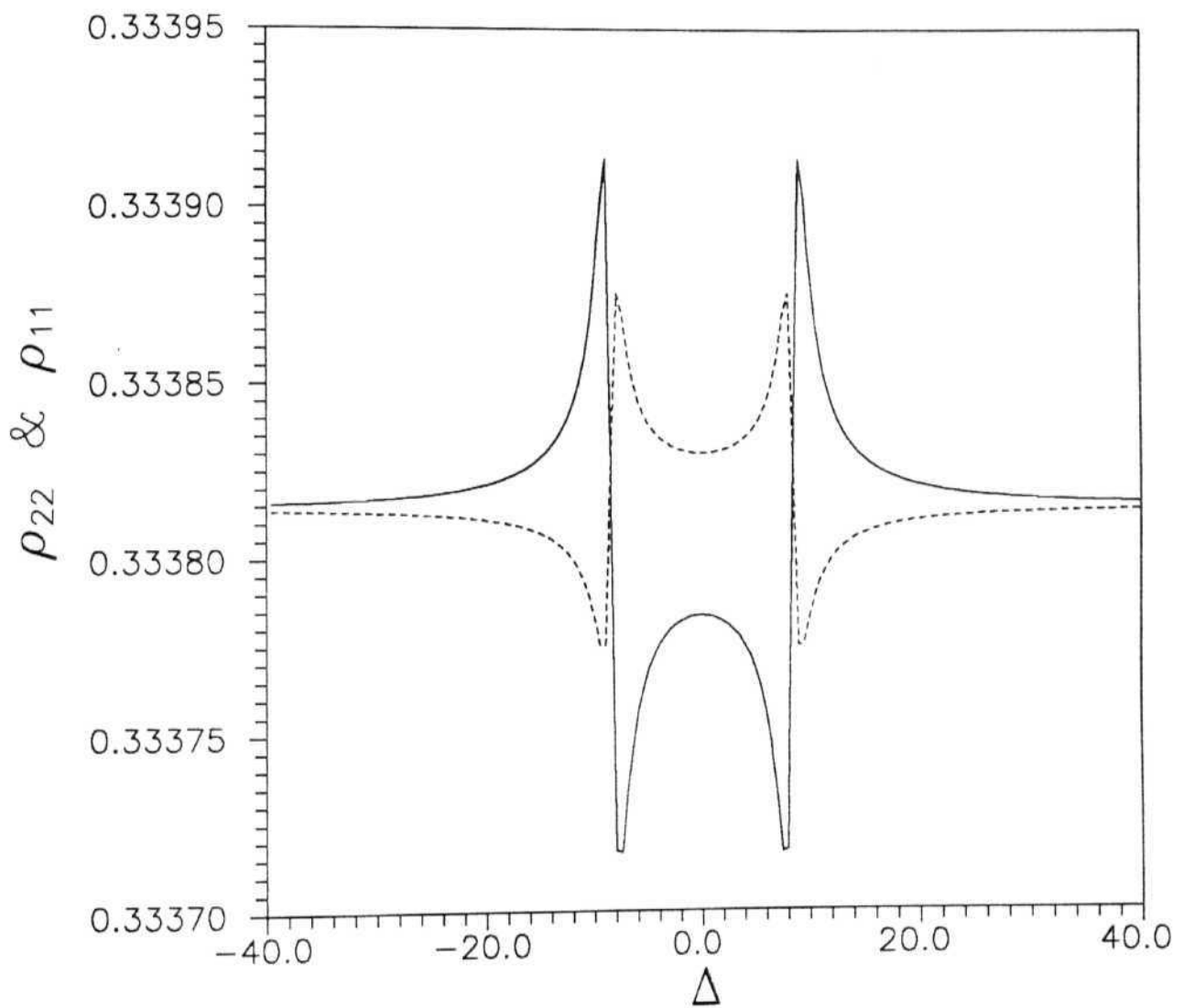


Fig. 6.2 (b): Population for level 1 and level 2 for $\Lambda_{12}=2.0$. Though these two populations cross each other, population of level 1 is more at the point of gain.

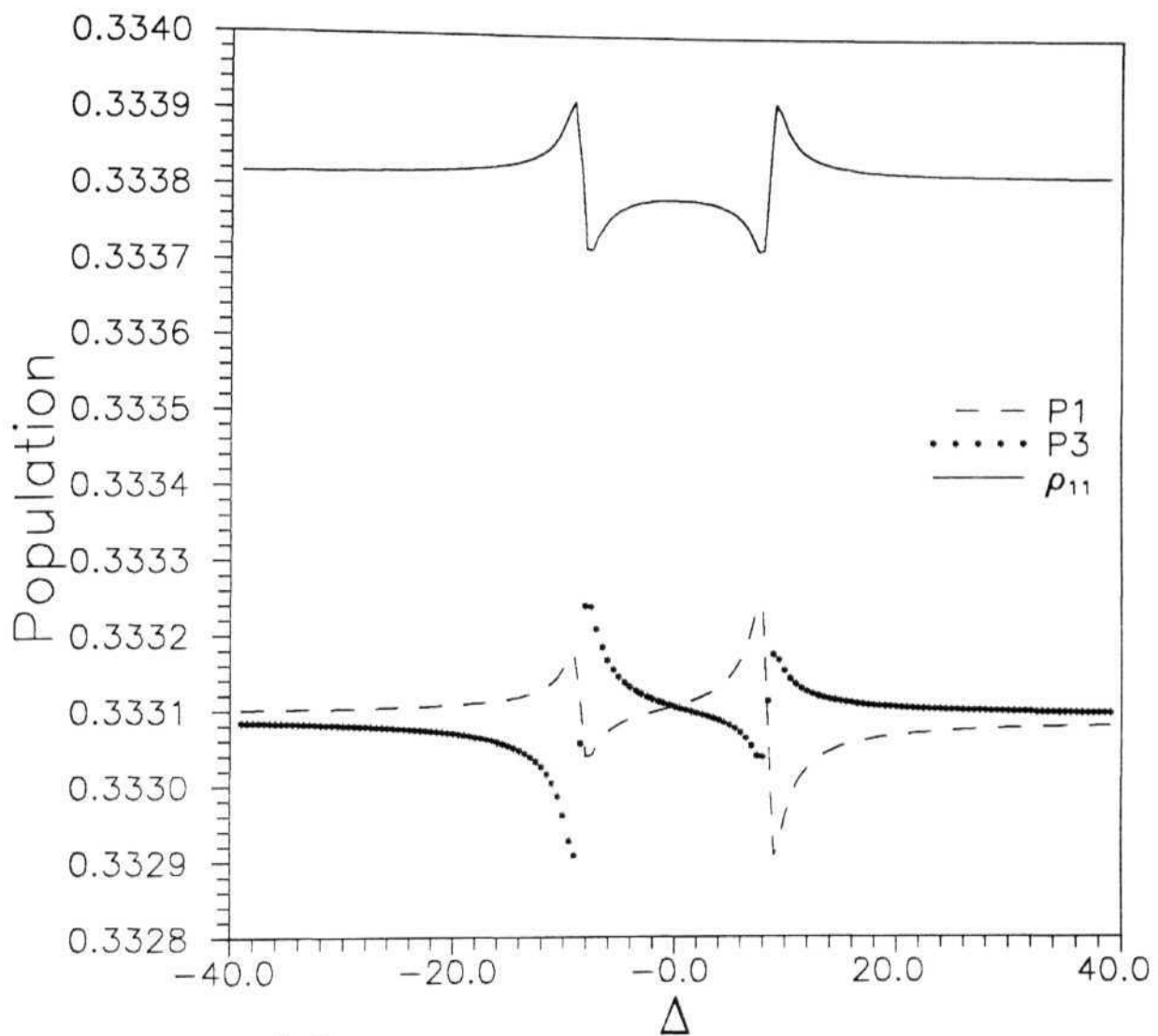


Fig.6.2(c): Population of dressed states Ψ_1 and Ψ_3 which are lower than that of level 1. (ρ_{11}). Population of Ψ_2 is zero.

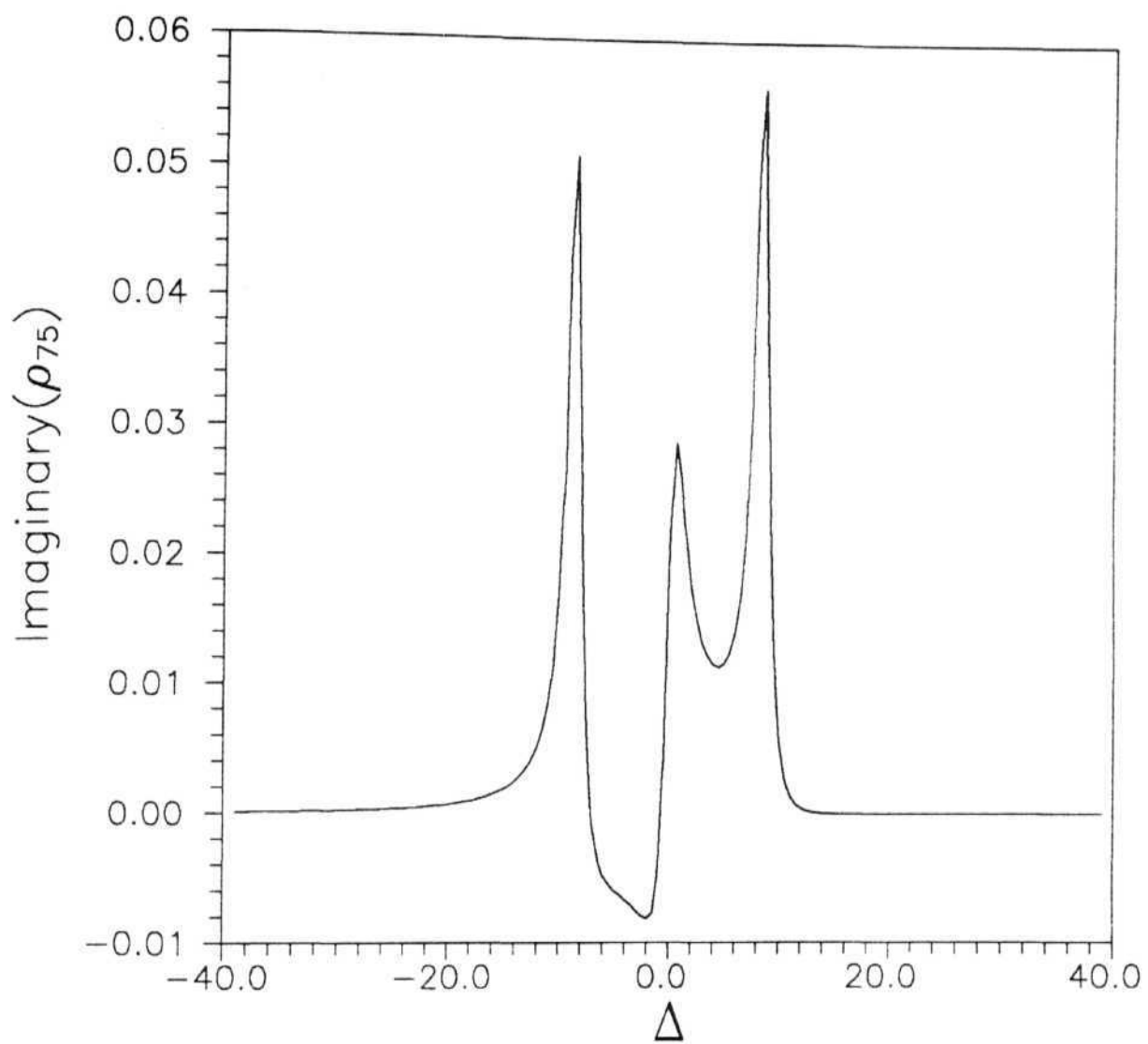


Fig. 6.3 (a): Absorption of probe (ρ_{75}) for $\rho_{65}=0.3+i0.3$.

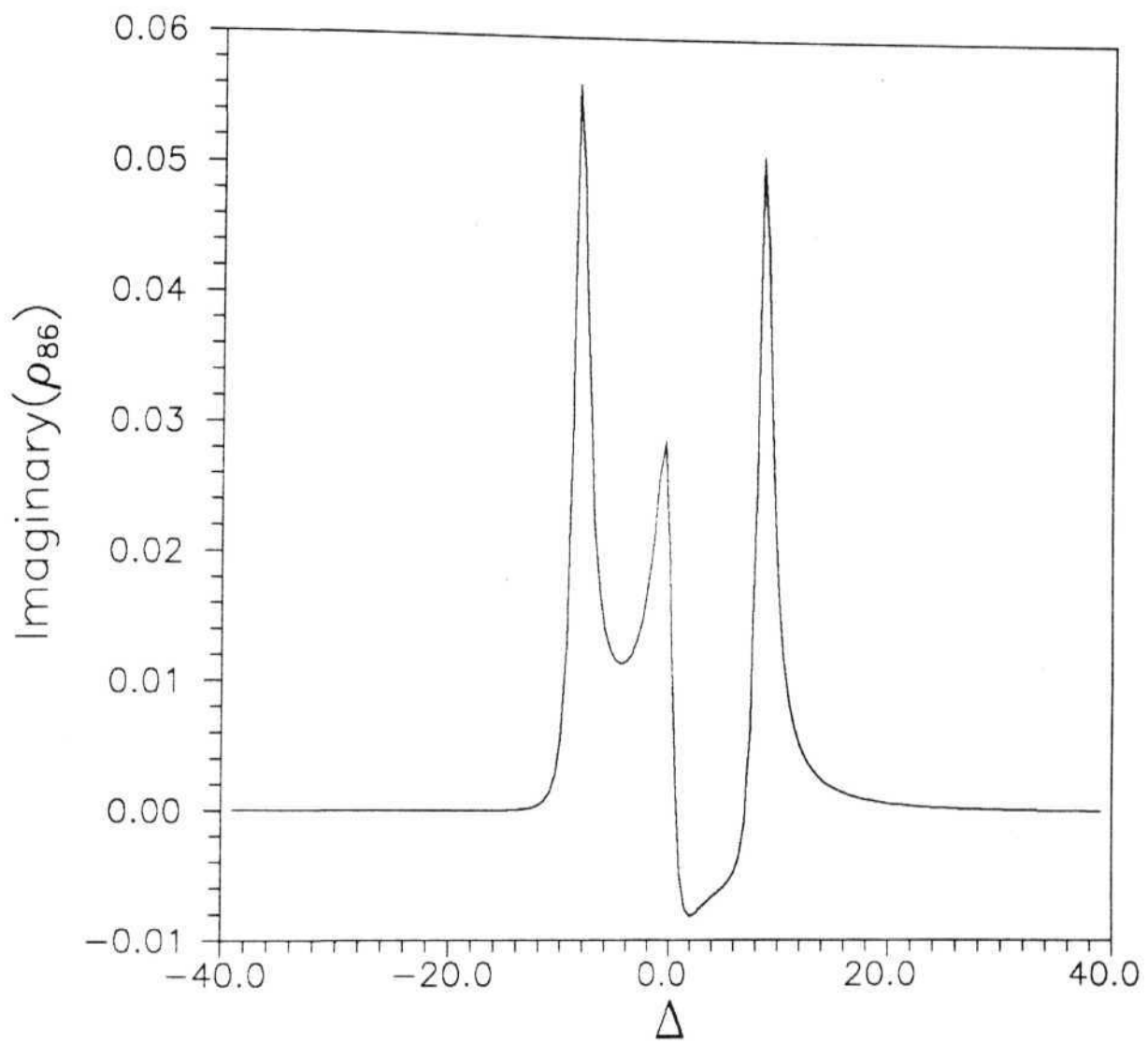


Fig. 6.3 (b): Absorption of probe (ρ_{86}) for $\rho_{65}=0.3+i0.3$.

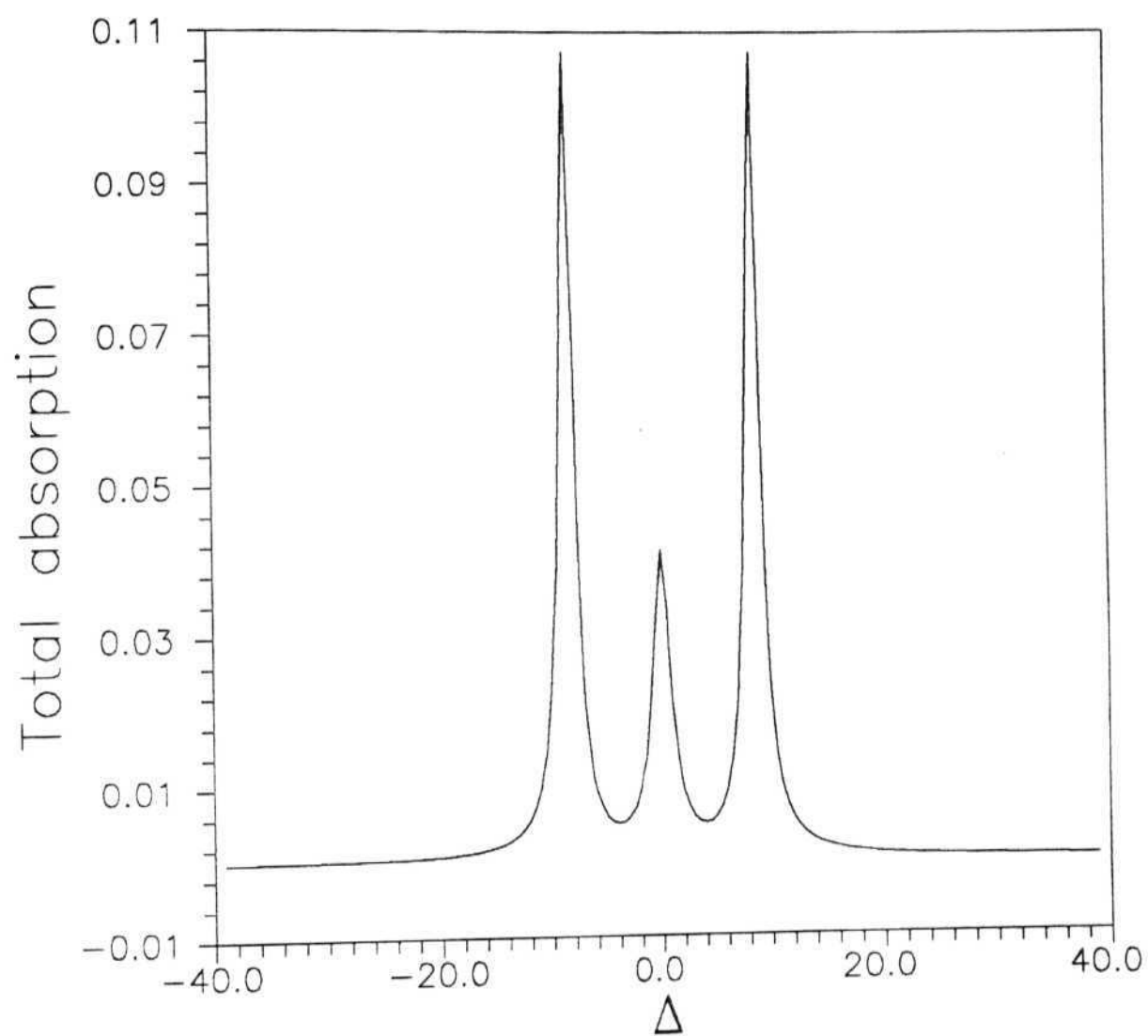


Fig. 6.3 (c): Total absorption of probe ($\rho_{86} + \rho_{75}$).

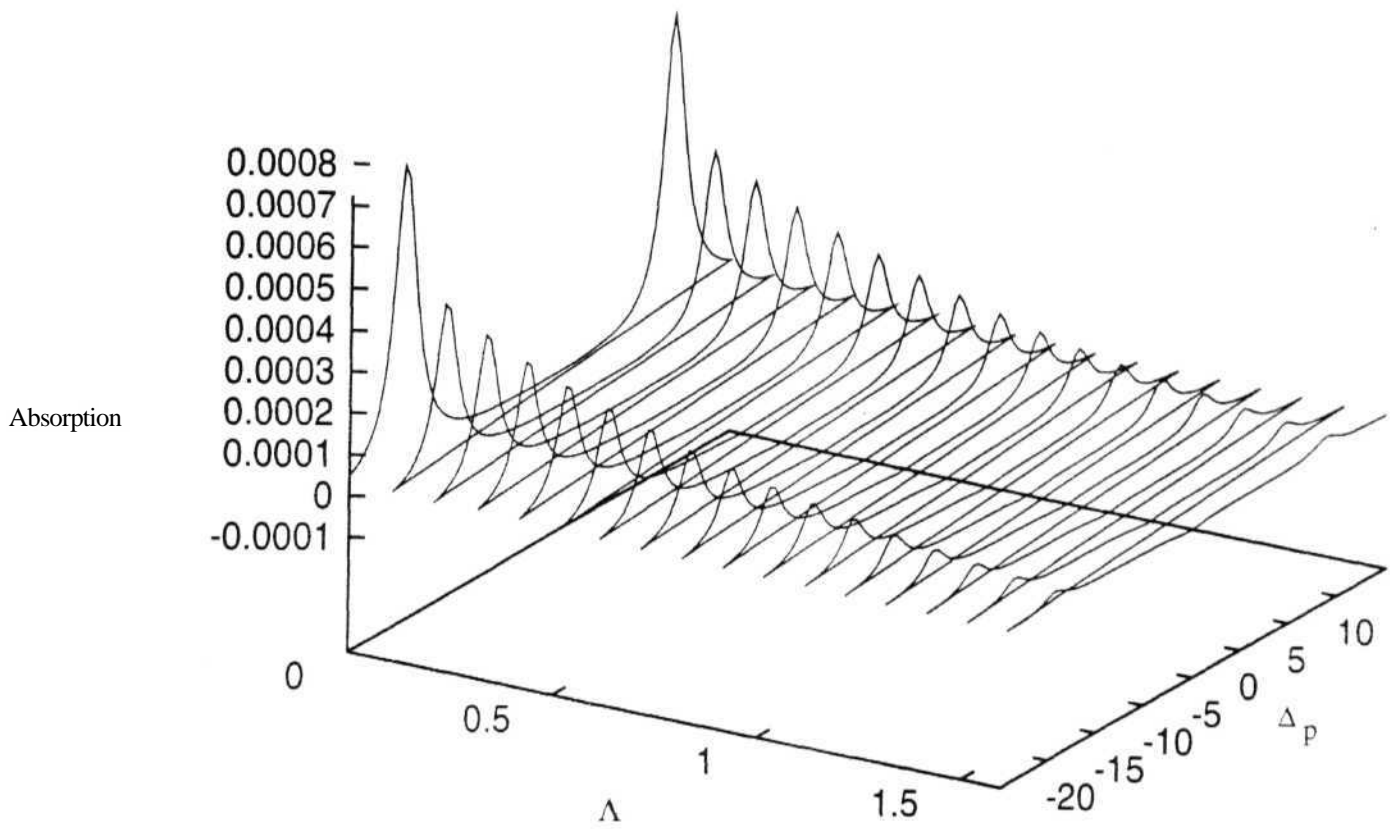


Fig. 6.4: Absorption as a function of probe detuning for various values of pump parameter

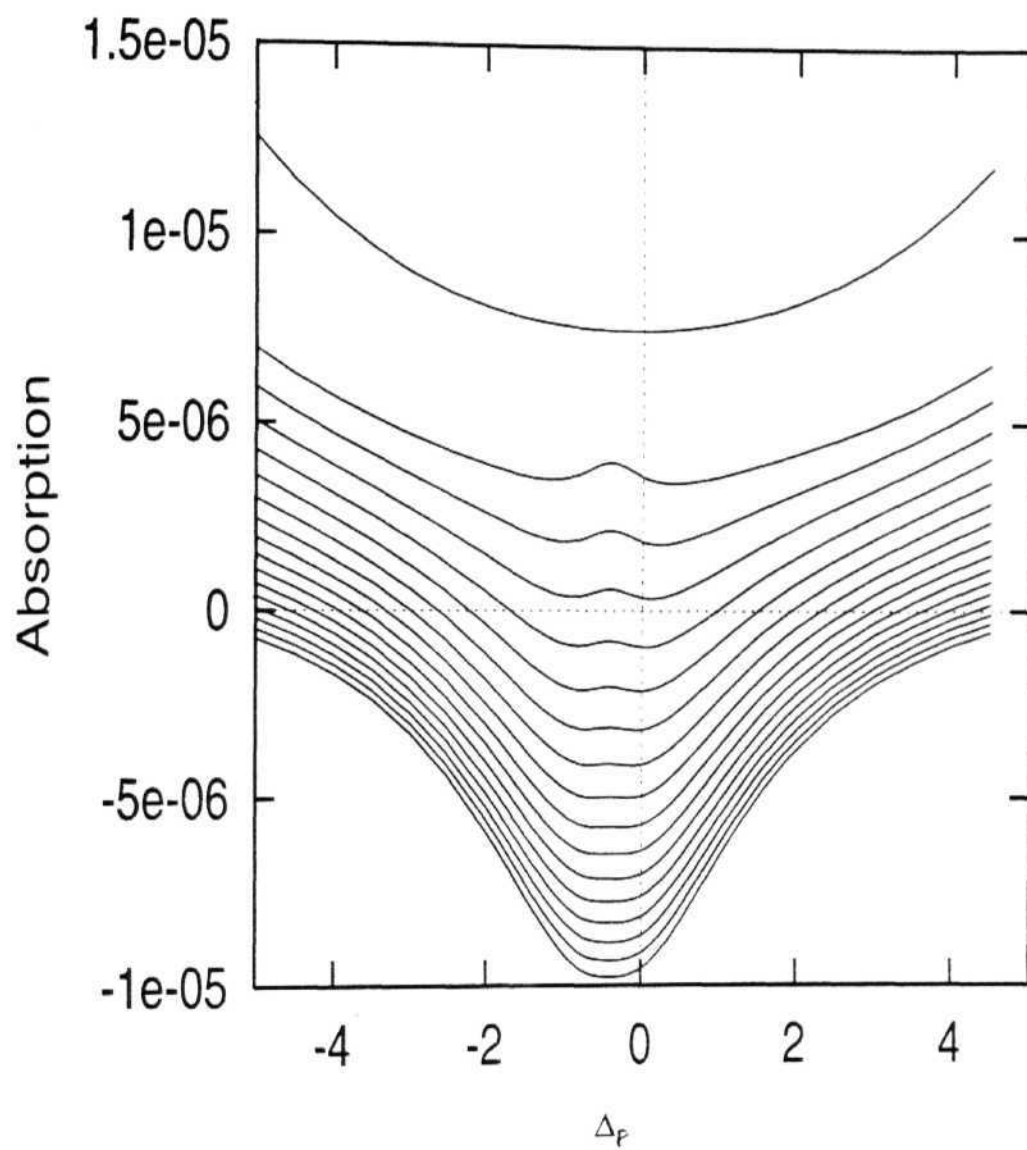


Fig. 6.5: Absorption as a function of probe detuning for various values of pump parameter

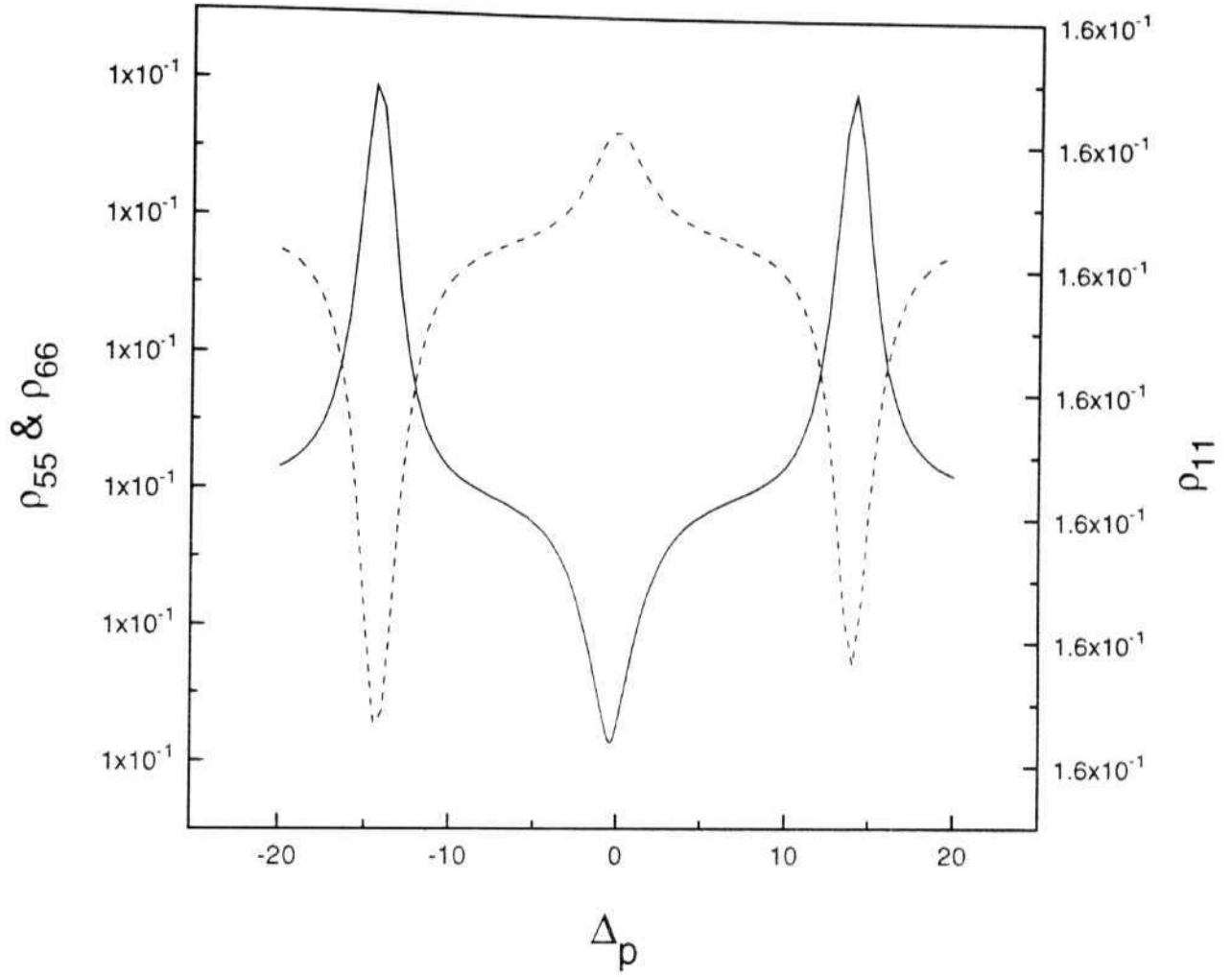


Fig. 6. 6 (a): Populations of levels 5 and 6 (Solid line, left axis), and of level 1(dashed line, right axis), for a pump parameter $A=0.5$.

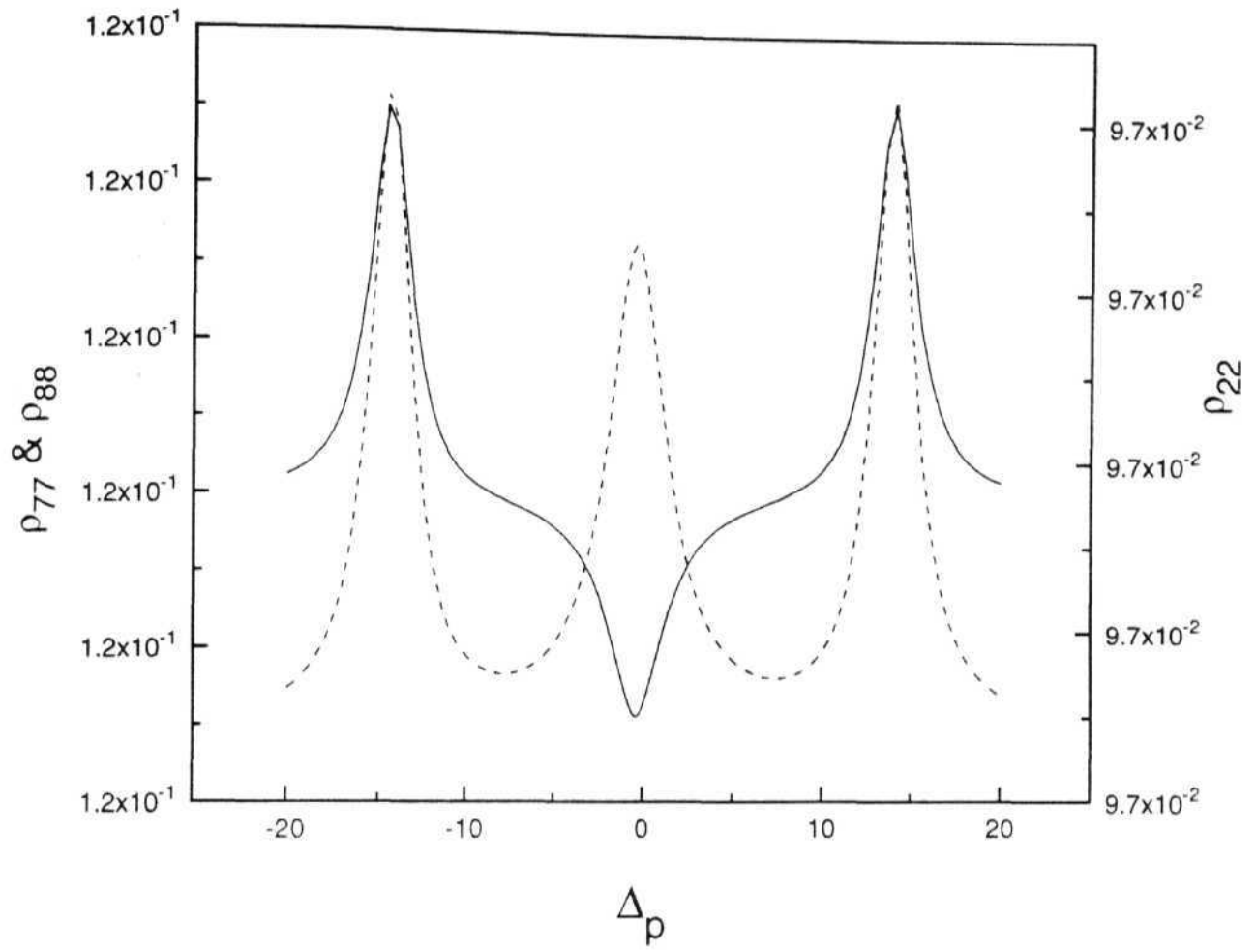


Fig. 6. 6 (b) Populations of levels 7 and 8 (Solid line, left axis), and of level 2 (dashed line, right axis), for a pump parameter $A=0.5$

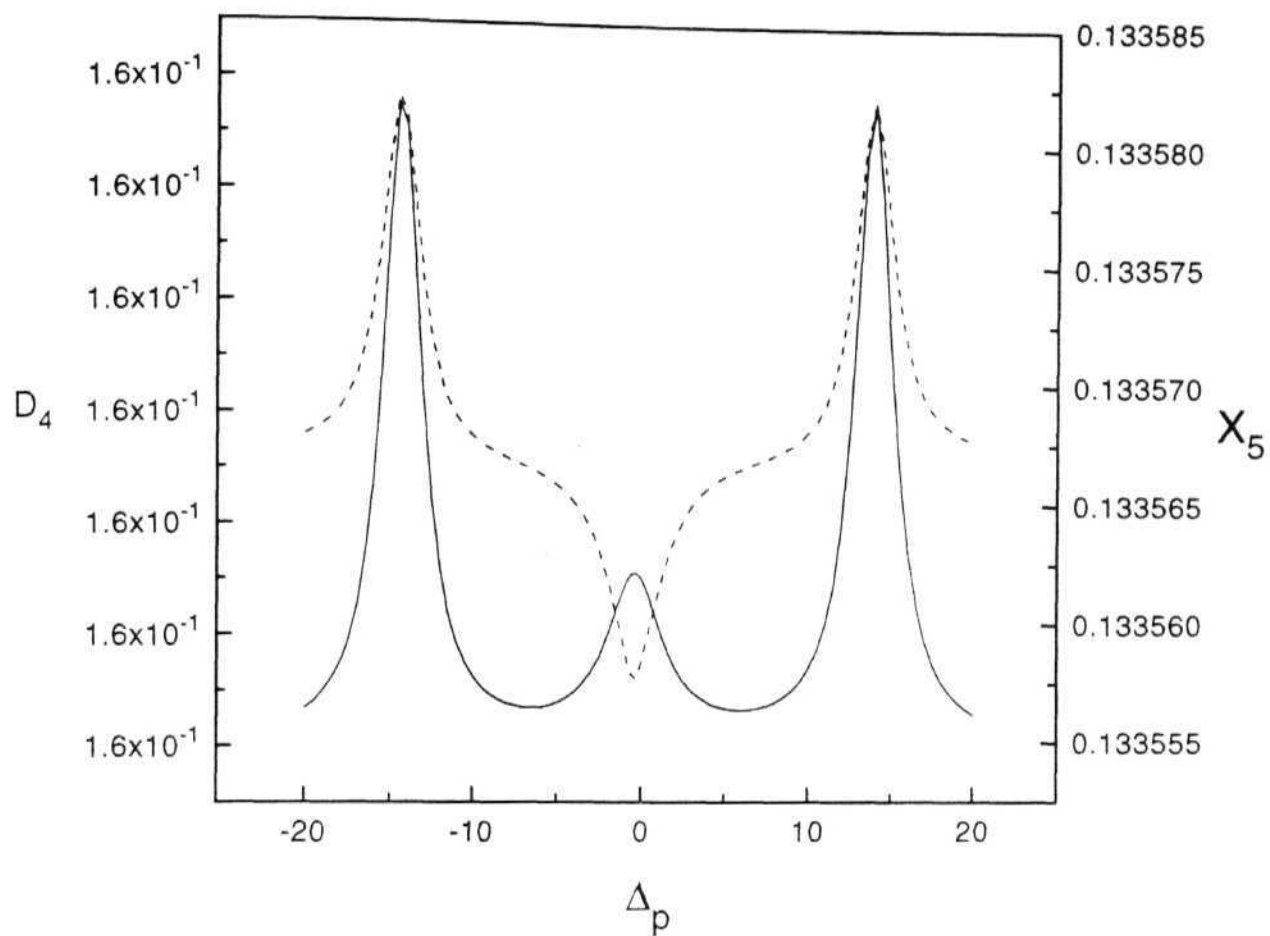


Fig. 6.6 (c) [Populations of the dressed states D_4 (Dashed line, left axis)) and X_5 (Solid line, right axis). Population of D_4 is more than that of X_5 , which corresponds to inversion in the dressed state.

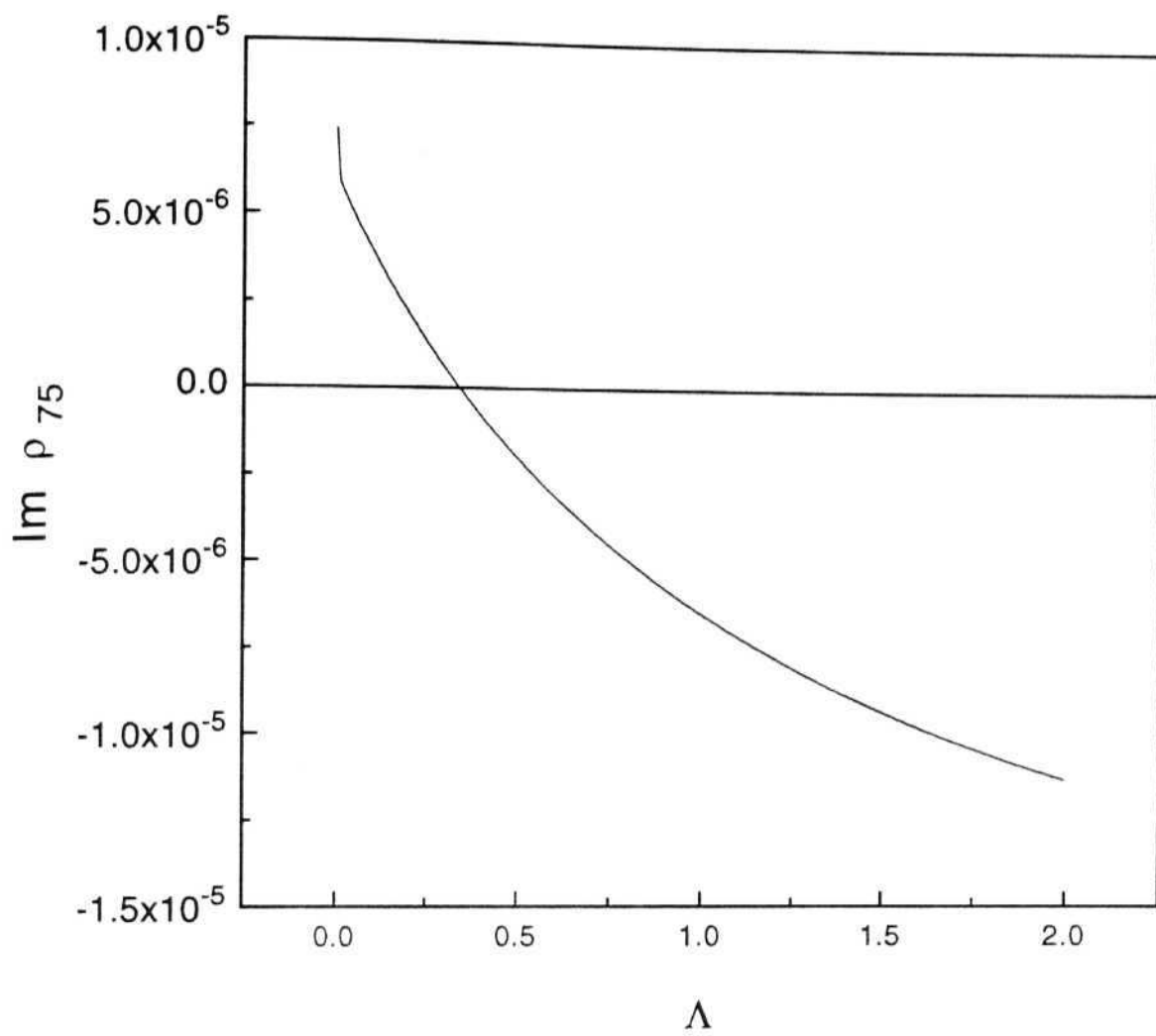


Fig. 6. 7 (a): Absorption of Gate configuration as a function of pump parameter Λ . Negative value implies gain.

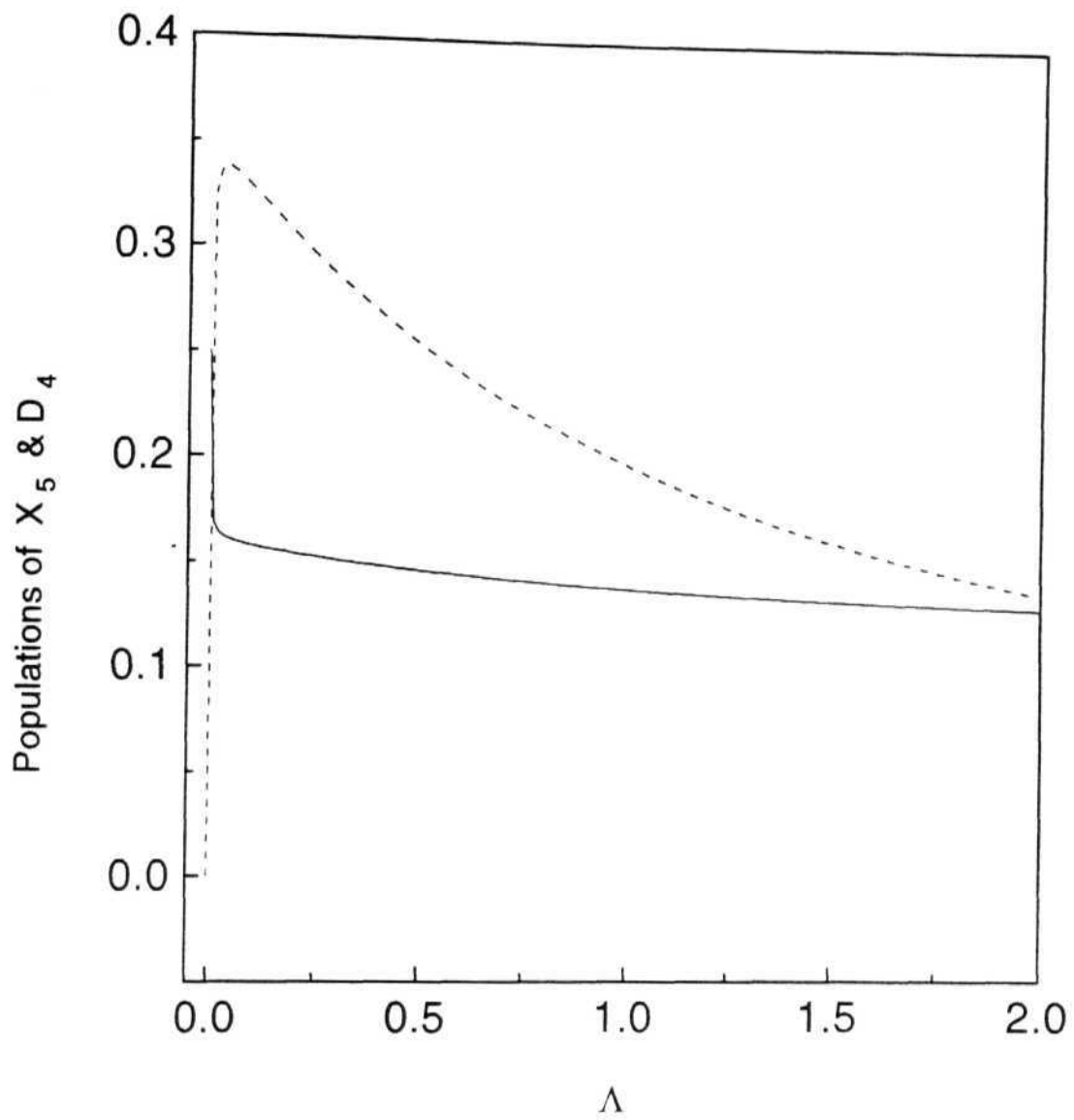


Fig. 6. 7 (b):Populations of X_5 (solid line) and D_4 (dashed line) for a value of $\Delta_p = -0.45$, which is the gain position.

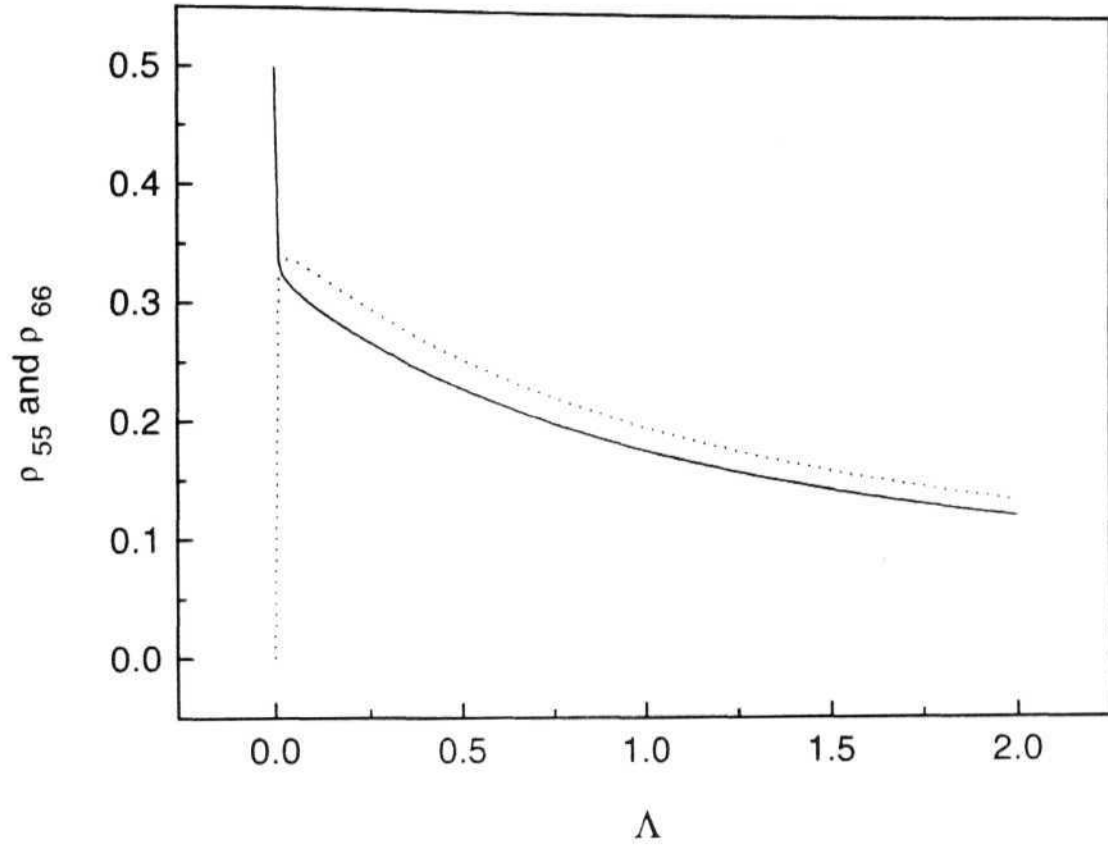


Fig. 6. 7 (c): Population of level 5 and 6 (solid line) and level 1 (dashed line), as a function of Λ , at $\Delta_p = -0.45$.

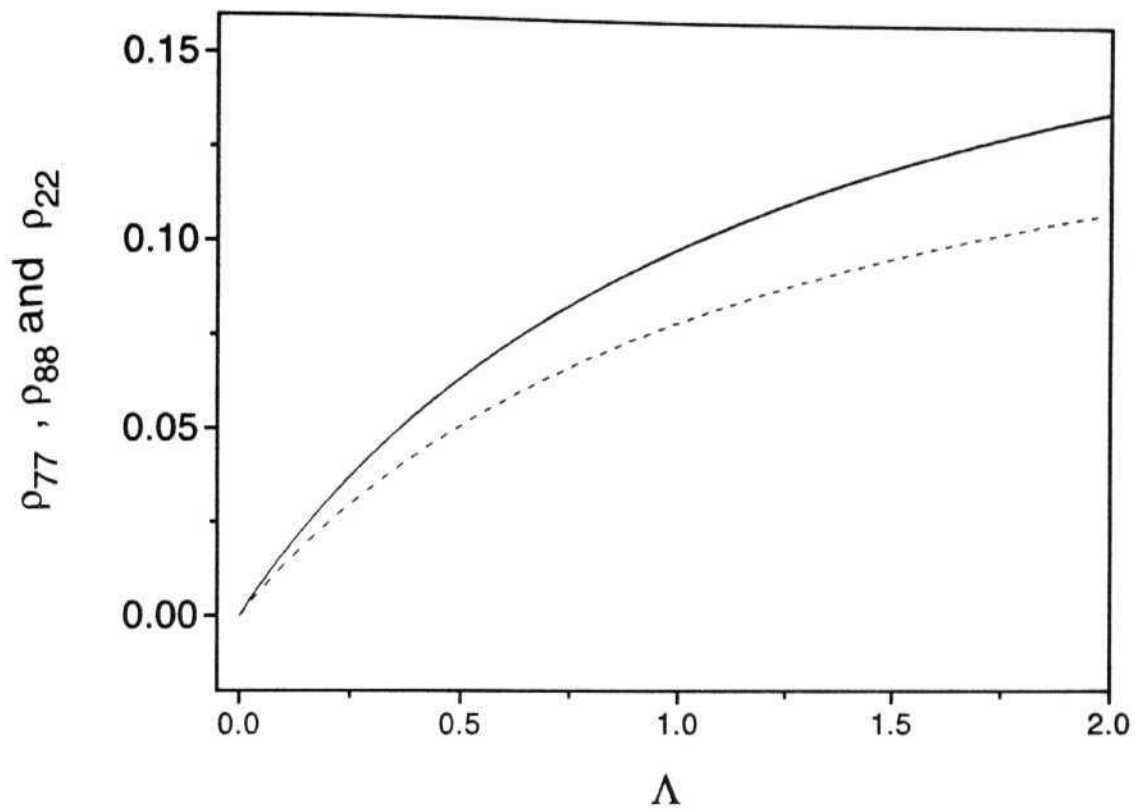


Fig 6.7 (d):Populations of levels 7 and 8 (solid line) and 2 (dashed line), as a function of Λ , at $\Delta_p=0.45$.

References

- [1] T. Hänsch and P. Toscheck, Z. Physik, 236, 213 (1970)
- [2] M. O. Scully, Quant. Opt. 6, 203 (1994) ; M. O. Scully, Phys. Rep. **219**, 191 and references therein
- [3] O. Kocharovskaya and P. Mandel, Quant. Opt. 6, 217 (1994); O. Kocharovskaya Phys. Rep. **219**, 175 (1992)
- [4] G. S. Agarwal, Phys. Rev. A 42, 686 (1990); Opt. Comm. 80, 37 (1990)
- [5] Y. Zhu and J. Lin, Phys. Rev A 53, 1767 (1996) :inversion in dressed states
- [6] Y. G. Arkhipin, Yu. I. Heller, Phys. Lett. A 98, 12 (1983)
- [7] S. E. Harris, Phys. Rev. Lett. 62, 1033(1989);
- [8] Surya P. Tewari and G. S. Agarwal, Phys. Rev. Lett. 56, 1811 (1986)
- [9] G. Z. Zhang, D. W. Tokaryk, B. P. Stoicheff and K. Hakuta, Phys. Rev. A 56, 813 (1997)
- [10] J. Gao, C. Guo, X. Guo, G. Jin, P. Wang, J. Zhao, H. Zhang, Y. Jiang, D. Waig and D. Jiang, Opt. Comm. 93, 323 (1992)
- [11] J. A. Bergou and P. Bogár, Phys. Rev. A 43, 4889 (1991)

Chapter VII

Threshold of Transparency

When a pump beam is a focussed Gaussian TEM_{00} mode travelling along the length of an optically thick sample, it leads to a transverse profile of transparency which varies also along the length of the sample. The spatial profile of transparency inside the sample depends on, besides other parameters, the intensity of the pump beam at the focal point of the Gaussian mode. In this chapter, a threshold intensity is defined at which transparency for the thick sample can be said to have set in. This threshold intensity is related to the relaxation rates and dipole matrix elements of the pump transition.

A spatial variation of the pump beam intensity leads to a spatial variation of the induced effects on the probe beam transmission. A transverse variation across the beam path has been shown earlier to lead to a transverse variation of the refractive index and hence to a induced lens-like behaviour of the medium [1]. Modification of such lensing effect due to the presence of associated absorption has also been examined [2]. In this chapter, a discussion is considered when the pump beam is a Gaussian beam which is focussed to obtain high energy density inside an optically thick sample. Because the intensity varies along the beam path also, there is a non-uniform modification of the probe absorption along the sample length. This variation needs to be taken into consideration when analysing the EIT effects.

In the present chapter, a study of longitudinal variation of absorption due to longitudinal variation of pump beam intensity in an optically thick sample is presented.

In particular, it is shown that a graph of axial absorption versus the log of the intensity of the pump beam suggests the definition of a threshold intensity at which the transparency in the thick sample may be said to have set in.

Consider a typical experimental configuration for EIT, which consists of a probe beam and a pump beam interacting with an atomic vapour in a cell of length L . The pump beam is a Gaussian beam of TEM₀₀ mode, focussed to the center of the cell, denoted by $z=0$, with a beam waist w_0 . The Rayleigh range of the probe beam, $b_p = k_p w_{p0}^2$ is taken to be much larger than that of pump beam $b = k w_0^2$. The probe beam can then be approximated by a plane wave, which is spatially uniform. k and k_p are the wave vectors and w_0 and w_{p0} are the beam waists of pump and probe beam respectively. The Rayleigh length of the pump beam is smaller than the length of the sample. The striped region of figure 7.1 depicts region in which atoms interact only with the probe beam, while the region which is hatched contains atoms which interact with pump beam also and their response to probe beam is hence modified. Therefore, atoms within the striped region are purely absorptive. Response of the atoms within the crossed region is obtained incorporating the shape of the pump beam.

In the following, the phenomenon of EIT in a three level model of the atom, consisting of ground state $|g\rangle$, an excited state $|e\rangle$ and a third state $|m\rangle$ is considered. Probe beam connects transition between $|g\rangle$ and $|e\rangle$. In presence of the pump beam which connects $|e\rangle$ to $|m\rangle$, absorption of the probe beam is modified following the susceptibility,

$$\chi^{(1)} = \frac{N}{\hbar} \frac{|d_{eg}|^2}{\Delta_{eg} - i\gamma_{eg} - \frac{|g_{me}|^2}{\Delta_{eg} + \Delta_{me} - i\gamma_{mg}}} \quad (7.1)$$

Here, N is the number of atoms in a unit volume, γ_{ij} is the transverse relaxation rate

of the coherence between levels $|i\rangle$ and $|j\rangle$. g_{me} is the Rabi frequency of the transition between levels $|m\rangle$ and $|e\rangle$. d_{eg} is the dipole matrix element of the transition between $|e\rangle$ and $|g\rangle$.

Propagation of the probe beam in the medium is governed by the paraxial equation

$$\left[\frac{i}{2k} \nabla_t^2 + \frac{\partial}{\partial z} \right] \mathcal{E}_1 = \frac{2\pi i\omega}{c} \chi^{(1)}(\omega) \mathcal{E}_1 \quad (7.2)$$

where

$$\nabla_t^2 = \frac{\partial^2}{\partial x^2} + \frac{\partial^2}{\partial y^2},$$

$k = \omega/c$ and $E = \mathcal{E}_1 \exp(i\omega t - ikz) + \text{c.c.}$. \mathcal{E}_1 is the slowly varying envelope for the probe field.

Spatial variation of the pump beam leads to a variation in the term $\chi^{(1)}$. The slowly varying envelope of the pump beam can be written as

$$\mathcal{E}_2(x, y, z) = \frac{E_{20} \exp(-ik_2 \cdot z)}{1 + i\xi} \exp \left(-\mathbf{k}_2 \cdot \left(\frac{x^2 + y^2}{b(1 + i\xi)} \right) \right),$$

where, \mathbf{k}_2 is the wave vector of the pump beam, $r = \sqrt{x^2 + y^2}$ is the transverse distance from the z -axis and

$$\xi = \frac{2(z - f)}{b},$$

The pump and probe beam are assumed to be collinear.

The Rabi frequency of the pump beam is given by $g = \frac{d_{me}}{\hbar} \mathcal{E}_2(x, y, z)$. This gives

$$\begin{aligned} |g|^2 &= \left| \frac{d_{me} E_{20}}{\hbar} \right|^2 \frac{1}{(1 + \xi^2)} \exp \left(\frac{-2(x^2 + y^2)}{b(1 + \xi^2)} \right) \\ &= \frac{g_0^2}{1 + \xi^2} \exp \left(-\frac{2r^2}{w^2(z)} \right) \end{aligned} \quad (7.3)$$

Along the axis, $r = 0$, and therefore,

$$g^2 = \frac{g_0^2}{1 + \xi^2}.$$

g_0 is the Rabi frequency of the pump beam at the focus.

Substituting envelope function of the pump in 7.1 and solving the equation 7.2 gives the effect of spatial profile of the pump beam on the probe absorption. In order to define the threshold intensity we concentrate on the axial case.

For the axial case, when $r \approx 0$, integrating equation (7.2) over the length of the medium gives

$$\ln \mathcal{E} = \int_{-L/2}^{L/2} \frac{\partial \mathcal{E}}{\mathcal{E}} = \int_{-L/2}^{L/2} \frac{2i\pi\omega}{c} \chi^{(1)}(z) dz,$$

where L is the length of the sample. Substituting for pump Rabi frequency $|g|^2$ in the expression 7.1 for $\chi^{(1)}(z)$ by its spatially varying factor $|g_0|^2/(1 + \xi^2)$ we get,

$$\sigma = \bar{\sigma} N \int_{-L/2}^{L/2} \frac{dz}{\Delta_{eg} - i\gamma_{eg} - \frac{|g_0|^2}{\Delta_{eg} + \Delta_{me} - i\gamma_{mg}} \frac{1}{1 + \xi^2}} \quad (7.4)$$

where $\bar{\sigma}$ is a constant given by

$$\bar{\sigma} = \frac{2\pi i\omega}{c} \frac{|d_{eg}|^2}{\hbar}.$$

This leads to

$$\sigma = \bar{\sigma} N \int_{-L/2}^{L/2} \frac{(1 + \xi^2).dz}{(1 + \xi^2)[\Delta_{eg} - i\gamma_{eg}] - \frac{|g_0|^2}{(\Delta_{eg} + \Delta_{me} - i\gamma_{mg})}} \quad (7.5)$$

Denoting

$$K_1 = -\frac{|g_0|^2}{\Delta_{eg} + \Delta_{me} - i\gamma_{eg}}$$

and

$$K_2 = \Delta_{eg} - i\gamma_{me}$$

the integral in expression 7.5 can readily be solved to give

$$\sigma = \bar{\sigma} N \frac{b}{2} \frac{1}{K_2} \left[\frac{2L}{b} - \frac{2K}{\sqrt{1+K}} \tan^{-1} \frac{L}{b\sqrt{1+K}} \right] \quad (7.6)$$

where $K = K_1/K_2$

Absorption coefficient in the absence (presence) of pump beam is denoted by $\alpha_o(\alpha)$ which is given by $\alpha_0 = -\text{Re}\bar{\sigma}NL/K(\alpha = -\text{Re}\sigma)$.

Figure 7.2 shows α/α_0 , as a function of log of the pump beam Rabi frequency $\log_{10} g_0$ for the ratio $L/b = 10^{-3}$. All the parameters are scaled to the coherence decay γ_{eg} . As the pump beam Rabi frequency g_0 is increased the absorption decreases and reaches an asymptotic value of zero. To quantify the fast change in absorption, a limiting curve is assumed as shown in figure 7.2. This curve intersects the absorption curve at $\alpha/\alpha_0 = 0.5$. In other words, the g_0 value at which α/α_0 reaches a value of 0.5 is taken to be the threshold value at which the transparency occurs. According to this picture there is finite large absorption below this threshold intensity and full transparency after it *.

Figure 7.3 shows variation of α for different values of L/b . Each one of them shows

*In an earlier publication, we had defined a reduction of absorption coefficient α to a value of $\alpha_0/10.0$ to be representing threshold transparency [4]. Considering the symmetrical nature of the profiles around threshold intensity in figure 7.2, we define here the induced transparency as reduction of α to $\alpha_0/2$.

a maximum absorption for small g_0 values, which approaches a minimum value sharply. The threshold intensity value increases as L/b increases.

Figure 7.4 shows variation of α for three different values of γ_{mg} . The threshold value is seen to increase with the value of γ_{mg} .

In figure 7.5, the threshold Rabi frequency is plotted against L/b values. It shows that as the sample length increases, the threshold intensity of transparency also increases.

The above results can be explained by noting that the shape of the pump beam is a hyperboloid of rotation [3]. The beam intensity is maximum at the focus and reduces gradually as one moves away from the focus. Therefore, the induced transparency follows a similar profile with a maximum at the focus and decreasing at the ends. This region forms a dumbbell centered at the focus, such that the atoms within this dumbbell are rendered transparent to the probe beam while the atoms outside the dumbbell are not. If the length of this dumbbell is less than that of the sample length, there exist atoms along the path of the probe beam which are absorptive. They absorb the probe beam and the transparency effect can not be observed. Roughly when the dumbbell length is of the order of the sample length, the induced transparency effect can be observed.

For a condition when $L/b \ll 1$, the variation of g_0 with L/b is seen to be linear (Figure 7.6). For this condition, a relation between threshold intensity and other parameters can be determined as follows.

Rewriting the equation 7.6 at threshold condition,

$$\frac{\alpha(\omega, |g_0|_{\text{Threshold}}^2)}{\alpha(\omega, |g_0|^2 \rightarrow 0)} = \frac{1}{2}$$

Which results in

$$\left[\frac{2L}{b} - \frac{2K}{\sqrt{1+K}} \tan^{-1} \frac{L}{b\sqrt{1+K}} \right] = \frac{L}{b}$$

$$\frac{2K}{\sqrt{1+K}} \tan^{-1} \frac{L}{b\sqrt{1+K}} = \frac{L}{b}. \quad (7.7)$$

For small values of $L/(b\sqrt{1+K})$,

$$\tan^{-1} \frac{L}{b\sqrt{1+K}} \approx \frac{L}{b\sqrt{1+K}}$$

and therefore, equation 7.7 gives

$$K = -1 = \frac{K_1}{K_2}.$$

Substituting for K_1 and K_2 for resonant situation

$$\frac{i|g_0|^2}{-i\gamma_{eg}\gamma_{mg}} = -1.$$

This results in

$$|g_0|^2 = \gamma_{eg}\gamma_{me}. \quad (7.8)$$

In other words, the Rabi frequency value at which the threshold transparency occurs for $L/b \ll 1$ regime, is equal to the square root of the product of two coherence decay terms γ_{eg} and γ_{mg} . Relation 7.8 may be used to estimate any one of the involved parameter as unknown while determining experimentally the value of g_0 under the conditions of validity of the above equation.

In conclusion, the probe absorption profile is seen to vary along the beam path, resulting in a dumbbell shaped profile. Since the probe absorption is not a complete zero, one needs to define onset of induced transparency. We define the transparency as reduction of absorption by half. This generates a region within the sample containing transparent atoms. If the length of this region is comparable to that of the sample length, the medium appears transparent. Otherwise, the probe beam will be absorbed by the atoms outside this region. The total axial absorption value for an optically thick sample reaches half its maximum value at $|g_0|^2 = \gamma_{eg} \cdot \gamma_{mg}$ for $L/b \ll 1$.

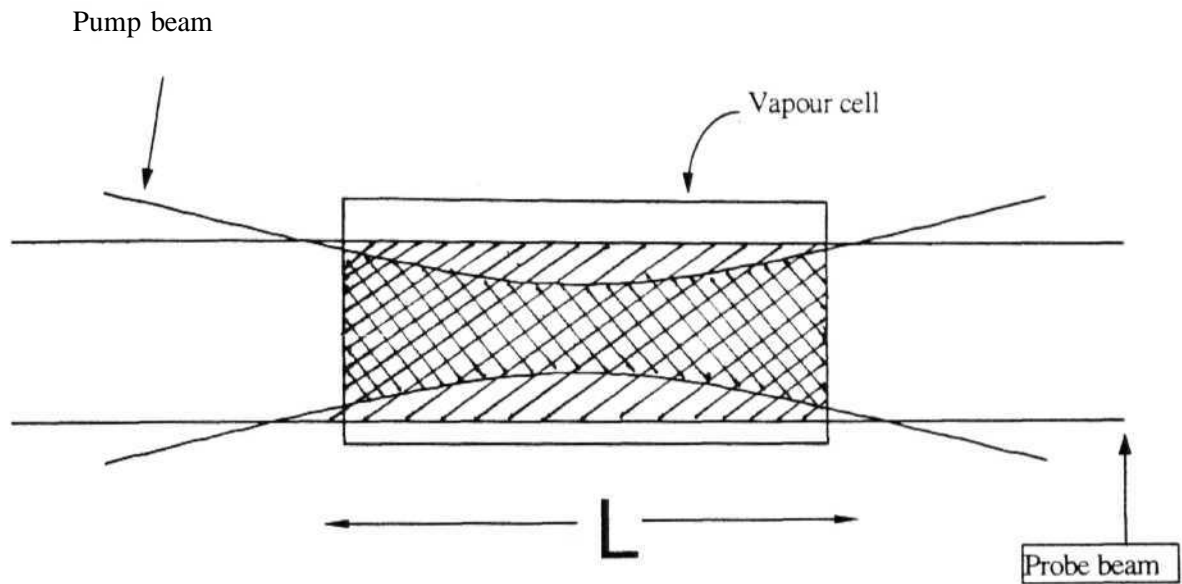


Fig.7.1: Figure showing the pump and probe beams interacting with the atomic medium within the sample cell. Probe beam is represented by a plane wave and pump beam is a focussed Gaussian forming the hyperboloid. Atoms within the striped region interact with the probe beam alone and atoms within the crossed region interact with both pump and probe beams.

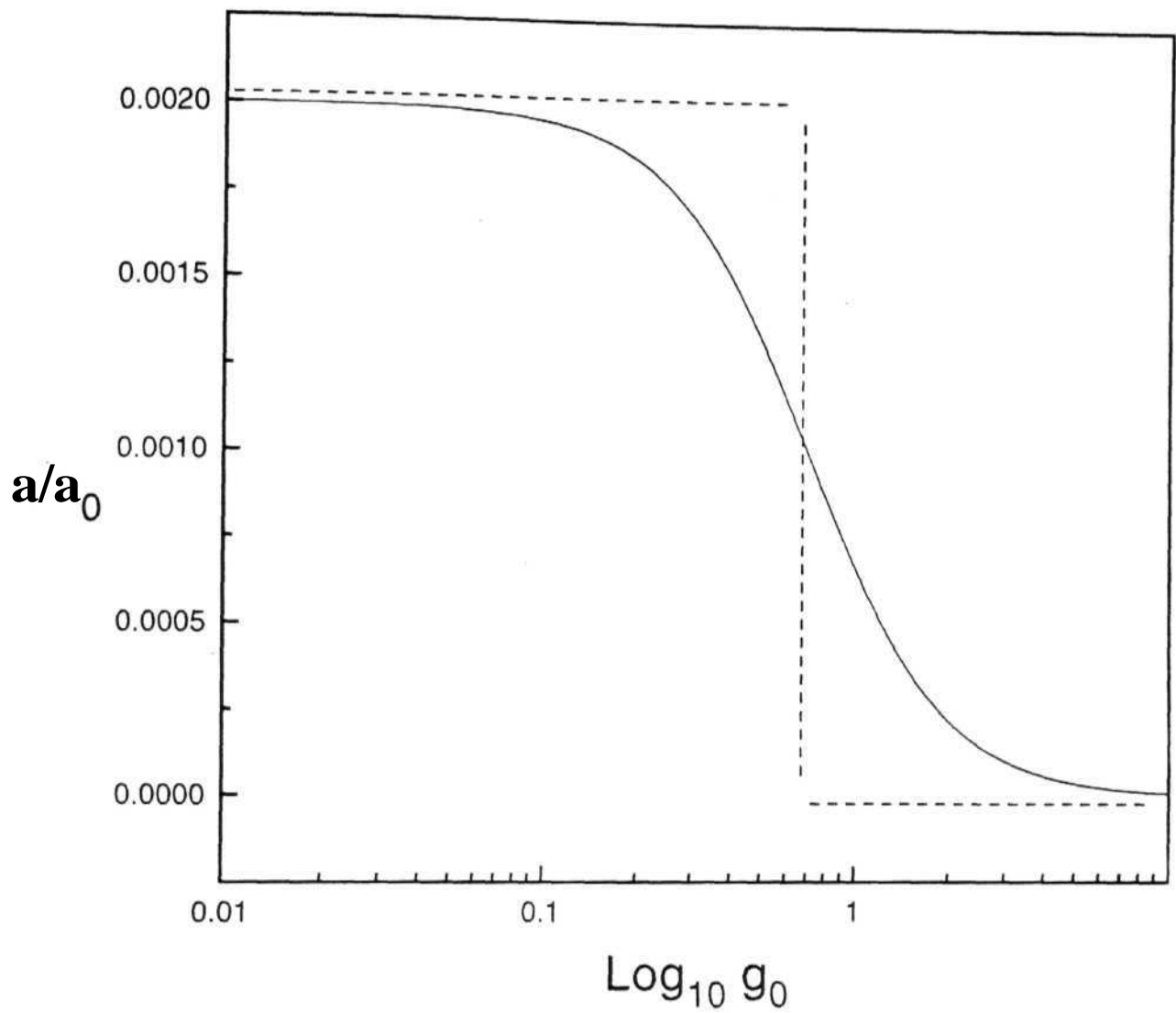


Fig. 7.2 : α/α_0 plotted against $\text{Log } g_0$. The absorption goes from maximum to minimum as g_0 is increased. The theoretical limit for threshold is shown by dashed lines.

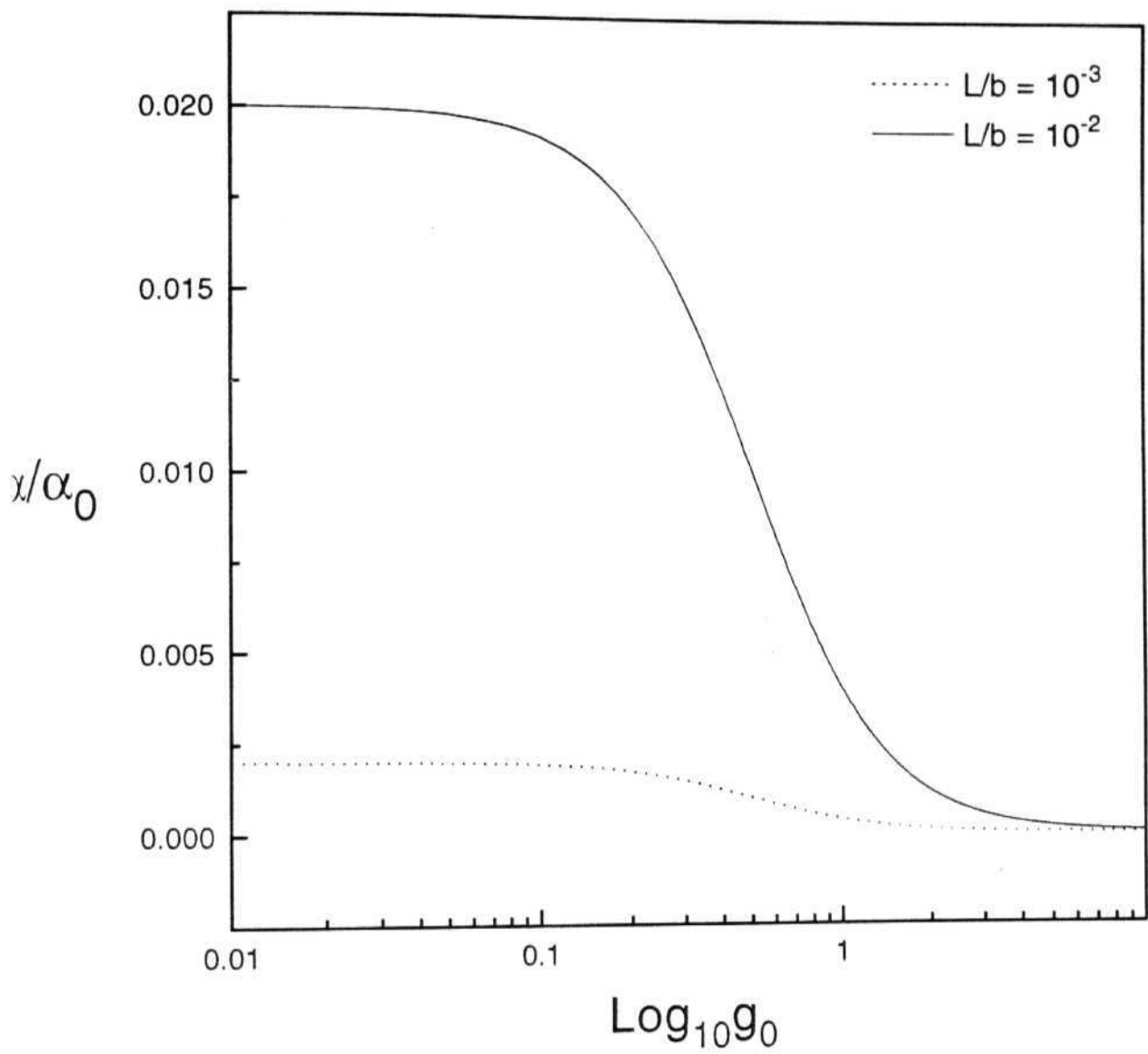


Fig. 7.3 a: α/α_0 plotted against $\text{Log } g_0$. For different values of L/b

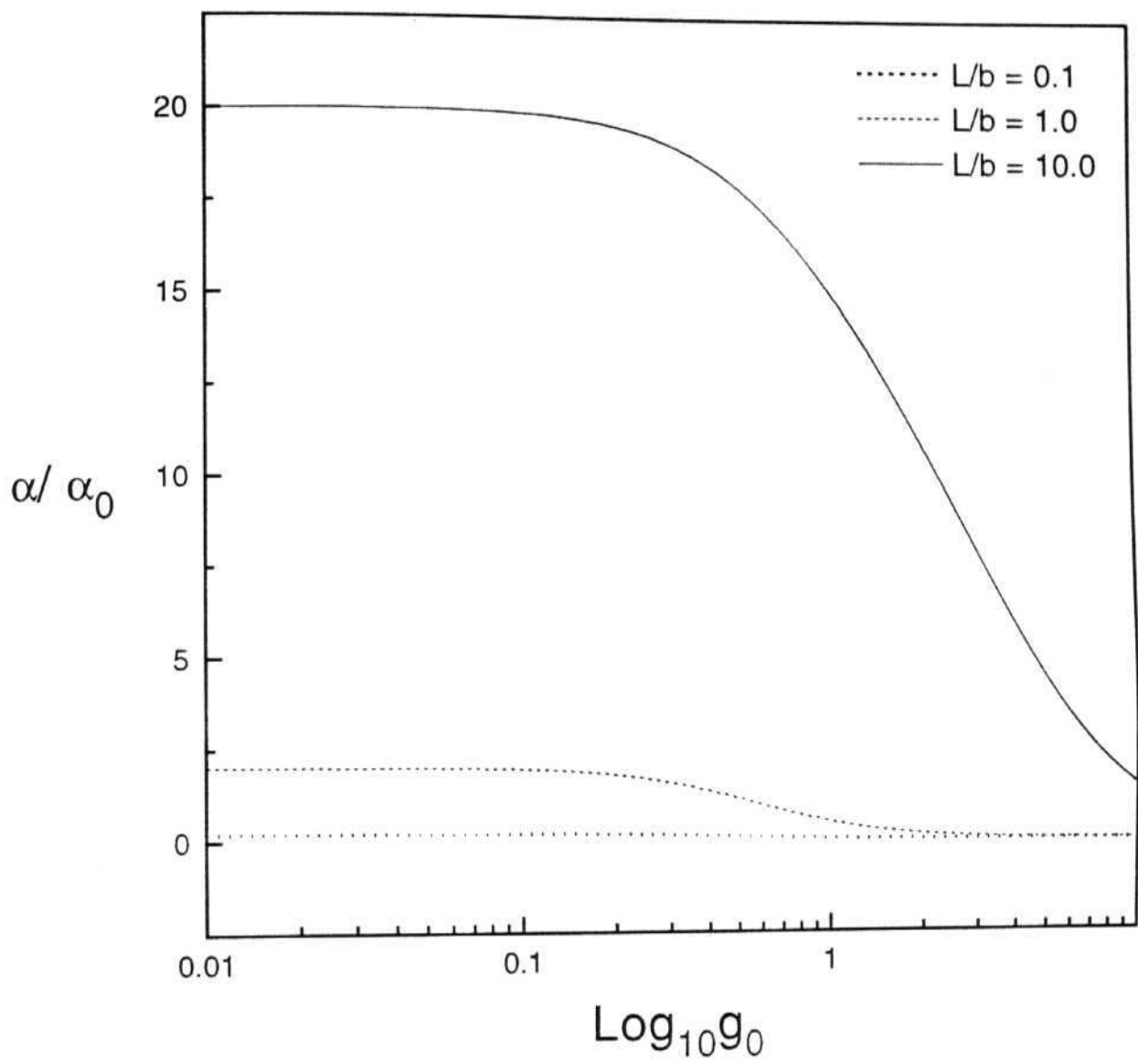


Fig. 7.3 b: α/α_0 plotted against $\text{Log } g_0$. For different values of L/b

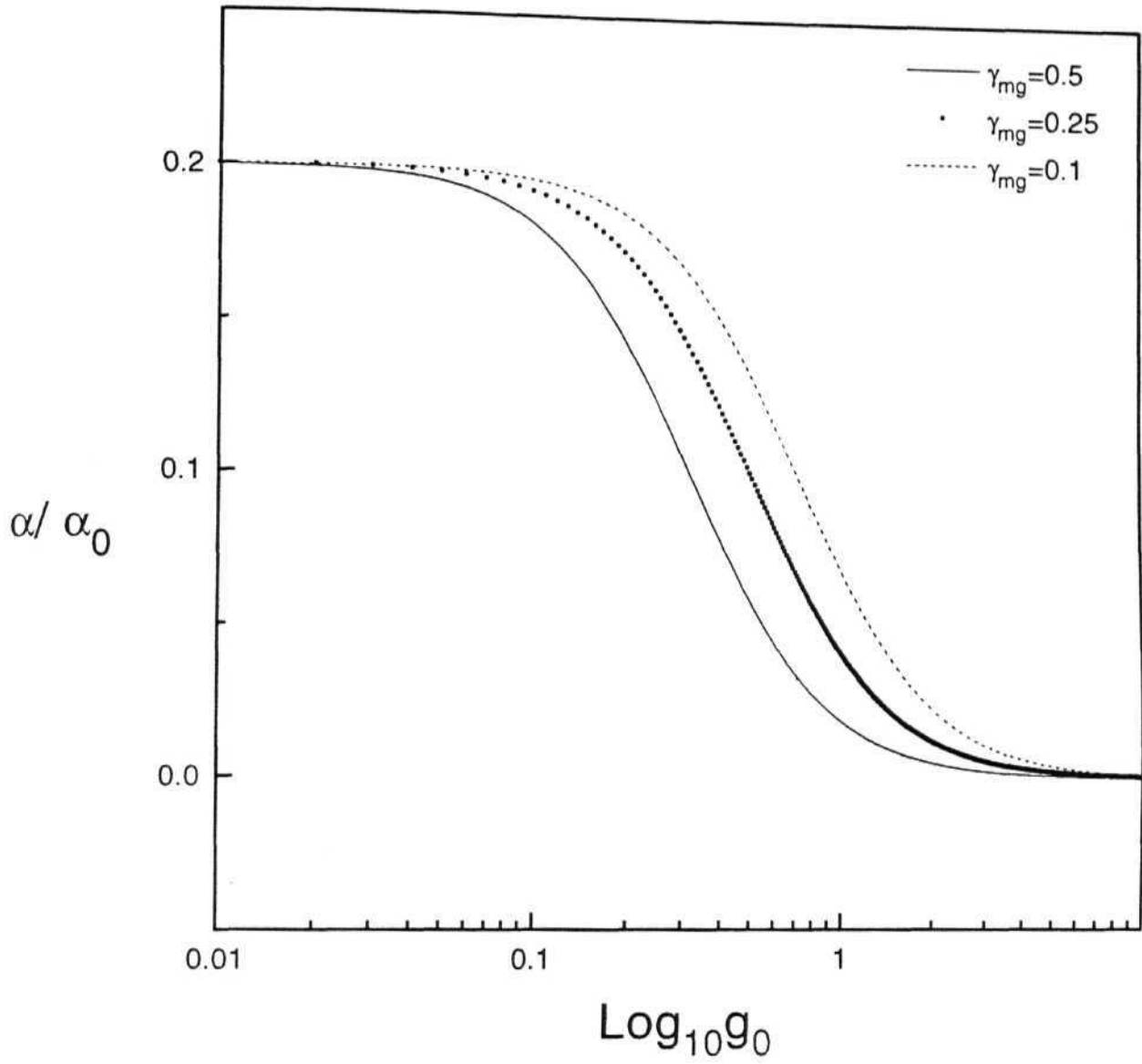


Fig. 7.4 : α/α_0 for $L/b=0.1$, for different values of γ_{mg} , the decay rate of coherence between level m and g.

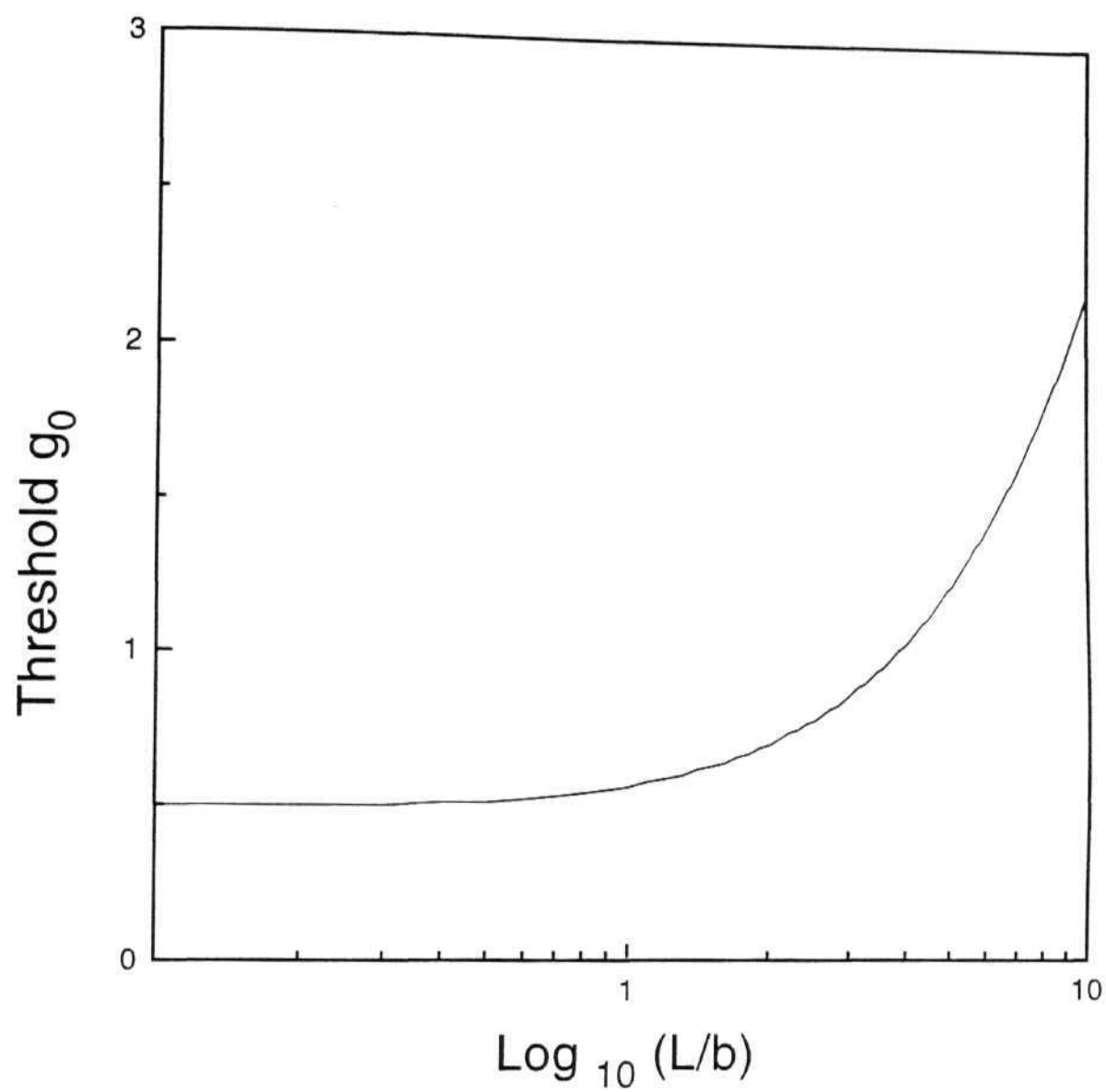


Fig. 7.5: Threshold g_0 for variation in $\text{Log}_{10} L/b$.

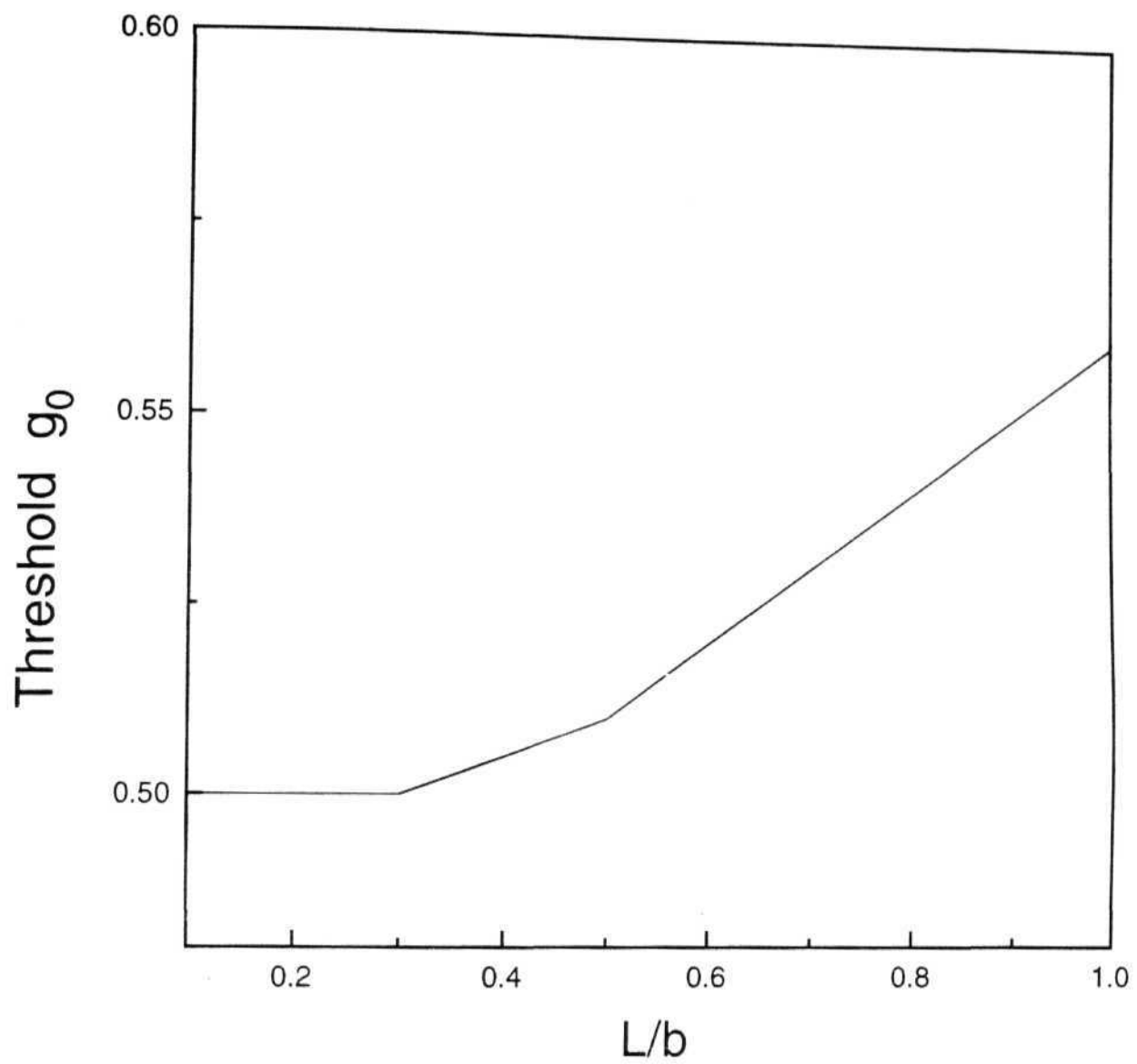


Fig. 7.6: Linear region of variation threshold g_0 for $L/b \ll 1$.

References

- [1] Richard R. Mosley, Sara Shepherd, David J. Fulton, Bruce D. Sinclair and Malcom S.Dunn, Phys. Rev. Lett. 74, 670 (1995)
- [2] Richard R. Mosley, Sara Shepherd, David J. Fulton, Bruce D. Sinclair and Malcom S.Dunn, Phys. Rev. A 53, 408 (1996)
- [3] A. Yariv, *Quantum Electronics*, John Wiley, N.Y. (1989), pp 119 Vol I , ed:-R. Balian, S. Haroche and S. Liberman, North Holland
- [4] S.P.Tewari & V.S.Ashoka, Proceedings of Workshop on Advanced Laser Spectroscopy, Indian Instt. of Technology, Kanpur, ed. H.D.Bist et. al., Allied Publishers, New Delhi, pp 213, (1996)

Equation 2.3

Where

$$\begin{aligned} D_1 &= \Delta_s + i\gamma_{12} & D_2 &= (\Delta_s + \Delta_p) + i\gamma_{27} & D_3 &= (\Delta_s + \Delta_p) + i\gamma_{24} \\ D_4 &= -\Delta_s + i\gamma_{12} & D_6 &= \Delta_p + i(\gamma_{12} + i\gamma_{23}) & D_7 &= \Delta_p + i(\gamma_{12} + \gamma_{24}) \\ D_8 &= -(\Delta_s + \Delta_p) + i\gamma_{23} & D_9 &= -\Delta_p + i(\gamma_{12} + \gamma_{23}) & D_{11} &= -\Delta_{34} + i(\gamma_{23} + \gamma_{24}) \\ D_{12} &= -(\Delta_p + \Delta_s) + i\gamma_{24} & D_{13} &= -\Delta_p + i(\gamma_{12} + \gamma_{24}) & D_{14} &= -\Delta_{34} + i(\gamma_{23} + \gamma_{24}) \end{aligned}$$

● **Answer:** (A)

[illegible]

[illegible]

$$\begin{aligned} D_1 &= \Delta_{05} + i(\gamma_{06} + \gamma_{65}) & D_2 &= \Delta_{75} + i(\gamma_{05} + \gamma_{57}) & D_3 &= \Delta_{05} - \Delta_{05} + i(\gamma_{05} + \gamma_{08}) \\ D_4 &= \Delta_{05} + i\gamma_9 & D_5 &= -\Delta_{05} + i(\gamma_{06} + \gamma_{65}) & D_6 &= 4i\gamma_{05} + 2i\gamma_{06} \\ D_7 &= \Delta_{76} + i(\gamma_{06} + \gamma_{67}) & D_8 &= \Delta_{05} + i(\gamma_{05} + \gamma_{08}) & D_9 &= \Delta_{06} + i(\gamma_{06} + \gamma_9) \end{aligned}$$

Appendix C

Clebsch-Gordon Coefficients

Combinations which lead to each $|F, m_F\rangle$ level used in the study are calculated using rules for addition of angular momentum*. Dipole matrix elements for transitions are calculated for these levels using the selection rules for transition between l, m_l, s and m_s values.

Formation of F levels according to $F=I+L+S$

F=2 levels

$$\begin{aligned}|F=2, m_F = 2\rangle &= \frac{1}{\sqrt{2}} \left| \frac{3}{2}, \frac{3}{2} \right\rangle \left| \frac{3}{2}, \frac{1}{2} \right\rangle - \frac{1}{\sqrt{2}} \left| \frac{3}{2}, \frac{1}{2} \right\rangle \left| \frac{3}{2}, \frac{3}{2} \right\rangle \\|F=2, m_F = 1\rangle &= \frac{1}{\sqrt{2}} \left| \frac{3}{2}, \frac{3}{2} \right\rangle \left| \frac{3}{2}, -\frac{1}{2} \right\rangle - \frac{1}{\sqrt{2}} \left| \frac{3}{2}, -\frac{1}{2} \right\rangle \left| \frac{3}{2}, \frac{3}{2} \right\rangle \\|F=2, m_F = 0\rangle &= \frac{1}{2} \left| \frac{3}{2}, \frac{3}{2} \right\rangle \left| \frac{3}{2}, -\frac{3}{2} \right\rangle + \frac{1}{2} \left| \frac{3}{2}, \frac{1}{2} \right\rangle \left| \frac{3}{2}, -\frac{1}{2} \right\rangle - \frac{1}{2} \left| \frac{3}{2}, -\frac{1}{2} \right\rangle \left| \frac{3}{2}, \frac{1}{2} \right\rangle \\&\quad - \frac{1}{2} \left| \frac{3}{2}, -\frac{3}{2} \right\rangle \left| \frac{3}{2}, \frac{3}{2} \right\rangle \\|F=2, m_F = -1\rangle &= \frac{1}{\sqrt{2}} \left| \frac{3}{2}, \frac{1}{2} \right\rangle \left| \frac{3}{2}, -\frac{3}{2} \right\rangle - \frac{1}{\sqrt{2}} \left| \frac{3}{2}, -\frac{3}{2} \right\rangle \left| \frac{3}{2}, \frac{1}{2} \right\rangle \\|F=2, m_F = -2\rangle &= \frac{1}{\sqrt{2}} \left| \frac{3}{2}, -\frac{1}{2} \right\rangle \left| \frac{3}{2}, -\frac{3}{2} \right\rangle - \frac{1}{\sqrt{2}} \left| \frac{3}{2}, -\frac{3}{2} \right\rangle \left| \frac{3}{2}, -\frac{1}{2} \right\rangle\end{aligned}$$

F=1 levels

$$\begin{aligned}|F=1, m_F = 1\rangle &= \sqrt{\frac{3}{10}} \left| \frac{3}{2}, \frac{3}{2} \right\rangle \left| \frac{3}{2}, -\frac{1}{2} \right\rangle - \frac{2}{\sqrt{10}} \left| \frac{3}{2}, \frac{1}{2} \right\rangle \left| \frac{3}{2}, \frac{1}{2} \right\rangle + \sqrt{\frac{3}{10}} \left| \frac{3}{2}, -\frac{1}{2} \right\rangle \left| \frac{3}{2}, \frac{3}{2} \right\rangle \\|F=1, m_F = 0\rangle &= \frac{3}{2\sqrt{5}} \left| \frac{3}{2}, \frac{3}{2} \right\rangle \left| \frac{3}{2}, -\frac{3}{2} \right\rangle - \frac{1}{2\sqrt{5}} \left| \frac{3}{2}, \frac{1}{2} \right\rangle \left| \frac{3}{2}, -\frac{1}{2} \right\rangle - \frac{1}{2\sqrt{5}} \left| \frac{3}{2}, -\frac{1}{2} \right\rangle \left| \frac{3}{2}, \frac{1}{2} \right\rangle\end{aligned}$$

*E. U. Condon and G. H. Shortley *The Theory of Atomic Spectra*, Cambridge, (1970), pp 76

$$\begin{aligned}
 & + \frac{3}{2\sqrt{5}} \left| \frac{3}{2}, -\frac{3}{2} \right\rangle \left| \frac{3}{2}, \frac{3}{2} \right\rangle \\
 |F=1, m_F = -1\rangle & = \sqrt{\frac{3}{10}} \left| \frac{3}{2}, \frac{1}{2} \right\rangle \left| \frac{3}{2}, -\frac{3}{2} \right\rangle - \frac{2}{\sqrt{10}} \left| \frac{3}{2}, -\frac{1}{2} \right\rangle \left| \frac{3}{2}, -\frac{1}{2} \right\rangle + \sqrt{\frac{2}{10}} \left| \frac{3}{2}, -\frac{3}{2} \right\rangle \left| \frac{3}{2}, \frac{1}{2} \right\rangle
 \end{aligned}$$

F=0 level

$$\begin{aligned}
 |F=0, m_F = 0\rangle & = \frac{1}{2} \left| \frac{3}{2}, \frac{3}{2} \right\rangle \left| \frac{3}{2}, -\frac{3}{2} \right\rangle - \frac{1}{2} \left| \frac{3}{2}, \frac{1}{2} \right\rangle \left| \frac{3}{2}, -\frac{1}{2} \right\rangle + \frac{1}{2} \left| \frac{3}{2}, -\frac{1}{2} \right\rangle \left| \frac{3}{2}, \frac{1}{2} \right\rangle \\
 & - \frac{1}{2} \left| \frac{3}{2}, -\frac{3}{2} \right\rangle \left| \frac{3}{2}, \frac{3}{2} \right\rangle
 \end{aligned}$$

Formation of different levels

F=1 levels of $S_{1/2}$

$$\begin{aligned}
 |F=1, m_F = +1\rangle & = -\frac{1}{2} \left| \frac{3}{2}, \frac{1}{2} \right\rangle |0, 0\rangle \left| \frac{1}{2}, \frac{1}{2} \right\rangle + \frac{\sqrt{3}}{2} \left| \frac{3}{2}, \frac{3}{2} \right\rangle |0, 0\rangle \left| \frac{1}{2}, -\frac{1}{2} \right\rangle \\
 |F=1, m_F = 0\rangle & = -\sqrt{\frac{1}{2}} \left| \frac{3}{2}, -\frac{1}{2} \right\rangle |0, 0\rangle \left| \frac{1}{2}, \frac{1}{2} \right\rangle + \sqrt{\frac{1}{2}} \left| \frac{3}{2}, \frac{1}{2} \right\rangle |0, 0\rangle \left| \frac{1}{2}, -\frac{1}{2} \right\rangle \\
 |F=1, m_F = -1\rangle & = -\frac{\sqrt{3}}{2} \left| \frac{3}{2}, -\frac{3}{2} \right\rangle |0, 0\rangle \left| \frac{1}{2}, \frac{1}{2} \right\rangle + \frac{1}{2} \left| \frac{3}{2}, -\frac{1}{2} \right\rangle |0, 0\rangle \left| \frac{1}{2}, -\frac{1}{2} \right\rangle
 \end{aligned}$$

F=2 levels of $S_{1/2}$

$$\begin{aligned}
 |F=2, m_F = 2\rangle & = \left| \frac{3}{2}, \frac{3}{2} \right\rangle |0, 0\rangle \left| \frac{1}{2}, \frac{1}{2} \right\rangle \\
 |F=2, m_F = 1\rangle & = \frac{1}{2} \left| \frac{3}{2}, \frac{3}{2} \right\rangle |0, 0\rangle \left| \frac{1}{2}, -\frac{1}{2} \right\rangle + \frac{\sqrt{3}}{2} \left| \frac{3}{2}, \frac{1}{2} \right\rangle |0, 0\rangle \left| \frac{1}{2}, \frac{1}{2} \right\rangle \\
 |F=2, m_F = 0\rangle & = \frac{1}{\sqrt{2}} \left| \frac{3}{2}, \frac{1}{2} \right\rangle |0, 0\rangle \left| \frac{1}{2}, -\frac{1}{2} \right\rangle + \frac{1}{\sqrt{2}} \left| \frac{3}{2}, -\frac{1}{2} \right\rangle |0, 0\rangle \left| \frac{1}{2}, \frac{1}{2} \right\rangle \\
 |F=2, m_F = -1\rangle & = \frac{\sqrt{3}}{2} \left| \frac{3}{2}, -\frac{1}{2} \right\rangle |0, 0\rangle \left| \frac{1}{2}, -\frac{1}{2} \right\rangle + \frac{1}{2} \left| \frac{3}{2}, -\frac{3}{2} \right\rangle |0, 0\rangle \left| \frac{1}{2}, \frac{1}{2} \right\rangle \\
 |F=2, m_F = -2\rangle & = \left| \frac{3}{2}, -\frac{3}{2} \right\rangle |0, 0\rangle \left| \frac{1}{2}, -\frac{1}{2} \right\rangle
 \end{aligned}$$

F=1 levels of $P_{1/2}$

$$\begin{aligned}
 |F=1, m_F = +1\rangle & = \frac{1}{2\sqrt{3}} \left| \frac{3}{2}, \frac{1}{2} \right\rangle |1, 0\rangle \left| \frac{1}{2}, \frac{1}{2} \right\rangle - \sqrt{\frac{1}{6}} \left| \frac{3}{2}, \frac{1}{2} \right\rangle |1, 1\rangle \left| \frac{1}{2}, -\frac{1}{2} \right\rangle \\
 & - \sqrt{\frac{1}{2}} \left| \frac{3}{2}, \frac{3}{2} \right\rangle |1, -1\rangle \left| \frac{1}{2}, \frac{1}{2} \right\rangle + \frac{1}{2} \left| \frac{3}{2}, \frac{3}{2} \right\rangle |1, 0\rangle \left| \frac{1}{2}, -\frac{1}{2} \right\rangle \\
 |F=1, m_F = 0\rangle & = \sqrt{\frac{1}{6}} \left| \frac{3}{2}, -\frac{1}{2} \right\rangle |1, 0\rangle \left| \frac{1}{2}, \frac{1}{2} \right\rangle - \sqrt{\frac{1}{3}} \left| \frac{3}{2}, -\frac{1}{2} \right\rangle |1, 1\rangle \left| \frac{1}{2}, -\frac{1}{2} \right\rangle
 \end{aligned}$$

$$\begin{aligned}
& -\sqrt{\frac{1}{3}}|\frac{3}{2}, \frac{1}{2}\rangle |1, -1\rangle |\frac{1}{2}, \frac{1}{2}\rangle + \sqrt{\frac{1}{6}}|\frac{3}{2}, \frac{1}{2}\rangle |1, 0\rangle |\frac{1}{2}, -\frac{1}{2}\rangle \\
|F=1, m_F = -1\rangle &= \frac{1}{2}|\frac{3}{2}, -\frac{3}{2}\rangle |1, 0\rangle |\frac{1}{2}, \frac{1}{2}\rangle - \sqrt{\frac{1}{2}}|\frac{3}{2}, -\frac{3}{2}\rangle |1, 1\rangle |\frac{1}{2}, -\frac{1}{2}\rangle \\
& -\sqrt{\frac{1}{6}}|\frac{3}{2}, -\frac{1}{2}\rangle |1, -1\rangle |\frac{1}{2}, \frac{1}{2}\rangle + \frac{1}{2\sqrt{3}}|\frac{3}{2}, -\frac{1}{2}\rangle |1, 0\rangle |\frac{1}{2}, -\frac{1}{2}\rangle
\end{aligned}$$

F=1 levels of D_{3/2}

$$\begin{aligned}
|F=1, m_F = 1\rangle &= \frac{\sqrt{6}}{5}|\frac{3}{2}, -\frac{1}{2}\rangle |2, 2\rangle |\frac{1}{2}, -\frac{1}{2}\rangle - \frac{1}{5}\sqrt{\frac{3}{2}}|\frac{3}{2}, -\frac{1}{2}\rangle |2, 1\rangle |\frac{1}{2}, \frac{1}{2}\rangle \\
& -\frac{\sqrt{6}}{5}|\frac{3}{2}, \frac{1}{2}\rangle |2, 1\rangle |\frac{1}{2}, -\frac{1}{2}\rangle + \frac{2}{5}|\frac{3}{2}, \frac{1}{2}\rangle |2, 0\rangle |\frac{1}{2}, \frac{1}{2}\rangle \\
& + \frac{\sqrt{3}}{5}|\frac{3}{2}, \frac{3}{2}\rangle |2, 0\rangle |\frac{1}{2}, -\frac{1}{2}\rangle - \frac{3}{5\sqrt{2}}|\frac{3}{2}, \frac{3}{2}\rangle |2, -1\rangle |\frac{1}{2}, \frac{1}{2}\rangle \\
|F=1, m_F = 0\rangle &= \frac{3}{5}|\frac{3}{2}, -\frac{3}{2}\rangle |2, 2\rangle |\frac{1}{2}, -\frac{1}{2}\rangle - \frac{3}{10}|\frac{3}{2}, -\frac{3}{2}\rangle |2, 1\rangle |\frac{1}{2}, \frac{1}{2}\rangle \\
& -\frac{\sqrt{3}}{10}|\frac{3}{2}, -\frac{1}{2}\rangle |2, 1\rangle |\frac{1}{2}, -\frac{1}{2}\rangle + \frac{\sqrt{2}}{10}|\frac{3}{2}, -\frac{1}{2}\rangle |2, 0\rangle |\frac{1}{2}, \frac{1}{2}\rangle \\
& -\frac{\sqrt{2}}{10}|\frac{3}{2}, \frac{1}{2}\rangle |2, 0\rangle |\frac{1}{2}, -\frac{1}{2}\rangle + \frac{\sqrt{3}}{10}|\frac{3}{2}, \frac{1}{2}\rangle |2, -1\rangle |\frac{1}{2}, \frac{1}{2}\rangle \\
& + \frac{3}{10}|\frac{3}{2}, \frac{3}{2}\rangle |2, -1\rangle |\frac{1}{2}, -\frac{1}{2}\rangle - \frac{3}{5}|\frac{3}{2}, \frac{3}{2}\rangle |2, -2\rangle |\frac{1}{2}, \frac{1}{2}\rangle \\
|F=1, m_F = -1\rangle &= \frac{3}{5\sqrt{2}}|\frac{3}{2}, -\frac{3}{2}\rangle |2, 1\rangle |\frac{1}{2}, -\frac{1}{2}\rangle - \frac{\sqrt{3}}{5}|\frac{3}{2}, -\frac{3}{2}\rangle |2, 0\rangle |\frac{1}{2}, \frac{1}{2}\rangle \\
& -\frac{2}{5}|\frac{3}{2}, -\frac{1}{2}\rangle |2, 0\rangle |\frac{1}{2}, -\frac{1}{2}\rangle + \frac{\sqrt{6}}{5}|\frac{3}{2}, -\frac{1}{2}\rangle |2, -1\rangle |\frac{1}{2}, \frac{1}{2}\rangle \\
& + \frac{1}{5}\sqrt{\frac{3}{2}}|\frac{3}{2}, \frac{1}{2}\rangle |2, -1\rangle |\frac{1}{2}, -\frac{1}{2}\rangle - \frac{\sqrt{6}}{5}|\frac{3}{2}, \frac{1}{2}\rangle |2, -2\rangle |\frac{1}{2}, \frac{1}{2}\rangle
\end{aligned}$$

It can be noted that $m_F=0$ sublevel of $F=1$ of $S_{1/2}$ is a Q_- state while the same one for $P_{1/2}$ is a Q_+ state. Similarly, $m_F=0$ of $F=2$ of $S_{1/2}$ is a Q_+ state and thus has a nonzero transition probability with $m_F=0$ of $F=1$ of $P_{1/2}$ level.

Appendix D

Dipole matrix elements

The electromagnetic fields that connect the transitions between various states of $S_{1/2}$, $P_{1/2}$ and $D_{3/2}$ are denoted in the following manner. In the cartesian coordinate system, the right and left circularly polarized light are denoted by

$$E^+ = \frac{\mathcal{E}}{2}(\hat{x} + i\hat{y}) \exp(i\omega t)$$

and

$$E^- = \frac{\mathcal{E}}{2}(\hat{x} - i\hat{y}) \exp(i\omega t)$$

The plane polarized light is denoted as

$$E_0 = \text{Re}[E^+ + E^-] = \mathcal{E}\hat{x} \exp(i\omega t).$$

The dipole matrix element $\langle i|E^\pm|j\rangle$ and $\langle i|E^0|j\rangle$ between states $|i\rangle$ and $|j\rangle$ are obtained by making use of the selection rules for orbital angular momenta *.

Dipole matrix elements for transitions $F=1$, $S_{1/2} \leftrightarrow F=1$, $P_{1/2}$

| | | $P_{1/2}$ | | |
|-----------|----|------------------------|------------------------|------------------------|
| | | -1 | 0 | +1 |
| $S_{1/2}$ | -1 | $-\frac{1}{6}$ | $-\frac{1}{3\sqrt{2}}$ | 0 |
| | 0 | $-\frac{1}{3\sqrt{2}}$ | 0 | $-\frac{1}{3\sqrt{2}}$ |
| | +1 | 0 | $-\frac{1}{3\sqrt{2}}$ | $\frac{1}{6}$ |

*H. A. Bethe and E. E. Salpeter, *Quantum Mechanics of one - and two -electron atoms*, Plenum, 1977, pp 254

Dipole matrix elements for transitions $F=2, S_{1/2} \leftrightarrow F=1, P_{1/2}$

| | | $P_{1/2}$ | | |
|-----------|----|-----------------------|-----------------------|------------------------|
| | | -1 | 0 | +1 |
| $S_{1/2}$ | -2 | $-\frac{1}{\sqrt{3}}$ | 0 | 0 |
| | -1 | $\frac{1}{2\sqrt{3}}$ | $-\frac{1}{\sqrt{6}}$ | 0 |
| | 0 | $\frac{1}{3\sqrt{2}}$ | $\frac{1}{3}$ | $-\frac{1}{3\sqrt{2}}$ |
| | +1 | 0 | $\frac{1}{\sqrt{6}}$ | $\frac{1}{2\sqrt{3}}$ |
| | +2 | 0 | 0 | $\frac{1}{\sqrt{3}}$ |

Dipole matrix elements for transitions $F=1, P_{1/2} \leftrightarrow F=1, D_{3/2}$

| | | $D_{3/2}$ | | |
|-----------|----|----------------------------------|----------------------------------|----------------------------------|
| | | -1 | 0 | +1 |
| $P_{1/2}$ | -1 | $-\frac{\sqrt{5}}{6}$ | $-\frac{1}{3}\sqrt{\frac{5}{2}}$ | 0 |
| | 0 | $-\frac{1}{3}\sqrt{\frac{5}{2}}$ | 0 | $-\frac{1}{3}\sqrt{\frac{5}{2}}$ |
| | +1 | 0 | $-\frac{1}{3}\sqrt{\frac{5}{2}}$ | $\frac{\sqrt{5}}{6}$ |

It is seen that the transition probability from states which are of the type Q_- to those of the type Q_+ are zero while the transition probability from states of the same type are finite. **In other** words, the transition probability between $m_F=0$ sublevel of $F=1$ of $S_{1/2}$ to $m_F=0$ of $P_{1/2}$ is zero. The transition from $m_F=0$ of $F=2$ level of $S_{1/2}$ to $m_F=0$ of $F=1$ of $P_{1/2}$ on the other **hand**, is **finite**.